Transverse load-spread of a voided bridge deck

Comparison between a grillage model and an orthotropic plate model

G. Hogendoorn

June 2021

Transverse load-spread of a voided bridge deck

Comparison between a grillage model and an orthotropic plate model

by

G. Hogendoorn

to obtain the degree of Master of Science
at the Delft University of Technology,

Student number:	4570928	
Project duration:	November 3, 2020 – June 23, 2021	
Thesis committee:	dr. ir. M.A.N. Hendriks	TU Delft, supervisor
	dr. ir. H.W.M. van der Ham	TU Delft
	dr. ir. P.C.J. Hoogenboom	TU Delft
	ing. R.K. Grift	Ballast Nedam
	ir. R.M. van Vught	Ballast Nedam

An electronic version of this thesis is available at http://repository.tudelft.nl/.

TU Delft Ballast Nedam

Preface

In September 2019, I started the master's program *Civil Engineering* at Delft University of Technology (TU Delft). During this study program, I followed courses in the direction of *Structural Engineering* and *Structural Mechanics*. In November 2020, I started with the last part of the master's program, which was the graduation research. This thesis is the final product of the graduation research.

During the graduation research, I studied the transverse load-spread of a voided bridge deck modelled as a grillage model, compared to an orthotropic plate model. The research topic was proposed by the contracting company Ballast Nedam, located in Nieuwegein. The graduation research started in November 2020 end lasted till June 2021.

This thesis is written for structural engineers interested in the modelling of voided concrete bridge decks. The reader of this thesis is supposed to have the knowledge associated to the bachelor's degree in civil engineering and has additional knowledge on: the theory of plates, (shape) orthotropy, theory on concrete and reinforcement design and finite element programming (i.e. SCIA-engineer, MIDAS, DIANA, etc).

I want to thank Ballast Nedam for offering me the opportunity to graduate at their company. Also a huge thank-you to Rob Grift, my main advisor during the whole research. During the whole project, you shared your knowledge, gave feedback and challenged me by giving me a lot of suggestions for subjects to look at. I also want to thank the members of the thesis committee, for their time, enthusiasm about the research topic and feedback and suggestions during the meetings.

G. Hogendoorn
Loenersloot, June 2021

Abstract

Problem statement
Orthotropic bridges can be modelled using a grillage model and an orthotropic plate model. The grillage model has some benefits (i.e.: shorter calculation time and easier to apply pre-stressing) compared to the orthotropic plate model. However, during the Blankenburgverbinding project Ballast Nedam experienced that the transverse load-spread of the grillage model can be lower compared to the orthotropic plate model. This potentially results into a less economical reinforcement design. The aim of this study is to investigate the differences in transverse load-spread of the grillage and orthotropic plate model and to make a judgement on the practical usability of the grillage model based upon the differences in reinforcement design.

Methodology
To test the hypothesis that the grillage model has less transverse load-spread compared to the orthotropic plate model and to quantify the impact on the reinforcement design, a case study on the bridge decks of the Blankenburgverbinding is carried out. The results of a grillage model are compared to an orthotropic plate model. In order to be able to judge whether to orthotropic plate model describes the correct behaviour of the bridge, this model is verified using a 3D plate model. In total, 3 different single-span, simply supported bridge deck layouts were modelled (straight, curved and curved with a skew angle).

Key results
The results of the 3D plate model are almost equal to the results of the orthotropic plate model. Both these models show the same transverse load-spread. The grillage model shows less transverse load-spread compared to the orthotropic plate model and the 3D plate model. This difference in load-spread increases with increasing eccentricity of the applied load. The torsional and transverse shear stiffness has the biggest impact on the transverse-load spread. When these stiffnesses are higher, the transverse load-spread increases. Lowering the stiffnesses results into less load-spread. In case of the curved bridge deck, the grillage model results in about 7.3% more reinforcement compared to the orthotropic plate model. For the curved and skewed deck the grillage model results into up to 4.7% more reinforcement compared to the orthotropic plate model.

Conclusion
The differences in design bending moments (Wood-Armer moments) are relatively small. Although the theoretical difference in amount of reinforcement is significant, the practical difference in reinforcement design between both models can be small. For example, the structural engineer is limited by the available space, detailing requirements and the available bar diameters. These limitations and rounding differences make that for some bridges it is possible to reduce for example 5% reinforcement and for some bridges such a reduction can be very hard to realise. In that case, the theoretical difference between the amount of reinforcement becomes very small or completely vanishes in practice.

Eventually, it depends on the situation whether the benefits of the grillage model outweigh the theoretically less economical reinforcement design. When there are a lot of repetitive bridge decks, it can be beneficial to use an orthotropic plate model. In that case, the orthotropic plate model has to be created only once and only a small reduction in the amount of reinforcement of one deck can add-up to a significant reduction for the whole project. When there is only one bridge deck to model, or all spans are unique, the benefits of the grillage model most likely outweigh the practical difference in the amount of reinforcement.

Contents

List of Figures

List of Tables

I

Introduction, theory and set-up of models

1 Introduction

An orthotropic voided bridge deck can be modelled using different kind of models. The most advanced and exact model is a full 3D model in which the full cross-section of the bridge deck is modelled. The finite elements of such a model are volume elements. Although this model gives the most exact description of the behaviour of the bridge deck, a full 3D model will need a lot of calculation time. Also, post-processing is needed to obtain the desired cross-sectional forces (such as normal forces, bending moments and torsional moments). These forces cannot be extracted from the 3D model directly. The 3D model can be simplified by modelling the cross-section using isotropic plates. For this 3D plate (or 2.5D model), the calculation time is already shorter compared to the 3D plate model, as there are less nodes compared to the 3D model. However, also for the 3D plate model it is needed to post-process the cross-sectional forces.

Another model that can be used to model an orthotropic bridge deck, is an orthotropic plate model. In this model, the orthotropic bridge deck is modelled as a flat plate, to which orthotropic stiffness properties are assigned. The calculation time of the orthotropic plate model will be shorter compared to the 3D and 2.5D models. The biggest benefit of the orthotropic plate model is that cross-sectional forces can be extracted from the results directly.

A third option is a grillage model. This model consists of a grid of longitudinal and transverse beams. These beams are rigidly connected in the nodes. The longitudinal beams represent the longitudinal and the transverse beams the transverse stiffness of the bridge deck. The biggest benefit of the grillage model is the short calculation time. A shorter calculation time means that it easier to adjust the design and see the effects of the adjustment faster. In the grillage model, it is also easier to apply pre-stressing.

The structural engineer always has to choose between the *simplicity* of the model and the desired *accuracy*. In general, a simpler model means less accuracy. This also holds for the grillage model. This model is the simplest model of the models discussed above. At the same time, this model is also the least accurate one.

1.1. Motivation of research

At the end of the summer of 2019, the BAAK-consortium (Ballast Nedam, DEME Group and Macquarie) started with the construction of the Blankenburgverbinding. In this project, a new highway in the Rotterdam port-area is build. This new highway (A24) connects the already existing highways A15 (near Rozenburg) and A20 (near Vlaardingen), see figure 1.1. As part of the new highway, several big structures needs to be build: a big tunnel passing the ”Nieuwe Waterweg” river (*Maasdeltatunnel*), a land tunnel (*Hollandtunnel*) and bridges for the connection roads of the intersections *Vlaardingen* and *Rozenburg*, see figure 1.1.

The bridges for the connection roads at the intersection with the A15 (intersection Rozenburg) are (partly) in-situ casted concrete bridge decks. The final situation of intersection Rozenburg can be seen in figure 1.1. It can be seen that the bridge decks are curved and the angle between the bridge deck and the support is not always 90°. This means that the bridge decks can be curved and have a skew agle as well. The in-situ casted bridge decks have voids in it to reduce self-weight and they are pre-stressed. The cross-section of these bridge decks can be seen in figure 1.2.

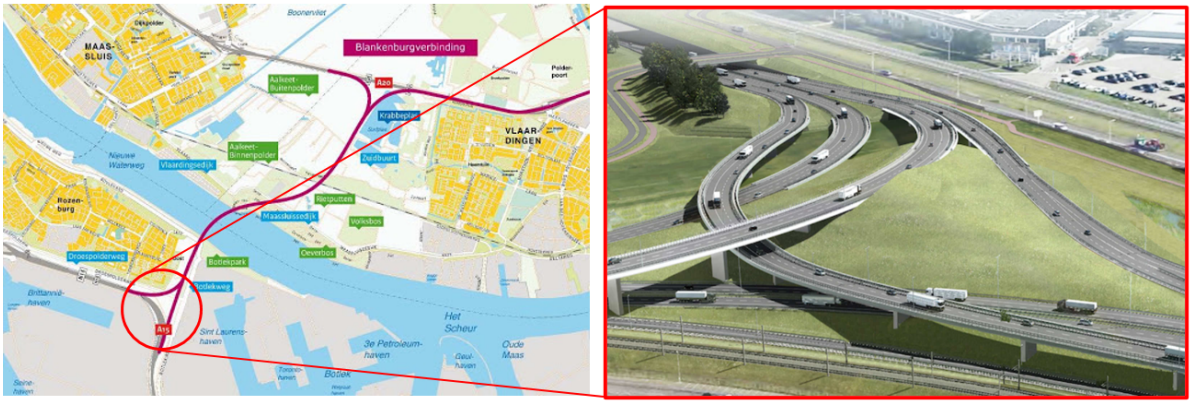

Figure 1.1: Blankenburgverbinding (left), intersection Rozenburg (right) (source: Rijkswaterstaat / ZJA)

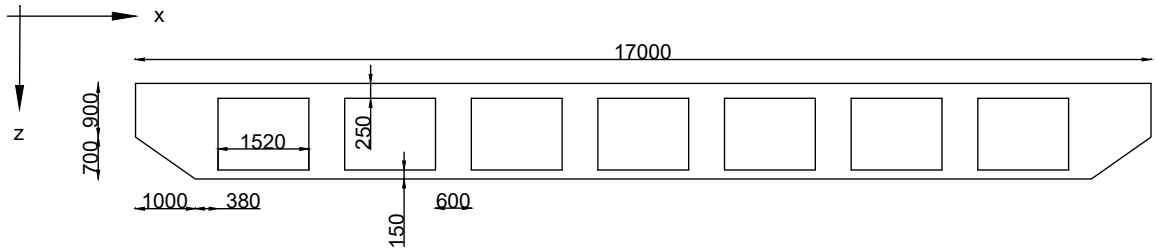

Figure 1.2: Cross-section bridge decks intersection Rozenburg

Figure 1.3 shows a top view of the bridge decks under construction. This photo was taken in March 2021. The 2 bridges on the top of the photo are completely casted in-situ. For the bridge at the top of the photo, the left span is already casted and the right span is under construction. In the span under construction, the reinforcement of the stiffeners and the top plate of the bridge deck can be seen. In the span, the color tone is a little bit more brown compared to the part above the support. This brown color comes from the wood of the moulds for the voids. Above and next to the support there are no voids. In this zone, the bridge deck is solid. The two bridges on the bottom consist of pre-casted beams with an in-situ casted top layer and solid in-situ casted integrated transverse beam. This is done to make a rigid connection above the supports.

During the preliminary design phase, Ballast Nedam modelled the bridge decks as an orthotropic plate model. In a later phase of the design, more detailed calculations were needed, such as the effect of the construction stages. These calculations were outsourced to the Turkish consultant firm SU-YAPI. They decided to model the bridge decks using a grillage model.

Eventually, the results of the grillage model (SU-YAPI) were compared to the orthotropic plate model (Ballast Nedam). It turned out that there was quite some agreement between both models. However, it seemed that the grillage model results into less transverse load-spread, especially for eccentric applied loads. Less transverse load-spread for example means that the maximum longitudinal bending moment is larger, as the applied loading spreads out over a smaller width of the bridge deck. When the differences in transverse load-spread are big, the grillage model could result into much more reinforcement. In that case, a reinforcement design based upon a grillage model would be less economical compared to for example and orthotropic plate model. This could potentially mean that the benefits of the grillage model (shorter calculation time, easier to see effects of adjustments and easier to apply pre-stressing) do not outweigh the the practical disadvantages of a model that is too conservative (i.e. more costs on reinforcement).

Figure 1.3: Top view bridge decks under construction (March 2021)

1.2. Research questions

The main research question is:

To which extend does the transverse load-spread of a voided orthotropic bridge deck modelled as a grillage model differ from an orthotropic plate model. And what does this mean for the practical usability of the grillage model in engineering practice?

This main research question can be answered by investigating the following sub-questions:

Validation of the models

- Do all models have the same transverse and longitudinal stiffness? How much do transverse and longitudinal strips, taken out of the complete models, deflect when they are all loaded in an similar way?
- How do the reaction forces and the deflections of the grillage model, orthotropic plate model and 3D plate model differ?
- Does the orthotropic plate model describe the behaviour of the voided bridge deck correctly? How does the transverse load-spread of the orthotropic plate model compare to a 3D plate model?

Differences in load-spread

- How do the longitudinal, transverse and torsional bending moment of the grillage and the orthotropic plate model differ? What does this means for the transverse load-spread.
- How does the eccentricity of the applied load influence the difference in transverse load-spread?
- Which stiffness parameter(s) has the biggest influence on the transverse load-spread of an orthotropic bridge deck?
- What is the difference in load-spread for a realistic load-combination for a bridge deck, taking into account self-weight, pre-stressing and traffic load? And which type of loading results into the biggest difference in load-spread?

Design bending moments

- To which extend are the design bending moments - used to design the reinforcement - different for the grillage and orthotropic plate model? What is the difference per direction and location (top and bottom) of the reinforcement and what is the difference of the sum of design bending moments?
- Does the difference of the design bending moment between both models depend on the layout of the bridge deck?
- What do the differences between the design bending moments mean for the reinforcement design and what does this mean for the usability of the grillage model in engineering practice?

Reinforcement design in practice

- How big are the step-sizes of the total amount of reinforcement per unit width of the bridge deck for realistic spacing and bar diameter?

1.3. Outline of research

In order to investigate the transverse load-spread of the grillage model and to compare it with the orthotropic plate model, the bridge decks of the Blankenburgverbinding were used as a case study. The correctness of the orthotropic plate model was verified using a 3D plate model. All 3 models (grillage, orthotropic plate and 3D plate model) were created in *SCIA-engineer*. The cross-section of the Blankenburgverbinding was applied to 3 different bridge deck layouts: a straight deck, a deck with a curvature (R=300 m) and a deck with the same curvature and a skew angle of 45°. The bridge decks of the case study were simply supported and had a span of 40 m.

The straight bridge deck was loaded with dummy loads in the middle of the span of the deck. These dummy loads were located at different positions in the transverse direction of the deck. Using these dummy loads, the transverse load-spread can be compared for different loads. Also, the effect of the eccentricity of the applied load can be investigated.

The curved and curved and skewed deck were loaded with self-weight, traffic load and pre-stressing. The pre-stressing was taken into account by reducing the self-weight of the bridge deck. Using the results of these bridge decks, the difference in transverse load-spread can be investigated for realistic loading. Using the design bending moments (Wood-Armer, 1968), the difference in amount of reinforcement between the grillage and orthotropic plate model can be determined.

1.4. Hypothesis

The engineers of Ballast Nedam compared their orthotropic plate model to the grillage model made by the engineering firm from Turkey. Based upon their observations, it is expected that the grillage model shows less transverse load-spread. It also stood out that the difference in load-spread between both models depends on the eccentricity of the applied load. The traffic load is an example of an eccentric load, as the more heavy loaded lanes are on the outside of the bridge deck. This means that the resultant of the traffic load lies outside the centre of gravity. The self-weight of the bridge is by definition a centric load as the resultant of the self-weight lies in the centre of gravity.

Longitudinal bending moment

When there is less transverse load-spread, the magnitude of the longitudinal bending moment over the transverse cross-section will have a larger range compared to a bridge deck that shows more load-spread. At the location where the load is applied, the longitudinal bending moment is larger compared to the remaining width of the deck.

When the transverse load-spread increases, a larger part of the load is taken by a wider part of the bridge deck. This lowers the longitudinal bending moment at the location where the load is applied and increases the longitudinal bending moment away from the point of application of the load. When the load-spreads out in the transverse direction, the magnitude of the longitudinal bending moments tend to get closer to each other.

Transverse bending moment
The transverse bending moment of a plate-like structure can be split-up into 2 parts. In transverse direction, the effect of lateral contraction (Poisson) contributes to the bending moment. The other part is a contribution of transverse load-spread: the load *travelling* in transverse direction results into a bending moment in transverse direction.

Lateral contraction
A positive bending moment is defined as a bending moment that causes tension on the bottom and compression on the top. Using a positive longitudinal bending moment applied to longitudinal plate strips, the effect of lateral contraction on the transverse bending moment can be explained. Figure 1.4 shows the cross-section of these longitudinal plate strips.

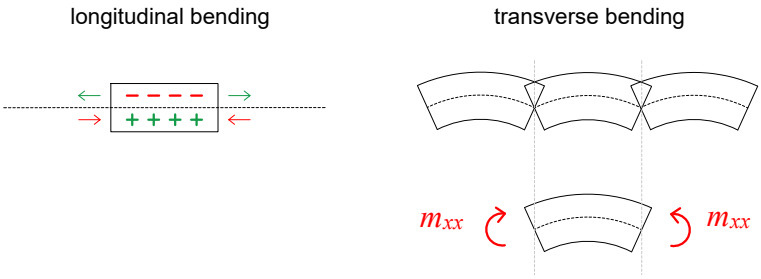

Figure 1.4: Transverse bending moment, effect of lateral contraction

In the left picture, the effect of a positive longitudinal bending moment (m_{yy}) can be seen. On the bottom of the plate strip there is tension and on the top there as compression. As a result of lateral contraction, the bottom part of the plate strip contracts in transverse direction, while the top part extends in transverse direction. This means that the plate strips deform as shown in the right picture of figure 1.4.

In reality, all longitudinal plate strips are connected and cannot deform as shown in the right picture of figure 1.4. To overcome this compatibility problem, there must be a bending moment in the transverse direction of the deck (m_{xx}). For isotropic plates this bending moment is equal to:

$$m_{xx} = \nu \cdot m_{yy} \tag{1.1}$$

For a voided isotropic bridge deck, the effect of lateral contraction can only happen in the top and bottom plate, the web-parts can expand and contract freely in transverse direction. This means that the effect of lateral contraction is smaller than shown in equation 1.1.

In the orhtotropic plate model, the effect of lateral contraction of the top and bottom plate is incorporated. For the grillage model, the effect of lateral contraction is not taken into account. The grillage model consists of a grid of 1D beams. These beams do not contract in lateral direction. This means that the transverse bending moment caused by lateral contraction will be 0 for the grillage model. In the orthotropic plate model, the transverse bending moment will have the same sign as the moment in longitudinal direction.

Transverse load-spread
As the transverse load spread of the grillage model is expected to be smaller compared to the orthotropic plate model, the transverse bending moment is also expected to to be smaller for the grillage model. In the grillage model, less load needs to be distributed in the transverse direction of the deck. From this, it can be expected that the transverse bending moment is lower.

Eccentricity and type of loading
The more eccentric applied load is expected to show a larger difference in transverse load-spread as this was also observed by the engineers of Ballast Nedam.

The self-weight of the bridge deck has no eccentricity, so it is expected that for this load case the difference in transverse load-spread will be small. The traffic load is applied according Load Model 1 (LM1) from the Eurocode. This load model consists of a uniform distributed load (UDL) and a tandem

axle system (TS). The magnitude of the tandem system has a larger variety over the different traffic lanes and thus a more eccentricity. It is expected that the tandem system contributes shows the biggest difference in load-spread.

Eventually, the load-spread of all loads together is compared. This is done without taking into account the pre-stressing and with taking account the pre-stressing. The pre-stressing is accounted for by lowering the self-weight. As it is expected that the self-weight shows a small difference between the load-spread of both models, it is expected that reducing the self-weight increases the overall difference in load-spread as the eccentric applied traffic loads have a larger relative contribution. So, when pre-stressing is taken into account, it is expected that the difference in load-spread increases.

1.5. Structure of the report

This report begins with the introduction of the *Blankenburgverbinding* case study. The cross-section and the layout of the bridge deck as well as the boundary and loading conditions can be found in chapter 2. Chapter 3, 4 and 5 are about the different models used to model the bridge deck of the Blankenburgverbinding case study. Chapter 3 is about the orthotropic plate model, chapter 4 the grillage model and chapter 5 introduces the 3D plate model. Each of these 3 chapters are split into 2 parts. The first part introduces the general theory of the model and in part 2, it is shown how the models of the Blankenburgverbinding case study are created.

The second part of this report is about the results of the models. In chapter 6, the longitudinal and transverse stiffnesses of the models are checked and compared to an analytical solution. To do this, strips in longitudinal and transverse direction are taken out of the models of the bridge deck. After validation of the models, the actual results of the complete bridge deck models are shown. This is done in chapter 7, 8 and 9. The results are shown per type of bridge deck layout. Chapter 7 shows the results of a straight bridge deck, chapter 8 of a curved and chapter 9 of a curved and skewed bridge deck. Also these chapters are supported by appendices showing a lot of graphs and other plots.

The final conclusions of the research as well as the discussion and recommendations for further research can be found in chapter 10.

2

The Blankenburg case study

This chapter introduces the case study of the Blankenburgverbinding. For this project, Ballast Nedam designed and constructed a number of bridges that connect the new A24 highway to the the existing A15. First, the cross-section of the bridge decks an the material properties are introduced. In the next section, the building process of the in-situ casted bridge decks of the Blankenburgverbinding is explained. In the last 2 sections the layout, boundary conditions and the applied loading applied to the decks is discussed.

2.1. Cross-section and material properties

The viaducts that are being build in the Blankenburgverbinding project more or less have the cross-section as shown a figure 2.1. At some locations, the deck is a little bit wider, which follows from traffic regulations such as a minimum required *line of sight* for curved roads. Beside, above and near the support, the deck is solid and the depth is a little bit higher. However, for this research, it is assumed that the bridge deck has a uniform cross-section in longitudinal direction.

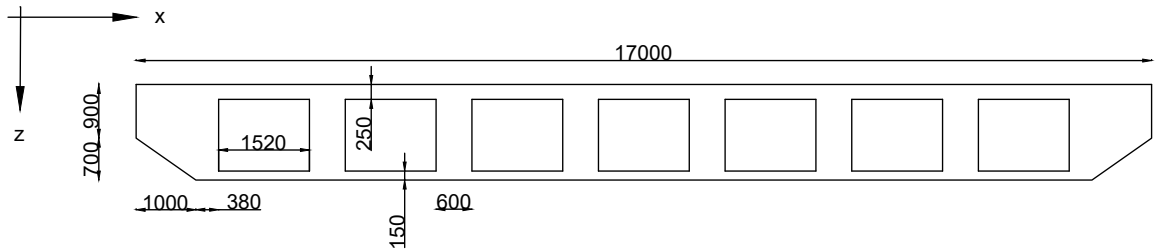

Figure 2.1: Cross-section of the bridge decks used for the Blankenburgverbinding (mm)

As shown in figure 2.1, the cross-section is not fully repetitive in transverse direction. On the edges of the deck, there is some extra material and there is a chamfer (1000 x 700 mm). For the grillage model it is possible to model 2 different longitudinal beams on the edge of the bridge deck. However, for the orthotropic plate model, it is not possible to model the extra stiffness and chamfer on the edge of the deck. This follows from the fact that for an orthotropic plate repetition is needed. A random located, or non-repetitive change in cross-section cannot easily be included in the orthotropic plate model. In order to be able to make a fair comparison between the grillage and the orthotropic plate model, it is decided to modify the cross-section such that there is a repetition of H-sections. For all models that will be compared in this thesis, the cross-sectional properties of the bridge deck will be based upon the modified cross-section, which is shown in figure 2.2.

The strength class of the concrete used for the bridge deck is C45/55. Table 2.1 shows all relevant material properties for this concrete strength class.

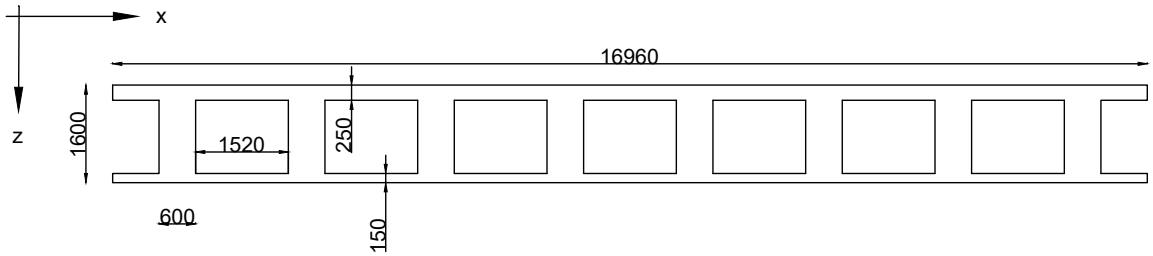

Figure 2.2: Modified cross-section used for all models (mm)

Table 2.1: Material properties concrete strength class C45/55

Concrete strength class C45/55			
Young's modulus	E	36 300	MPa
Shear modulus	G	15 125	MPa
Poisson's ratio	ν	0.2	-
Specific weight	ρ	2500	kg/m^3

The cross-sectional area of the bridge deck shown in figure 2.2 is equal to

$$\begin{aligned} A &= b \cdot h - n \cdot A_{void} \\ &= 16.96 \cdot 1.6 - 8 \cdot 1.52 \cdot 1.2 = 12.544\,\text{m}^2 \end{aligned}$$

2.2. Building process

The bridge decks of the intersection Rozenburg are casted in-situ. This means that it is needed to build a temporarily supporting frame. This frame has two functions: the formwork can be build on it, and the frame carries the self-weight of the freshly casted concrete. In case of the Blankenburgverbinding, there is a land-strip which may not be loaded as there is crucial infrastructure (such as cables and pipes) in the ground. Also, 2 spans of the viaduct need to be build above the highway A15 while the road is still in use. For these 2 locations (the land-strip and the A15), the temporally frame supporting the formwork and the self-weight of the concrete is called a *table structure*. The table structure above the A15 can be seen in figure 2.3. Left from the table structure, a completed span of one of the viaducts can be seen.

Figure 2.3: Table structure above highway A15, top view (left) and side view (right)

On top of the table structure, a scaffolding is placed. With this scaffolding, the desired vertical alignment and shape of the bridge deck can be created. The formwork of the bridge decks is placed on top of the scaffolding. The formwork can be seen in figure 2.4.

The locations that are indicated in figure 2.4, are the following ones: The gaps for the bearings are sawn out of the formwork and the bearings are positioned at their correct position. A very tiny part of the cut-out needed for the bearing, can be seen at (1). During the first cast, the concrete is casted till the level of the wooden slats, indicated with (2). The wooden slats are located at the top level of the bottom plate of the bridge deck. After the first cast, the remaining part of the deck is casted. With the help of the wooden slats, the pouring seam is more aesthetic. The anchors indicated with (3) are casted in the concrete of the bottom plate. When the bottom plate is cured, these anchors can be used to fit the formwork when the remaining part of the deck is casted. There is also a row of anchors at a higher level (4), these anchors are used to connect a temporarily fence to the bridge deck. In the back of the picture (5), an already casted deck can be seen. On the face of this already casted deck, the connectors of the pre-stressing strands are protected with a foil.

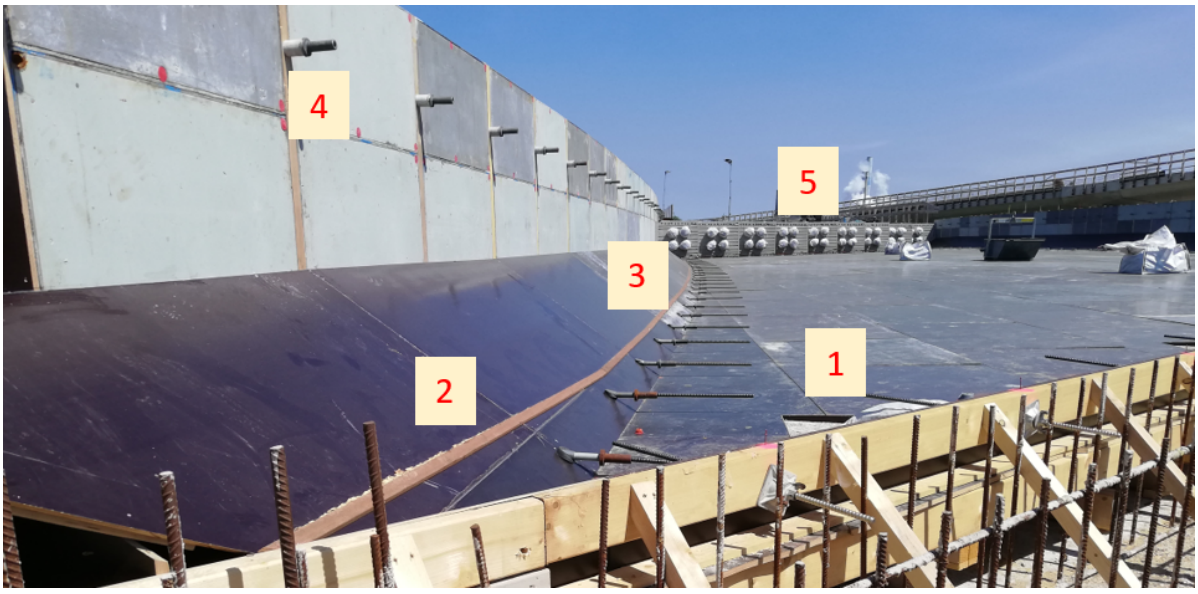

Figure 2.4: formwork, including: 1. cut-out for the bearing, 2. wooden slats, 3/4. anchors and 5. already casted deck

The transverse reinforcement is placed on top of the formwork. To ensure enough concrete cover, the reinforcement lays on concrete spacers. After the installation of the transverse reinforcement, the shear reinforcement of the stiffeners is added. The horizontal part of the U-shaped shear reinforcement is connected to the transverse reinforcement bars. To make the shear reinforcement stable, the separate shear bars are connect with reinforcement bars in the longitudinal direction of the deck. After the installation of the shear reinforcement, the longitudinal reinforcement bars are placed in between the shear reinforcement. The width between the shear reinforcement is about 1.5 m. The longitudinal reinforcement bars lay on top of the transverse bars. The reinforcement in the bottom plate as well as the shear reinforcement can be seen in figure 2.5.

After the installation of the reinforcement of the bottom plate, the concrete of the bottom plate can be casted. In this first cast, the concrete is casted till the level of the wooden slats that are placed on the formwork (figure 2.4). A few days after the casting of the bottom plate, the formwork of the voids is installed. In between this formwork, the 600 mm wide stiffeners will be casted. After the second cast, the formwork for the voids is enclosed with concrete. As this formwork cannot be removed, it is also called *lost formwork*. The casing pipes that are used for the pre-stressing strands, are installed in between the shear reinforcement of the stiffeners. The formwork for the voids as well as the installation of the casing pipes can be seen in figure 2.6. In this picture, the workers walk on top of the already casted bottom plate of the bridge deck.

Figure 2.5: Transverse, longitudinal and shear reinforcement

Figure 2.6: Formwork for the voids and installation of casing pipes for pre-stressing

Eventually, the reinforcement of the top deck is put in place. This reinforcement consists of several layers. In the transverse direction of the deck, there is a combination of global and local behaviour. The local behaviour is the result from traffic that is located in between the stiffeners. This traffic causes hogging and sagging bending moments in the transverse direction of the top plate. The hairpins of the shear reinforcement are enclosed by longitudinal reinforcement bars. This ensures that the node, in which the tensile force of the shear reinforcement is transferred into a compressive stress diagonal, is strong enough (truss analogy). The reinforcement of the top plate, as well as the lost formwork and the bars enclosing the hairpins of the shear reinforcement can be seen in figure 2.7.

Figure 2.7: Reinforcement top plate, hairpins and formwork of the voids

After the the installation of all reinforcement, the reaming part of the deck is casted. This is done by pouring every stiffener until the bottom level of the top plate. When this level is reached, the top plate is casted. During the casting of the concrete, the table structure deflects as it has to carry the self-weight of the fresh concrete. This deflection is already accounted for by adding this deflection to the shape of the formwork. The deflected formwork has the desired shape of the bridge deck. However, the deflection of the formwork may not be too big, as the already casted and cured bottom plate must be able to follow the same deflection.

Before the formwork and the table structure can be removed, the bridge deck is pre-stressed. For every new deck that is connected to an already casted deck, the pre-stressing strands are connected using connectors. Eventually, the casing pipes of the pre-stressing strands are filled with grout. During this process, the air inside the casing pipes must be able to flow out. This can be done by installing ventilation tubes. These tubes are located at the highest levels of the casing pipes. When the grout starts to flow out of the ventilation tubes, the grouting is stopped.

2.3. Layout of the deck and boundary conditions

Figure 2.8 shows a top view of the viaducts of the Blankenburgverbinding under construction. This photo was taken in March 2021. From above, it becomes clear that the bridge decks are curved. The direction of the curvature changes for some bridge decks, this can be seen in figure 2.9. In the front, the left edge of the bridge deck is convex and in the back the left edge is concave. Also the supports of the bridge decks are not always perpendicular to the longitudinal direction of the deck. This means that the bridge decks also have a skew angle.

Figure 2.8: Top view of Blankenburg viaducts under construction (March 2021)

Figure 2.9: Change of direction of curvature

For the case study, 3 different layouts of the bridge deck were modelled: a straight deck, a curved deck with a radius of curvature of 300 m, and a deck with the same radius of curvature plus a skew angle of 45°. For all decks, one single span of 40 m has been modelled. The bridge deck with a radius of curvature of 300 m and a skew angle of 45° is one of the most extremely-shaped bridge decks that will be build in the *Blankenburgverbinding* project. The three different bridge deck layouts used for the case study can be seen in figure 2.10.

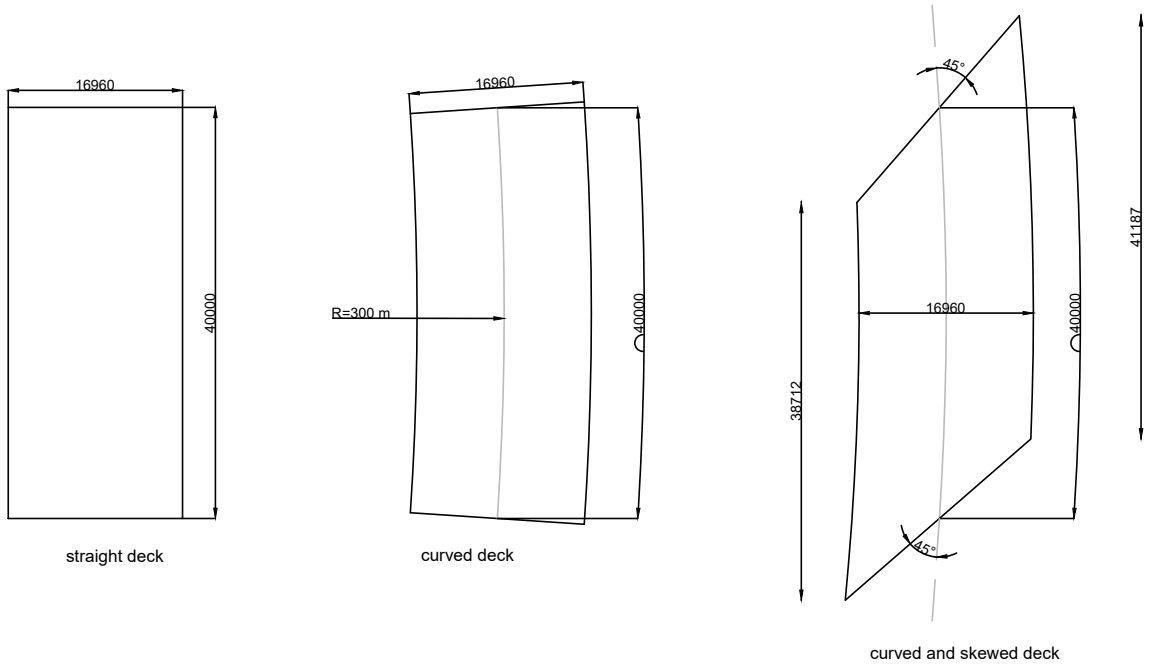

Figure 2.10: Layout of the bridge decks analysed (top view) (mm)

On both ends, the decks are simply supported with point supports. For all models, the position of

the point supports is based upon the grid of the grillage model. For the grillage model, it is not possible to support the bridge decks along the complete edges. Instead, the supports are located on the ends of the longitudinal beams. To make the models comparable, the supports of the orthotropic plate and 3D plate model are located at the same position.

For the grillage and orthotropic plate model, the supports are located at the level of the neutral axis. In the 3D plate model, the supports are located at the level of the bottom plate. This means that one edge of the bridge deck must be supported with a roller. The roller support ensures that there are no support reactions in the in-plane direction of the bridge deck. For the 3D plate model, in-plane support reactions would generate an undesired bending moment, as the supports of the 3D plate model are not at the level of the neutral axis. The supports and the support conditions can be seen in figure 2.11.

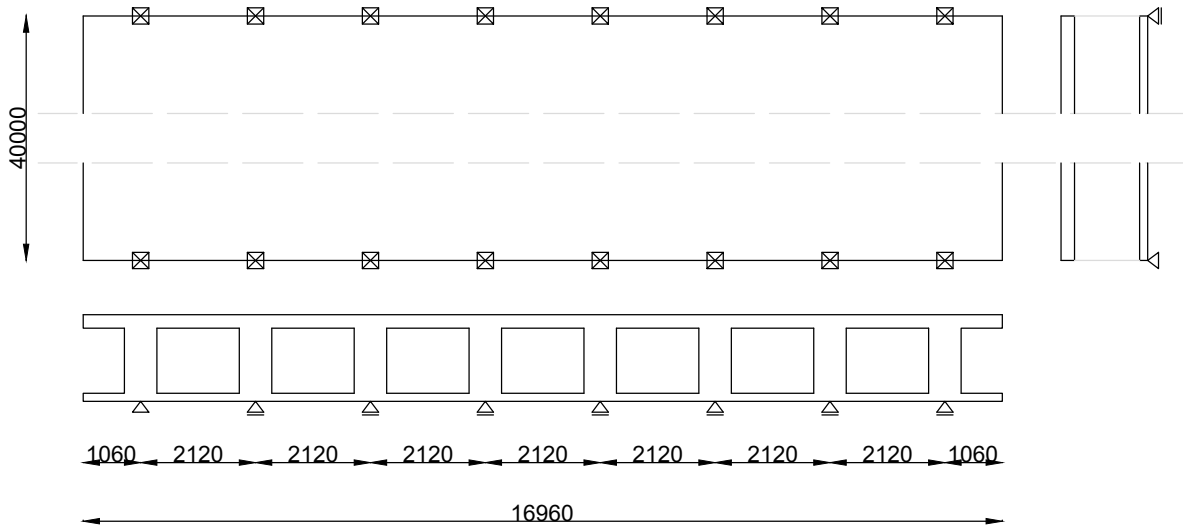

Figure 2.11: Supports bridge decks case study, top view and side view (mm)

2.4. Loading

The models of the bridge deck will be loaded with 3 different loads. The type of load that is applied depends on the goal of the analysis. For the straight bridge deck, the goal is to verify the models and to investigate the differences in transverse load-spread depending on the eccentricity of the applied load. The models of the straight deck layout are loaded with the self-weight of the bridge, as well as a variety of dummy loads. These dummy loads consist of a distributed load in the middle of the span, as well as several point loads above the stiffeners. The point-loads are applied one-by-one, so the relationship between the eccentricity of the applied load and the differences in transverse load spread can be investigated.

The bridge deck with the curved and curved + skew layout is loaded with the self weight as well as the traffic load. This loading is a realistic loading, which is also used in engineering practice. The self-weight is relatively big and is more or less centric applied. For the traffic load, the opposite holds: the magnitude of the force is relatively small and the eccentricity is relatively big. This follows from the fact that the more heavy traffic is positioned close to the edge of the bridge.

According to the hypothesis, more eccentricity, leads to a bigger difference in transverse load spread for the grillage model. The balance between the self-weight and the traffic load determines the overall eccentricity of the applied load. From this realistic loading, it can be concluded whether the difference in load spread is significant or not in engineering practice.

All bridge deck layouts are loaded by the self-weight. In order to be sure that the self-weight is identical for every model, the self weight is applied manually instead of automatically by *SCIA-engineer*. In case the self-weight is applied automatically, the self-weight of the grillage and 3D plate model is too high as a result of overlapping beams or plate parts.

For the grillage and 3D plate model, the self-weight can be applied as a q-load acting on the longitudinal beams, for the orthotropic plate model, the self-weight can be applied as a surface load. For every model, the numerical calculation of the self-weight is a little bit different and for the grillage model, it depends on the grid, that is why the self-weight will be calculated in the chapters concerning the models.

Table 2.2 gives an overview of which bridge deck layout is loaded with which load. The dummy loads and the traffic load will be discussed in the following sections. The self-weight of the deck will be calculated in the chapters in which the creation of the models will be discussed.

Table 2.2: Overview of loads and bridge layouts

	deck layout		
	straight	curved	curved and skewed
Self-weight	x	x	x
Pre-stressing (indirect)		x	x
Traffic load		x	x
Dummy loads	x		

2.4.1. Pre-stressing

In the longitudinal direction of the bridge deck, the deck of the *Blankenburgverbinding* is pre-stressed. As a result of the stress in the pre-stressing cable and the shape of the pre-stressing cable, part of the self-weight of the bridge deck is compensated by a distributed load acting in the opposite direction of the the gravitational force. This means that the longitudinal pre-stressing reduces the longitudinal bending moments. Of course, the pre-stressing doesn't lower the reaction forces of the bridge deck.

To account for pre-stressing, it was chosen to make an assumption on which part of the self-weight of the deck is compensated by pre-stressing. It is assumed that in the final situation, after pre-stressing losses, 75% of the self-weight is compensated by pre-stressing. This means that only 25% of the self-weight of the bridge contributes to the longitudinal bending moments.

In the final situation, the bridge deck is also loaded by asphalt and other loads (i.e. fences and

barriers). It is assumed that these loads have a magnitude of about 10% of the self weight. This means that, in the final stage, the pre-stressing compensates about 75 - 10 = 65% of the self-weight. This comes down to a self-weight of 35% when accounting for pre-stressing.

2.4.2. Dummy loads

The straight bridge deck is loaded with dummy loads. These dummy loading consists of several load cases of point loads and one load case with a distributed load in over the transverse direction of the deck. All the load cases of the dummy loads are applied in the middle of the span.

Each point load has a different eccentricity with respect to the centre of gravity of the bridge deck. Which means that every point load gives a different torque to the bridge deck. In order to avoid local bending of the top plate of the deck, the point loads are applied above the stiffeners. As the transverse cross-section of the bridge deck is fully symmetrical, only the left part of the bridge is loaded with the point loads. Point loads applied to the right part of the bridge deck will give the same results, but then mirrored. Load case 6 (LC6) is a load that does not have an eccentricity. As there is no stiffener in the middle of the deck, it was needed to split up the point load into two separate point loads positioned above the stiffeners next to the middle of the deck. Figure 2.12, shows all the load cases of the dummy loads, positioned along the transverse cross-section, in the middle of the span.

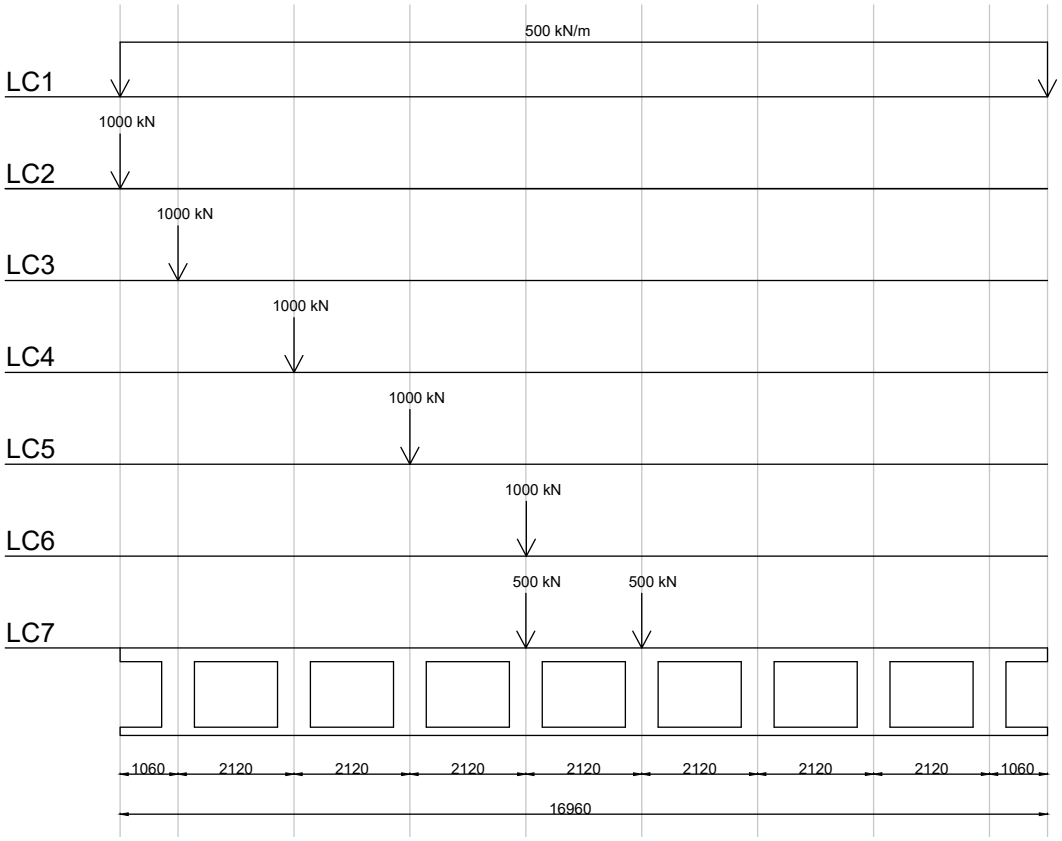

Figure 2.12: Load cases of the dummy loads, positioned along the transverse cross-section, in the middle of the span (mm)

By analysing the results each load case separately, it can be determined whether there is a relationship between the difference in transverse load spread and the eccentricity of the applied loading.

2.4.3. Traffic load

The traffic load is based upon Load Model 1 (LM1) from Eurocode EN 1991-2 *(Eurocode 1 "Actions on structures", part 2: "Traffic loads on bridges")* [6]. LM1 consists of a uniform distributed load (UDL) and a tandem-axle system (TS). According to the EN 1991-2, the carriageway of the bridge needs to be divided into notional lanes each having a width of 3 m. The maximum number of notional lanes is 3. For each of these notional lanes, the magnitude of the uniform distributed load (UDL) and the tandem axle load is different.

Table 2.3 shows the magnitude of UDL and TS for each of the three lanes and the remaining area of the bridge. The values in table 2.3 are based upon EN 1991-2. According to the EN 1991-2, the UDL from the needs to be multiplied with a factor α_{qi} and the tandem load with a factor α_{Qi}. These factors follow from the national annex, for which in this case the Dutch national annex was used. In case it is assumed that there are 2 million trucks/lane/year, the α-factors are equal to: α_{q1} = 1.15 (lane 1) and α_{qi} = 1.4 (all other lanes). And for the tandem loads, α_{Qi} = 1. These α-factors are already included in table 2.3, which means that table 2.3 gives the characteristic values for UDL and TS.

Table 2.3: Traffic loading LM1 (Eurocode EN 1991-2)

	q_{ik} / UDL (kN/m^2)	Q_{ik} / TS, per axle (kN)
Lane 1	10.35	300
Lane 2	3.50	200
Lane 3	3.50	100
Remaining area	3.50	-

Figure 2.13 shows the top view of the tandem axle system, for each lane. The tandem axle system consists of 2 axles with a width of 2 m and distance of 1.2 m in the longitudinal direction of the bridge.

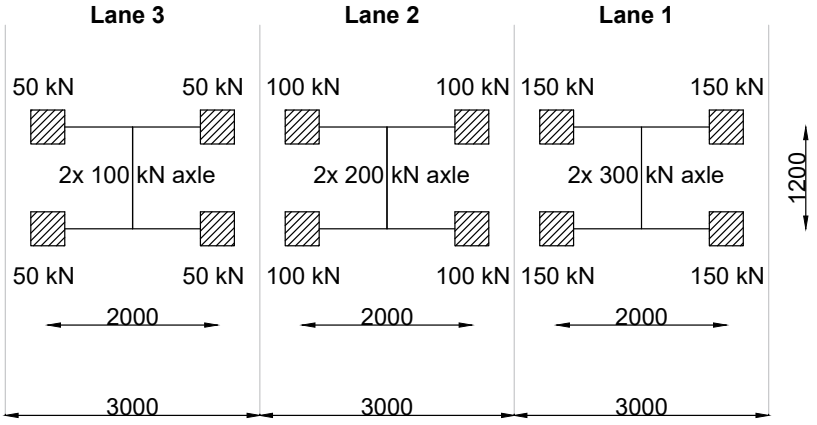

Figure 2.13: Top view of the tandem axle system (mm)

The number and the layout of the notional lanes is based upon the with and the position of the carriageway. The width of the carriageway is equal to the width of the bridge deck over which the traffic *could* drive. Areas that are separated from the traffic by a *hard* barrier may be excluded from the with of the carriageway.

For the viaducts of the *Blankenburgverbinding*, there is a concrete curb edge with a height of 200 mm and a width of 1100 mm on both edges of the deck, see figure 2.14. This concrete curbs avoid traffic from driving on the outer 1100 mm of the bridge deck. The total width of the bridge is 16.96 m, this means that the width of the carriageway is equal to 16.96 - 2 · 1.1 = 14.76 m.

According to the Eurocode 2, a carriageway with a width of ≥ 9 m, has 3 notional lanes. This means that 9 m of the carriageway is occupied with 3 lanes and that there is a remaining area of 14.76 - 9 = 5.76 m. Figure 2.15 shows the cross-section of the bridge deck, the layout of the notional traffic lanes and a side view of the uniform distributed traffic loading (UDL) and the point loads from the axles of the tandem system (TS).

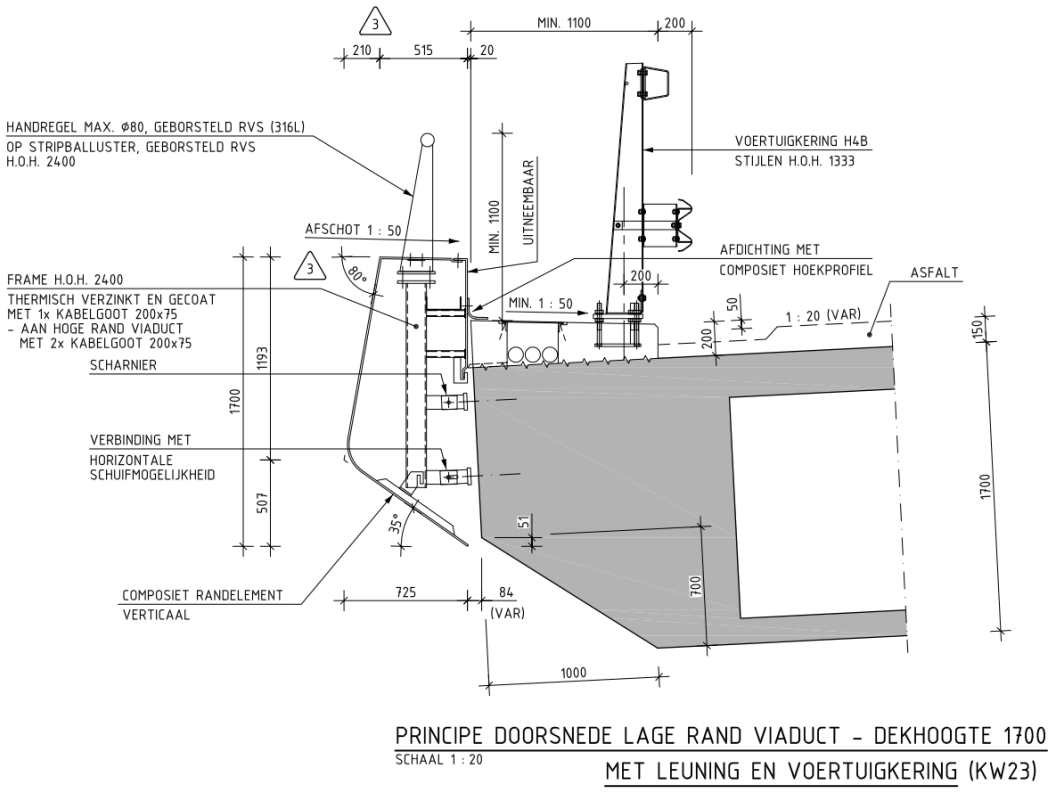

Figure 2.14: Cross-section of the edge of the viaduct, *Blankenburgverbinding*

2.4.4. Load combinations

The curved and curved and skewed bridge deck layouts are loaded with self-weight (SW), pre-stressing (indirectly, 0.35*SW) and the traffic loads (UDL and TS). In order to obtain the bending moments as a result of the sum of all loads and the sum of all loads in which also the effect of pre-stressing is taken into account, 2 different load combinations were created. The first load-combination is the sum of all load-cases. The second load-combination includes the pre-stressing. Of course, this load-combination cannot be used to look at the support reactions of the bridge deck, as the pre-stressing only changes the internal system of the bridge decks. The piers still need to carry the whole system.

Sum of all loads, excluding pre-stressing

1. SW + UDL + TS

Sum of all loads, including pre-stressing

2. 0.35 * SW + UDL + TS

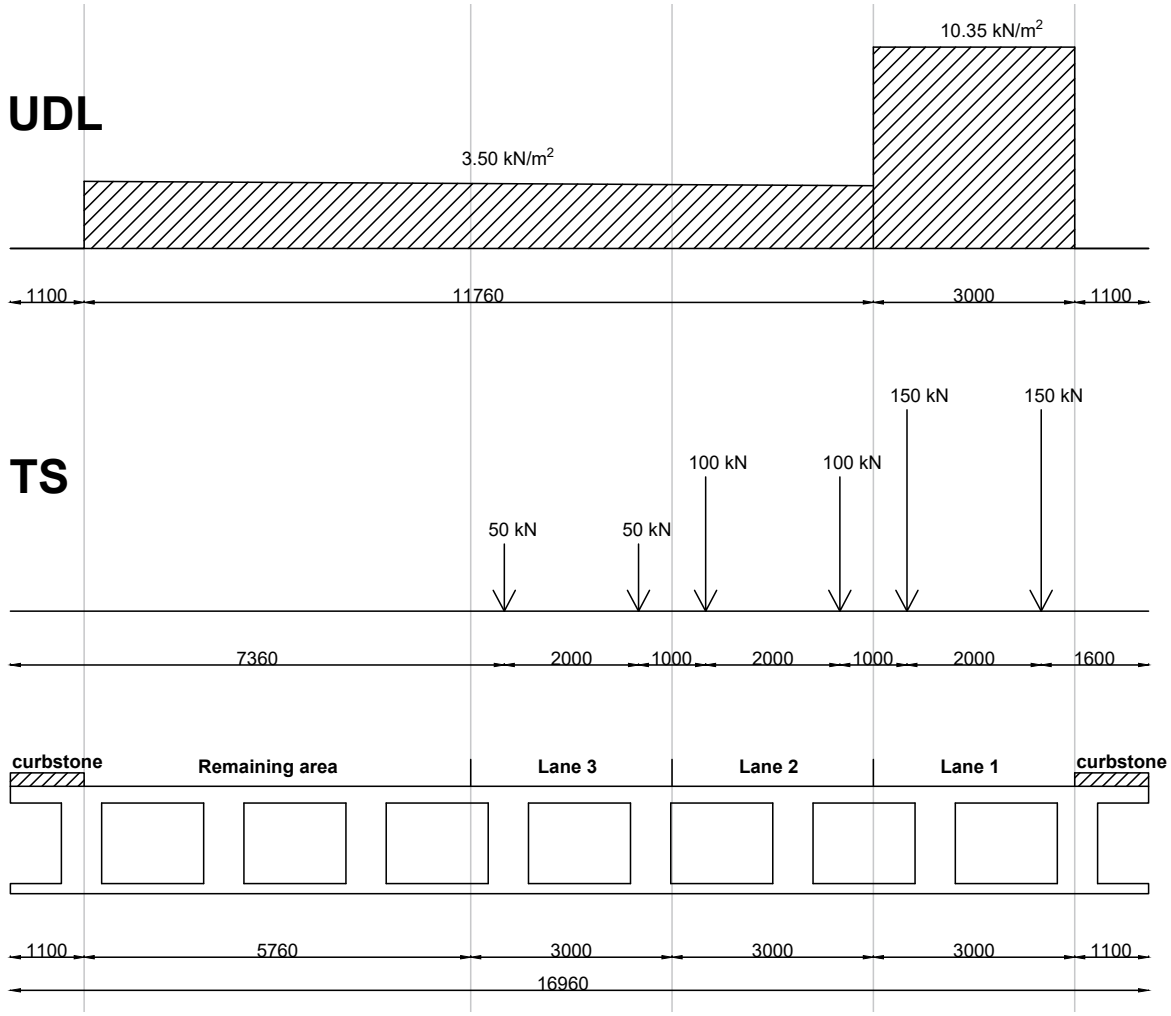

Figure 2.15: Cross-section of the bridge deck, lane layout and side view of traffic load (UDL and TS) (mm)

3

Orthotropic plate model

The first model that will be used in this thesis is the orthotropic plate model. This model can be derived from the plate theory of an isotropic plate. For an orthotropic concrete bridge deck, the orthotropy is introduced by the irregular shape of the cross-section. This kind of orthotropy is also called *shape orthotropy*. Another source of orthotropy can be the material properties (the strength of timber depends on the direction). In the case of an orthotropic concrete bridge deck, non-homogeneous material behaviour doesn't play a role. That is why the orthotropic plate model is purely based upon shape orthotropy. In the first section of this chapter, the theory of an shape orthotropic plate will be introduced.

The second part of this chapter discusses the set-up of the orthotropic plate model. For both directions, the in- and out-of-plane stiffness properties are calculated. These stiffness properties consist of: normal, bending, shear and torsional stiffness. Next, it is shown how the model is set-up in SCIA-engineer. It is shown how the direction of the local coordinate system is adjusted for the curved deck, so the orthotropic material properties follow the correct direction. In the last section, it is shown how the loads are applied to the orthotropic plate model.

3.1. Theory of shape orthotropic plates

For the orthotropic plate model, the stiffness properties are derived from the ordinary plate theory. For shape orthotropic plates, there are stiffeners under or in between the plate in 1 or 2 directions. The added stiffness of these stiffeners is evenly distributed over a unit width. In practice, this means that the stiffness properties of the repeated cross-section is calculated and divided by the width of these repeated cross-section. The theory of shape orthotropic plates, as well as the elaboration of the stiffness properties for the cross-section considered in this thesis, is presented in the remaining part of this section. The theory of shape orthotropic plates is mainly based upon *"Plates and FEM: Surprises and Pitfalls"*, written by Johan Blaauwendraad [2].

3.1.1. Axial stiffness

For in-plane action, there are two external forces that can act on the plate (p_x and p_y). These external forces cause internal stresses (σ_{xx}, σ_{yy} and σ_{xy}), multiplying these stresses with the thickness of the plate, gives the normal force components per unit width: n_{xx}, n_{yy} and n_{xy}. The in-plane constitutive relations of a plate read

$$\begin{aligned} \varepsilon_{xx} &= \frac{1}{E}(\sigma_{xx} - \nu\sigma_{yy}) \\ \varepsilon_{yy} &= \frac{1}{E}(\sigma_{yy} - \nu\sigma_{xx}) \\ \gamma_{xy} &= \frac{2(1+\nu)}{E}\sigma_{xy} \end{aligned} \tag{3.1}$$

In formula 3.1, the stresses σ can be replaced by forces $n = \sigma t$, written in stiffness formulation, this results in the following formulation of the axial stiffness per unit width

$$\begin{Bmatrix} n_{xx} \\ n_{yy} \\ n_{xy} \end{Bmatrix} = \frac{Et}{1-\nu^2} \begin{bmatrix} 1 & \nu & 0 \\ \nu & 1 & 0 \\ 0 & 0 & (1-\nu)/2 \end{bmatrix} \begin{Bmatrix} \varepsilon_{xx} \\ \varepsilon_{yy} \\ \gamma_{xy} \end{Bmatrix} \tag{3.2}$$

For the orthotropic plate, the axial stiffness of the *'extra'* material in x and y-direction must be added to the axial stiffness formulation for the general plate (3.2). To do this, the *'extra'* material is spread out over the spacing. Assume a stiffener spacing of a and an axial stiffness of EA, then the axial stiffness distributed over a unit width becomes EA/a. In matrix notation, the axial stiffness formulation becomes

$$D = \frac{Et}{1-\nu^2} \begin{bmatrix} 1 & \nu & 0 \\ \nu & 1 & 0 \\ 0 & 0 & (1-\nu)/2 \end{bmatrix} + \begin{bmatrix} EA_x/a & 0 & 0 \\ 0 & EA_y/b & 0 \\ 0 & 0 & 0 \end{bmatrix} \tag{3.3}$$

written in one matrix

$$D = \begin{bmatrix} \frac{Et}{1-\nu^2} + \frac{EA_x}{a} & \nu\frac{Et}{1-\nu^2} & 0 \\ \nu\frac{Et}{1-\nu^2} & \frac{Et}{1-\nu^2} + \frac{EA_y}{b} & 0 \\ 0 & 0 & Gt \end{bmatrix} \tag{3.4}$$

In finite element software, the entries of the D-matrix for axial stiffness, are often denoted as

$$\begin{aligned} d_{11} &= \frac{Et}{1-\nu^2} + \frac{EA_x}{a} \\ d_{22} &= \frac{Et}{1-\nu^2} + \frac{EA_y}{b} \\ d_{12} &= \nu\frac{Et}{1-\nu^2} \end{aligned} \tag{3.5}$$

3.1.2. Bending stiffness

When a plate is loaded in the out-of-plane direction, bending and shear deformation can will be observed. The shear deformation is only observed for thick plates, or when there is a voided deck in which the top plate can translate with respect to the bottom plate, which is also called shear deformation. Taking into account shear deformation means that the Mindlin-Reissner plate theory is adopted. The constitutive equations for plate bending read

$$\begin{aligned} m_{xx} &= D(\kappa_{xx} + \nu\kappa_{yy}) \\ m_{yy} &= D(\kappa_{yy} + \nu\kappa_{xx}) \\ m_{xy} &= \frac{1}{2}D(1-\nu)\rho_{xy} \end{aligned} \tag{3.6}$$

with

$$D = \frac{Et^3}{12(1-\nu^2)} \tag{3.7}$$

In matrix notation, the relation between bending moments and bending deformation (curvature), becomes

$$\begin{Bmatrix} m_{xx} \\ m_{yy} \\ m_{xy} \end{Bmatrix} = D \begin{bmatrix} 1 & \nu & 0 \\ \nu & 1 & 0 \\ 0 & 0 & (1-\nu)/2 \end{bmatrix} \begin{Bmatrix} \kappa_{xx} \\ \kappa_{yy} \\ \rho_{xy} \end{Bmatrix} \tag{3.8}$$

Again, it is assumed that the stiffness of stiffer parts is spread out over a unit width of the orthotropic. The general stiffness relation for plate bending can be rewritten as

$$\begin{Bmatrix} m_{xx} \\ m_{yy} \\ m_{av} \end{Bmatrix} = \begin{bmatrix} D_{xx} & D_{\nu} & 0 \\ D_{\nu} & D_{yy} & 0 \\ 0 & 0 & D_{av} \end{bmatrix} \begin{Bmatrix} \kappa_{xx} \\ \kappa_{yy} \\ \rho_{xy} \end{Bmatrix} \tag{3.9}$$

In this matrix, D_{xx} and D_{yy} are the bending stiffness in x- and y-direction, per unit width. D_v is the off-diagonal rigidity, which follows from lateral contraction. Instead of using m_{xy} for the torsional moment and D_{xy} for the torsional stiffness, m_{av} and D_{av} are used. This follows from the fact that there is only one unique twisting deformation ρ_{xy} ($\rho_{xy} = \rho_{yx}$, by definition). However, the torsional stiffness can be different in both directions ($D_{xy} \neq D_{yx}$), which means that $m_{xy} \neq m_{yx}$. This results in the following relations for the torsional moments.

$$\begin{aligned} m_{xy} &= D_{xy}\rho_{xy} \\ m_{yx} &= D_{yx}\rho_{xy} \\ m_{xy} + m_{yx} &= (D_{xy} + D_{yx})2\rho_{xy} \\ m_{av} &= D_{av}\rho_{xy} \end{aligned} \tag{3.10}$$

with

$$\begin{aligned} m_{av} &= \frac{1}{2}(m_{xy} + m_{yx}) \\ D_{av} &= \frac{1}{2}(D_{xy} + D_{yx}) \end{aligned} \tag{3.11}$$

In a FEM-analysis of an orthotropic plate, the torsional moment m_{av} will be shown in the results. This means that result needs to be post-processed in order to get the torsional moment components m_{xy} and m_{yx}. This post-processing can be done using formula 3.12. With these formulas, the mean torsional moment m_{av} will be divided according to the ratio of the stiffness in x- and y-direction.

$$\begin{aligned} m_{xy} &= \frac{2i_{xy}}{i_{xy} + i_{yx}} m_{av} \\ m_{yx} &= \frac{2i_{yx}}{i_{xy} + i_{yx}} m_{av} \end{aligned} \tag{3.12}$$

3.1.3. Shear stiffness

According to the Minlin-Reissner plate theory, the constitutive relations for shear read

$$\begin{aligned} v_x &= D_\gamma \gamma_x \\ v_y &= D_\gamma \gamma_y \end{aligned} \tag{3.13}$$

The shear stiffness of the orthotropic plate can be obtained by creating a shear-frame of the cross-section. In this frame, there are horizontal and vertical beam members that represent a unit width of the cross-section. The shear stiffness then follows from the shear deformation and the vertical applied load.

3.2. Blankenburg case

For the orthotropic plate model, the cross-sectional stiffness properties are calculated based upon the theory of chapter 3. The contribution of the stiffener parts are evenly distributed over a unit width of the cross-section. This results in stiffness properties per unit plate width, like for ordinary isotropic plates.

The cross-section used for the Blankenburgverbinding is shown in figure 2.1. In transverse direction, there is no repetition as the edges of the bridge deck are chambered. For the orthotropic plate model, there must be a repetition of identical cross-sections. When modelling the cross-section of the Blankenburgverbinding, the edges of the bridge deck must be approximated, while for the grillage model this approximation is not necessary.

In order to get a fair comparison between both models, the cross-section of the deck used for the Blankenburgverbinding is simplified. For both the orthotropic plate model and the grillage model, a repetition of H-shaped cross-sections is assumed. This modified cross-section is shown in figure 3.1.

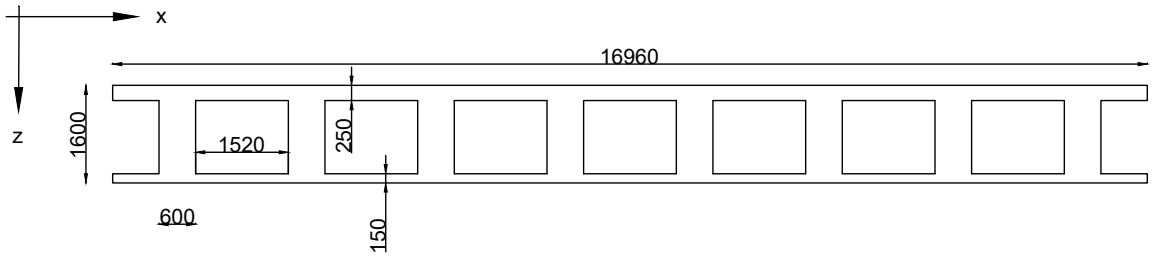

Figure 3.1: Modified cross-section of the bridge deck (mm)

In the following calculations, the coordinate system presented in figure 2.2 is adopted. The x-axis runs in the transverse direction of the orthotropic deck, the y-axis runs in the longitudinal direction of the deck, into the displayed plane. The vertical direction coincides with the z-axis, with its positive direction downward.

Table 3.1 gives an overview of all the stiffness parameters of the orthotropic plate. These stiffness parameters are being calculated in the following sections.

Table 3.1: Overview of stiffness parameters for the orthotropic plate model

stiffness component	description	value	
in-plane			
d_{11}	axial stiffness in x-direction	1.5125	10^4 MN/m
d_{22}	axial stiffness in y-direction	2.7453	10^4 MN/m
d_{12}	in-plane Poisson effect	3.0250	10^3 MN/m
d_{33}	in-plane shear stiffness	6.0500	10^3 MN/m
out-of-plane			
D_{11}	bending stiffness in x-direction (about y-axis)	7.0079	10^3 MN m
D_{22}	bending stiffness in y-direction (about x-axis)	8.7590	10^3 MN m
D_{12}	lateral contraction (bending) of plate parts	1.4016	10^3 MN m
D_{33}	average of torsional stiffness in x- and y-direction	2.6420	10^3 MN m
D_{44}	shear stiffness in x-direction	2.6205	10^2 MN/m
D_{55}	shear stiffness in y-direction	4.2807	10^3 MN/m

3.2.1. Axial stiffness

The axial stiffness of the orthotropic deck follows from the thickness of the sum of the top and bottom plate. Next to the plates, the stiffeners add axial stiffness to the cross-section. The effect of the stiffeners is spread out over to width over which the stiffeners are spaced. To calculate the axial stiffness, equation 3.5 is used.

x-direction

In the transverse direction, the flow of normal stresses runs trough the top and bottom plate of the deck. At the location of the stiffener, the flow of normal stresses also runs trough a part of the height of the stiffener. This means that the axial stiffness in x-direction, is bigger than the axial stiffness of the top and bottom plate only.

In order to determine which height of the stiffener contributes to the axial stiffness, a 2D-plate model is created in *SCIA-engineer*. Both the top and bottom plate are loaded with an axial force. In figure 3.2, the trajectories of the principal normal force are shown. It can be seen that the height over which the normal force spreads out is very limited compared to the thickness of the top and bottom plate. For this reason, it is assumed that the axial stiffness in x-direction comes from the top and bottom plate only. The stiffness component d_{11} can be calculated as follows:

$$d_{11} = \frac{36\,300 \cdot (0.25 + 0.15)}{1 - 0.2^2} = 15.125 \times 10^3\ \text{MN/m}$$

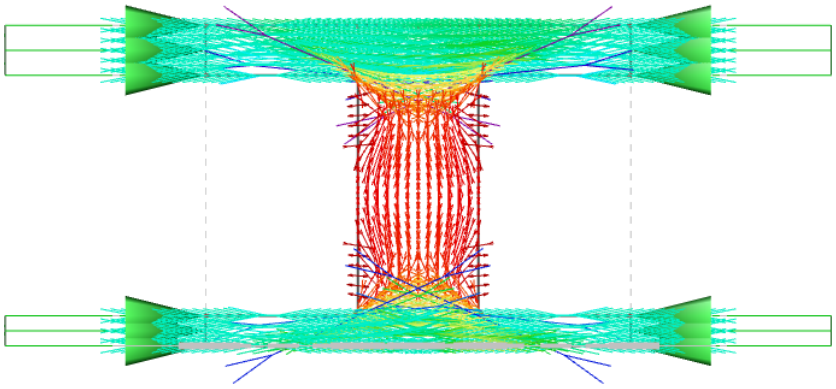

Figure 3.2: Principal normal-stress trajectories (n_2) for axial loading.

y-direction

For the y-direction, the axial stiffness comes from the top and bottom plate and the presence of stiffeners with cross-sectional area A_y and spacing b. A part of the cross-section in y-direction is shown in figure 3.3.

Again, the thickness of both plates can summed up to determine the stiffness of the plate parts. The stiffness of the stiffeners with dimensions 600 ×1200 mm each and a spacing of $b = 2120$ mm, is added to every 2120 mm deck width. To determine the stiffness per unit deck width, the stiffness of the stiffeners is divided by the spacing b. This results into the following axial stiffness component d_{22}:

$$d_{22} = \frac{36\,300 \cdot (0.25 + 0.15)}{1 - 0.2^2} + \frac{36\,300 \cdot 1.2 \cdot 0.6}{2.12} = 27.453 \times 10^3\ \text{MN/m}$$

Lateral contraction

For the top and bottom plate of the deck, lateral contraction can be observed as an effect of Poisson. This lateral contraction can only be observed in the plate-parts of the cross-section, as the stiffeners do not touch each other. When a stiffener is compressed in longitudinal direction, it can freely expand in transverse direction. This means that when the cross-section is compressed in longitudinal direction, the stiffeners cannot give rise to any stresses in transverse direction. The lateral contraction component

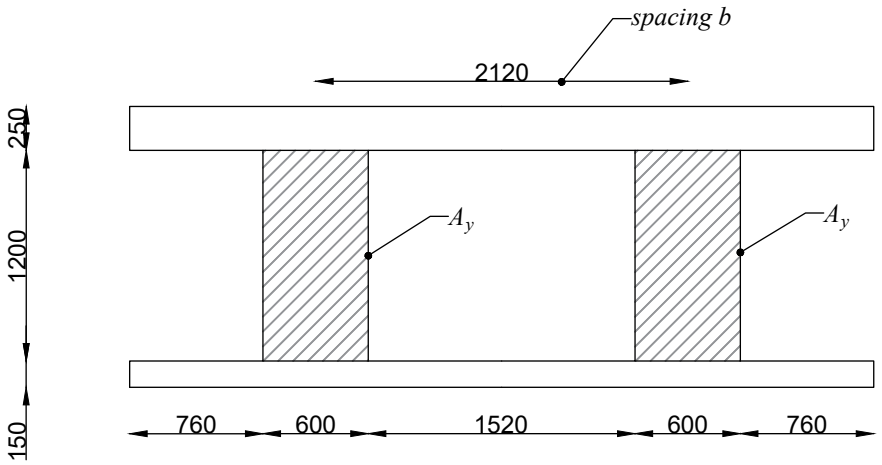

Figure 3.3: Part of the cross-section in y-direction (mm)

of the axial stiffness (d_{12}) can be based upon the transverse axial stiffness (d_{11}), as this component consists of the plate-parts only.

$$d_{12} = \nu \cdot d_{11} = 0.2 \cdot 15.125 \times 10^3 = 3.025 \times 10^3 \text{ MN/m}$$

In-plane shear
For the in-plane shear stiffness, it is assumed that the stiffeners do not play a role. Of course the stiffeners partly prevent the top and bottom plate from in-plane shear deformation. It is assumed that the in-plane shear stiffness of the plate follows from the shear modulus G and the sum of the thickness of the top and bottom plate.

$$d_{33} = Gt = 15\,125 \cdot (0.25 + 0.15) = 6.050 \times 10^3 \text{ MN/m}$$

3.2.2. Bending stiffness

The bending stiffness follows from the moment of inertia per unit width in longitudinal and transverse direction.

x-direction
In x-direction, the bending stiffness is determined by the top and bottom plate of the deck. It is assumed that the bottom and top plate act as one cross-section, which means that the Steiner-rule is applied. The bending stiffness must be calculated per unit width, which is equal to 1 m. The cross-section for bending in x-direction is shown in figure 3.4.

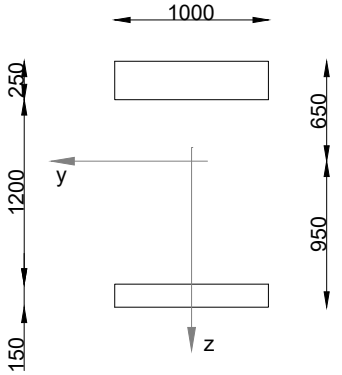

Figure 3.4: Cross-section for bending in x-direction (mm)

The neutral axis for this cross-section is at 650 mm from the top. This can be calculated using:

$$\bar{z}_{NC} = \frac{250 \cdot 125 + 150 \cdot 1525}{250 + 150} = 600\,\text{mm}$$

The second moment of inertia for bending around the y-axis is equal to:

$$I_y = \frac{1}{12} \cdot 0.25^3 + 0.25 \cdot 0.525^2 + \frac{1}{12} \cdot 0.15^3 + 0.15 \cdot 0.875^2 = 0.185\,\text{m}^4/\text{m}$$

The bending stiffness D_{11} can be found by multiplying the second moment of inertia per unit width with the Young's modulus and the factor $\frac{1}{1-\nu^2}$, because the cross-section is in fact a plate:

$$D_{11} = EI_y = \frac{1}{1 - 0.2^2} \cdot 36\,300 \cdot 0.185 = 7.0079 \times 10^3\,\text{MN m}$$

y-direction

In y-direction, the bending stiffness is determined by repeating cross-section with a width of 2120 mm, consisting of the top and bottom deck and one stiffener. Due to the factor $\frac{1}{1-\nu^2}$, the plate-parts (or flange-like parts) have a higher effective stiffness than the stiffener (the web-like part). The stiffness of these plate parts is equal to $E_{eff-plate} = \frac{1}{1-0.2^2} \cdot 36\,300 = 37\,813\,\text{MPa}$.

First, the bending stiffness EI_y is calculated per 2120 mm width, this result will be divided by 2.12 m, in order to arrive at the bending stiffness per unit width. The cross-section for bending in y-direction is shown in figure 3.5.

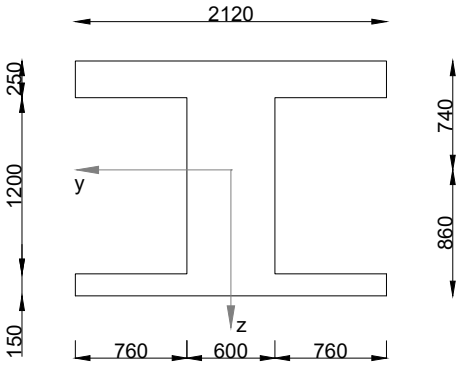

Figure 3.5: Cross-section for bending in y-direction (mm)

The neutral axis for this cross-section is at 740 mm from the top. In order to calculate the position of the neutral axis, the difference in effective stiffness of the plate parts needs to be taken into account, see the table 3.2.

Table 3.2: Calculation of ES_y and EA to determine $\bar{z}_{NC}$

part of cross-section	b (mm)	t (mm)	A (m^2)	z_{NC} (mm)	E_{eff} (MPa)	ES_y (MPa)	EA (m^4)
top plate	2120	250	0.530	125	37 813	2505	20 041
stiffener	600	1200	0.720	850	36 300	22 216	26 136
bottom plate	2120	150	0.318	1525	37 813	18 337	12 024
$\sum$	-	-	-	-	-	**43058**	**58201**

The position of the neutral axis can be calculated as follows:

$$\bar{z}_{NC} = \frac{ES_y}{EA} = \frac{43\,058}{58\,201} = 740\,\text{mm}$$

Table 3.3 shows the calculation of the bending stiffness in the longitudinal direction of the bridge deck, per 2.12 m width.

Table 3.3: Bending stiffness orhtotropic plate in longitudinal direction, per 2.12 m

	b	t	d	E_{eff}	I_y	EI_y
part of cross-section	(mm)	(mm)	(mm)	(MPa)	(m^4)	(MN m^2)
top plate	2120	250	615	37 813	0.2032	7684
stiffener	600	1200	110	36 300	0.0951	3453
bottom plate	2120	150	785	37 813	0.1966	7432
$\sum$	-	-	-	-	-	**18569**

The bending stiffness in longitudinal direction can be found by dividing the bending stiffness per 2.12 m by 2.12, this results into the following longitudinal bending stiffness per unit plate width:

$$D_{22} = \frac{18\,569}{2.12} = 8.7590 \times 10^3 \text{ MN m}$$

Torsion

The torsional of a voided deck can be based upon the torsional moment of inertia of a cross-section in transverse direction. Compared to the torsional moment of inertia of a cross-section in transverse direction, the torsional moment of inertia of a cross-section in the longitudinal direction can be neglected. So, for the transverse direction I_{yx} is equal to I_t divided by the width of the deck (b). As $i_{xy} \approx 0$, the average torsional stiffness per unit length (i_{av}) is equal to I_t divided by two times the the width of the deck:

$$\begin{aligned} i_{xy} &\approx 0 \\ i_{yx} &= \frac{I_t}{b} \\ i_{av} &= \frac{1}{2}\left(i_{xy} + i_{yx}\right) \approx \frac{I_t}{2b} \end{aligned} \tag{3.14}$$

The torsional moment of inertia (I_t) of the transverse cross-section can be calculated using the Bredt formula:

$$I_t = \frac{4A^2}{\sum \frac{b_i}{t_i}} \tag{3.15}$$

In this equation A is the enclosed area by the elements of the cross-section and b_i/t_i is the width over thickness ratio for each element in the cross-section. For a voided deck, the biggest part of the torsional stiffness comes from the top and bottom plate and the outer stiffeners. The inner stiffeners can be neglected as their contribution is very small compared to the rest of the cross-section. The shaded area of the cross-section shown in figure 3.6 shows which part of the cross-section is taken into account in the calculation of the torsional stiffness.

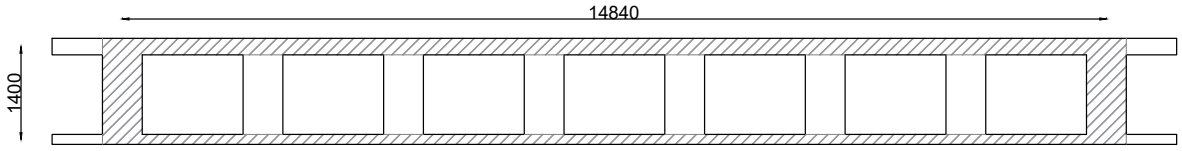

Figure 3.6: Area taken into account to calculate the torsional stiffness

Table 3.4 gives an overview of b and t for each element. The enclosed area is based upon the area within the centre lines of the considered elements of the cross-section: $A = 14.84 \cdot 1.4 = 20.776\,m^2$.

Table 3.4: Torsional stiffness: b_i/t_i

part of cross-section	b_i (mm)	t_i (mm)	b_i/t_i (-)
top plate	14 840	250	59.36
bottom plate	14 840	150	98.93
2x outer stiffener	1200	600	2x 2.00
$\sum$	-	-	**162.29**

Using $A = 20.776\,\text{m}^2$ and $\sum b_i/t_i = 162.29$, I_t can be calculated as:

$$I_t = \frac{4 \cdot 20.776^2}{162.29} = 10.64\,\text{m}^4$$

The torsional stiffness of the transverse cross-section was also determined using *ShapeBuilder*, which is a finite element program that is able to determine cross-sectional properties. In *ShapeBuilder* the complete cross-section, including all stiffeners, has been analysed. From this analysis it follows that $I_t = 11.85\,\text{m}^4$. This is about 11% more than the hand-calculation. As part of the cross-section is neglected, the hand-calculation provides a slightly lower torsional moment of inertia. However, 11% is still a significant error, so it was decided to use the solution from *ShapeBuilder* instead of the hand-calculation.

$$i_{av} = \frac{11.85}{2 \cdot 16.96} = 0.349\,\text{m}^3$$

$$D_{33} = 15\,125 \cdot \frac{0.349}{2} = 2.6420 \times 10^3\,\text{MN m}$$

Basically, the calculation of the torsional stiffness of a voided deck comes down to the torsional moment of inertia of the transverse cross-section, divided by 4 times the width of the deck. In *"Aantekeningen over wringing", (2008)* [5], written by dr. ir. P.C.J. Hoogenboom, the torsional stiffness is also defined in this way.

In order to find out whether *SCIA-engineer* uses the same definition for the torsional stiffness, two *Nadai's plates* [1] with identical geometry has been modelled. One of the plates was modelled as an isotropic plate, the other plate was modelled as an orthotropic plate. The torsional stiffness component (D_{33}) assigned to the orthotropic plate was calculated as if it was the isotropic plate. It turned out that both plates show the same torsional deformation, meaning that the definition used in this report is identical to the definition of the torsional stiffness of *SCIA-engineer*. The plate models used to verify whether the torsional stiffness parameter was defined correctly, as well as the results of these models can be found in appendix A.

[1] *Nadai's plate:* square plate subjected to pure twist, using two couples of point loads in opposite direction [2]

3.2.3. Shear stiffness

x-direction

The shear-stiffness in the x-direction (transverse direction) can be determined using a shear frame. In this shear frame, one box-like cross-section is modelled as a frame. As a result of the interaction between the webs (the stiffeners) and the bottom and top plate, a more extensive derivation and verification of the shear frame was needed. This derivation and verification is presented in appendix C. This appendix presents the shear frame model that has been used to determine the shear stiffness. In this shear frame model, the thickness of the top and bottom plate is higher in the zone of the web. This extra thickness is equal to the effective height of the top and bottom plate determined in chapter 6. The result of the shear frame is verified with the analytical solution of a semi-rigid supported beam with support settlement and a 2D plate model, in which the voids are modelled using plate openings.

The shear deformation of the shear frame model of appendix C can be used to calculate the shear stiffness of the deck in the x-direction. This results into the following calculation of D_{44}:

$$\begin{aligned} \delta &= 80.9\,\text{mm} \\ \gamma_x &= \frac{\delta}{b} = \frac{80.9}{2120} = 3.816 \times 10^{-2}\,\text{rad} \\ D_{44} &= \frac{v_x}{\gamma_x} = \frac{10}{3.816 \times 10^{-2}} = 2.6205 \times 10^{2}\,\text{MN/m} \end{aligned}$$

y-direction

The shear stiffness in the y-direction is equal to the shear area A_{sy} times the shear modulus G, see equation 3.16. The shear area is based upon the area of the stiffeners (A_{web}). The stiffeners can be compared to the web of a H-section. For these sections, the shear force is transferred by the webs only. For the case of the orthotropic bridge deck, the areas contributing the the shear stiffness are marked in figure 3.7.

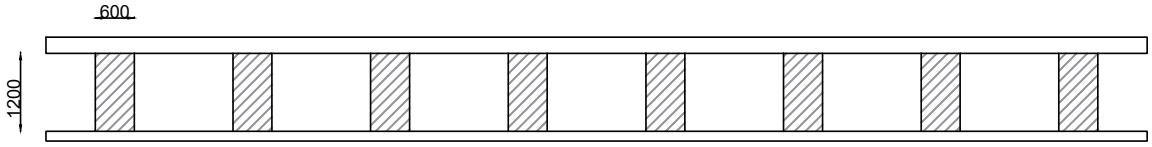

Figure 3.7: Areas contributing to shear stiffness in y-direction

$$\begin{aligned} D_{55} &= GA_{sy} \\ A_{sy} &= \frac{A_{web}}{\eta} \end{aligned} \tag{3.16}$$

For the rectangular shape of the stiffeners, the shape factor η is equal to 6/5. Each of the 8 stiffeners have a dimension of 0.6 x 1.2 m. The shear modulus is equal to $G = 15\,125\,\text{MPa}$, this means that the shear stiffness in y-direction is equal to:

$$D_{55} = 15\,125 \cdot \frac{8 \cdot 0.6 \cdot 1.2}{6/5} = 7.2600 \times 10^{4}\,\text{MN/m}^2$$

This is the shear stiffness for the whole width of the deck. So, the shear stiffness per unit width is equal to:

$$D_{55} = \frac{7.2600 \times 10^{4}}{16.96} = 4.2807 \times 10^{3}\,\text{MN/m}$$

3.2.4. Mesh and local coordinate system

In the orthotropic plate model, the stiffness parameters depend on the direction. This means that it is important that for each finite element, the local coordinate system is aligned correctly.

Straight deck

Figure 3.8 shows the mesh of the orthotropic plate model of the straight bridge deck. In the right figure the orientation of the local coordinate system can be seen on finite element level. It can be observed that for each finite element, the local coordinate system points in the exact same direction. The red arrows (x-axis) points in the transverse direction of the deck and the green arrows (y-axis) point in the longitudinal direction of the deck. This means that all orthotropic stiffness parameters are taken into account correctly.

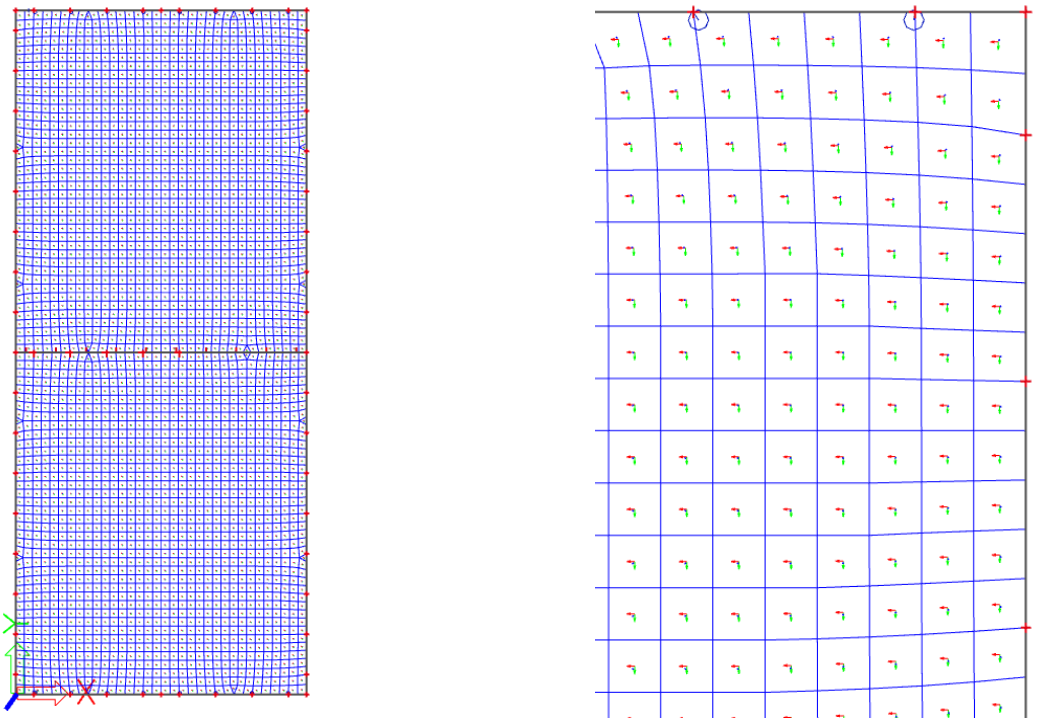

Figure 3.8: Finite element mesh of the straight deck (left) and zoomed-in (right)

Curved decks

For the curved and curved and skewed bridge deck, it is important that the local longitudinal axis follows direction of the longitudinal stiffeners. Otherwise, the orthotropic stiffness parameters do not match with the model and the orientation of the local coordinate system.

The curvature of the bridge deck follows the shape of a perfect circle segment. This circle has one unique radius in the longitudinal direction of the bridge. In the transverse direction, an infinite amount of circle segments can be drawn. These segments have a radius between 300 m $\pm$ 8.48 m (half the width of the bridge deck). All these circle segments have the same centre, which can also be called the *centre of curvature*.

At any location, the transverse direction of the bridge deck can be found by drawing a line towards the centre of curvature. This means that every local x-axis must point in the direction of the centre of curvature. As the coordinate system is orthogonal, the local y-axis automatically follows the tangent of every local circle segment describing the curvature, which is the longitudinal direction of the bridge deck.

Figure 3.9 shows the elements and the local coordinate system for the top right and bottom right corner of orthotropic plate model of the curved bridge deck. In these pictures, it can be observed that the local transverse direction (red x-axis) is parallel to the transverse edges of the deck. The local longitudinal direction (green y-axis) is always parallel to the longitudinal edges of the bridge deck. This

means that the orientation of the local coordinate system is correct and that that orthotropic stiffness parameters are coupled to the right directions in every single finite element.

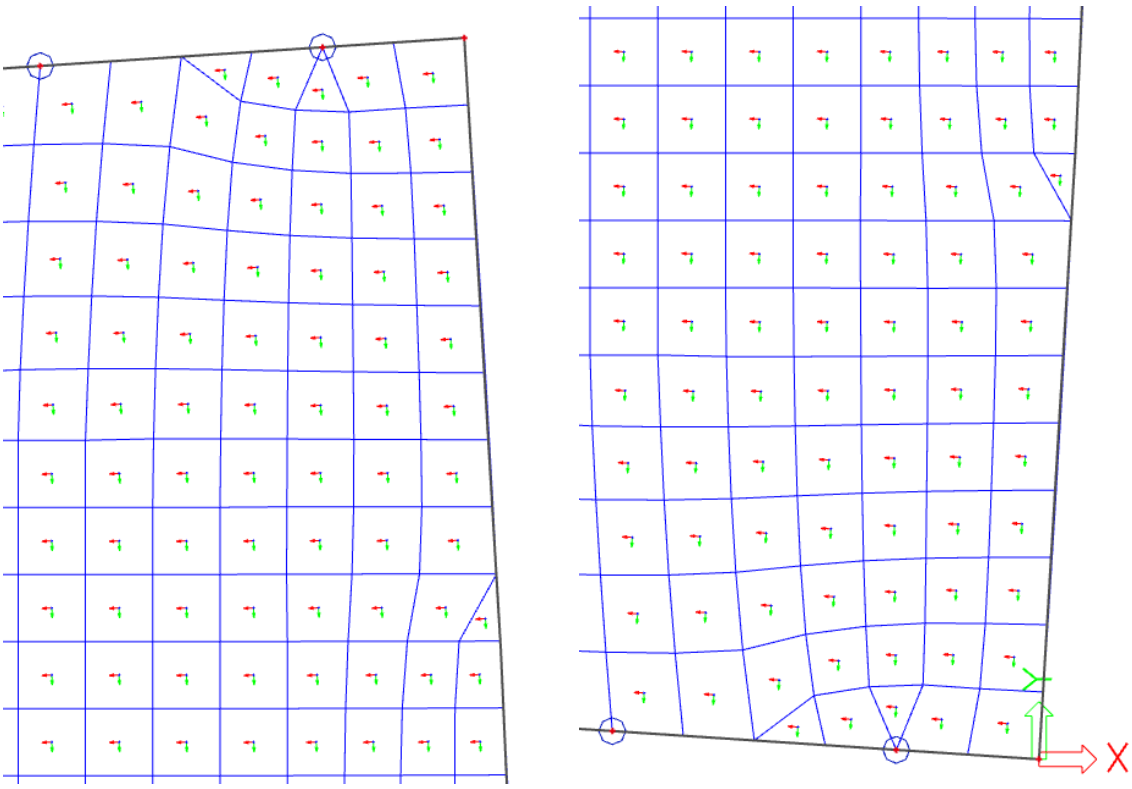

Figure 3.9: Local coordinate system of the curved deck, top right corner (left) and bottom right corner (right)

3.2.5. Loading

This section shows the different types of loading applied to the bridge decks modelled as an orthotropic plate.

Self-weight

The self-weight of the bridge deck is applied as a uniform distributed load over the surface of the deck. This uniform distributed self weight can be calculated using an equivalent thickness of the bridge deck. In this way, the self-weight is equally spread out over the width of the deck, which also applies to the stiffness parameters of the orthotropic plate model. The cross-sectional area of the deck is equal to $A = 12.544\,\text{m}^2$. The width of the deck is equal to $w = 16.96\,\text{m}$. From this, it follows that the equivalent thickness is equal to

$$t_{eq} = \frac{A}{w} = \frac{12.544}{16.96} = 0.74\,\text{m}$$

The specific weight of concrete the deck is assumed to be equal to $\rho = 2500\,\text{kg/m}^3$. This means that the uniform distributed load is equal to

$$Q_{sw} = t_{eq} \cdot \rho \cdot g = 0.74 \cdot 2500 \cdot 10 = 18.49\,\text{kN/m}^2$$

Figure 3.10 shows the uniform distributed self-weight applied to the orthotropic plate model.

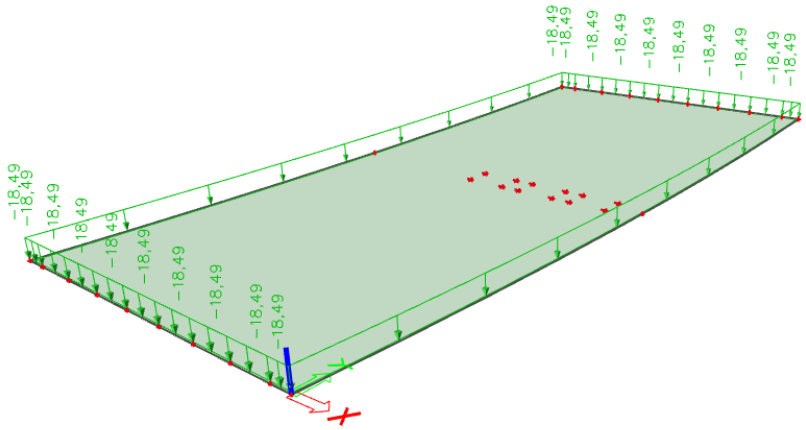

Figure 3.10: Self-weight applied to the orthotropic plate model

Dummy and traffic loads

The dummy loads of the straight bridge deck and the traffic loads (UDL and TS) of the curved and curved and skewed deck are directly applied to the orthotropic plate model. These loads are applied in the middle of span of the bridge deck. Figure 3.11 shows the orthotropic plate model loaded with the dummy load of LC3. The orthotropic plate loaded with the traffic load (UDL and TS) is shown in figure 3.12.

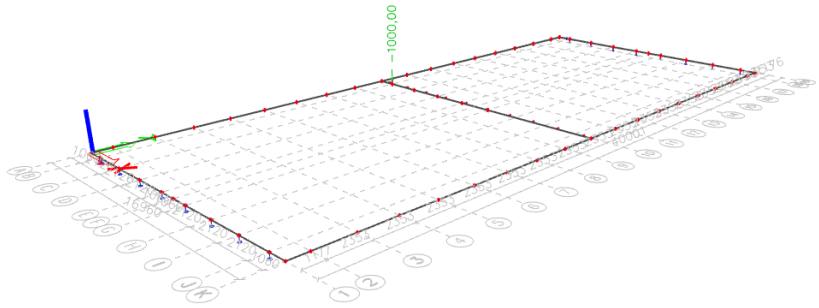

Figure 3.11: Dummy load (LC3) applied to the orthotropic plate model

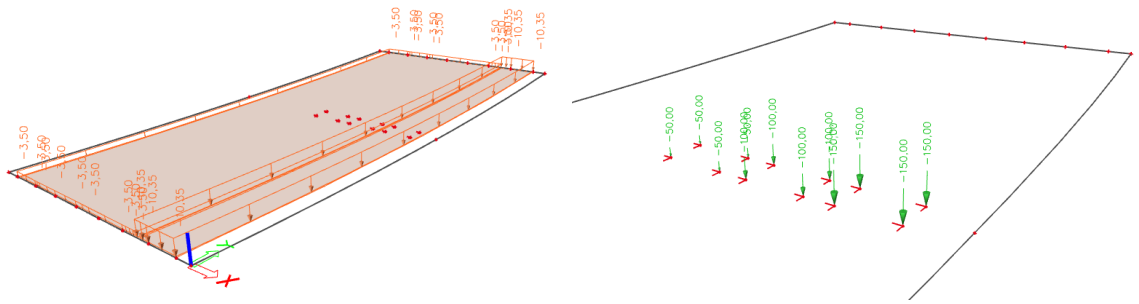

Figure 3.12: Traffic load (left: UDL and right: TS) applied to the orthotropic plate model (curved bridge deck)

4

Grillage model

In this chapter, the theory of the grillage model is introduced. A grillage model consists of a grid in which longitudinal beams represent the longitudinal stiffness of the deck and transverse beams represent the transverse stiffness of the deck. The software Midas civil provides a spacial wizard to create the grid of the grillage model automatically. However, for this study, it was decided to create all models in the same software. This means that also the grillage model is created in SCIA-engineer.

The second part of this chapter shows the set-up of the grillage model for the Blankenburg case study. The cross-section of the longitudinal and transverse beams is shown, as well as the calculation of their cross-sectional properties. For the grillage model, the loading needs spacial attention, as the position of the load could be in between the beams of the grillage model. This means that the load needs to be transferred towards the adjacent beams. The calculation of these equivalent loads is shown at the end of the chapter.

4.1. Theory of grillage modelling

The grillage model consists of a grid of longitudinal and transverse beams. The longitudinal beams of this grid represent the stiffness of the deck in the longitudinal direction and the transverse beams the stiffness of the deck in transverse direction.

Figure 4.1 shows an example of a grillage model applied to a hybrid bridge deck. This bridge deck consists of steel beams in the longitudinal direction and on top there is a concrete slab. In the longitudinal direction, the stiffness comes from the steel beam and the concrete slab, while in the transverse direction, the stiffness is equal to the stiffness of the concrete slab only.

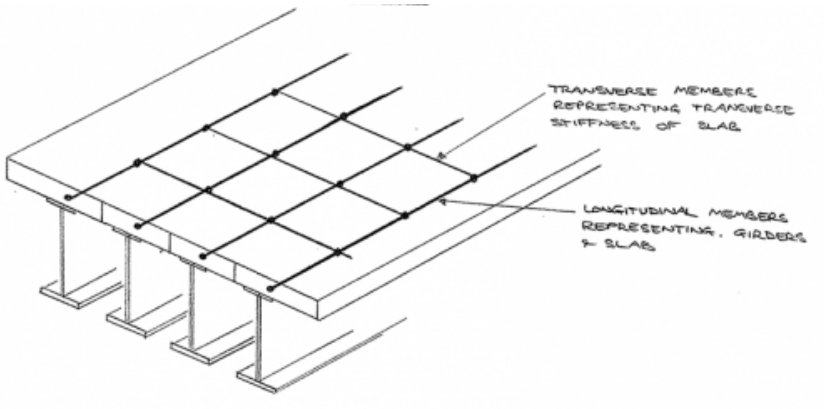

Figure 4.1: Example of a grillage model (Structville)

At each intersection of longitudinal and transverse beams, there is a node. At these nodes, the beams are rigidly connected. This means that the bending moment of the longitudinal beam interacts with the torsional bending moment of the transverse beam and vice versa.

4.1.1. Layout of the grid

For the layout of the grid of the grillage model, there are some recommendations. These recommendations were found at [7] and [3]. In general, it is recommended to use an odd number of grid-lines, especially for the transverse beams. By doing this, there are is always a beam in the middle of the span of the bridge, which makes it easier to apply a load at mid-span.

In case the bridge deck already exists of beam-like sections, the grid lines are placed along the centre lines of these beams. If the spacing between these beams is too big, there can be an extra grid-line along the centre line of the left over slab in between the beams. This can for example be applied to a T-girder bridge deck.

If the grillage model is applied to a slab bridge, the distance between the edge and the outer longitudinal grid lines needs to be equal to 0.3d, where d is the depth of the slab. Figure 4.2 shows a transverse cross-section of the edge of a slab. In this cross-section, the flow of shear stresses following from torsion can be seen. At 0.3d, the flow of stresses makes a turn which causes a concentrated shear force (S_x) at 0.3d. In order to be able to capture this concentrated shear force in the most accurate way, it is preferred that the longitudinal member is at the same location as the concentrated shear force, which is at 0.3d for a slab.

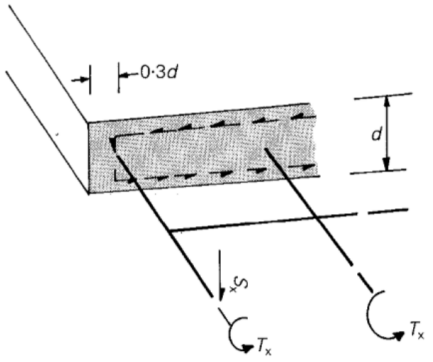

Figure 4.2: Torsion at the edge of the grillage model (Hambly) [3]

According to Shreedhar [7] and Hambly [3] the grillage model gives the best results when the ratio between the spacing of the longitudinal and transverse grid lines is somewhere between 1.0 and 2.0. In case the spacing of the longitudinal grid lines is already defined by the existing beam-like members, the spacing of the transverse members can easily be calculated.

The following list gives and overview of the recommendations discussed above, among some other recommendations that apply to the grid of the grillage model.

- In case of already existing beams, the grid lines are placed along the centre lines and, if needed, along the centre lines of parts in between the beams.
- For slabs, the longitudinal grid lines needs to be placed at a distance of 0.3d from both edges, where d is the depth of the slab.
- Grid lines should be placed along the lines connecting bearings.
- In each direction, it is preferred to have a minimum of 5 grid lines.
- It is preferred that grid lines are placed orthogonal.
- Grid lines in general should coincide with the centre of gravity of the section. Some shift can be made by using eccentricities.
- In case of a continuous support, the spacing between the transverse grid lines needs to be reduced in order to be able to capture strong peaks around the support.
- The ratio between the spacing in longitudinal and transverse direction should preferably lie between 1.0 and 2.0.

4.1.2. Cross-sectional properties

This part shows the theory related to the calculation of the cross-sectional properties of the grillage model.

Bending

The bending stiffness EI of both the longitudinal and transverse beams can easily be assigned to the model by calculating the moment of inertia I, both for the strong and weak axis of the beam. The bending stiffness of the beams can be found be multiplying the moment of inertia with the Young's modulus E.

The moment of inertia for bending around the y- and z-axis can be calculated using the general formula for a rectangular section:

$$I = \frac{1}{12}bh^3 + Ad^2 \tag{4.1}$$

This formula already includes the rule of Steiner as d is the distance between the local centre of gravity and the centre of gravity of the whole cross-section. And A the cross-sectional area of the rectangle considered.

Shear

In order to account for the shear stiffness, one can assign a certain shear area to the the longitudinal and transverse beams. This shear area can be derived from the shape of the grillage member (i.e. the area of the web for a H-section) or the shear deformation derived from other models.

If the shear deformation (γ) is known, the shear area can be calculated using

$$A_s = \frac{V}{G\gamma} \tag{4.2}$$

Torsion

According to *Bridge Deck Behaviour*, written by *E.C. Hambly* [3], the torsional stiffness of the longitudinal beams of a voided bridge deck, can be calculated using equation 4.3.

$$I_t = \frac{2h^3 d' d''}{d' + d''} w \tag{4.3}$$

In this equation, h is the centre to centre distance of the top and bottom plate, d' and d'' the thickness of the top and bottom plate and w the width of the longitudinal beams in the grillage model. The torsional stiffness calculated with equation 4.3 approximately comes down to the torsional stiffness of the transverse cross-section per unit width multiplied with the width of one longitudinal beam, divided by 2. The division by 2 follows from the fact that in a plate there is torsion in 2 directions, while in a beam there is only torsion in 1 direction.

For the transverse beams, the torsional stiffness can be calculated based upon the cross-section of the individual beams, using the formula of Bredt.

4.1.3. Output of results

For the grillage model, the bending moment M_y of the transverse beam, interacts with the bending moment M_x of the longitudinal beams. As this interaction is concentrated in the nodes of the grillage model, the bending moment output of the grillage model is discontinuous. In each of the nodes, there are jumps in the bending moment diagrams.

Figure 4.3 shows an example of the output of the grillage model, in this case the transverse bending moment. According the E. C. Hambly [3], the discontinuous output of the grillage model can be converted into a continuous line without jumps. This can be done by taking the average value in every node. Or, int other words, the average of he value just before and just after the node. This, results into the true transverse bending moment diagram, plotted with the blue in figure 4.3.

According to E. C. Hambly [3], the torsional moment of the bridge deck can be found by taking the average of the torsional moment of the longitudinal and transverse beam, at each node of the grillage model. In case the width of the longitudinal and transverse beams is not equal, the torsional moment first must be divided by the width of the beam, before the average value can be calculated.

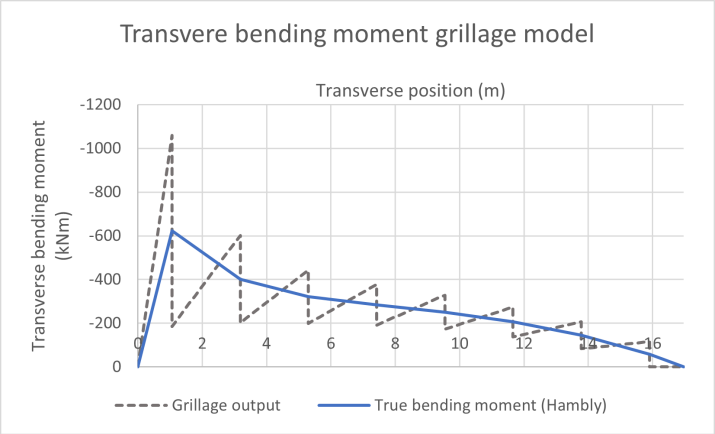

Figure 4.3: Transverse bending moment: grillage output vs. true bending moment diagram

4.2. Blankenburg case

The grillage model of the Blankenburg case is created in *SCIA-engineer*. It was chosen to create all models in the same software, in order to be sure that the material parameters, loading and the possibilities for post-processing were identical for all models. However, *Midas civil* provides a special wizard to create a grillage model. This means that in practice it would be more convenient to use Midas instead of SCIA-engineer to create the grillage model.

In this section, first the grid layout of the Blankenburg case study is introduced. Then, the stiffness parameters of the longitudinal and transverse beams are calculated. The last section shows how the different loads are applied to the grillage model.

4.2.1. Layout of the grid

In longitudinal direction, the bridge deck of the Blankburgverbinding has 8 repeating shapes that can be handled as 8 longitudinal beams. Each of the stiffener parts and half of the plate part in between them, will be modelled as one longitudinal beam in the grillage model. The spacing between the stiffeners is equal to 2.12 m, which means that the spacing of the longitudinal grid lines is also equal to 2.12 m. The cross-section of the longitudinal beams of the grillage model can be seen in figure 4.4.

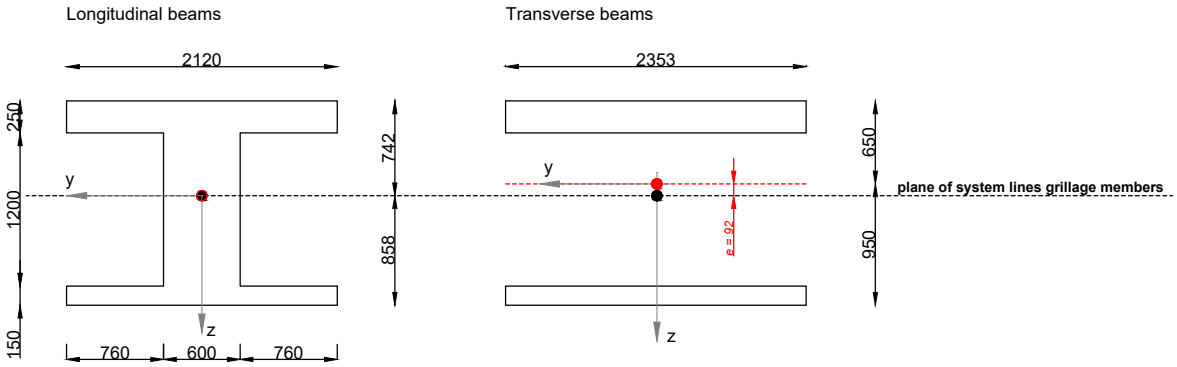

Figure 4.4: Cross-section longitudinal and transverse beams grillage model (mm)

On the edges of the deck, the longitudinal grid lines are positioned at 1.06 m, which is not equal to 0.3d. However, the commendation of 0.3d is based upon a slab. In case of the *Blankenburgverbinding*, the flow of shear stresses caused by torsion is more or less equal to a flow of stresses through the top and bottom plate and the 2 outer beams, which is shown in figure 4.5. This means that the concentrated shear force of the bridge deck is in the 2 outer web-parts. Which is at the location of the centre of gravity of the 2 outer longitudinal beams. This is in line with the recommendations of the grid-layout.

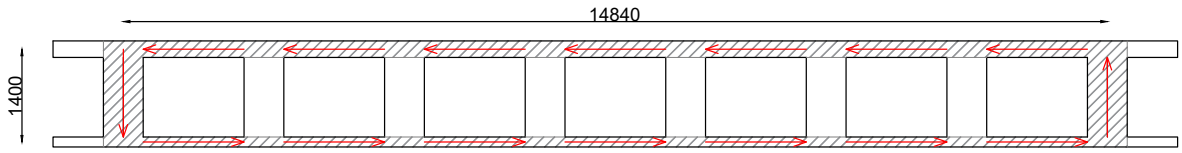

Figure 4.5: Shear-flow due to torsion

The spacing of the transverse beams is determined using 2 requirements: (1) the ratio between the spacing of the longitudinal and transverse beams is somewhere between 1.0 and 2.0 and (2) the number of transverse members is required to be odd, in order to have a transverse member in the middle of the span.

Table 4.1 shows an overview of possible numbers of transverse beams, which are all odd numbers. The total length of the bridge is equal to 40 m. This means that in case of 11 transverse beams, the spacing is equal to 40 / 11 = 3.636 m. The ratio between the spacing's is then equal to 3.636 / 2.12 = 1.72. This calculation can be repeated for all other rows of table 4.1.

Table 4.1: Overview parameters grillage model

# transverse beams	**spacing** (m)	**ratio** (-)
11	3.636	1.72
13	3.077	1.45
15	2.667	1.26
17	2.353	1.11

Eventually, it was chosen to use 17 transverse beams. This means that the spacing between the transverse grid lines is equal to 2.353 m and that the ratio between the spacing is equal to 1.11, which is between 1.0 and 2.0. Also the cross-section of the transverse beams can be seen in figure 4.4.

For the curved and curved and skewed bridge deck layout, the longitudinal and transverse beams are identical to the ones used for the straight bridge deck. However, the longitudinal beams are curved and the transverse beams are pointing in the direction of the centre of curvature. In this way, the longitudinal and transverse beams are pointing in the same direction as the longitudinal and transverse direction of the orthotropic plate model.

For the skewed bridge deck, the spacing of some of the transverse beams is different. This is needed to make the grid-layout fit. In the zone of the skew, the transverse beams end at a support. The transverse beams with a different spacing also have different stiffness properties compared to the other transverse beams, as they also represent a different width in the longitudinal direction of the bridge deck. Figure 4.6 shows the grid layout of the grillage model, for the straight, curved and curved and skewed deck.

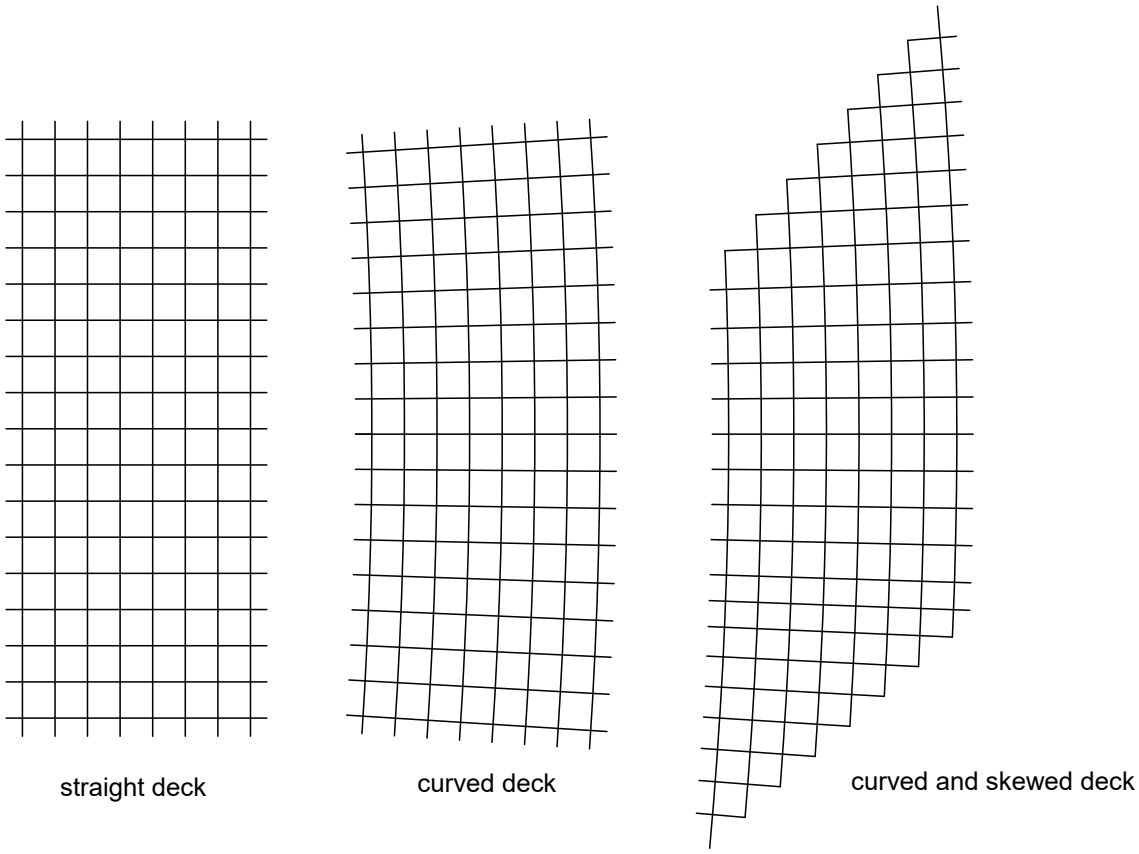

Figure 4.6: Grid-layout of the grillage model

4.2.2. Cross-sectional properties

In the sections below, the cross-sectional properties of the longitudinal and transverse beams of the grillage model are calculated. For both beams, the moment of inertia for bending and torsion has been determined. In transverse direction, there is also a relatively big contribution of shear deformation.

The shear stiffness of a beam can be accounted for by assigning a certain shear area to it. For the transverse beams, the shear area is determined based upon the result of the shear frame used for the orthotropic plate. For the sake of completeness the longitudinal beams will also be given a shear area, which will be equivalent to the one assigned to the orthotropic plate model.

Table 4.2 shows an overview of the most important dimensional and cross-sectional parameters of the grillage model.

Table 4.2: Overview parameters grillage model

description		**longitudinal beams**	**transverse beams**	**unit**
number of beams	N	8	17	-
length per beam	l	40.000	16.960	m
beam width	b	2.120	2.358	m
cross-sectional area	A	1.568	0.941	m^2
moment of inertia	I_y	4.9488	4.3609	$10^{-1}\,m^4$
	I_z	3.3920	4.3425	$10^{-1}\,m^4$
torsional moment of inertia	I_t	1.0907	0.0398	m^4
shear area	A_s	60.00	4.0767	$10^{-2}\,m^2$
eccentricity	e_s	-	92	mm

Longitudinal beams
The cross-section of the longitudinal beams can be found in figure 4.4. The bending and torsional moment as well as the shear stiffness of the longitudinal beams are calculated below.

The origin of the local coordinate system coincides with the centre of gravity of the cross-section. The z-axis coincides with the middle of the cross-section, as the cross-section is symmetrical with respect to the vertical axis. The y-axis lies 742 mm from the top of the cross-section. The location of the y-axis can be calculated as follows:

$$\overline{z}_{NC} = \frac{2120 \cdot 250 \cdot 125 + 600 \cdot 1200 \cdot 850 + 2120 \cdot 150 \cdot 1525}{2120 \cdot 250 + 600 \cdot 1200 + 2120 \cdot 150} = 742\,\text{mm}$$

Bending
The calculation of I_y and I_z is presented in table 4.3. In this table, only d_z is presented, as all centres of gravity of the separate elements lie at $y = 0$.

Table 4.3: moment of inertia longitudinal beams

part	b (mm)	h (mm)	A (m^2)	d_z (mm)	I_y ($10^{-1}\,m^4$)	I_z ($10^{-1}\,m^4$)
top flange	2120	250	0.530	617	2.0453	1.9850
web	600	1200	0.720	108	0.9480	0.2160
bottom flange	2120	150	0.318	783	1.9556	1.1910
$\sum$	**-**	**-**	**1.568**	**-**	**4.9488**	**3.3920**

Shear
For the grillage model, the shear area in the longitudinal direction is kept the same as for the orthotropic plate model. For the orthotropic plate it was assumed that the shear area in longitudinal direction is equal to the area of the stiffeners divided by η. Each longitudinal beam has one stiffener, so the shear area per longitudinal beam is equal to the area of a stiffener (which is the web-part of the cross-section) divided by η:

$$A_s = \frac{A_{web}}{\eta} = \frac{1.2 \cdot 0.6}{1.2} = 6.000 \times 10^{-1}\,\text{m}^2$$

Torsion
The torsional stiffness of the longitudinal beams can be calculated using equation 4.3. From this equation, it follows that the torsional stiffness if the longitudinal beams must be equal to

$$I_t = \frac{2 \cdot 1.4^3 \cdot 0.25 \cdot 0.15}{0.25 + 0.15} \cdot 2.12 = 1.0907\,\text{m}^4$$

Transverse beams
The cross-section of the longitudinal beams can be found in figure 4.4. The bending and torsional moment as well as the shear stiffness of the transverse beams are calculated below.

The origin of the local coordinate system coincides with the centre of gravity of the cross-section. The z-axis coincides with the middle of the cross-section, as the cross-section is symmetrical in the vertical axis. The y-axis lies 650 mm from the top of the cross-section. This follows from the fact that the top plate (the top flange) is thicker than the bottom plate (bottom flange). The location of the y-axis can be calculated as follows:

$$\overline{z}_{NC} = \frac{2353 \cdot 250 \cdot 125 + 2353 \cdot 150 \cdot 1525}{2353 \cdot 250 + 2353 \cdot 150} = 650\,\text{mm}$$

Bending
The calculation of the moment of inertia of the transverse beams can be found in table 4.4. The vertical distance between the centre of gravity and the centre of gravity of the whole cross-section is denoted as d_z. In horizontal direction, this distance is equal to 0 ($d_y = 0$).

Table 4.4: moment of inertia transverse beams

part	b (mm)	h (mm)	A (m^2)	d_z (mm)	I_y ($10^{-1}\,m^4$)	I_z ($10^{-1}\,m^4$)
top flange	2353	250	0.588	525	1.6520	2.7141
bottom flange	2353	150	0.353	875	2.7089	1.6285
$\sum$	-	-	**0.941**	-	**4.3609**	**4.3425**

Shear

The shear stiffness of the transverse beams can be controlled with the shear area A_y. According to Hambly, the shear area can be found using equation 4.4. In this equation V and γ are the applied shear force and the shear deformation. The shear stiffness of the bridge deck of the Blankenburgverbinding can be found in appendix C (page 143).

$$A_s = \frac{V}{G\gamma} \tag{4.4}$$

Filling in the values from the shear frame model:

$$\gamma = \frac{\delta}{l} = \frac{80.9}{2120} = 3.816 \times 10^{-2}\,\text{rad}$$
$$A_s = \frac{10}{15\,125 \cdot 3.816 \times 10^{-2}} = 1.732 \times 10^{-2}\,m^2/m$$

As the shear force $V = 10\,\text{MN/m}$, the shear area A_s needs to be multiplied with the width of the transverse beams. This results into a shear area of $A_s = 1.732 \times 10^{-2} \cdot 2.353 = 4.0767 \times 10^{-2}\,m^2$.

Torsion

The calculation of the torsional moment of inertia of the transverse beams can be found in table 4.5. Parameter k_1 is calculated using equation 4.6, for the calculation of I_t equation 4.5 is used.

$$I_t = k_1 t^3 b \tag{4.5}$$

the value k_1 depends on the ratio $b/t \geq 1$, where b is the width and t is the thickness of a rectangular part of the cross-section. For $b/t \to \infty$, $k_1 = \frac{1}{3}$.

$$k_1 = \frac{1}{3}\left(1 - 0.63\frac{t}{b}\left(1 - \frac{t^4}{12b^4}\right)\right) \tag{4.6}$$

Table 4.5: Torsional moment of inertia transverse beams

part	b (mm)	t (mm)	k_1 (-)	I_t ($10^{-2}\,m^4$)
top flange	2353	250	0.3110	1.1434
bottom	2353	150	0.3199	0.2540
$\sum$	-	-	-	**1.3975**

Eccentricity

The system lines of the grillage model are all drawn in one plane. For both the longitudinal as well as the transverse beams, the location of the system lines is indicated with the black dot in figure 4.6.

In the same figure, the centre of gravity of both cross-sections is indicated with a red dot. For the longitudinal beam, the centre of gravity coincides with the system line. However, for the the transverse

beams, the centre of gravity lies above the plane of the system lines. This means that the transverse beams must have an eccentricity assigned to it.

The distance between the centre of gravity and the system line is equal to 92 mm. So, the eccentricity of the transverse beams, in the z-direction is equal to $e_z = 92$ mm.

4.2.3. Loading

The dummy load-cases involving point loads (LC2 - LC7), can be applied at the nodes where the longitudinal beams intersect with the mid-span transverse beam. LC1 concerns a distributed load, which is applied over the full length of the transverse beam. This means that for this load case, the load is also applied in between the nodes. Figure 4.7 shows how LC1 and LC3 are applied to the grillage model.

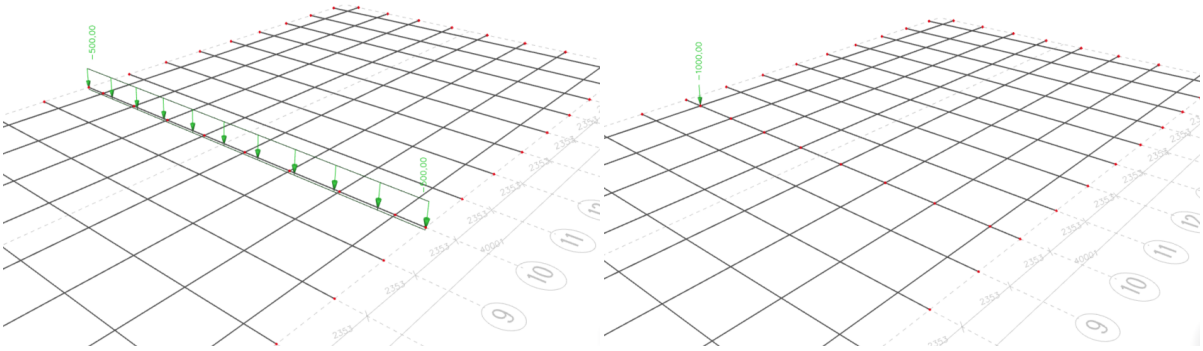

Figure 4.7: Grillage model loaded with LC1 (left) and LC3 (right)

The curved and skewed deck will be loaded with the self-weight of the deck and a traffic load, instead of the dummy loads. For the self-weight of the bridge deck, an equivalent distributed load has been calculated. This distributed load is applied at the 8 longitudinal beams of the grillage model.

Also for the traffic load, an equivalent loading must be calculated, as this loading must be applied on the longitudinal beams. The traffic load consists of 2 parts, a uniform distributed load (UDL) and point loads coming from tandem systems (TS). The UDL can be turned into equivalent distributed loads acting on the longitudinal beams. The tandem loads must be shifted in transverse direction. Based on force and moment equilibrium, part of the point load goes to the longitudinal beam on the left and part goes to the beam on the right of the point load.

Self-weight

The longitudinal beams of the grillage model already contain all the material of the bridge deck. In other words, the cross-sectional area of the longitudinal beams sums-up to the total cross-sectional area of the deck. This means that the deck can be loaded with it's self-weight by assigning the self-weight of the longitudinal beams. The transverse beams only add transverse and torsional stiffness of the deck, but doesn't add any extra material.

The cross-sectional area of the longitudinal beams of the grillage model is equal to

$$A = 1.568\,\text{m}^2$$

The specific weight of the concrete is assumed to be equal to (see table 2.1, page 10)

$$\rho = 2500\,\text{kg/m}^3$$

This means that the self-weight of each longitudinal beam is equal to

$$q_{SW} = A \cdot \rho \cdot g = 1.568 \cdot 2500 \cdot 10 = 39.2\,\text{kN/m}$$

So, each longitudinal beam must be loaded with $q_{SW} = 39.2$ kN/m to load the bridge deck with its self-weight. Figure 4.8 shows the grillage model of the curved bridge deck loaded with its self-weight.

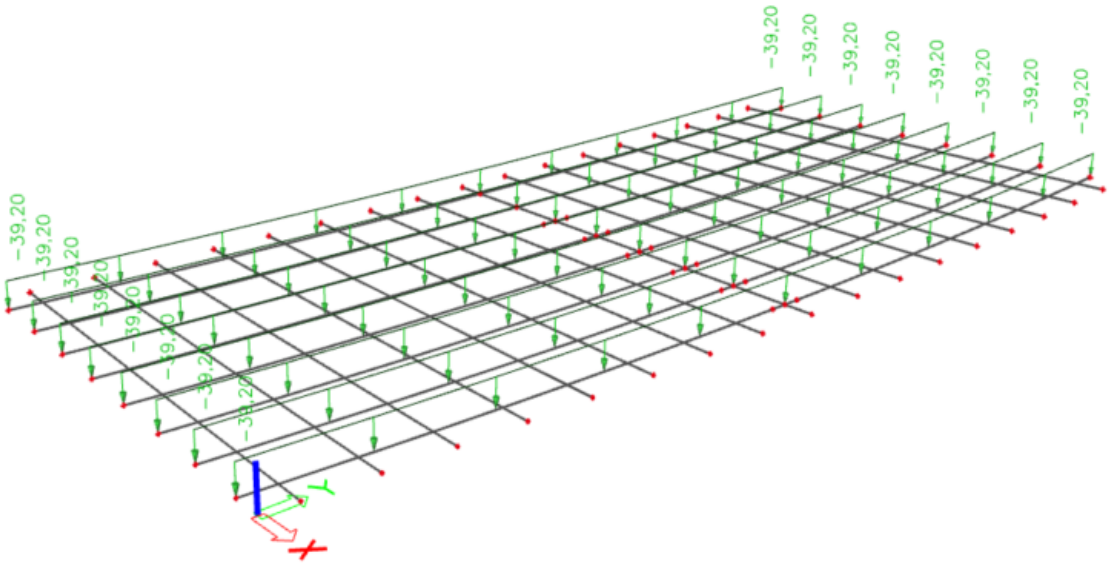

Figure 4.8: Grillage model curved deck subjected to self-weight

Traffic load

For the grillage model, all the loads are applied to the longitudinal beams. However, the point loads of the tandem system are not necessarily located at the same position as the longitudinal beams. Also, the uniform distributed load runs in the transverse direction of the bridge, which means that the UDL also acts in between the longitudinal beams. This problem can be solved by distributing the point loads from the tandem system towards the longitudinal beams and transferring UDL into concentrated loads and distribute them towards the longitudinal beams.

Tandem system (TS)

First, the point loads from the tandem system will be distributed. The position of the point loads from the tandem system, as well as the position of the longitudinal beams of the grillage model, can be seen in figure 4.9. The longitudinal beams are marked with the black dots.

The point loads can be distributed by thinking of a fictitious, simply supported beam in between the longitudinal beams of the grillage model. Figure 4.9 shows the fictitious beam for the right tandem load in lane 1 (F_1). For force F_1, part of the force goes to longitudinal beam I and part of the force goes to beam J. The part that goes to beam I is equal to support reaction at the left end of the fictitious beam and the part that goes to beam J is equal to the support reaction of the at the right end of the fictitious beam.

The length of the fictitious beam is equal to the distance between the longitudinal beams in the grillage model, which is equal to 2120 mm. The distance between F_1 and longitudinal beam I is equal to 1580 mm and the distance between F_1 and J is equal to 540 mm. By using moment equilibrium, the reaction force at the left and right end of the fictitious beam can be calculated. From this, it follows that

$$\frac{2.12 - 1.58}{2.12} \cdot 150 = 38.21\,\text{kN}$$

goes to longitudinal beam **I** and

$$\frac{2.12 - 0.54}{2.12} \cdot 150 = 111.79\,\text{kN}$$

goes to beam **J**.

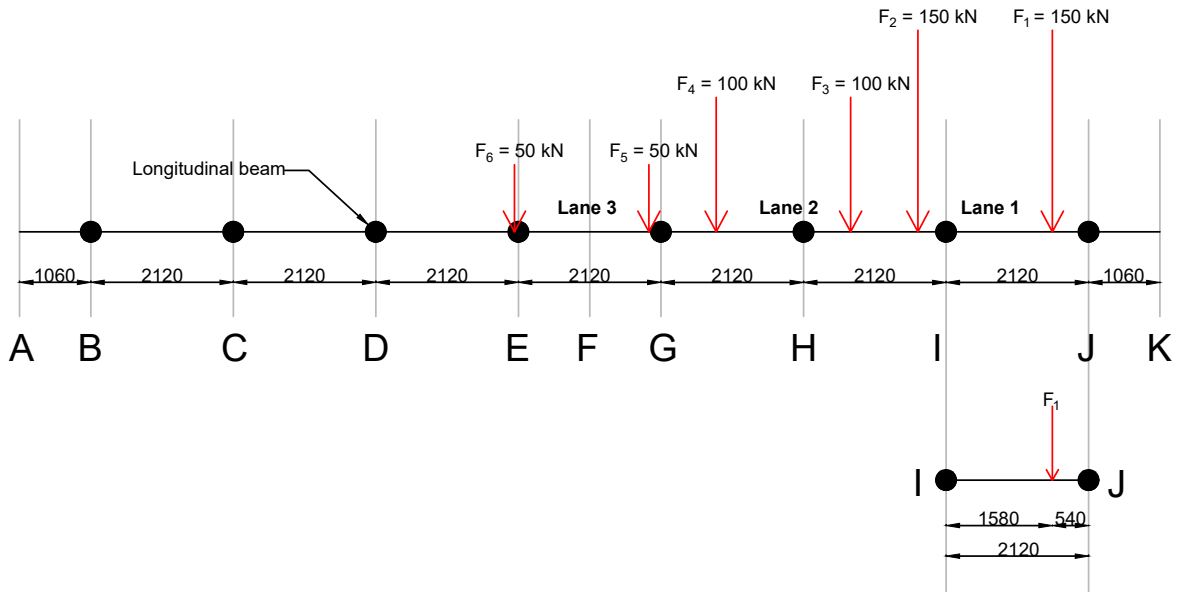

Figure 4.9: Transverse cross-section: position of the tandem loads and the longitudinal beams of the grillage model (mm)

The calculation above, can be applied to each of the the point loads F_1 till F_6 (see figure 4.9). Table 4.6 shows the distance between the point load and the 2 adjacent beams (one on the left and one on the right). The remaining columns of the table show which part of the load goes to which longitudinal beam. The unloaded longitudinal beams (A, B and C) are left out of the table. For every lane, the subtotal force of the longitudinal beams is shown, eventually this is needed to apply the loads of the curved and skewed bridge deck. The last row of table 4.6 shows the sum of the forces for all traffic lanes together, these values can be used for the curved deck.

Table 4.6: Distribution of forces tandem system (grillage model)

F_i (kN)	**distance** (m)		**force per longitudinal beam** (kN)					
	left	right	**D**	**E**	**G**	**H**	**I**	**J**
Lane 1								
F_1 = 150	1.58	0.54	-	-	-	-	38.21	111.79
F_2 = 150	1.70	0.42	-	-	-	29.72	120.28	-
			0	**0**	**0**	**29.72**	**158.49**	**111.79**
Lane 2								
F_3 = 100	0.70	1.42	-	-	-	66.98	33.02	-
F_4 = 100	0.82	1.30	-	-	61.32	38.68	-	-
			0	**0**	**61.32**	**105.66**	**33.02**	**0**
Lane 3								
F_5 = 50	1.94	0.18	-	4.25	45.75	-	-	-
F_6 = 50	2.06	0.06	1.42	48.58	-	-	-	-
			1.42	**52.83**	**45.75**	**0**	**0**	**0**
$\sum$			**1.42**	**52.83**	**107.08**	**135.38**	**191.51**	**111.79**

The curved deck and the curved and skewed deck are both loaded with the tandem system. For both bridge deck layouts, the tandem system is positioned in the middle of the span. In case of the curved deck, all the tandem systems are aligned, which means that the each beam is loaded with the sum of the equivalent forces, shown in the last row of table 4.6.

For the skewed deck, the tandem systems are not aligned. This means that the longitudinal position of the tandem system depends on the lane. For example, beam G is loaded with 61.32 kN coming from lane 2 and 45.75 kN coming from lane 3. As both tandem systems have a different position in the longitudinal direction of the deck, they must be applied separately. This means that for the skewed deck one has to look for the subtotal per traffic lane, which can be found in table 4.6. Figure 4.10 shows the point loads of the tandem system applied to the grillage model of the curved and curved and skewed bridge deck.

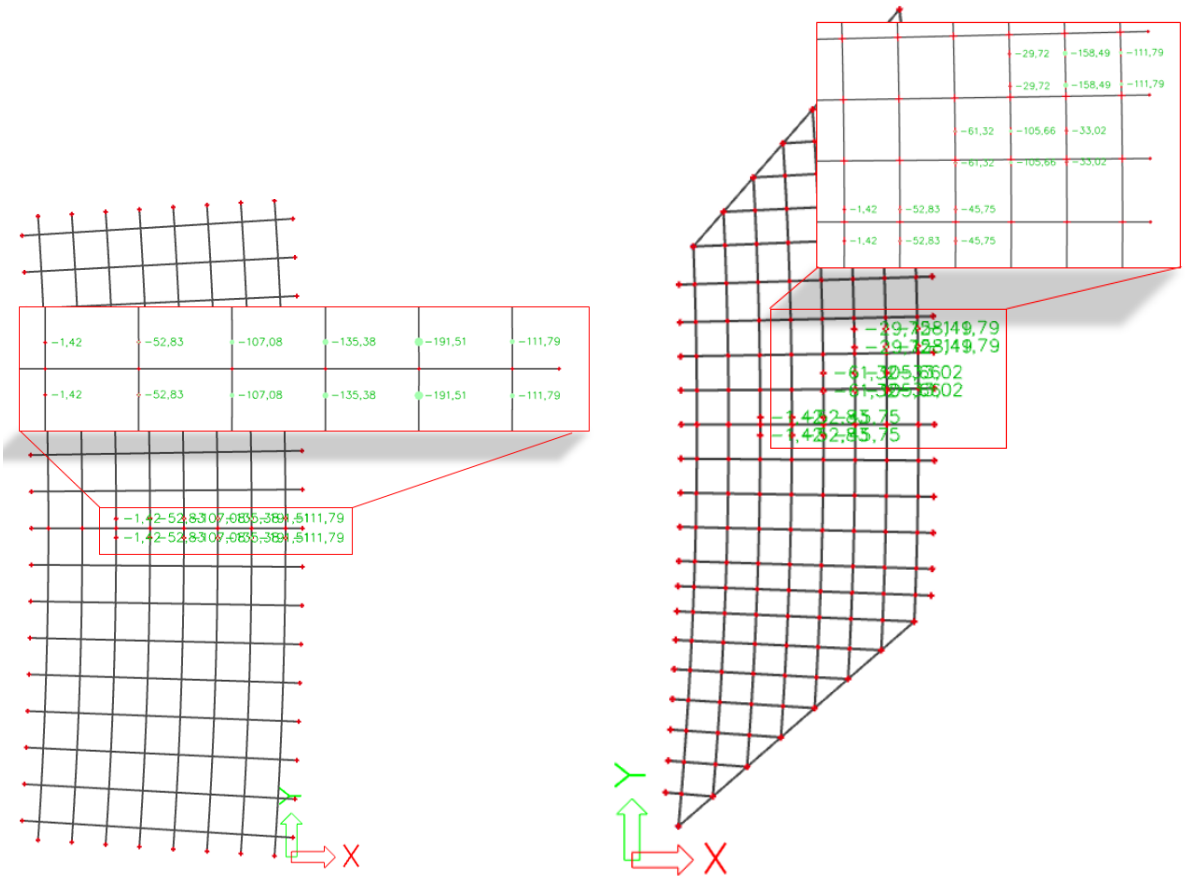

Figure 4.10: Grillage model curved deck (left) and curved and skewed deck (right), loaded with TS

Uniform distributed load (UDL)

Also for the uniform distributed load (UDL), the force can only be applied at the longitudinal beams of the grillage model. Figure 4.11 shows the transverse cross-section of the deck, the position of the uniform distributed load and the position of the longitudinal beams. The UDL can be split-up into a part of 3.50 kN/m^2 and a part of 10.35 - 3.50 = 6.85 kN/m^2, which can be seen in figure 4.12.

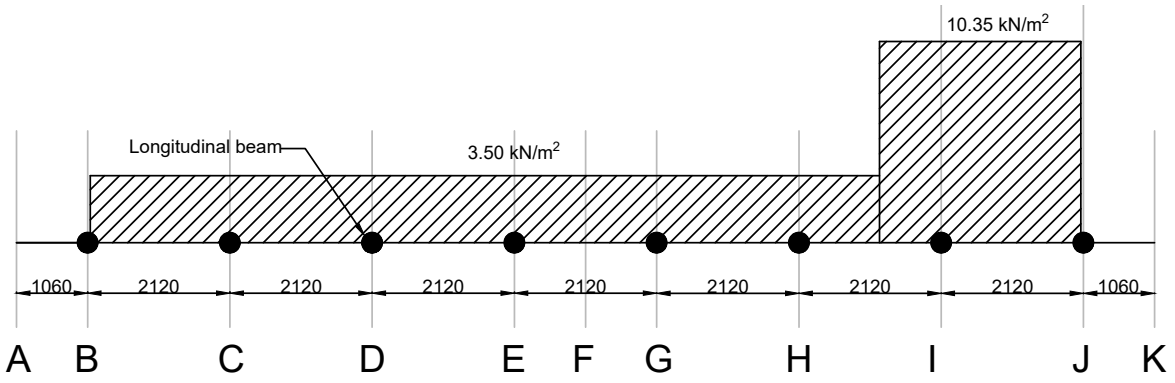

Figure 4.11: Transverse cross-section: position of the uniform distributed load (UDL) and the longitudinal beams of the grillage model (mm)

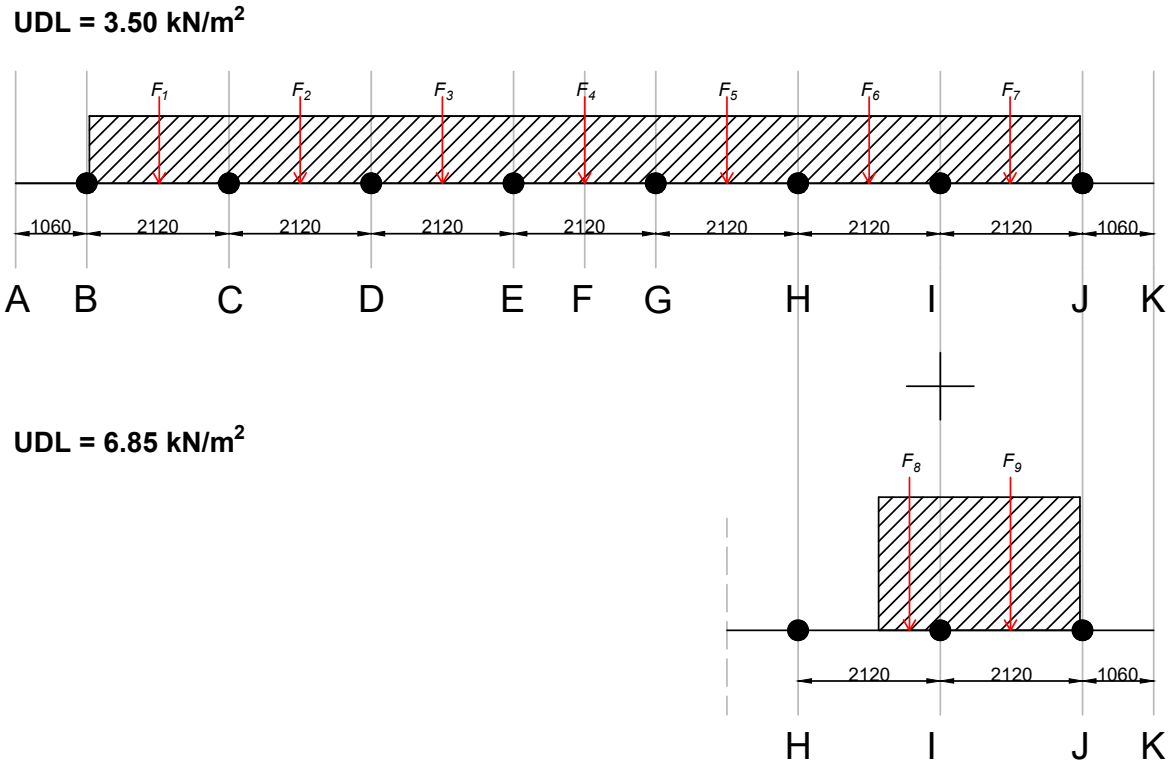

Figure 4.12: Equivalent concentrated loads and split-up of UDL (mm)

In order to distribute the UDL over the longitudinal beams, the UDL is transferred into equivalent, concentrated loads between each longitudinal beam. These equivalent point loads are indicated with the red arrows, called F_1 till F_7 for UDL = 3.50 kN/m^2 and F_8 and F_9 for UDL = 6.85 kN/m^2. The equivalent point loads can be distributed in the same way as was done for the point loads of the tandem system.

Table 4.7 shows the values of the equivalent loads F_1 till F_9. This equivalent load can be calculated by multiplying the uniform distributed load (kN/m^2) with the width over which UDL acts (m). This results into an equivalent load with unit (kN/m), which can be read from the first column of table 4.7. For most fields, the width over which UDL acts is equal to 2.12 m. This results into an equivalent load of

$$3.50 \cdot 2.12 = 7.42\,\text{kN/m}^2$$

For F_1, F_7, F_8, F_9 the values are different, as the width over which UDL acts is smaller and/or the value of UDL is equal to 6.85 kN/m^2 instead of 3.50 kN/m^2. For F_1 and F_7 the width over which UDL acts is equal to 2.08 m, which means that $F_{1,7} = 7.28$ kN/m. In the case of F_8 and F_9, the width is equal to 0.92 m and 2.08 m respectively. As UDL = 6.85 kN/m^2, this results into

$$F_8 = 6.85 \cdot 0.92 = 6.30\,\text{kN/m}$$
$$F_9 = 6.85 \cdot 2.08 = 14.25\,\text{kN/m}$$

The next 2 columns of table 4.7 show the distance between the equivalent load and the 2 adjacent longitudinal beams. The remaining columns of the same table show which part of the load goes to which longitudinal beam. The last row of table 4.7 shows the sum of the q-loads for each of the longitudinal beams.

Table 4.7: Distribution of forces uniform distributed load (UDL) grillage model

F_i (kN/m)	**distance** (m)		**q-load per longitudinal beam** (kN/m)							
	left	right	**B**	**C**	**D**	**E**	**G**	**H**	**I**	**J**
UDL = 3.50 kN/m^2										
F_1 = 7.28	1.08	1.04	3.57	3.71	-	-	-	-	-	-
F_2 = 7.42	1.06	1.06	-	3.71	3.71	-	-	-	-	-
F_3 = 7.42	1.06	1.06	-	-	3.71	3.71	-	-	-	-
F_4 = 7.42	1.06	1.06	-	-	-	3.71	3.71	-	-	-
F_5 = 7.42	1.06	1.06	-	-	-	-	3.71	3.71	-	-
F_6 = 7.42	1.06	1.06	-	-	-	-	-	3.71	3.71	-
F_7 = 7.28	1.04	1.08	-	-	-	-	-	-	3.71	3.57
UDL = 6.85 kN/m^2										
F_8 = 6.30	1.66	0.46	-	-	-	-	-	1.37	4.93	-
F_9 = 14.25	1.04	1.08	-	-	-	-	-	-	7.26	6.99
$\sum$			**3.57**	**7.42**	**7.42**	**7.42**	**7.42**	**8.79**	**19.61**	**10.56**

The equivalent uniform distributed load of the grillage model is shown in figure 4.13. In this figure, the loading is applied to the curved deck.

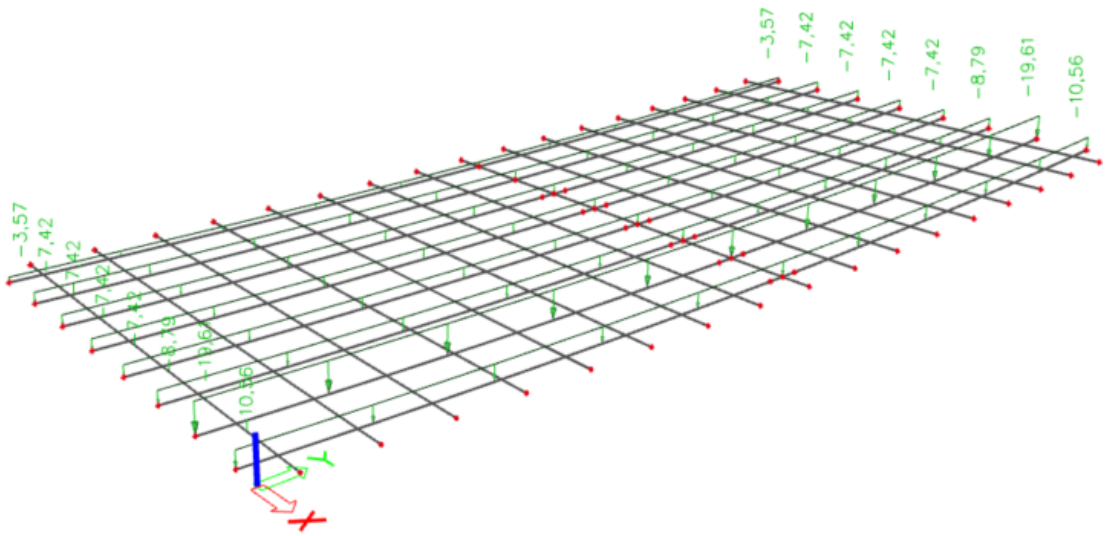

Figure 4.13: Uniform distributed load applied to the grillage model

5

3D plate model

In order to verify the orthotropic plate model, the bridge deck of the Blankenburg case study is compared to and 3D plate model. This model consists of an 3D assembly of 2D isotropic plates. As this model is slightly less advanced as and full 3D model, the 3D plate model can also be called an 2.5D model. The theory of the 3D plate model is introduced in the first part of this chapter. Also the 3D plate model is created in SCIA-engineer. The downside of the 3D plate model is the fact that the cross-sectional forces (i.e.: bending moments) cannot be extracted from the model directly. These cross-sectional forces need to be calculated by hand, based upon the forces or stresses for each individual plate part. Alternatively, the bending moments can be calculated indirectly. This indirect method is used for this study.

In the second part of this chapter, it is shown how the 3D plate model of the Blankenburg case study is created. Due to the overlap of plates and the interaction of the web and top and bottom plate, the top and bottom plate in the zone of the web are created using an orthotropic plate. The calculation of the orthotropic stiffness properties is shown in this chapter. Eventually, it is shown how the loading is applied to the 3D plate model.

5.1. Theory of 3D plate model

The 3D plate model consists of a spatial assembly (3D) of 2D plate or shell elements. The system lines of these plate parts are located at the the centre lines of the part of the cross-section they represent. These separate plate part are rigidly connected in the nodes. Figure 5.1 shows an example of 3D plate model of a bridge deck stiffened by box beams.

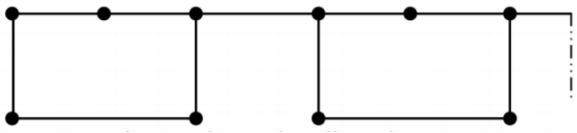

Figure 5.1: 3D plate model of a bridge deck stiffened by box beams [2]

The elements used are plane isotropic elements. These elements can both take membrane as well as bending action. In finite element codes, these elements are often called *shell* elements. However, generally the elements are not curved and the interaction between membrane and bending action is not at stake, which are typical properties for shell elements. As the elements of the 3D plate model misses these properties, it is better to use the name *membrane-bending* element [2].

5.1.1. Overlapping and missing material

When creating a 3D plate model, the system lines of the 2D plates are drawn. Generally, the system line is equal to the (local) neutral axis of the plate part. On both sides of the system lines, half of the thickness of the plate is added.

This means that there is an overlap of material at locations were a vertical plate (web) intersects with a horizontal plate (flange). Figure 5.2 shows how this overlap of plates looks like. In this figure,

the flange part is grey and the webs are white. The system lines of both the flange and plate intersect in a node. The locations at witch material is overlapping are marked with red.

When the web intersects in the middle of a flange there is overlapping of plate parts only. However, in case the web intersects on the edge of the flange, in the outer corner material is missing. The area of missing material is equal to the extra material situated in the overlapping part, which can also be seen in figure 5.2.

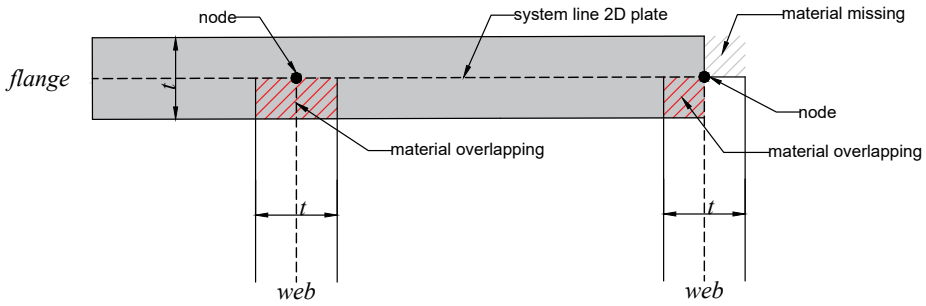

Figure 5.2: Overlapping and missing material where flange and web parts meet

In practice, the overlap of material means that in the longitudinal direction the normal and bending stiffness of the total cross-section is a too high. In case the web part intersects at the end of the flange, the plate part that is missing is equal to the overlapping plate part. This means that the net cross-sectional area of the 3D plate model is equal to the cross-sectional area of the real cross-section. If the stiffness E of both plate parts is equal, the normal stiffness EA is equal.

However, material of the 3D plate model still has a different orientation with respect to the neutral axis of the total cross-section. This means that for a web connected to the end of a flange, the moment of inertia of the model is still different compared to the real cross-section.

The overlapping and missing of material at intersections of plate parts can be solved by creating separate plate parts over the width of the web. This means that for each point at which a flange is connected to a web, 2 extra nodes must be created. Along the flange, this results into one node where the web starts, one node where the system line of the web is connected to the flange and one node where the web ends, see figure 5.3.

Over the thickness of the web, the thickness of the flange is reduced and the plate parts have an eccentricity, equal to $t/4$. The eccentricity is equal to the distance between the system line and the neutral axis of the plate part, which is indicated with a red line in figure 5.3.

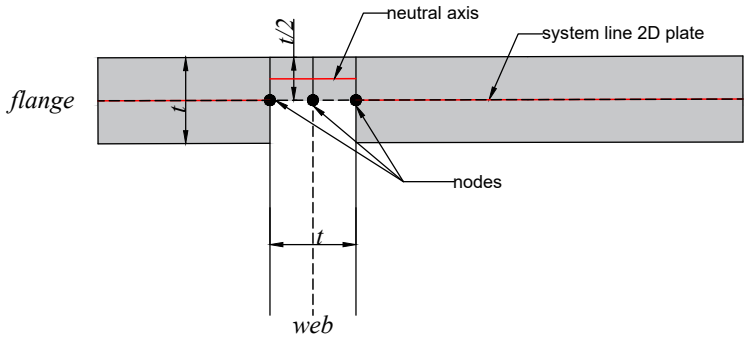

Figure 5.3: Overlapping and missing material where flange and web parts meet

When adopting the modifications shown in figure 5.3, the material of the 3D plate model is positioned at the exact same location as the real cross-section. This means that the axial and bending stiffness in longitudinal direction is equal to the real cross-section.

5.1.2. Stiffness of the web-zone

In the zone of the stiffener, there is a rigid connection between the horizontal plate (flange-part) and vertical orientated stiffener (web-part). This part of the cross-section can be seen in figure 5.4. Figure 5.4a shows the real cross-section of this zone. In the 3D plate model, the web-zone connects three elements: a flange coming from the left, a flange coming from the right and the web. All of these three elements share the same red node, see figure 5.4b. In figure 5.4b and 5.4c the web-part is shifted downward.

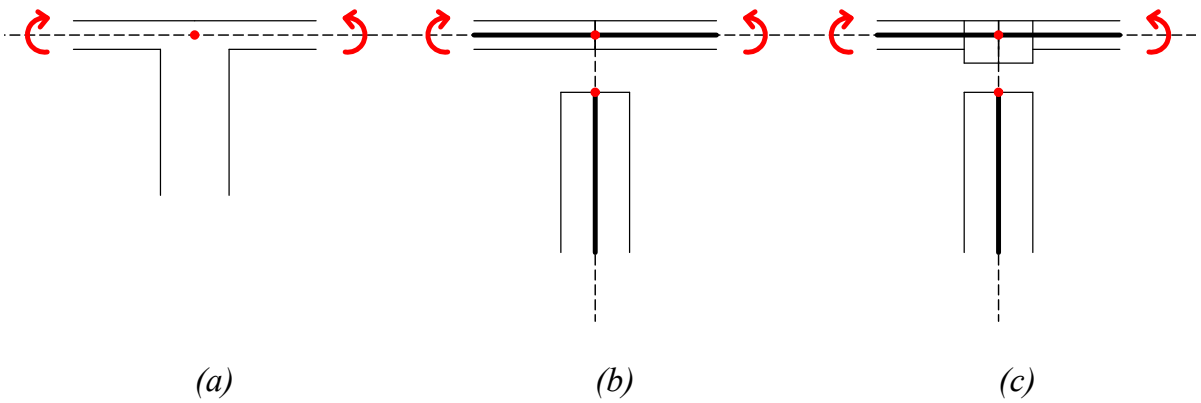

Figure 5.4: Web-zone 3D plate model (transverse cross-section). *(a): real cross-section, (b): 3D plate model, (c): 3D plate model with higher stiffness in web-zone*

In the shared node, there is a transfer of forces and bending moments between the top plate and the stiffener. However, this transfer of forces and moments occurs in this node only. This means that over the width of the web there is no transfer of stresses between the top plate and the web. Which results into a constant bending stiffness EI over the length of the top plate. For figure 5.4b, this means that the bending moment acting on the top plate causes a constant curvature over the length of the top plate. This follows from equation 5.1. For the real cross-section (figure 5.4a), the bending stiffness in the zone of the web is higher than the remaining part of the top plate. From equation 5.1 it follows that for the real cross-section the curvature κ varies over the length of the top plate.

$$\kappa = \frac{M}{EI} \tag{5.1}$$

Figure 5.4c shows a solution of how the top plate can be made stiffer in the zone of the web. In this figure it can be seen that in the zone of the web, the top plate is made thicker. Now, the top plate is stiffer in the zone of the web, which also means that the curvature isn't constant over the length of the top plate. The extra thickness added to the top and bottom plate in the web-zone can be based upon the area over which the web-part is activated.

The area in which the web is activated can determined by creating a separate 2D plate model of the web-zone. The flanges of web-zone can be loaded with a normal force, this normal force partly flows through the web, which can be made visible with the stress trajectories of the major principle stress. The height over which the web is activated must be added to thickness of the top and bottom plate in the transverse direction of the bridge deck. As the extra height is on the side of the web only and the system line of the web-zone must be at the same level of the remaining plate parts of the top and bottom plate of the bridge deck, the plates in the web-zone must have an eccentricity.

Orthotropic plate web-zone

Both in transverse and longitudinal direction, the web-zone of the top and bottom plate needs to have a modified thickness in order to have an accurate transverse and longitudinal stiffness. For both directions, the thickness of the web-zone plate can be different. This means that the web-zone plate of the 3D plate model must be orthotropic.

Orthotropy caused by 2 different plate heights in 2 different directions is a standard source of orthotropy that can be chosen in SCIA-engineer. This kind of orthotropy can for example be found in a *wide slab floor* system, in which continuous seams lower the plate thickness in one direction. In the

other the direction, the full thickness of the plate contributes to the stiffness of the plate. This kind of orthotropy can be used to assign different plate thicknesses of the web-zone plate for the longitudinal and transverse direction.

5.1.3. Extraction of results

The results that can be directly extracted from the 3D plate model are the support reactions and the deflections. The total bending moment over a particular section is less easy to extract, as the bending moment of the total cross-section is equal to the sum of membrane and bending action of each individual plate part.

Longitudinal bending moment (indirect method)

The longitudinal bending moment can also be extracted from the 3D plate model. The easiest way to do this is using an indirect method. For this method, one needs to determine the slope of the normal force diagram of each of the web parts. The normal force diagram of the webs can be plotted by making a *section* over the transverse direction of the bridge deck.

Figure 5.5 shows an example of the normal force diagrams of the webs of a 3D plate model. The distribution of longitudinal bending moment over a transverse cross-section can be determined using the slope of the normal force diagrams. For the Blankenburg case, there is a repetition of 8 H-like cross-section in the longitudinal direction of the bridge deck. These 8 cross-sections have identical moment of inertia (I) and Young's modulus E.

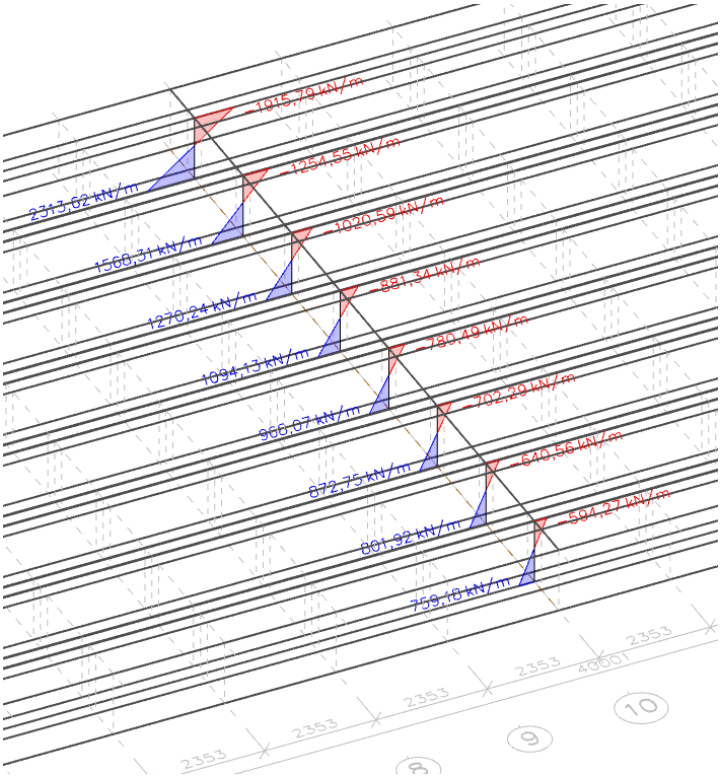

Figure 5.5: Normal force diagrams web parts

The slope of the normal force diagram is proportional to the bending moment. This follows from the fact that the slope of the normal force diagram is proportional to the curvature κ (slope of strain diagram). To find the curvature, the normal force diagram of the webs needs to be divided through the width of the web b and the Young's modulus E. For each web, these values are the same, which means that the ratio's between the slopes of the normal force diagram are identical to the ratio's between κ.

The relationship between the bending moment M and the curvature κ is equal to

$$M = EI\kappa \tag{5.2}$$

As EI is identical for every H-section, the ratio between κ is equal to the ratio between the bending moment. This also means that the ratio between the bending moments is equal to the ratio between the slopes of the normal force diagrams of the webs. The total bending moment acting on the mid-span cross-section can be distributed over the different longitudinal strips proportionally.

When a point load F or a distributed load q (with $F = qw$) is applied in the middle of the span of the deck, the total longitudinal bending moment is equal to

$$M = \frac{1}{4}Fl \tag{5.3}$$

5.2. Blankenburg case

The 3D plate model of the Blankenburg bridge deck is created in *SCIA-engineer*. The cross-section is build-up using 5 different types of plates. Figure 5.6 shows the transverse cross-section of the 3D plate model of the Blankenburg case. In this figure, the system lines of the different plate parts are indicated with different colors.

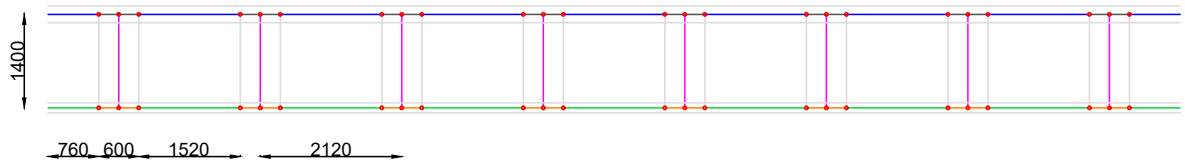

Figure 5.6: Transverse cross-section 3D plate model Blankenburg case

In the zone where the web and flange part intersect, there are 3 nodes. Each node in the middle is shared by a flange and a web. In these points, there is a rigid connection between the flange and the web. The other 2 nodes are there to connect the different top or bottom plate to the top or bottom plate of the web-zone. This makes it possible to assign different properties to the top and bottom plate in the web-zone.

The spacing between the system lines of the top and bottom plates is equal to 1400 mm, which is equal to the centre to centre distance of the top and bottom plate. The first web begins at 760 mm from the edge of the deck. The thickness of the webs is equal to 600 mm and the spacing of the stiffeners is equal to 1520 mm. From this, it follows that the centre to centre distance of the webs is equal to 1520 + 600 = 2120 mm.

Table 5.1 shows an overview of the properties of the 5 different plates used to create the 3D plate model of the bridge deck of the Blankenburgverbinding. All plates have a length of 40 m (in case of the straight deck layout). There are 9 isotropic top plates (blue lines figure 5.6), 7 of them have a width of 1520 mm and the ones on the edges have a width of 760 mm. The thickness of the top plate is equal to 250 mm and there is no eccentricity (system line coincides with the centre line). For the other plate parts, the same kind of characteristics can be read from table 5.1.

Table 5.1: Plate parts of 3D plate model, colors according to figure 5.6

part of cross-section	**number**	**width** w (mm)	**thickness** t (mm)	**eccentricity** e (mm)	**type**
top plate	9	7 x 1520 2 x 760	250	0	isotropic
bottom plate	9	7 x 1520 2 x 760	150	0	isotropic
web	8	1400	600	0	isotropic
web-zone top plate	16	300	L: 167, T: 357	-53.5	orthotropic
web-zone bottom plate	16	300	L: 101, T: 240	45.0	orthotropic

The plate parts in the web zone of the top and bottom plate have a width of 300 mm, this means that there are 2 of these plates at the end of every 600 mm wide web. The plates in the web zone are orthotropic. The orthotropy of these plates is assigned by assigning 2 different plate thicknesses in 2 directions. In table 5.1, *L* means *longitudinal direction* and *T* means *transverse direction*. In transverse direction, the extra thickness needs to be added to the top plate, at the side of the web. This means that the web-zone top and bottom plate needs to have an eccentricity. For the top plate, the centre line needs to shift 53.5 mm downwards with respect to the system line and for the bottom plate, the centre line needs to shift 45.0 mm upwards.

The properties of the orthotropic plates of the web-zone are determined in the following section 5.2.1, page 59. Figure 5.7 and figure 5.8 give a 3D view of the 3D plate model of the straight, curved and curved and skewed deck layout.

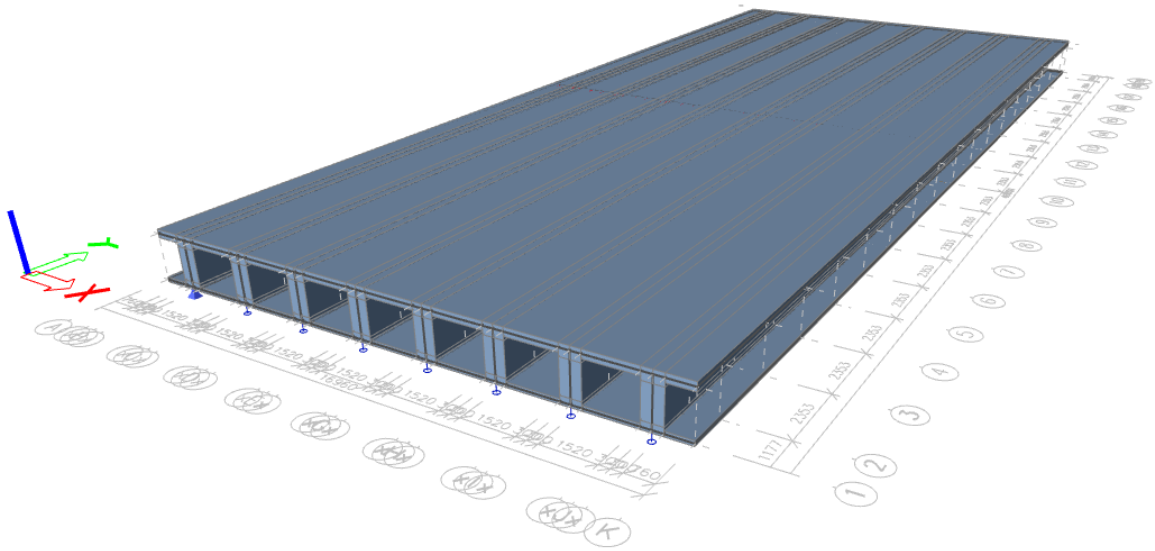

Figure 5.7: 3D plate model straight bridge deck

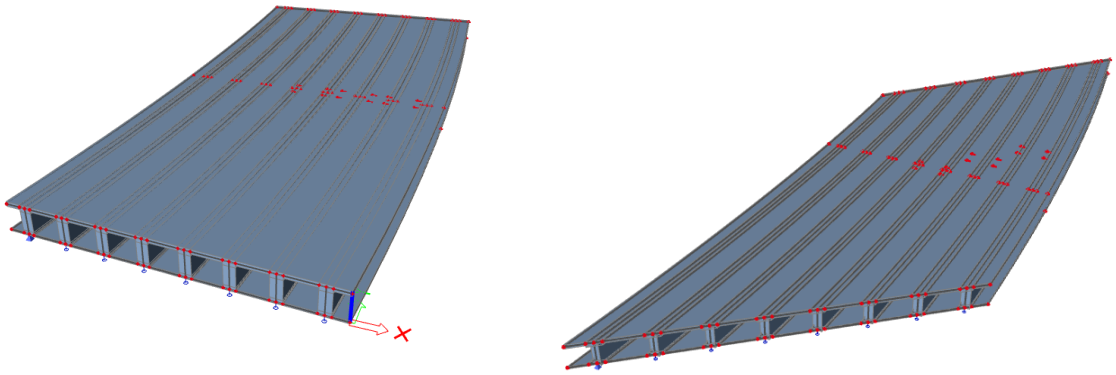

Figure 5.8: 3D plate model curved (left) and curved and skewed (right) bridge deck

5.2.1. Orthotropic plates web-zone

In this section, the thickness of the orthotropic plate of the web-zone in longitudinal and transverse direction is determined. The eccentricity of the plates is determined by the thickness needed in the transverse direction of the deck. This transverse thickness of the web-zone is the sum of the thickness of the top or bottom plate and the part of the web that is activated while putting a normal stress on the top and bottom plate (flange parts).

The thickness of the web-zone of the top and bottom plate is determined using the condition that the cross-section of the 3D plate model has the same location of the neutral axis and the same moment of inertia as the real cross-section. The position of the neutral axis of the web-zone plates is already determined by the eccentricities needed for the transverse direction. These eccentricities need to be taken into in the calculation of the location of the neutral axis and the moment of inertia.

Transverse direction

The activated zone of the web has been determined using a 2D plate model. In this model, a part of the transverse cross-section is modelled. The cross-section is modelled as a rectangular plate with a thickness of 10 mm and openings in it. In the transverse direction, the flanges are loaded with a distributed load. This means that the top and bottom flange are loaded with the same stress. This plate was also used to determine the transverse axial stiffness of the orthotropic plate, see figure 3.2, page 27.

Figure 5.9 shows the trajectories of the major principle stress. From this figure, it becomes clear that part of the stresses from the flanges also flow through a limited part of the web.

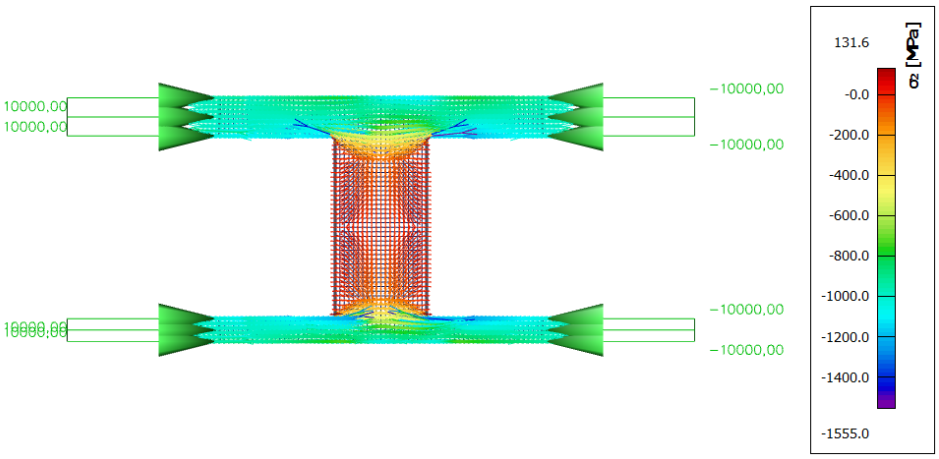

Figure 5.9: Trajectories major principle stress

The area over which the web is influenced is assumed to be a segment of a circle. The radius of this circle segment can be calculated by using the *sagitta* (equation 5.4). Based upon the *sagitta* and the radius of the circle, the area of the circle segment can be calculated. This area will be divided by the width of the web, this results into an equivalent effective height of the web-zone. This equivalent effective height is added to the thickness of the top or bottom plate. Figure 5.10 shows the definition of the parameters used in equation 5.4.

$$R = \frac{s}{2} + \frac{l^2}{8s} \tag{5.4}$$

$$A = \frac{R^2}{2}\left(\alpha - \sin\left(\alpha\right)\right) \tag{5.5}$$

with

$$\alpha = 2\arcsin\left(\frac{l}{2R}\right) \tag{5.6}$$

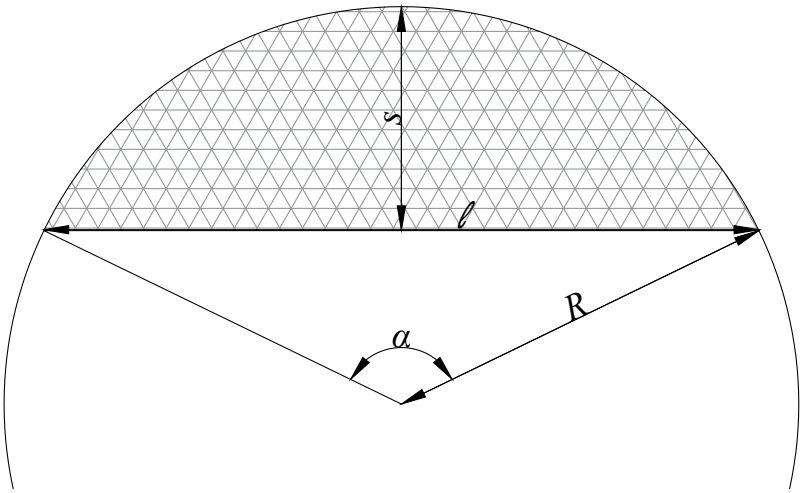

Figure 5.10: Variables related to the sagitta, radius, and area of a circle segment

Top plate

For the top plate, the circle segment running through the activated part of the web is shown in figure 5.11. In this figure, the color scale of the stress trajectories has been changed, in order to get a more clear border between the circle segment and the rest of the web. On the figure, the 250 mm thick top flange measured 75 mm. The sagitta of the circle segment measured 46 mm. This means that the sagitta is equal to $s = 250/75 \cdot 46 = 153\,\text{mm}$.

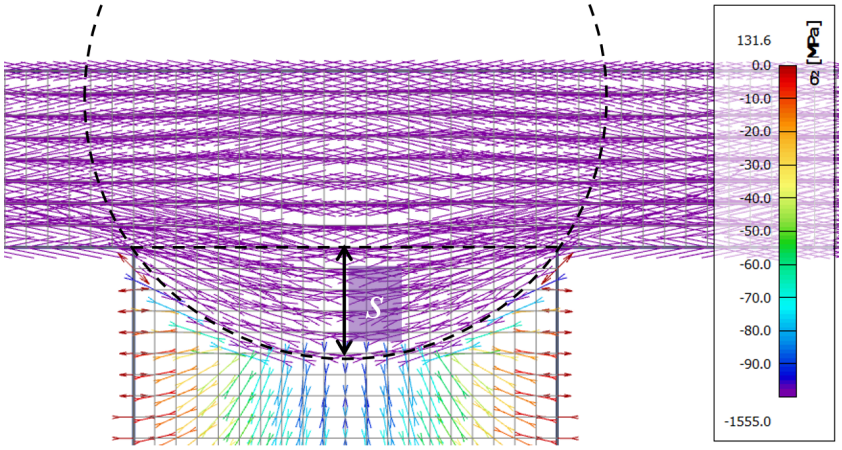

Figure 5.11: Circle segment activated web-zone (top-plate)

Now, the radius R and the area A of the circle segment of the top plate can be calculated:

$$R = \frac{153}{2} + \frac{600^2}{8 \cdot 153} = 370\,\text{mm}$$

$$A = \frac{370^2}{2}\left(1.89 - \sin\left(1.89\right)\right) = 64\,428\,\text{mm}^2$$

Over the width of the web, a rectangular plate with an equivalent height is assumed. The equivalent height is chosen such that the area of the rectangular plate has the same area as the circular segment. This means that the area of the circular segment must be divided by the width of the web, in order to determine the equivalent effective height. The equivalent effective height for the top plate is equal to $64\,428/600 = 107\,\text{mm}$. Together with the thickness of the top plate of 250 mm, this results into a thickness of $h = 250 + 107 = 357\,\text{mm}$.

Bottom plate

In figure 5.12 the circle segment of the activated web-zone next to the bottom plate can be seen. The 150 mm thick bottom plate measured 44 mm on the figure and the sagitta of the circle segment measured 38 mm. This means that for the bottom plate the sagitta is equal to $s = 150/44 \cdot 38 = 130\,\text{mm}$.

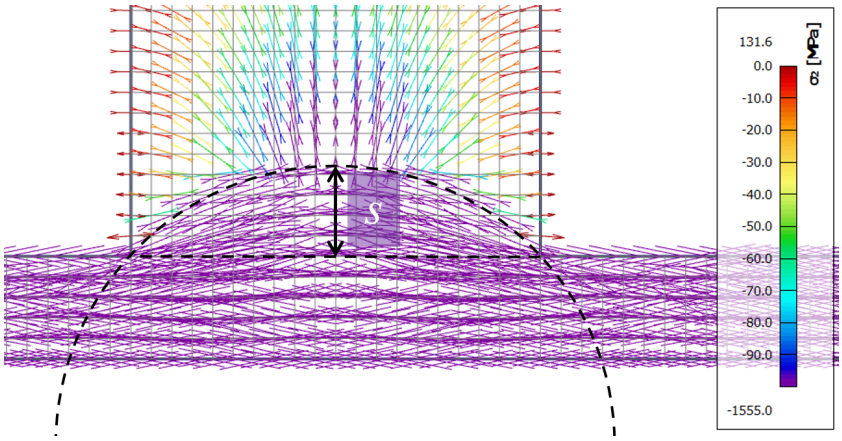

Figure 5.12: Circle segment activated web-zone (bottom-plate)

Now, the radius R and the area A of the circle segment for the bottom plate can be calculated:

$$R = \frac{130}{2} + \frac{600^2}{8 \cdot 130} = 412\,\text{mm}$$

$$A = \frac{412^2}{2}\left(1.63 - \sin\left(1.63\right)\right) = 53\,702\,\text{mm}^2$$

The equivalent effective height for the bottom plate is equal to $53\,702/600 = 90\,\text{mm}$. Together with the thickness of the bottom plate of 150 mm, this results into a thickness of $h = 150 + 90 = 240\,\text{mm}$.

Implementation

From the analysis above, it followed that a thickness of 107 mm must be added to the top plate and a thickness of 90 mm must be added to the bottom plate in the web-zone. These extra thicknesses must be added on the side of the web only, which means that the plate parts in the zone of the web must have an eccentricity with respect to the plane in which they are drawn (the system lines). Figure 5.13 shows the top and bottom plate in the zone of the web. In this figure, the thick lines are the system lines, these lines coincide with the level at which the plates are drawn. The red lines are the neutral axes of the top and bottom plate in the web-zone. The gap between the system line and the red line is the eccentricity of the plates in the web-zone. For the top plate, the eccentricity is equal to 53.5 mm and for the bottom plate the eccentricity is equal to 45.0 mm.

Longitudinal direction

By applying the plate thicknesses and eccentricities shown in figure 5.13. The 3D plate model is too stiff for bending in longitudinal direction. In fact, the extra plate thicknesses in the zone of the web must only be added in transverse direction. This can be solved by applying an orthotropic plate in the zone of the web. For this situation, an orthotropic plate with different thicknesses in each direction can be used. In total, 4 different thicknesses can be assigned: for both orthogonal directions a membrane and a bending thickness.

The plate thickness found for the transverse direction, must be assigned to the bending thickness of the orthotropic plate. This can be concluded from figure 5.4. For bending in longitudinal direction, the bending stiffness of the cross-section comes from the membrane thickness of the top and bottom plate. In steel design, the stresses are often assumed to be constant over the height of the flanges. This means that the top and bottom flange are assumed to be loaded in full tension or compression. This assumption is also made for this particular case. The contribution of the top and bottom plate to the total bending stiffness comes from the normal forces in the plates.

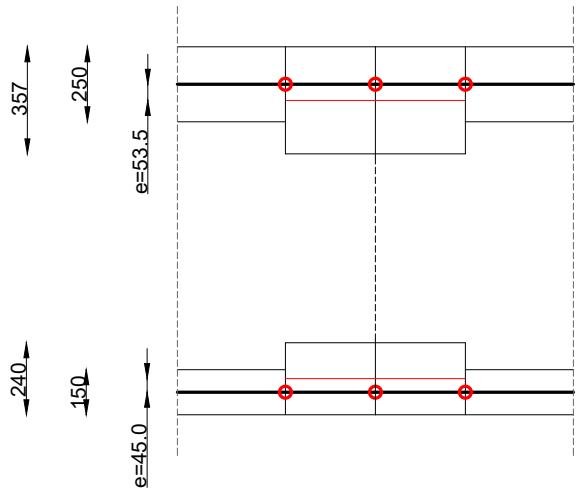

Figure 5.13: Thicknesses and eccentricity top and bottom plate in the web-zone (mm)

For the transverse direction the plates in the zone of the web must have an eccentricity. In *SCIA-engineer*, this eccentricity determines the position of the plate with respect to the plane in which it is drawn. This means that one particular plate can only have one eccentricity, which also is the case for orthotropic plates. This means that the position of the neutral axis of the top and bottom plate in the zone of the web is already determined. The only unknown are the *membrane* thicknesses of these plates in longitudinal direction. These thicknesses can be determined by satisfying two equations: the web-zone of the 3D model must have the same position of the neutral axis and the same moment of inertia as the real cross-section.

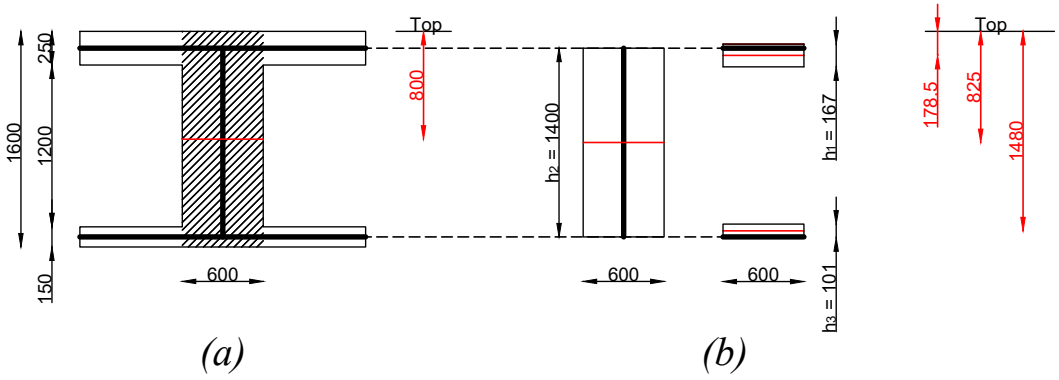

Figure 5.14: Real web-zone *(a)* and web-zone of 3D plate model *(b)* (mm)

The neutral axis of the web-zone of the real cross section (shaded area in figure 5.14a) is at 800 mm from the top. The moment of inertia of the same web-zone is equal to:

$$I = \frac{1}{12} \cdot 600 \cdot 1600^3 = 2.048 \times 10^{11}\ \text{mm}^4 \tag{5.7}$$

In figure 5.14b the web-zone of the 3D plate model is show. In order to make the drawing more clear, the top and bottom plate are shifted towards the right. For each of the 3 elements, the position of their neutral axis is predefined. The thicknesses h_1 and h_3 of the top and bottom plate are the two unknowns. The position of the neutral axis and the moment of inertia of the cross-section shown in figure 5.14b can be calculated as follows:

$$
\begin{aligned}
z_{NC} &= \frac{h_1 \cdot 178.5 + 1400 \cdot 825 + h_3 \cdot 1480}{h_1 + 1400 + h_3} = 800\,\text{mm} \\
I &= \frac{1}{12} \cdot 600 \cdot h_1^3 + 600 \cdot h_1 \cdot 621.5^2 + \\
&\quad \frac{1}{12} \cdot 600 \cdot 1400^3 + 600 \cdot 1400 \cdot 25^2 + \\
&\quad \frac{1}{12} \cdot 600 \cdot h_3^3 + 600 \cdot h_3 \cdot 680^2 = 2.048 \times 10^{11}\,\text{mm}^4
\end{aligned}
\tag{5.8}
$$

Solving set of equations 5.8 results into $h_1 = 167\,\text{mm}$ and $h_3 = 101\,\text{mm}$. These thicknesses are assigned to the membrane thickness of the orthotropic plate in longitudinal direction.

Error axial stiffness

The membrane plate thicknesses in longitudinal direction result into a small error of the axial stiffness in longitudinal direction. This follows from the fact that the total cross-sectional area of the 3D plate model is bigger than the real cross-section (figure 5.14a). In the real cross-section the total cross-sectional area is:

$$A_{real} = 600 \cdot 1600 = 0.96\,\text{m}^2$$

In the 3D plate model this cross-sectional area is equal to:

$$A_{3D-plate} = 600 \cdot (167 + 1400 + 101) = 1.00\,\text{m}^2$$

This means that the web-zone of the 3D plate has an axial stiffness which is 4.5% too stiff. This is such a small difference that it will be neglected.

5.2.2. Loading

Also the 3D plate model is loaded with dummy loads, self weight and traffic load. The dummy loads are applied in the same way as for the other models. Figure 5.15 shows 2 examples of the dummy load-cases applied to the 3D plate model (LC1 and LC3).

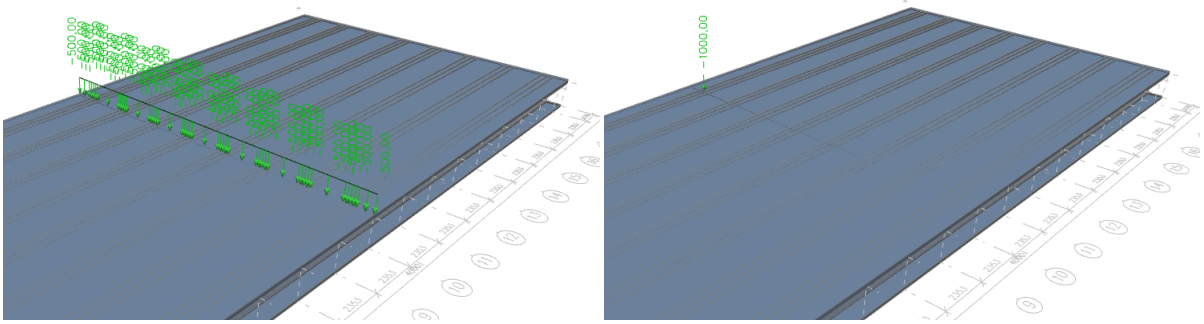

Figure 5.15: 3D plate model loaded with LC1 (left) and LC3 (right)

Self-weight

In order to avoid local bending of the top plate, the self-weight of the deck is applied as distributed loads at the position of the webs. This means that the self-weight of the deck is applied in the same way as was done for the grillage model. Above each web, the 3D plate model is loaded with a line load of $q = 39.20\,\text{kN/m}$. This is the same load as applied to the the longitudinal beams of the grillage model. Figure 5.16 shows how the self-weight is applied to the 3D plate model.

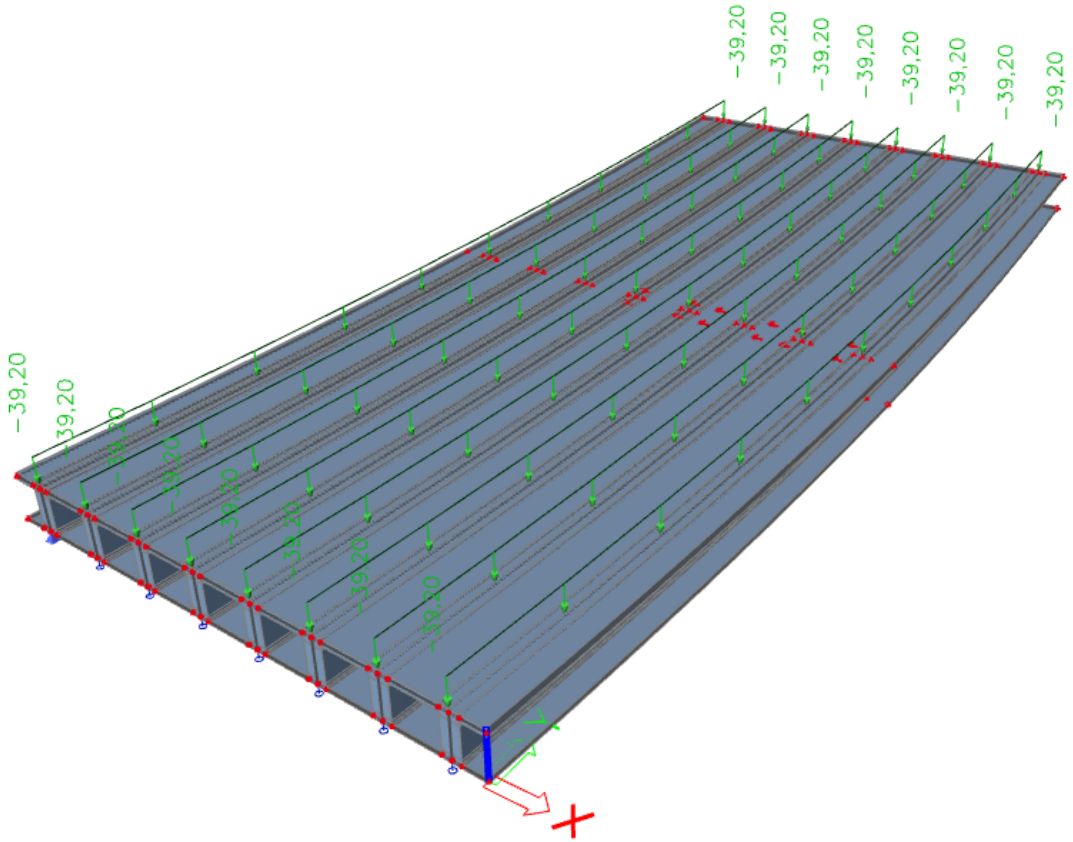

Figure 5.16: 3D plate model loaded with the self-weight

Traffic load

The traffic load of the tandem system (TS) applied to the 3D plate model can be seen in figure 5.17. The left figure shows the TS applied to the curved deck and in the right figure the TS is applied to the curved and skewed deck. For the curved deck, the TS is aligned in the transverse direction. For the skewed deck, the longitudinal position is different for every notional lane.

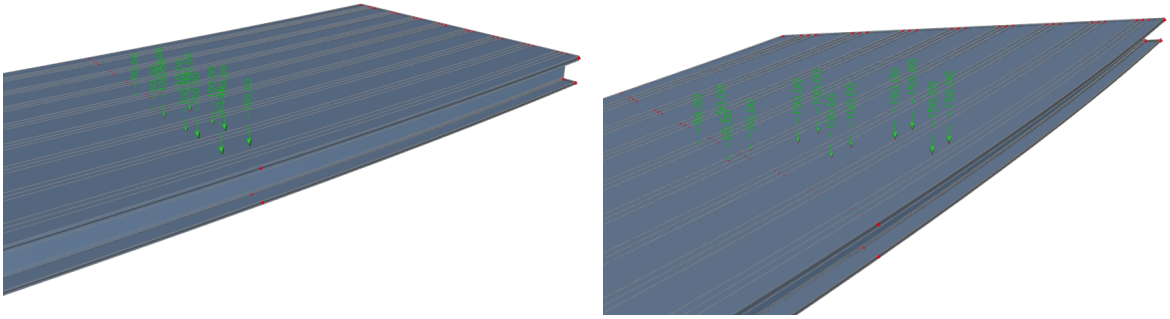

Figure 5.17: 3D plate model loaded with the tandem system, curved deck (left) and curved and skewed deck (right)

The uniform distributed load (UDL) is applied to the 3D plate model in the same way as for the grillage model. The UDL is applied above the stiffeners to avoid local action of the top plate of the bridge deck. Figure 5.18 shows the uniform distributed load applied to the 3D plate model.

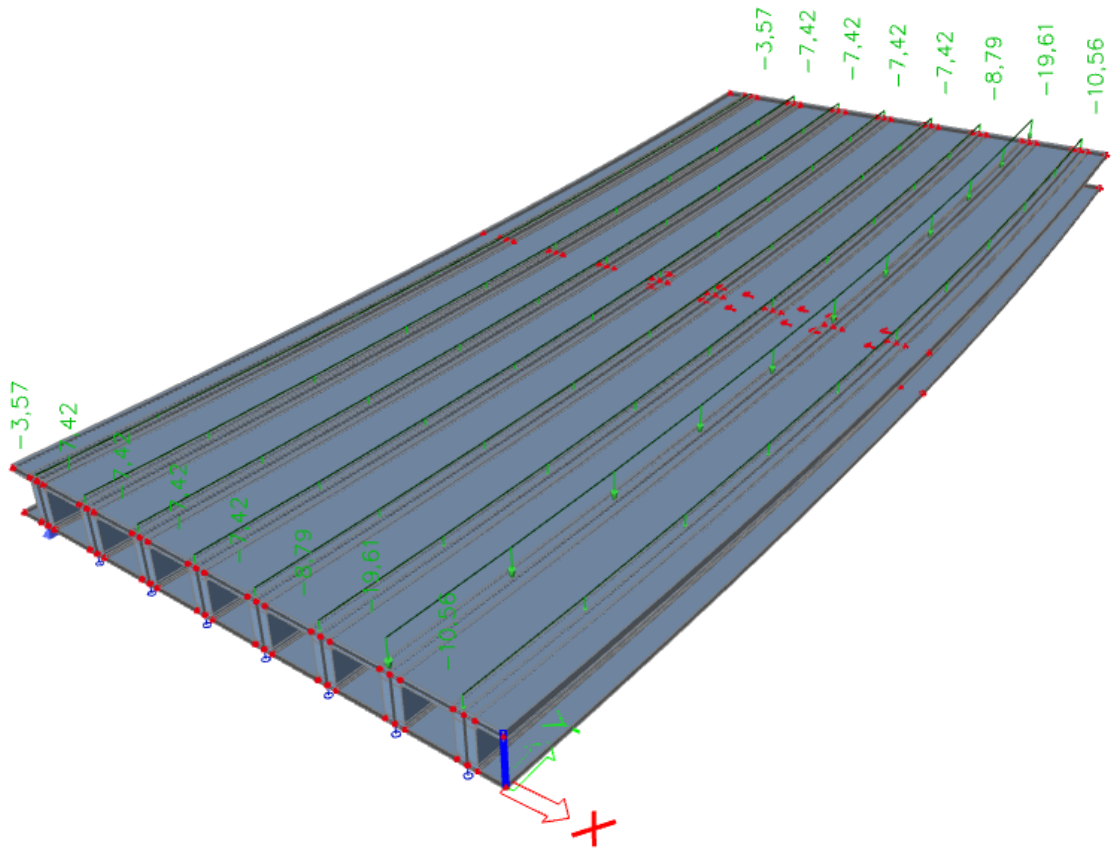

Figure 5.18: 3D plate model loaded with the uniform distributed load (curved deck)

II

Verification and results

6

Verification of stiffness

The first verification of the 3 different models of the bridge deck is the comparison between their longitudinal and transverse stiffness. In both directions, the stiffnesses of the models are compared to each other and they are compared to the analytical solution of the Timoshenko beam. In order to be able to make a fair comparison between the models and the analytical solution of the Timoshenko beam, the bridge deck is divided into a longitudinal and a transverse strip.

These strips are located in such a way that their cross-section is identical to the longitudinal and transverse beams of the grillage model. This is the easiest way to make equivalent strips for all models. The longitudinal strips have a width of 2.12 m and a length of 40 m and the transverse strips have a width of 2.353 m and a length of 16.96 m. Figure 6.1 shows the longitudinal (green) and transverse (red) strips, drawn in the 3D plate model.

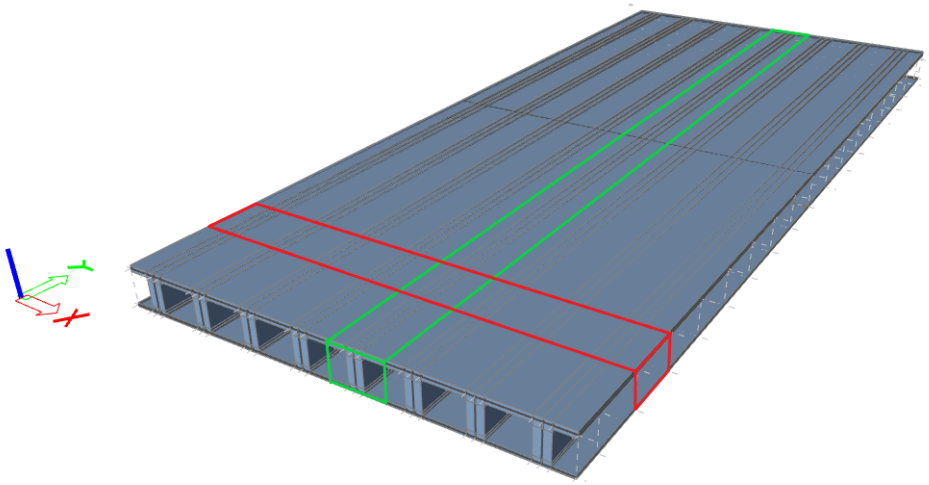

Figure 6.1: Longitudinal (green) and transverse (red) strip

6.1. Longitudinal direction

All strips in longitudinal direction have a width of 2.12 m. This width is equal to the with of the beams of the grillage model. The longitudinal strips are simply supported in both ends. The length of the strips is 40 m. In the middle of the span, the strips are loaded with a distributed load of $q = 500\,\text{kN/m}$, or a point load of $F = 1060\,\text{kN}$ in case of the grillage model and the analytical solution. The mechanical scheme of the longitudinal strips is shown in figure 6.2.

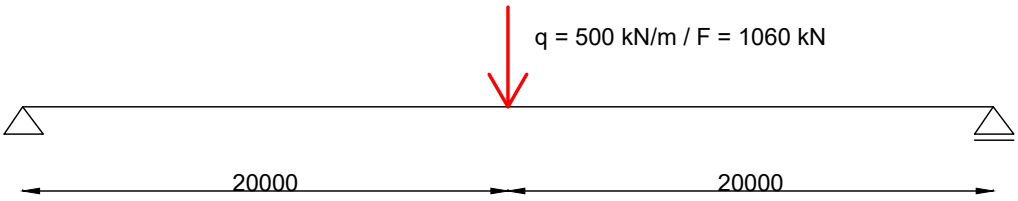

Figure 6.2: Mechanical scheme longitudinal strip (width=2120 mm)

Grillage model

The longitudinal strip of the grillage model consists of 1 longitudinal beam. This beam cannot be loaded with a distributed load, so the distributed load has been converted into a point load. This point load has a magnitude of $F = 500 \cdot 2.12 = 1060\,\text{kN}$. Figure 6.3 shows the deformed shape of the longitudinal strip from the grillage model. The maximum deflection is equal to 79.8 mm.

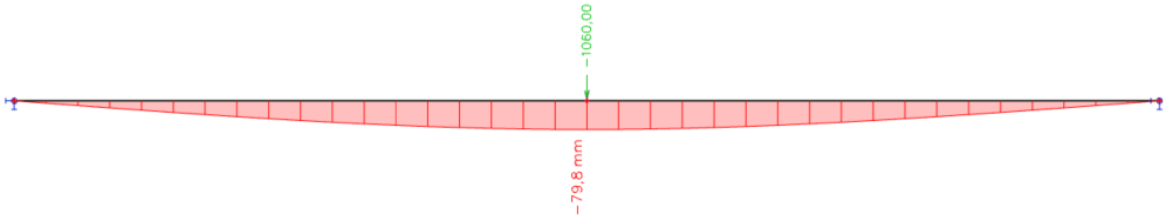

Figure 6.3: Deflection longitudinal strip grillage model (w_{max} = 79.8 mm)

Orthotropic plate model

For the orthotropic plate model, the maximum deflection of a longitudinal strip is equal to 79.8 mm. The deflected shape of this strip is shown in figure 6.4.

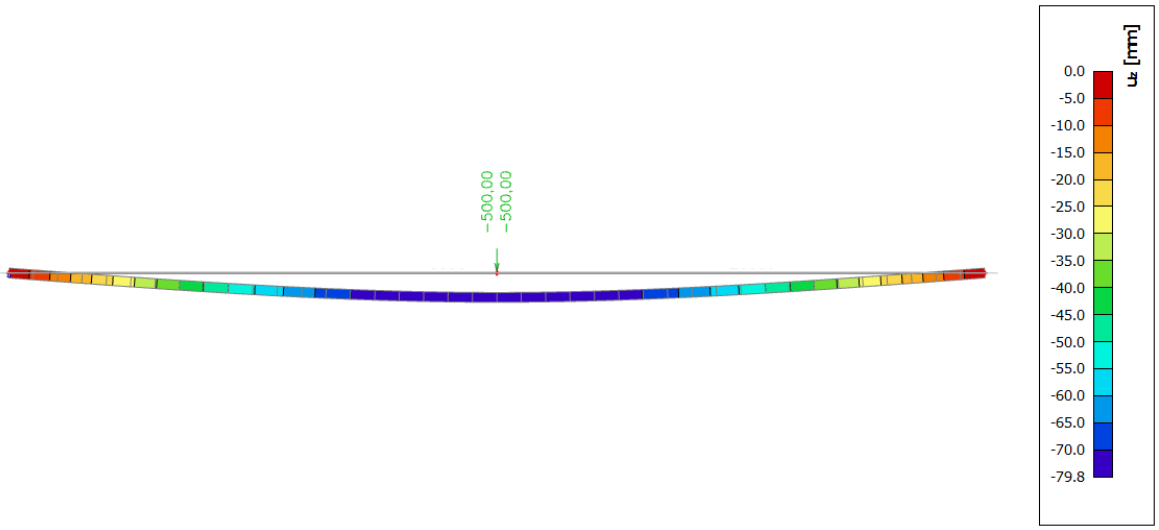

Figure 6.4: Deflection longitudinal strip orthotropic plate model (w_{max} = 79.8 mm)

3D plate model

The longitudinal strip of the 3D plate model consists of a spatial assembly of plates that form a H-section. At the ends, the bottom flanges of of the H-section are supported over the full width. The load is applied as a distributed load, which means that - at mid-span - the full width of the top flange is loaded. Figure 6.5 shows the deformed shape of the longitudinal strip taken out of the 3D plate model. The maximum deflection of this strip is equal to 79.4 mm.

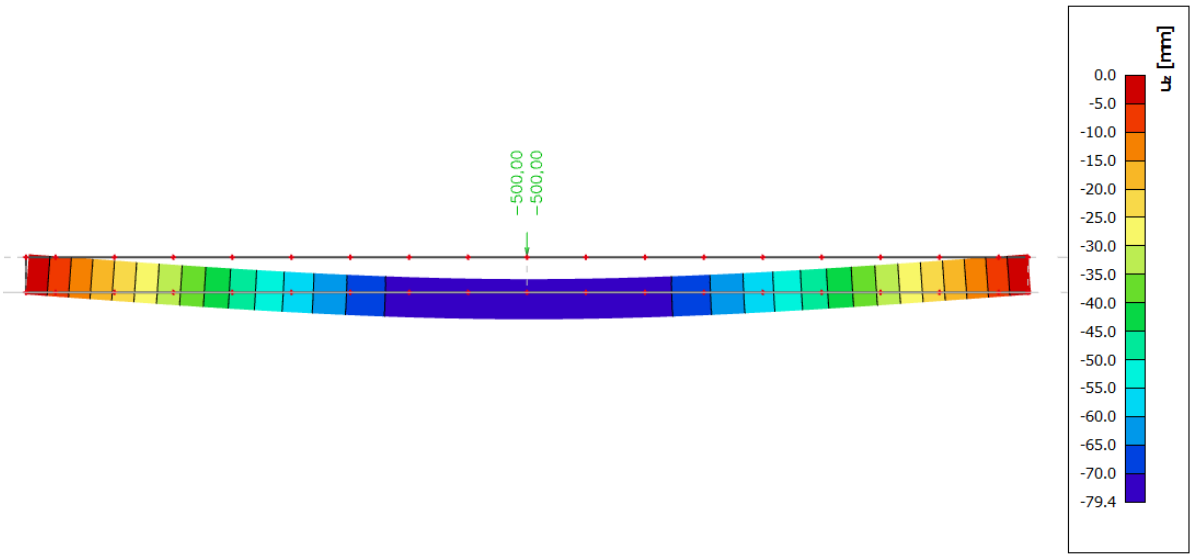

Figure 6.5: Deflection longitudinal strip 3D plate model (w_{max} = 79.4 mm)

Analytical solution

According to the forget-me-not of a simply supported Timoshenko beam with a point load at mid-span, the mid-span deflection is equal to [4]:

$$w = \frac{1}{48}\frac{Fl^3}{EI} + \frac{1}{4}\frac{Fl}{k_s} \tag{6.1}$$

The bending stiffness EI of the longitudinal strip is equal to the bending stiffness of the longitudinal beam from the grillage model. This bending stiffness is equal to:

$$EI = 36.3 \cdot 4.9488 \times 10^{11} = 1.7964 \times 10^{13}\,\text{kN mm}^2$$

The shear stiffness k_s can be calculated using the longitudinal shear stiffness of the orthotropic plate model (D_{55}).

$$D_{55} = 7.2600 \times 10^4\,\text{MN/m}^2 k_s = b \cdot D_{55} = 2.12 \cdot 7.2600 \times 10^4 = 9.075 \times 10^6\,\text{kN/m}$$

With $F = 1060$ kN and $l = 40\,000$ mm, according to equation 6.1 is equal to:

$$w = \frac{1}{48}\frac{1060 \cdot 40\,000^3}{1.7964 \times 10^{13}} + \frac{1}{4}\frac{1060 \cdot 40\,000}{9.075 \times 10^6} = 79.8\,\text{mm}$$

6.2. Transverse direction

For the transverse direction, the strips has a width of 2.353 m, which is equal to the width of a transverse beam of the grillage model. Again, the strips are simple supported in both ends. The transverse strips have a length of 16.96 mm. The loading consists of 2 distributed loads of $q = 500\,\text{kN/m}$ each, or a point load of $F = 1176.5\,\text{kN}$ each in case of the grillage model and the analytical solution. The loads are located above the 2 stiffeners in the middle of the span. This is at $7/16 \cdot l$ from the supports. The loading is not applied at mid-span, as for the 3D plate model this will result into local bending of the top plate. The mechanical scheme and the loading conditions of the transverse strip is shown in figure 6.6.

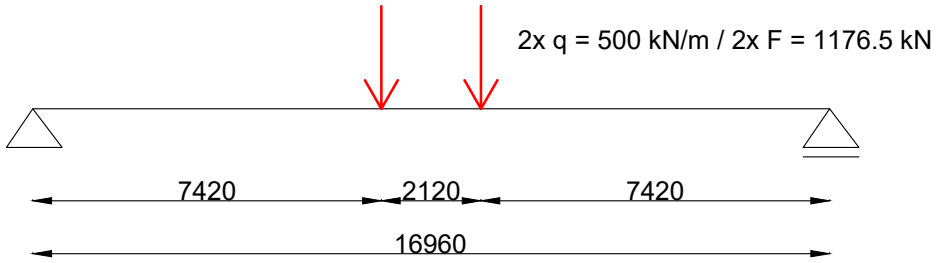

Figure 6.6: Mechanical scheme transverse strip (width=2353 mm)

Grillage model

The transverse strip of the grillage model is equal to the transverse beam of the grillage model. Figure 6.7 shows the deflected shape of this strip. The deflected shape clearly shows a combination of bending and shear deformation. At mid-span, the maximum deflection is equal to 28.9 mm.

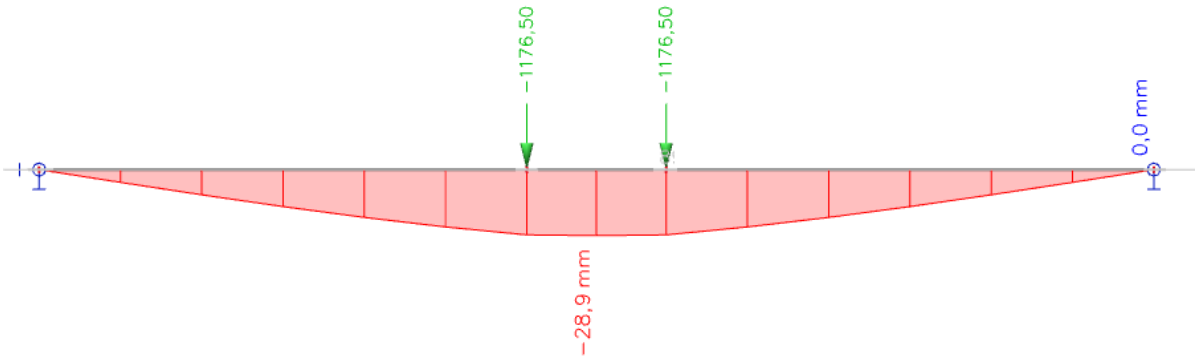

Figure 6.7: Deflection transverse strip grillage model (w_{max} = 28.9 mm)

Orthotropic plate model

For the orthotropic plate model, the maximum deflection of a transverse strip is equal to 28.8 mm. The deflected shape of this strip is shown in figure 6.8. Also this strip clearly shows a combination of bending and shear deformation.

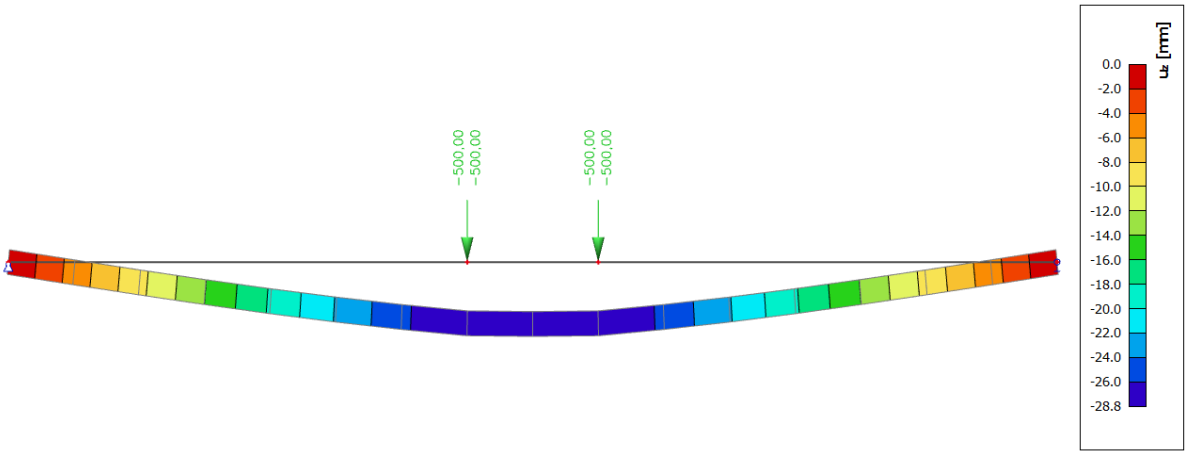

Figure 6.8: Deflection transverse strip orthotropic plate model (w_{max} = 28.8 mm)

3D plate model

The transverse strip of the 3D plate is supported at the bottom plate. In he field, the stiffeners force that the top and bottom plate act together. However, this is not the case for the top and bottom plate on the edges. This means that the total deflection of this strip will be a summation of global bending and shear deformation, but also local bending of the outer bottom plates.

In order to avoid local bending of the bottom plate the top and bottom plate are forced to act together by adding a plate that connects the top and bottom plate. The connection between the top and bottom plate and the dummy plate is a hinged connection. The thickness needed for the dummy plate was determined by looking at the relation between the thickness of this plate and the maximum deflection. It is assumed that only local bending of the bottom plate depends on the thickness of the dummy plate. When the total deflection of the strip doesn't decrease anymore, it can be assumed that the local bending of the bottom plate has vanished.

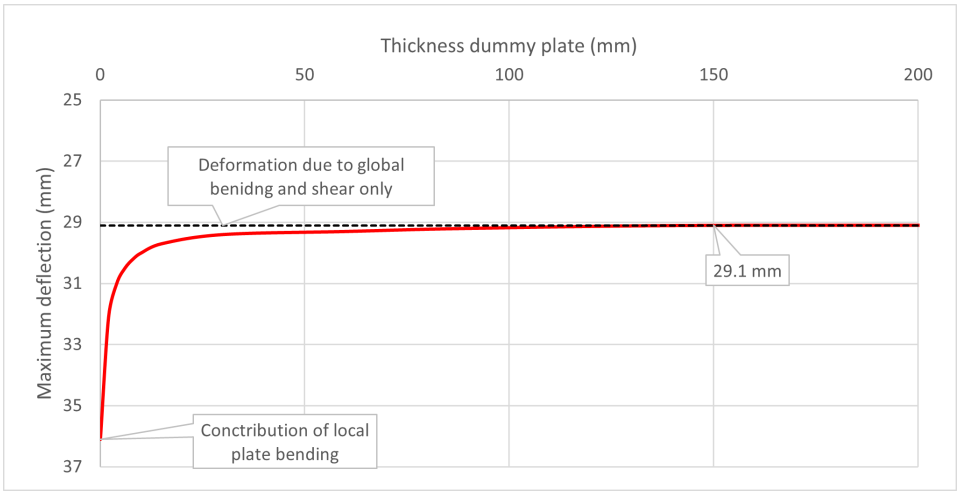

Figure 6.9: Relationship thickness dummy plate and maximum deflection (3D plate model)

Figure 6.9 shows the relation between the thickness of the dummy plate and the maximum deflection of the transverse strip of the 3D model. Please notice that the y-axis runs from 25 to 37 mm. From figure 6.9, it becomes clear that there is an asymptote at a deflection of 28.6 mm. Starting from a plate thickness of about 250 mm, the red line meets the asymptote. This means that for a plate thicknesses of 250 mm or thicker, the effect of local bending of the bottom plate can be assumed to be zero. The remaining part of the deflection is due to global bending and shear deformation.

In the transverse strip of the 3D model, the dummy plate has a thickness of 250 mm. From figure 6.9, it becomes clear that for a thicker plate, the maximum deflection does not decrease further. So, it

can be assumed that the transverse strip shown in figure 6.10 shows a deformed shape due to global bending and shear deformation. The maximum deflection is equal to 29.1 mm.

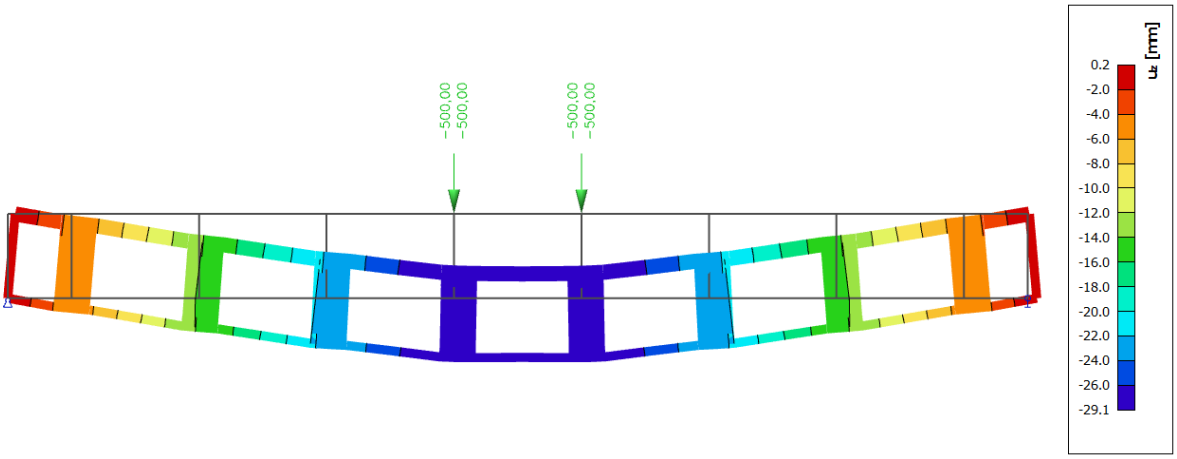

Figure 6.10: Deflection transverse strip 3D plate model (w_{max} = 29.1 mm)

Analytical solution
In the transverse direction of the bridge deck, the strips deform due to a combination of bending and shear deformation. The analytical solution that combines both these deformations is the Timoshenko beam. Equation 6.2 shows the general differential equation of the Timoshenko beam [8].

$$\begin{aligned} EI\frac{\mathrm{d}^2\varphi}{\mathrm{d}x^2} - k_s\left(\frac{\mathrm{d}w}{\mathrm{d}x} + \varphi\right) &= 0 \\ k_s\left(\frac{\mathrm{d}^2w}{\mathrm{d}x^2} + \frac{\mathrm{d}\varphi}{\mathrm{d}x}\right) &= -q \end{aligned} \tag{6.2}$$

The Timoshenko beam can be solved for the situation shown in figure 6.11. In this figure, a is the distance between the left support and the point load. Due to the point load the beam must be split into two fields. Using the relations of equations 6.3, and the boundary and interface conditions of table 6.1, the deflection of the Timoshenko beam can be solved.

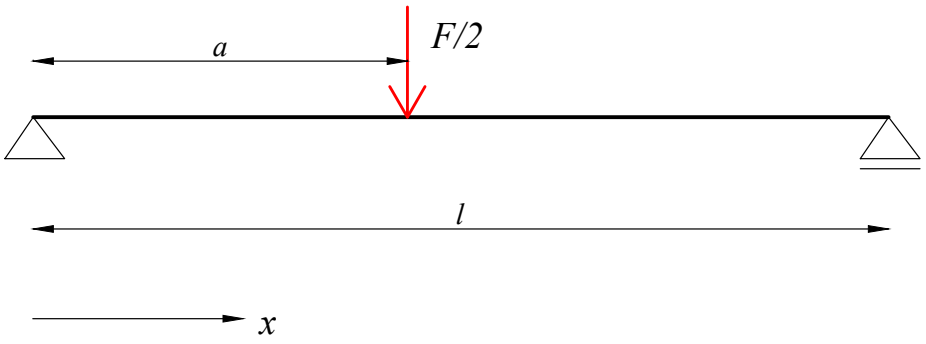

Figure 6.11: Model Timoshenko beam

$$\begin{aligned} q &= 0 \\ \gamma &= \frac{\mathrm{d}w}{\mathrm{d}x} + \varphi \\ M &= -EI\frac{\mathrm{d}^2w}{\mathrm{d}x^2} \\ V &= k_s \cdot \gamma \end{aligned} \tag{6.3}$$

Table 6.1: Overview of boundary and interface conditions Timoshenko beam

boundary conditions		**interface conditions**
$x = 0$	$x = L$	$x = a$
$w_1 = 0$	$w_2 = 0$	$w_1 = w_2$
$M_1 = 0$	$M_2 = 0$	$M_1 = M_2$
		$\phi_1 = \phi_2$
		$V_1 + F/2 + V_2 = 0$

The solution to the Timoshenko beam can be found using *Maple*. In order to find the solution to the load case of the transverse strip, the deflection due to F_1 and F_2 must be added (see figure 6.12). The deflection due to a single field is defined as w_{ab}, where index a is equal to the index of the load and index b is the field. For the total deflection, three different fields are distinguished (w_1, w_2 and w_3). Here, the indices represent the field. The boundaries of these fields, as well as the the total deflection per field can be found in table 6.2.

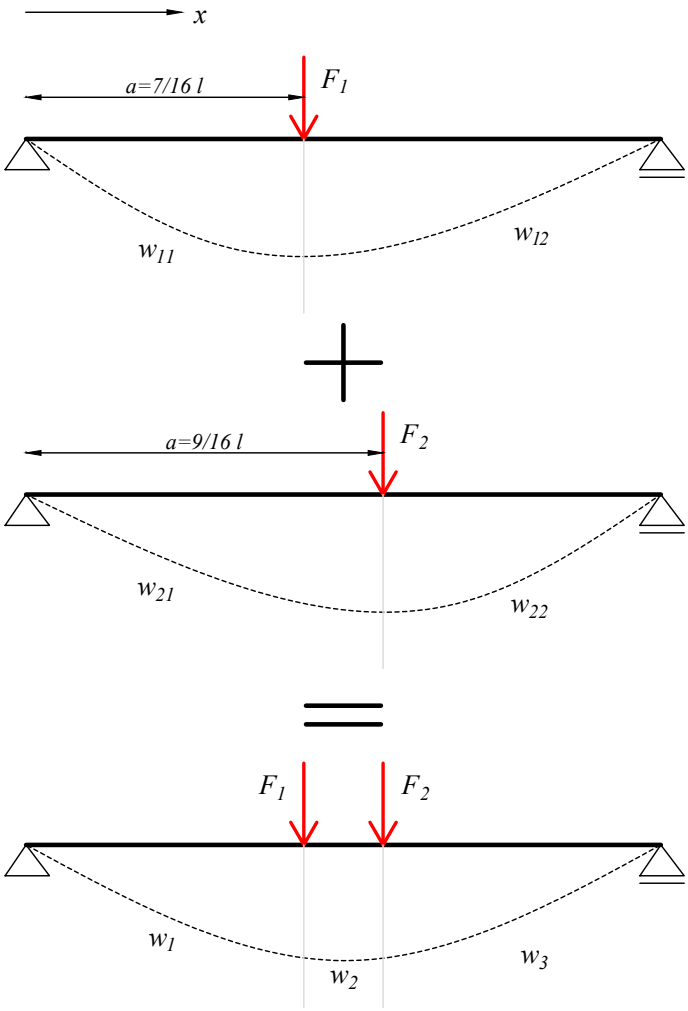

Figure 6.12: Summation of deflections Timoshenko beam

Table 6.2: Sum of deflections, split into 3 fields

field	boundaries	total deflection
1	$0 \leq x \leq \frac{7}{16}l$	$w_1 = w_{11} + w_{12}$
2	$\frac{7}{16}l \leq x \leq \frac{9}{16}l$	$w_2 = w_{12} + w_{21}$
3	$\frac{9}{16}l \leq x \leq l$	$w_3 = w_{12} + w_{22}$

As the loading of the transverse strip is symmetrical, the total maximum deflection can be found in the middle of the span. So, the analytical solution to the maximum deflection of the Timoshenko beam with one point load at $a_1 = \frac{7}{16}l$ and the other point load at $a_2 = \frac{9}{16}l$, can be found by taking w_2 and setting $x = \frac{1}{2}l$:

$$w_2\left(x = \frac{1}{2}l\right) = \frac{1001}{49152}\frac{Fl^3}{EI} + \frac{10752}{49152}\frac{Fl}{k_s} \tag{6.4}$$

In this formula, F is the sum of both forces and both forces must be equal, otherwise the maximum deflection is not at $x = \frac{1}{2}l$. So: $F = F_1 + F_2$, with $F_1 = F_2 = 1176.5\,\text{kN}$. So: $F = 2353\,\text{kN}$. The factors $\frac{1001}{49152}$ and $\frac{10752}{49152}$ from equation 6.4 are almost equal to the factors from the analytical solution

of a Timoshenko beam with only one point load in the middle of the span ($\frac{1}{48}$ and $\frac{1}{4}$). In case of the transverse strip, the point loads are close to mid-span. So, it makes sense that the difference between these factors is very small.
For the transverse strip, the bending stiffness EI is equal to the Young's modulus times the second moment of inertia of the transverse beam of the grillage model:

$$EI = 36.3 \cdot 4.3609 \times 10^{11} = 1.5830 \times 10^{13}\,\text{kN mm}^2$$

The shear stiffness k_s is equal to stiffness component D_{44} from the orthotropic plate model times the width of the transverse strip:

$$k_s = 2.353 \cdot 2.6205 \times 10^{5} = 616\,603\,\text{kN/mm}$$

Filling in the stiffness parameters, load and span of the transverse strip into equation 6.4, results into a deflection of:

$$w = \frac{1001}{49\,152} \cdot \frac{2353 \cdot 16\,960^3}{1.5830 \times 10^{13}} + \frac{10\,752}{49\,152} \cdot \frac{2353 \cdot 16\,960}{616\,603} = 28.9\,\text{mm}$$

2D plate model
For all models, the (shear) stiffness of the transverse strips depends on the effective height of the web-zone of the 3D plate model (section 5.2.1) in any way. In the 3D plate model, the effective height of the web-zone is a direct input parameter for the orthotropic plates in the web-zone. For the orthotropic plate and grillage model, the effective heights of the top and bottom plate in the web-zone are used as an input parameter for the transverse shear stiffness calculation, which is shown in appendix C. The shear stiffness calculation eventually results into the shear stiffness parameters D_{44} (orthotropic plate model), A_s (grillage model) and k_s (Timoshenko beam).

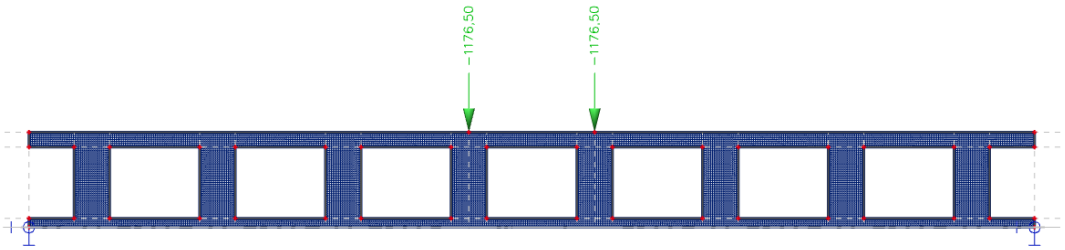

Figure 6.13: 2D plate model transverse strip

A model that does not depend on the transverse shear stiffness calculation shown in appendix C, is a 2D plate model. In this model, the transverse cross-section of the deck is modelled using a vertical orientated plate with openings in it, see figure 6.13. In the out-of-plane direction, this plate has a thickness of 2.353 m, which is equal to the width of the transverse strips.

For the 2D plate model it is important to have a finite element mesh that is coarse enough. The size of the finite elements was determined by assuming at least 6 nodes over the thickness of the smallest zone. This smallest zone is the bottom plate of the bridge deck. The thickness of the bottom plate is 150 mm, so the size of the finite elements must be equal to $h = 150/(6-1) = 30$ mm. Figure 6.14 shows the finite element mesh of part of the 2D plate model.

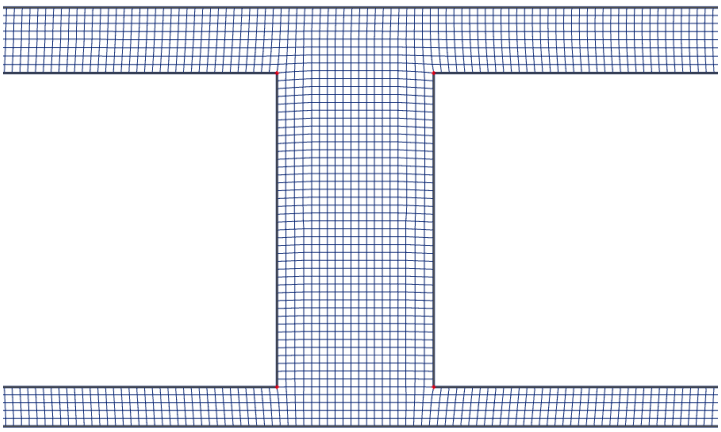

Figure 6.14: Mesh 2D plate model ($h \approx 30$ mm)

From figure 6.15, it becomes clear that the maximum deflection of the 2D plate model is equal to 28.8 mm.

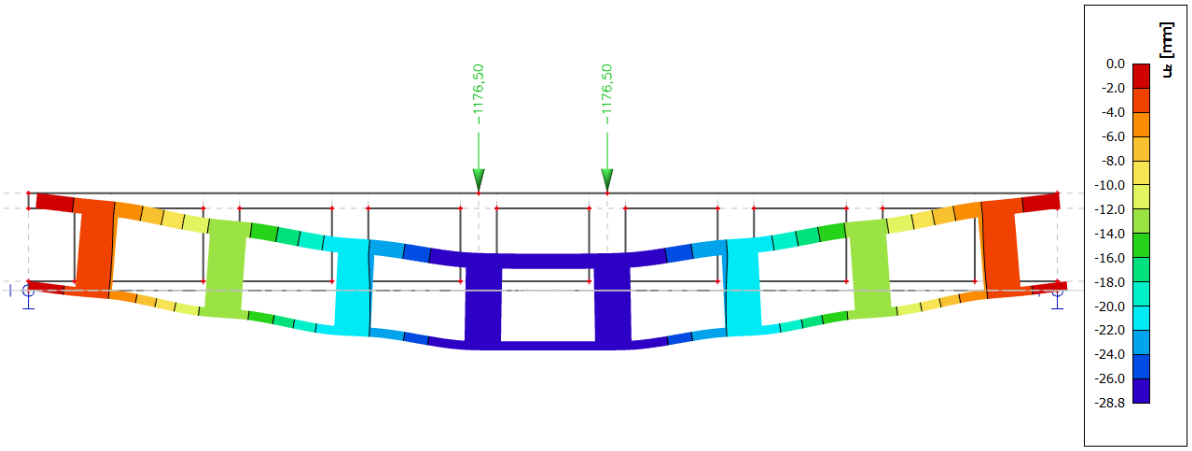

Figure 6.15: Deflection transverse strip 2D plate model ($w_{max} = 28.8$ mm)

6.3. Conclusions

Table 6.3 gives an overview of the deflections (w) of the longitudinal and transverse strips taken out of the 3 different models of the bridge deck and the analytical solutions. For both the longitudinal as well as the transverse direction, the relative difference (%) with respect to the analytical solution is shown.

Table 6.3: Overview of maximum deflections strip models (mm)

model	**longitudinal strip**		**transverse strip**	
	w_{max}	%	w_{max}	%
Analytical	79.8	-	28.9	-
Grillage	79.8	-	28.9	0.0
Orthotropic plate	79.8	-	28.8	-0.3
3D plate	79.4	-0.5	28.9	0.0
2D plate	-	-	28.8	-0.3

From the results of the strip models, it can be concluded that:

- In both directions, the relative difference between the models is insignificant. The biggest difference between the deflections of the strips is only 0.5%. This means that all models have the same stiffness in the longitudinal and transverse direction of the deck;
- The transverse stiffness parameters of the analytical, grillage, orthotropic plate and 3D plate model are reliable. The independent 2D plate model showed the same maximum deflection / stiffness as the other transverse strips.

7

Straight deck

In this chapter, the results of the straight bridge deck are shown. This bridge deck was loaded with dummy loads. The results of the curved and curved and skewed bridge deck layout are presented in chapter 8 and 9.

In this chapter, the results of the grillage model, orthotropic plate and 3D plate model are compared. This comparison is done for: reaction forces, bending moments, mid-span deflection and shear forces. For the reaction forces, mid-span deflection and longitudinal bending moment, the results of the orthotropic plate model are compared to the 3D plate model. For all other type of results, the results of the 3D plate model are not considered.

The conclusions that can be drawn on the results of the straight bridge deck are shown in the last section of this chapter.

7.1. Reaction forces

For all models, the reaction forces can be extracted directly from SCIA-engineer. In the graphs presented, the supports are labeled according to the labelling of the longitudinal grid-lines. This labelling can be seen in figure 7.1. In this figure, the supports are indicated with a blue circles and a blue square at grid line B.

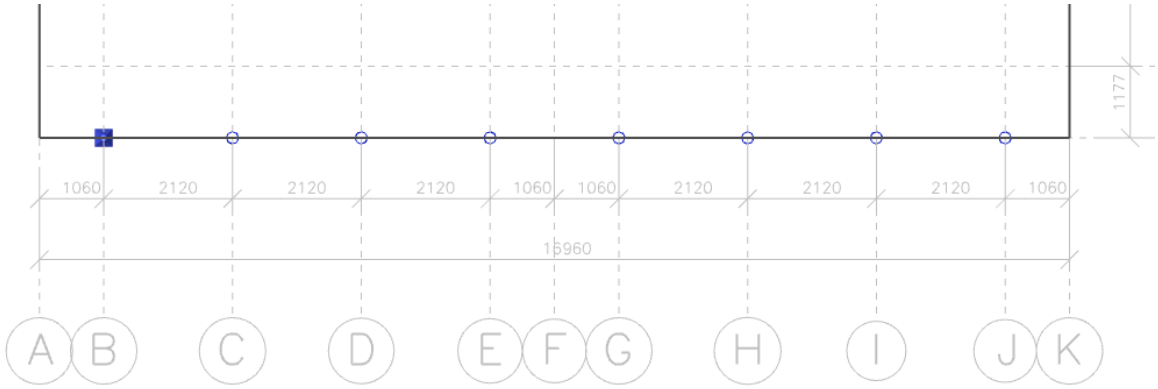

Figure 7.1: Names of the supports

Figure 7.2 shows the reaction forces for LC1, LC3, LC6 and LC7 of the straight deck. A complete overview of the reaction forces for load-case 1 till 7 can be found in appendix E. In the graphs of figure 7.2, the names of the supports are indicated along the x-axis. This naming is derived from the position of the supports with respect to the grid-lines of the models, see figure 7.1

For all load-cases, the sum of the reaction forces is equal to 4240 kN for LC1 and 500 kN for the other load-cases, per edge of the deck. This is equal to half of the force applied for these load-cases.

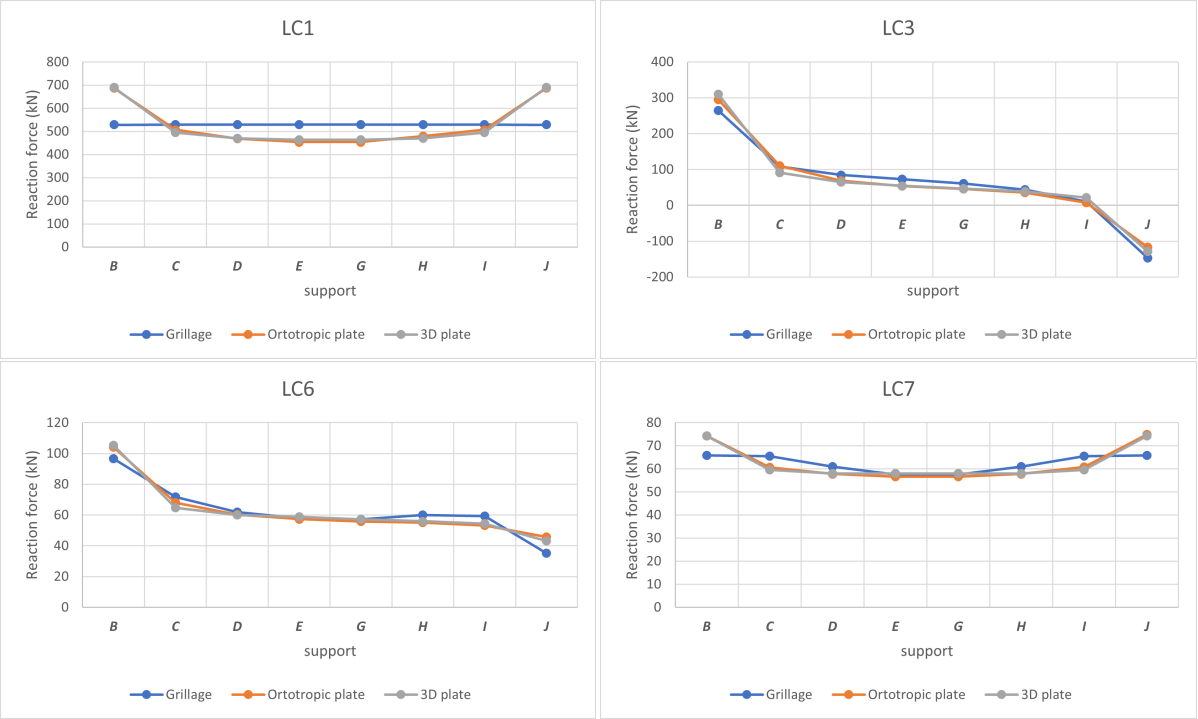

Figure 7.2: Reaction forces straight deck: LC1, LC3, LC6 and LC7

This means that for all models the condition of equilibrium is met: the sum of the applied force is equal to the sum of the reaction forces.

From figure 7.2, it follows that the reaction forces of the orthotropic plate model and the 3D plate model are almost overlapping. This is the case for all load-cases, also the ones for which the reaction forces are presented in appendix E only. The reaction forces of the grillage model are clearly different compared to the other 2 models.

The orthotropic plate and 3D plate model give higher support reactions at the outer supports, for the load-case of a distributed load (LC1). The grillage model, results in an almost constant reaction force over the different support in transverse direction of the deck.

This can be attributed to the concentrated shear force on the edge of a plate. From plate theory, it follows that this concentrated shear force is equal to $V = m_{xy}$ [2]. For the grillage model, this concentrated shear force is not observed as the grillage model consists of beam elements.

As a result of the peaks at the outer supports, it is difficult to draw conclusions on the transverse load-spread based upon the reaction forces. load-case 3 for example, shows for the grillage model the lowest support reaction at the position of the point load (LC3). In order to make equilibrium with the applied force, the remaining supports have to take a larger part of the applied force, which is also observed. This could indicate that the grillage model shows more transverse load-spread compared to the orthotropic plate and 3D plate model. However, the effect of the concentrated shear force of the orthotropic plate and 3D plate model and the difference in transverse load-spread could interfere. This means that it is not possible to distinguish the effects and to judge which effect is stronger.

In order to be able to draw conclusions on the transverse load-spread of the different models, it is easier to look at the longitudinal bending moments.

7.2. Mid-span deflection

In this section, the grillage model, orthotropic plate model and 3D plate model are being compared by looking at the deflection at the middle of the span. This is done by plotting the deflection line over the mid-span transverse cross-section of the bridge deck. Figure 7.3 shows the mid-span deflection lines for the load-case with the distributed load (LC1).

For the grillage model and orthotropic plate model, the deflection is independent from the height of the deck. However, for the 3D plate model the deflection depends on the vertical position one is looking

at. The deflection of the 3D plate model plotted in the graphs of figure 7.3 is at the top of the deck.

In the left graph of figure 7.3, the vertical axis runs from 0-100 mm deflection. For the right graph, the scaling is adjusted to 75-85 mm, which gives a clearer picture of the differences between the deflection lines of the 3 models. For both graphs, the vertical axis runs from 0-16.96 m, which is equal to the width of the bridge decks.

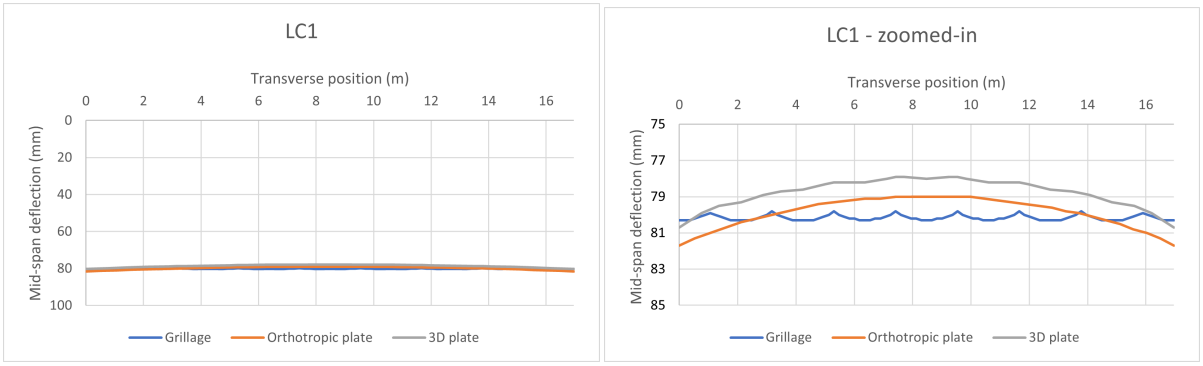

Figure 7.3: Mid-span deflection LC1

The left graph of figure 7.3 shows that for LC1 the absolute values of the mid-span deflections of all models are almost identical. However, the right graph shows that for the grillage model, the shape of the deflection line is different compared to the other 2 models. For the grillage model, one can observe local deflection of the mid-span transverse beam in between the longitudinal beams. For all longitudinal beams, the mid-span deflection is more or less identical.

For the orthotropic plate model and the 3D plate model, the shape of the deflection line is almost identical. The difference between the orthotropic plate model and the 3D plate model is almost constant over the whole mid-span cross-section. The deflection line of the orthotropic plate model is more smooth compared to the 3D plate model.

For the orthotropic plate model, the stiffness of the stiffeners is distributed over the whole width of the deck, while for the 3D plate model, the longitudinal stiffness varies over the transverse direction of the deck. The deflection line of the 3D plate model also shows local deflection in between the stiffeners, which is also observed for the grillage model. For the grillage model, this local deflection is larger compared to the 3D plate model, as the local load-spread in longitudinal direction is limited by the width of the transverse beams.

Figure 7.4 shows the deflections in the middle of the span for LC2 till LC7. For each model, these lines are shown in a different graph. For all graphs, the scale of the vertical and horizontal axis is identical. The horizontal axis runs from 0-16.96 m, which is equal to the width of the bridge deck. In addition to the graphs of figure 7.4, the for each load-case the minimum, maximum and mean deflection are listed in table 7.1.

Table 7.1: Minimum, maximum and average mid-span deflection. *G = grillage model, OP = orthotropic plate model and 3DP = 3D plate model*

	min. (mm)			**max.** (mm)			**average** (mm)		
load-case	**G**	**OP**	**3DP**	**G**	**OP**	**3DP**	**G**	**OP**	**3DP**
LC1	79.8	79.0	77.9	80.3	81.7	80.7	80.1	79.8	78.7
LC2	2.5	5.5	5.5	19.5	16.2	15.0	9.5	9.5	9.5
LC3	3.2	5.9	5.9	16.8	14.5	14.2	9.4	9.4	9.4
LC4	4.7	6.7	6.6	14.2	12.7	12.4	9.4	9.3	9.3
LC5	6.4	7.6	7.5	12.0	11.1	10.9	9.4	9.3	9.2
LC6	8.1	8.6	8.5	10.2	10.1	9.7	9.4	9.3	9.2
LC7	9.0	9.2	9.0	9.9	9.7	9.5	9.4	9.3	9.2

From figure 7.4 and table 7.1, it becomes clear that for the orthotropic plate model and the 3D plate model, the deflections are almost identical. For all load-cases, the difference between the minimum,

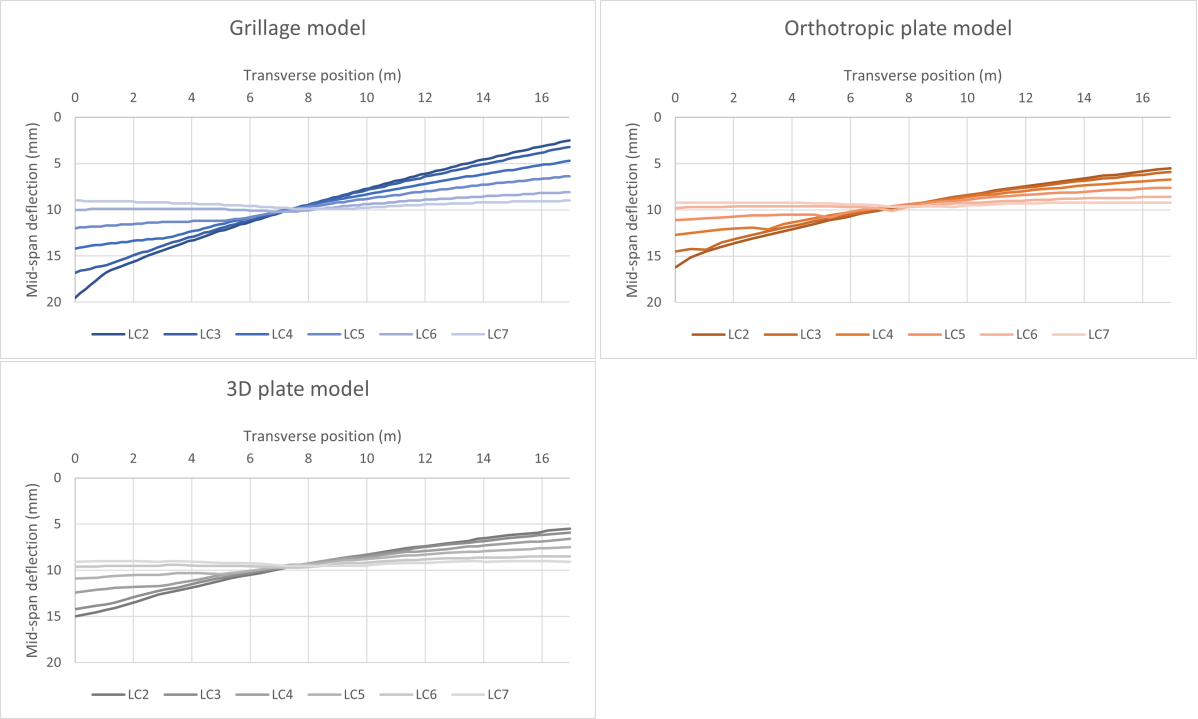

Figure 7.4: Mid-span deflection LC2 till LC7, per model

maximum and mean deflection is relatively small.

The deflection of the grillage model is clearly different from the other 2 models. From table 7.1, it can be read that the mean deflection of the grillage model is close to the mean deflection of the other models. However, the minimum and maximum deflections of the grillage model deviate from the other models. This effect becomes larger for more eccentric applied loads.

From these observations, it can be concluded that the deflection line of the grillage model is a summation of 2 effects. The grillage model deflects in the same way as the other 2 models and on top of that, the deck rotates a bit around its longitudinal axis. The magnitude of this rotations depends on the eccentricity of the applied force. Eventually, the rotation lowers the minimum deflection and increases the maximum deflection, but the total area under the deflection line does not change.

7.2.1. Guyon-Massonnet

The transverse load-spread can also be verified using Guyon-Masssonnet. The theory of this method is introduced in appendix D (page 145). Shortly speaking, the bridge deck is divided into 9 nodes in the transverse direction of the bridge deck. To each nodes belongs a *coefficient of lateral distribution* (k). From this coefficient k, it can be determined which part of the load goes to which node. The coefficient k is determined as the local deflection of the deck $w(y)$ over a transverse cross-section, divided by the average deflection (w_0) in the transverse direction of the bridge deck.

For each of the 3 models, the mid-span deflection (as shown in figure 7.4) can be used to determine the coefficient of lateral distribution k. This can be done by dividing each local deflection by the mean deflection over the transverse cross-section. This results into the coefficients of lateral distribution of the 3 models. These values can be compared to the theoretical values of k following from Guyon-Massonnet. For the Blankenburg case, the calculation of the coefficients of lateral distribution from the Guyon-Massonnet method can be found in appendix D.

Figure 7.5 shows the coefficients of lateral distribution for each of the 3 models and the theoretical result of Guyon-Massonnet (k_α for $\alpha = 0.68$ and $\alpha = 1$) for the bridge decks loaded with LC3 and LC7. The k-values of Guyon-Massonnet are indicated with k0.68 (as $\alpha = 0.68$ for the Blankenburg case) and k1 which are de k-values for a torsion stiff case.

In figure 7.5, it can be seen that for LC3 the results of the orthotropic plate and the 3D plate model

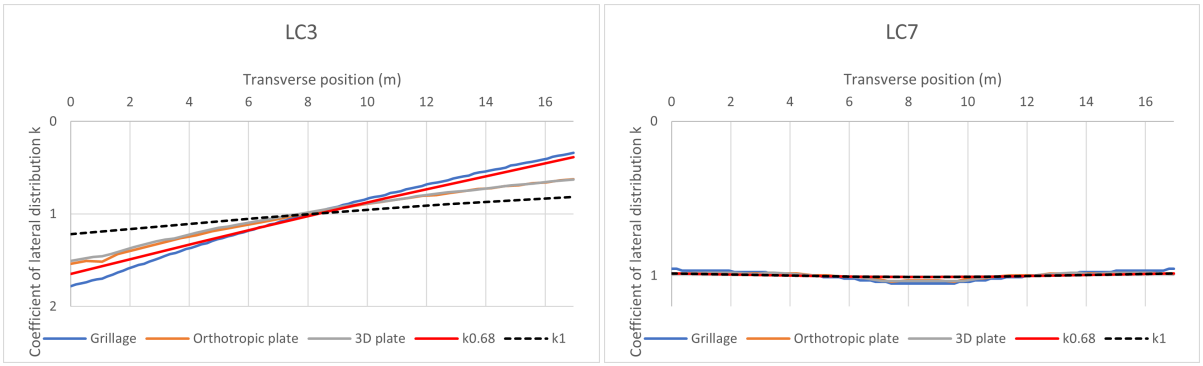

Figure 7.5: Coefficients of lateral distribution k, LC3 and LC7

are almost identical. The coefficient of lateral distribution for the grillage model does deviate from the other 2 models. The result of Guyon-Massonnet (k0.68, figure 7.5) is closest to the result of the grillage model. However, for the left part of the bridge deck ($\approx$ 0-8 m), the red line of k0.68 lies just as far from the result of the grillage model and the results of the other 2 models. The results of the orthotropic plate and 3D plate model are closer to k1 (torsion stiff case) compared to the grillage model. From this, it can be concluded that the grillage model has a lower torsional stiffness compared to the other 2 models.

For LC7, the coefficients of lateral distribution are almost equal to 1 for all models and the results of Guyon-Massonnet (k_α for $\alpha = 0.68$ and $\alpha = 1$). load-case 7 consists of 2 centric applied point loads. This loading results in an almost uniform deflection of the mid-span transverse cross-section, which means that $k \approx 1$. In the middle of the bridge deck, the k-values of the grillage model are slightly larger compared to the other models and on both edges, the k-values are slightly smaller. This shows that also for LC7, the grillage model shows less transverse load-spread compared to the other models.

The k-values for the Blankenburg case (k0.68) are closest to the grillage model, however the Guyon-Massonnet is an approximation and the transverse shear stiffness is not incorporated in this method. That makes it hard to compare the values of k0.68 to the 3 models and draw conclusions based upon their relative differences. Instead, it can be concluded that the results of Guyon-Massonnet showed that the grillage model has less torsional stiffness compared to the other 2 models as the results of the orthotropic plate and 3D plate model are closer to k1 (torsion stiff) compared to the grillage model. Also from the coefficients of lateral distribution, it follows that the grillage model shows less transverse load-spread.

7.3. Bending moments

In the following section, the longitudinal, transverse and torsional moment of the different models are compared. The longitudinal and transverse bending moments are given per width of beams of the grillage model, which is 2.12 m for the longitudinal and 2.353 m for the transverse beams. The longitudinal bending moments are shown for all models (grillage, orthotropic plate and 3D plate). The transverse and torsional bending moments are shown for the grillage and orthotropic plate model only.

7.3.1. Longitudinal bending moments

For the grillage model, the longitudinal bending moments can be directly extracted from the individual longitudinal beams. For the orthotropic plate model, it is needed to integrate the bending moments over the same with as the width of the longitudinal beams of the grillage model in order to be able to compare the results. These integration strips had the same width as the longitudinal beams of the grillage model. In the integration strips, the bending moment is over the width of the integration strip. This results into 8 bending moment diagrams that can be compared to the 8 bending moments diagrams of the longitudinal beams of the grillage model.

Figure 7.6 shows a 3D top view of the the grillage model. This figure includes the bending moment diagrams for longitudinal bending for each of the 8 longitudinal beams. The green lines on both ends of the deck, mark the line at which the deck is supported. The red line marks grid line 10, which is the grid line in the middle of the span.

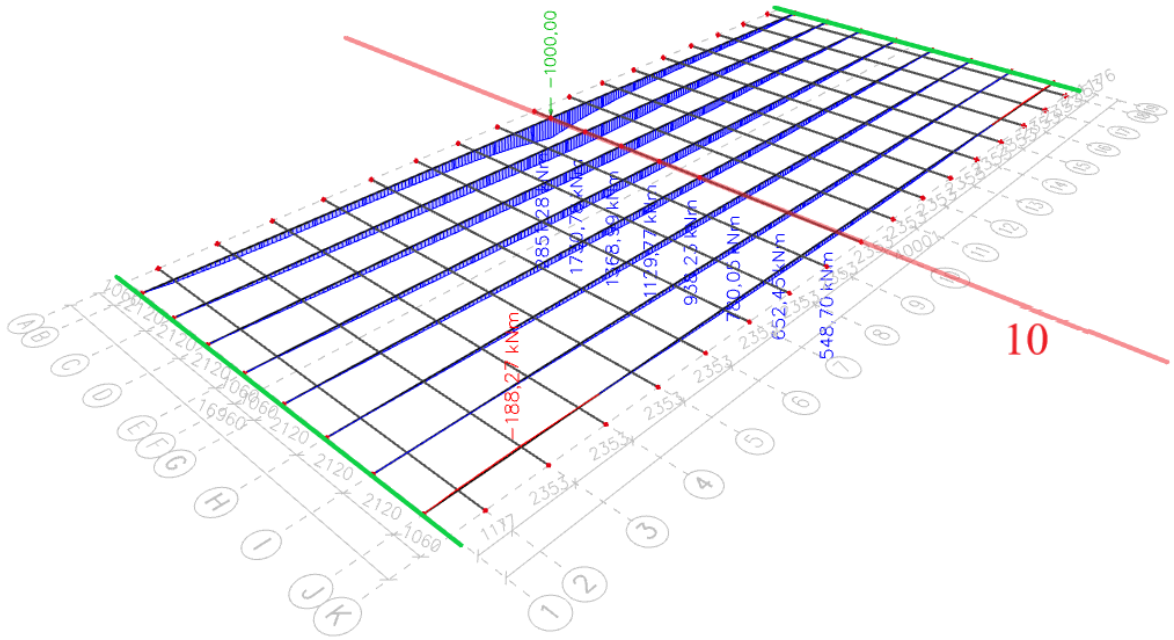

Figure 7.6: Longitudinal bending moments (M_y) of the grillage model (LC3)

Figure 7.7 shows the longitudinal bending moments of the grillage model. Again, the middle of the span (grid line 10) is marked with the red line and the lines along which the point supports are located are marked with green.

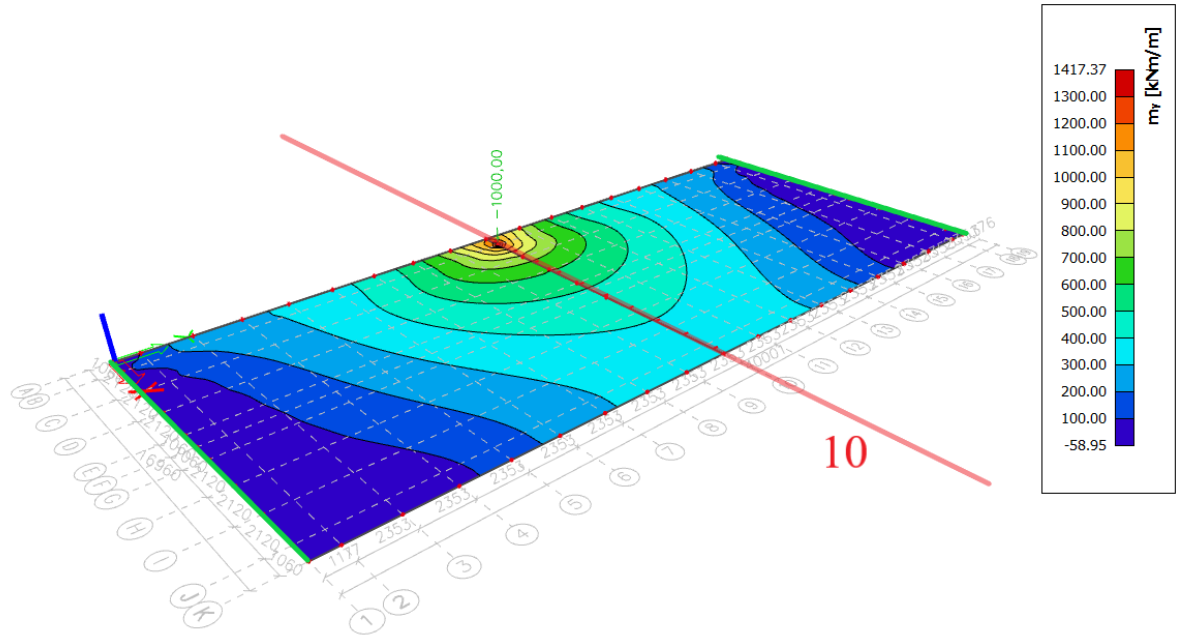

Figure 7.7: Longitudinal bending moments ($m_y y$) of the orthotropic plate model (LC3)

In order to be able to compare the longitudinal bending moments of the orthotropic plate model to the longitudinal bending moments of the grillage model, 8 sections were created in the middle of the span (along grid line 10) of the orthotropic plate. Each of the sections has a width of 2120 mm, which is equal to the width of each of the 8 longitudinal beams from the grillage model. Over each section, the

average longitudinal bending moment can be plotted, this plot can be seen in figure 7.8. The average longitudinal bending moment over the section is multiplied with the width of the section, in order to obtain the to total longitudinal bending moment acting on a plate strip with a width of 2120 mm. These bending moments are one-to-one comparable to the bending moments of longitudinal members of the grillage model.

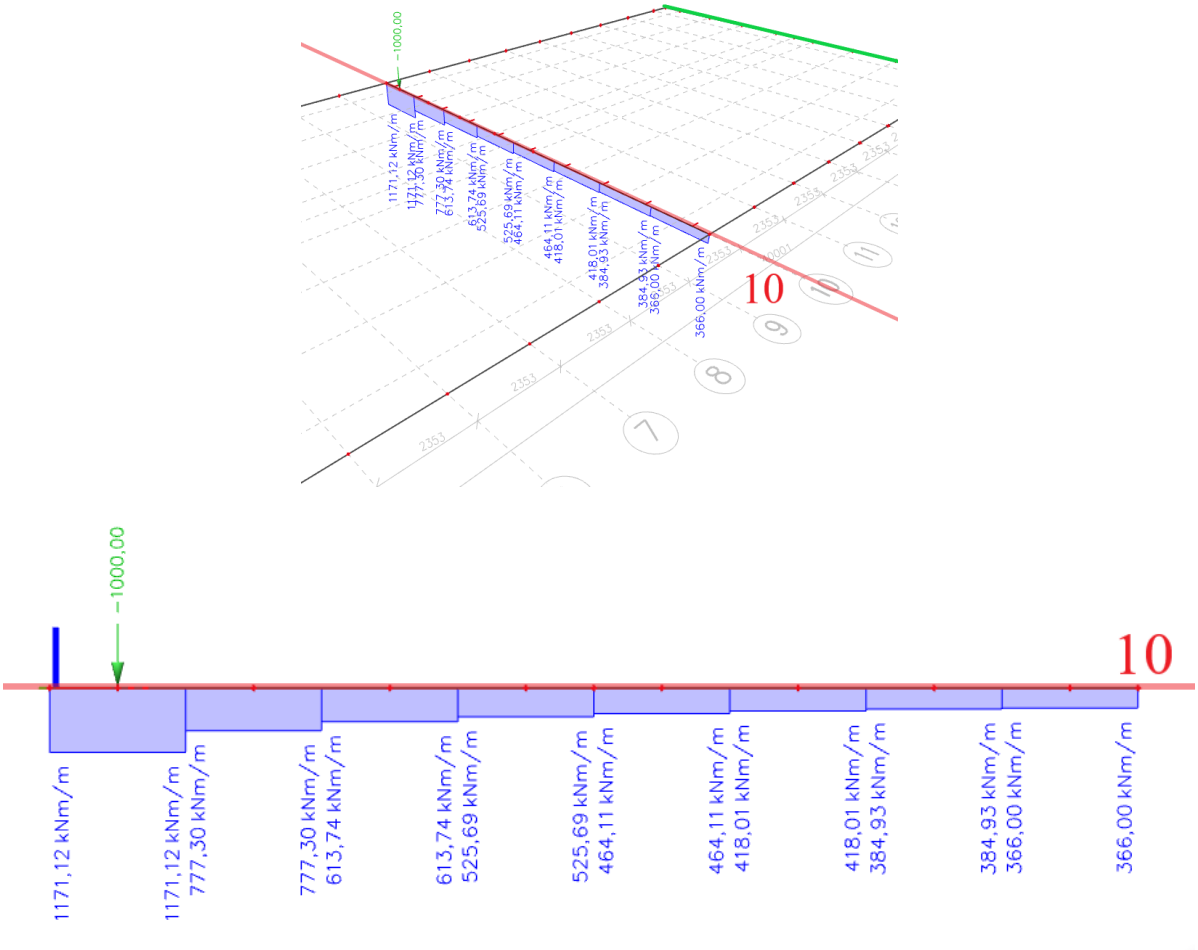

Figure 7.8: Average longitudinal bending moment over 8 sections (w=2120 mm) along grid line 10 (LC3)

Figure 7.9 shows the longitudinal bending moments in the middle of the span of the deck, for 4 of the 7 load-cases. The results for all the load-cases can be found in appendix E (page 151). For all load-cases, it can be observed that the global maximum longitudinal bending moment is always higher for the grillage model compared to the orthotropic plate model and the 3D plate model. For the load-case of the transverse distributed load (LC1), the results of all models are almost identical. The difference in the global maximum is about 1% with respect to the 3D plate model. For all load-cases, the longitudinal bending moments of the orthotropic plate model is almost equal to the longitudinal bending moments of the 3D plate model.

The load-cases with the point loads show a larger difference in longitudinal bending moment. Load-case 3, is a load-case in which the point load is applied with a big eccentricity with respect to the shear centre of the bridge deck. The point load of LC3 is applied at grid-line B. From figure 7.9, it follows that the longitudinal bending moment at the position of the point load (grid-line B) is larger for the grillage model compared to the orthotropic plate and 3D plate model.

On the opposite side of the deck, the opposite is observed: here the bending moment of the orthotropic plate and 3D plate model is larger compared to the grillage model. This means that for the grillage model, there is less transverse load-spread compared to the orthotropic plate and 3D plate model. For the orthotropic plate and 3D plate model, the minimum and maximum bending moment are

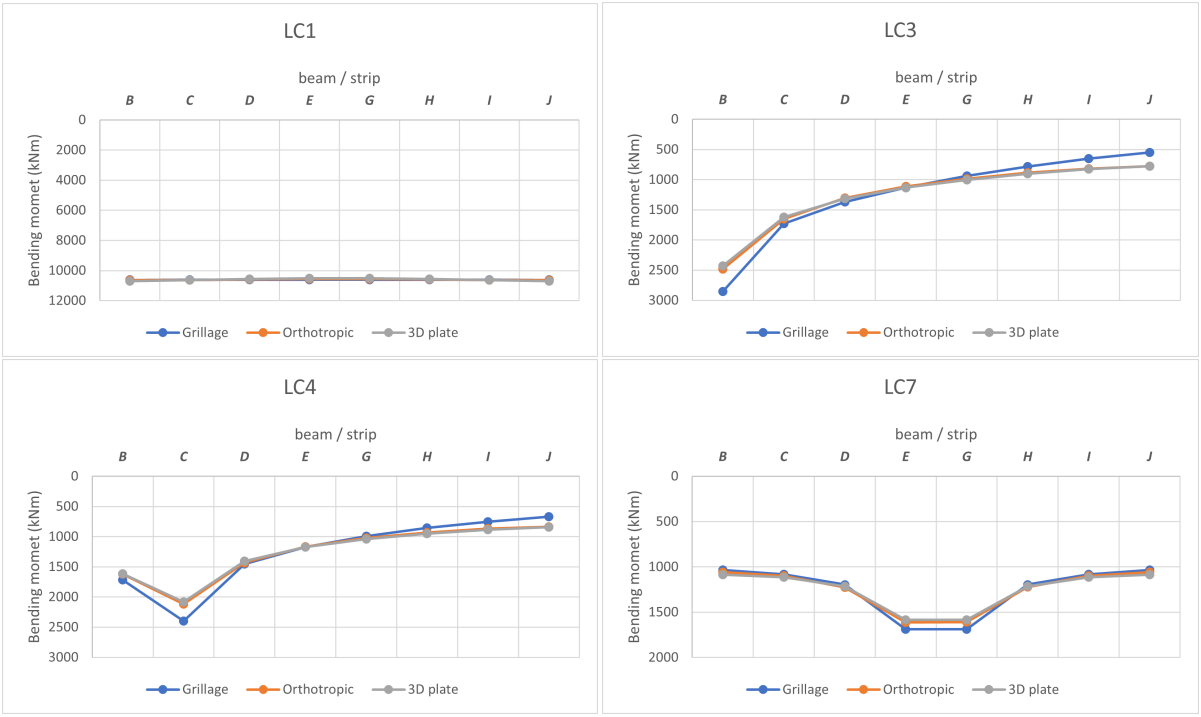

Figure 7.9: Longitudinal bending moments for LC1, LC3, LC4 and LC7

closer to each other, which means that the load has spread out more evenly in the transverse direction of the deck.

In the grillage model, a larger part of the loading stays in the zone at which the load is applied. As the sum of the bending moments over the whole mid-span cross-section must be equal for all 3 models (the loading is identical, so over each transverse cross-section the total longitudinal bending moment must also be identical), this means that the plate part away from the point load is loaded less.

For all other load-cases, it is observed that the grillage model shows less transverse load-spread compared to the orthotropic plate and 3D plate model. Also for the centric loaded deck (LC7), it can be observed that the longitudinal bending moment in the zone of the load is larger for the grillage model and in other zones the bending moment of the grillage model is smaller. However, for LC7, the difference in transverse load-spread is smaller compared to for example LC2. The transverse load-spread of the orthotropic plate model is more or less identical to the load-spread of the 3D plate model.

Figure 7.10 shows the global maximum longitudinal bending moment for the different load-cases. The different load-cases are plotted along the horizontal axis of the graph, with decreasing eccentricity of the applied load.

From the graph of figure 7.10, it becomes clear that, with increasing eccentricity of the applied load, the global maximum bending moment of all 3 models increases. The global maximum bending moment of the orthotropic plate and 3D plate model are almost identical for all load-cases. However, LC2 shows a clear difference between the orthotropic plate and 3D plate model. For LC2, the point load is applied on the outer edge of the deck. In the orthotropic plate model, this edge is too stiff, as the stiffness of the stiffener is spread out over the spacing of the stiffeners. As stiffer parts take more load, it is expected that the slightly larger longitudinal bending moment of the orthotropic plate model can be attributed to this higher stiffness.

The difference between the grillage and orthotropic plate model is about 5% for LC7 and increases till 15% for LC2. The difference in load-spread between the grillage and the other 2 models increases with the eccentricity of the applied load.

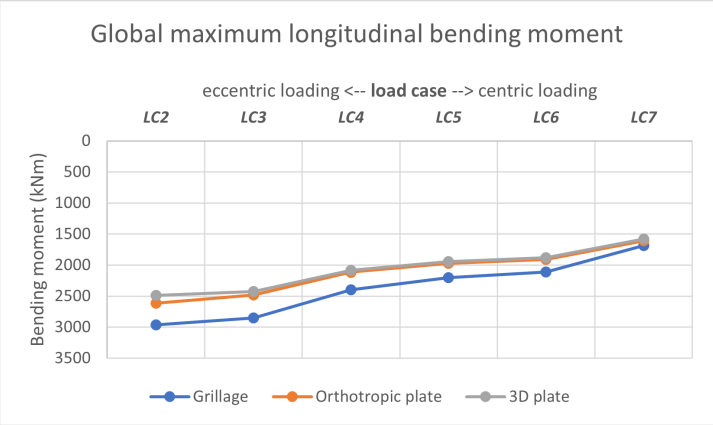

Figure 7.10: Global maximum longitudinal bending moment

7.3.2. Transverse bending moments

Next to the moments in the longitudinal direction of the deck, the moments in the transverse direction can be checked. For both models, the transverse bending moments that are extracted are located in the middle of the span.

The transverse beams of the grillage model have a width of 2353 mm. The transverse bending moment of the orthotropic plate model can be compared to the grillage model by taking the bending moment of a transverse strip with the same width as the transverse beam of the grillage model. Figure 7.11 shows the orthotropic plate model, loaded with LC3. The green boundaries mark a transverse strip that coincides with the mid-span transverse beam of the grillage model.

In figure 7.11, the transverse bending moment of the orthotropic plate model is plotted over 3 different transverse sections. One section is in the middle of the span, the other 2 sections are located at a distance equal to half the width of the transverse beams of the grillage model. This means that the area enclosed by the green lines coincides with the mid-span transverse beam of the grillage model. So, this area can be seen as a transverse plate strip with a width of 2353 mm.

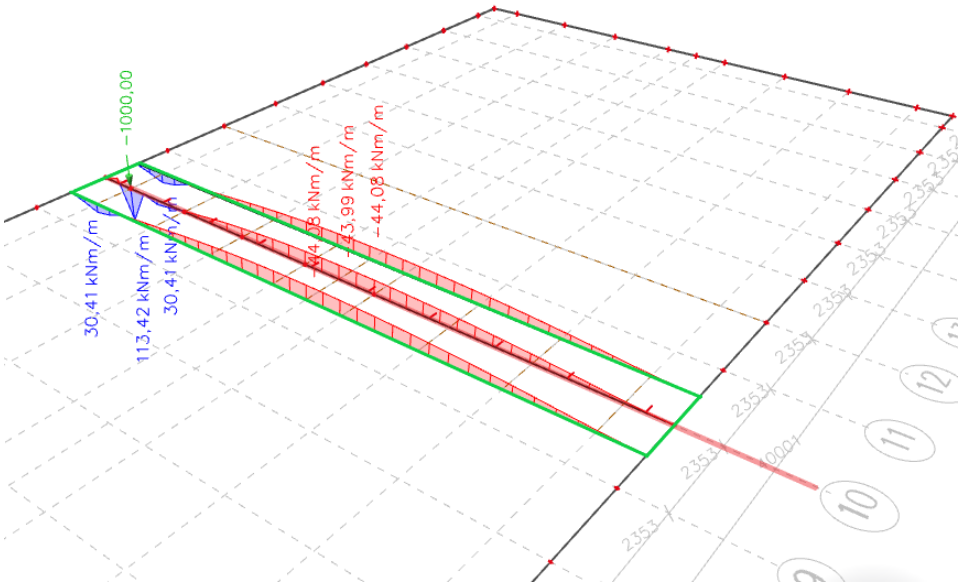

Figure 7.11: Transverse bending moment at 3 sections, in and around the middle of the span

From figure 7.11, it becomes clear that the transverse bending moment at the mid-span section is different from the other 2 sections. This means that the transverse bending moment varies over the longitudinal direction of the bridge deck. Which also means that the transverse bending moment is not

constant over the width of the transverse plate strip. As a result of this, it will not be accurate to take the transverse bending moment over the section in the middle of the span of the deck and multiply this with the width of the transverse beams of the grillage model. Especially in the zone at which the force is applied, this method would result in big errors.

A more accurate way to extract the transverse bending moments from the orthotropic plate model is to create sections in the longitudinal direction of the deck. These sections are located in the middle of the span and have a length of 2353 mm, see figure 7.12. In transverse direction, the sections are located at the same position as the longitudinal beams of the grillage model. This means that the transverse position of the sections is identical to the position of the nodes of the grillage model. Next to the sections located at the position of the longitudinal beams, there are 2 extra sections, one on each edge of the deck. Figure 7.12 gives an example for which the orthotropic plate model is loaded with LC3. The average transverse bending moment over each of the 10 sections (8 above the webs and 2 on the edges of the bridge deck) with a length of 2353 mm, is shown in this figure.

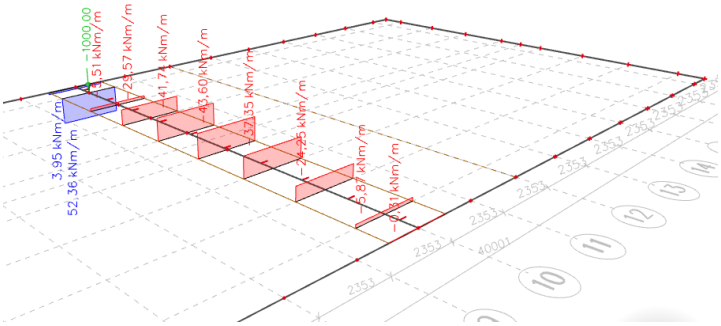

Figure 7.12: Sections in the orthotropic plate model at which the average transverse bending moment is determined, LC3

The next step is to determine the average transverse bending moment over each section and multiply this value with 2353 mm. By plotting these bending moments along the transverse direction of the bridge deck, one can obtain the transverse bending moment diagram of the orthotropic plate model. This diagram can be compared to that of the grillage model. Figure 7.13 shows the transverse bending moment diagrams of the models loaded with LC1. This load-case concerns a distributed force in the transverse direction in the middle of the span of the bridge deck.

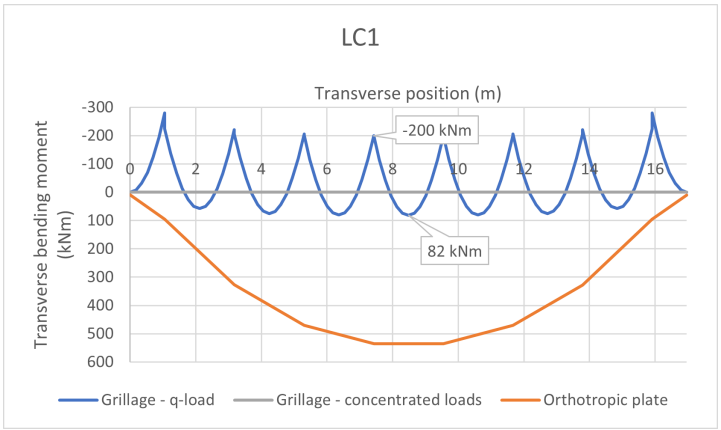

Figure 7.13: Transverse bending moments for LC1 (uniform distributed load)

In figure 7.14, it can be seen that for LC1 the transverse bending moments diagram of the grillage model is much different compared to the orthotropic plate model. LC1 consists of a uniformly distributed load running in transverse direction in the middle of the span. For the grillage model, this means that the mid-span transverse beam, can be compared to a continuous beam with multiple spans, supported with springs and loaded with a q-load. Such a load-case will result into the same bending moment

pattern as is obtained from the grillage model.

In the middle of the deck, the hogging bending moment is equal to 200 kNm, the sagging bending moment is equal to -82 kNm. According to theory, the difference between these 2 bending moments should be equal to $\frac{1}{8}ql^2$, where $q = 500\,\text{kN/m}$ and $l = 2.12\,\text{m}$ (the spacing between the longitudinal beams).

The transverse q-load of LC1 can also be applied to the grillage model by using equivalent concentrated forces. These concentrated forces can be applied at the position of the longitudinal beams. The magnitude of the q-load is equal to 500 kN/m, the spacing between the longitudinal beams is equal to 2.12 m. That means that the equivalent concentrated must be equal to 500 x 2.12 = 1060 kN. When LC1 is applied with equivalent loads, the transverse bending moment of the grillage model is equal to 0. This means that the applied concentrated forces are directly transferred towards the support, by means of the longitudinal beams. As can be expected, there is no transverse load-spread for LC1.

For the orthotropic plate model loaded with LC1, the transverse bending moment diagram is much different compared to the grillage model. For the orthotropic plate model, there is also an effect of the lateral contraction. The bending moments in longitudinal direction also causes bending moments in transverse direction. The transverse bending moment for LC1 for the orthotropic plate model can most likely be fully attributed to the effect of lateral contraction (Poisson's effect) instead of being an effect of transverse load-spread.

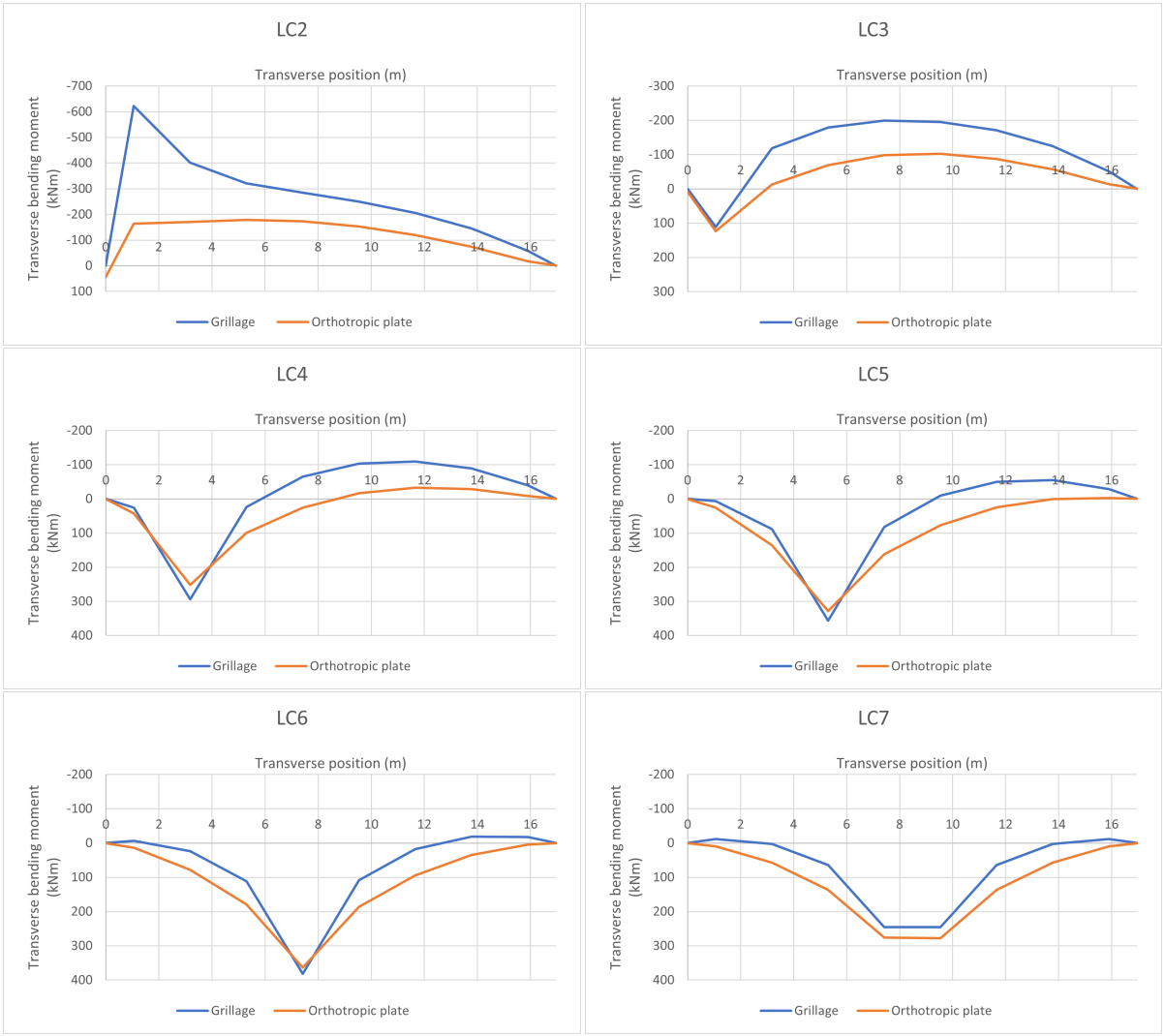

Figure 7.14: Transverse bending moment diagrams LC2 till LC7

The transverse bending moment diagrams of the load-cases concerning the point loads (LC2 till LC7) are shown in figure 7.14. The transverse bending moments are evaluated along a transverse section along the mid-span of the bridge deck (grid line 10). Again, the transverse bending moment diagrams show the true transverse bending moments for the grillage model instead of the direct grillage output (see figure 4.3) and the transverse bending moments evaluated at the sections shown in figure 7.12.

From figure 7.14, it becomes clear that LC2 shows the biggest difference between the transverse bending moment diagrams of both models. LC2, concerns a point load applied at the edge of the deck. For the grillage model, this means that the point load is applied on a cantilevering part of the transverse beam in the middle of the span. In between the point at which the load is applied and the first longitudinal beam (beam B), the transverse beam is not able to transfer any bending moment. This results into a big hogging bending moment at longitudinal beam B, which also rises the bending moment in the remaining part of the transverse beam, right from beam B.

For the orthotropic plate, there is no cantilevering part on the outer edges of the bridge deck. As a result of shear stresses, the applied point load on the edge of the beam is able to spread out in the longitudinal direction of the deck. This results into a much smaller hogging bending moment at the location of longitudinal beam B for the orthotropic plate model, which also reduces the bending moment right from beam B.

The remaining load-cases show that for both models, the transverse bending moment is almost equal at the point at which the load is applied. In the areas away from the point at which the load is applied, the difference between both models is clearly larger. In these areas, the transverse bending moment of the grillage model is smaller compared to the orthotropic plate model.

These observations are in line with the hypothesis. As the Poisson's effect is not included in the grillage model, the contribution of lateral contraction to the transverse bending moment will be 0. For the orthotropic plate model, the Poisson's effect will contribute to the transverse bending moment, next to the contribution of transverse load-spread.

7.3.3. Torsional moments

The torsional moment of the grillage model can be found by taking the average of the torsional moment of the longitudinal and transverse beams. As the width of the longitudinal and transverse beam is not equal, the torsional moment must be divided by the width of the beams, before the average value can be calculated. Figure 7.15 shows the torsional moments for the longitudinal and transverse beams of the grillage model loaded with LC2.

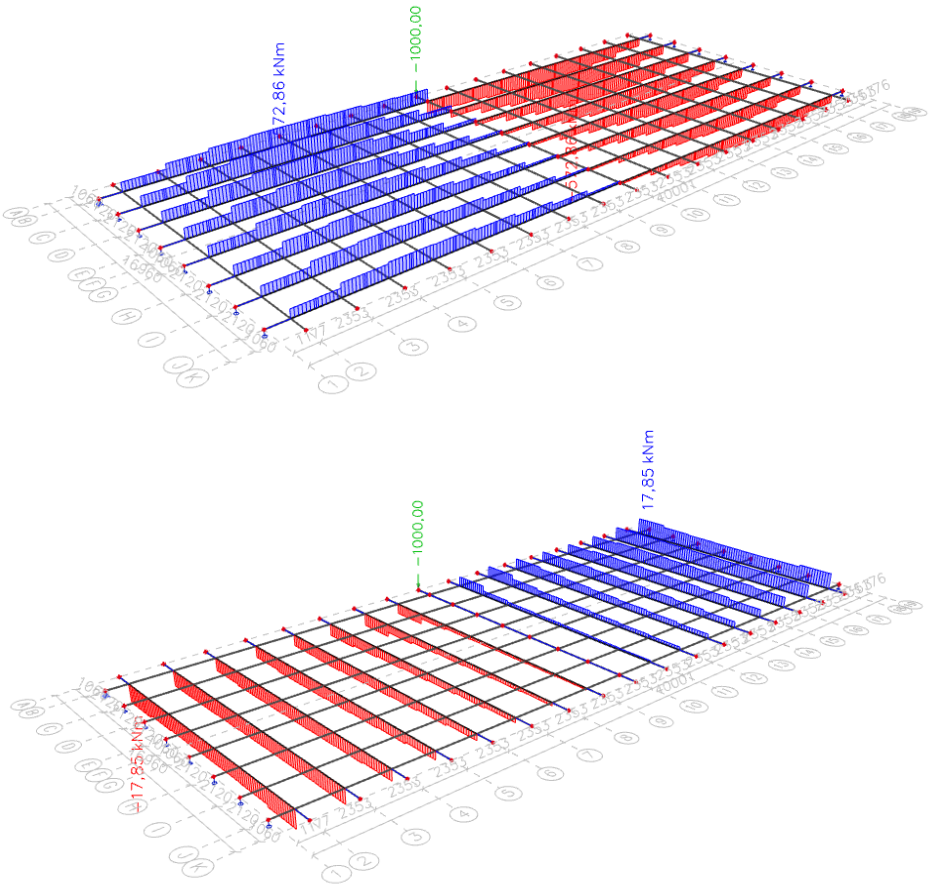

Figure 7.15: Torsional moments grillage model. Longitudinal beams (top) and transverse beams (bottom, LC2)

For the orthotropic plate model, the torsional moments can be extracted from *SCIA-engineer* by plotting a contour plot. Figure 7.16 shows the torsional moment for the orthotropic plate model loaded with LC1 till LC7.

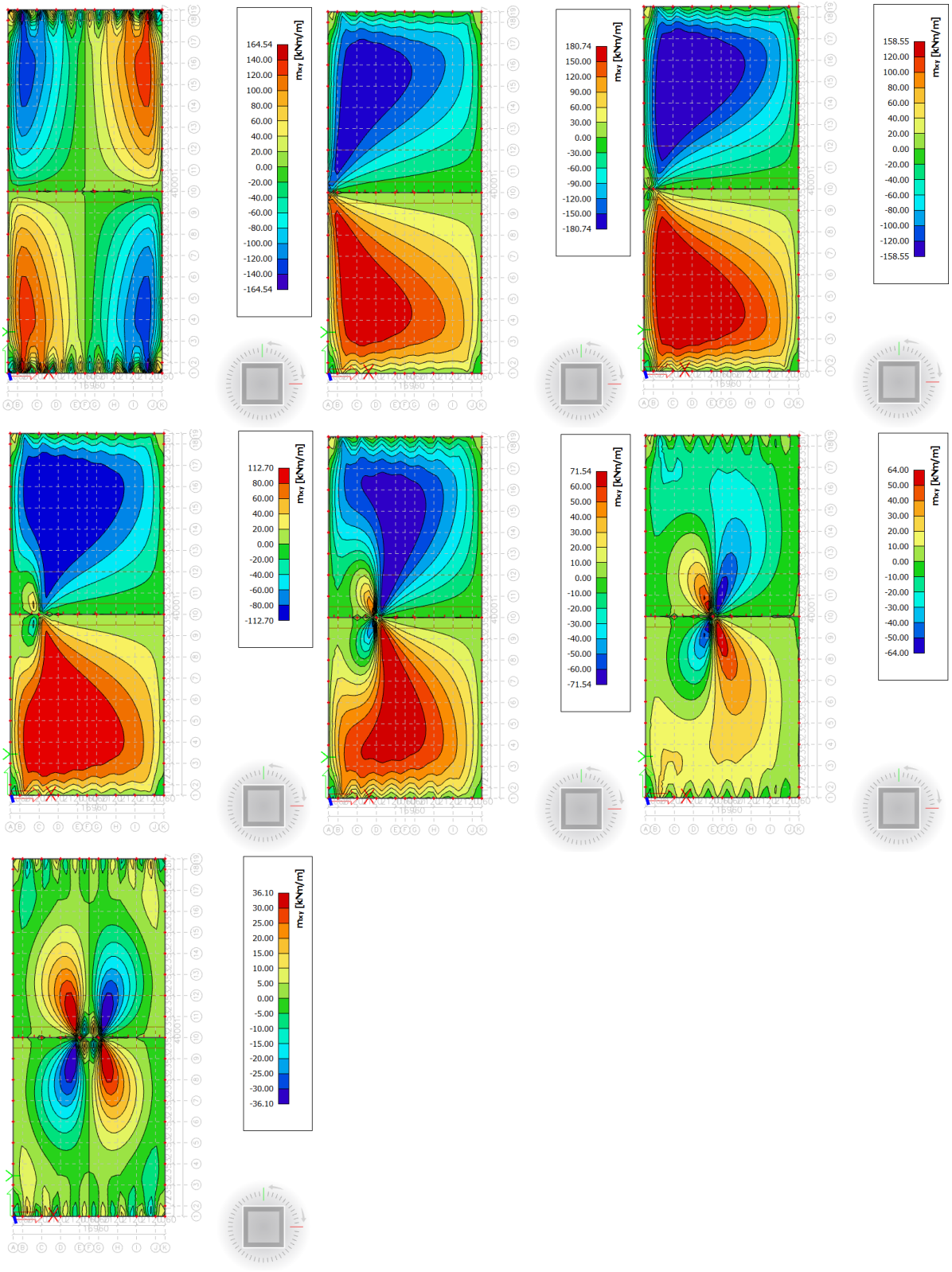

Figure 7.16: Torsional moments orthotropic plate model. LC1 till LC7

Table 7.2 gives an overview of the maximum torsional moments of the grillage model and the orthotropic plate model for each of the 7 load-cases. The torsional moments are given per unit width. So, the presented values have the unit kNm/m. In the last column of table 7.2, the relative difference between the grillage and the orthotropic plate model is given (in %).

Table 7.2: Torsional moments (kNm/m)

load-case	**grillage**	**orthotropic plate**	**difference** (%)
LC1	0.00	165	-100
LC2	132	181	-27
LC3	114	159	-28
LC4	80.1	113	-29
LC5	50.0	71.5	-30
LC6	22.5	64.0	-65
LC7	11.4	36.1	-69

From table 7.2, it becomes clear that for the orthotropic plate model the torsional moments are much larger compared to the grillage model. The biggest difference can be found for LC1, which is a uniform distributed load over the middle of the span. In the grillage model, this load-case results into longitudinal bending moments only. The transverse bending moments that were observed are a result of local bending of the transverse beams. As lateral contraction is not included in the grillage model, the longitudinal bending moment does not interact with the transverse direction. This means that there is a bending moment in one direction only, which results into zero torsional moment.

In the orthotropic plate model, the longitudinal bending moment interacts with the transverse bending moments as a result of lateral contraction. The interaction between both directions results into a torsional moment in the orthotropic plate model. Also for the other load-cases, the torsional moment of the grillage model is much lower due to the fact that the transverse bending moment is much smaller compared to the grillage model. For the load-cases with a small eccentricity (LC6 and LC7), the difference between the grillage and ortotropic plate model increases.

7.3.4. Parameter-study

In order to find out how the transverse load-spread depends on the transverse stiffness, a parameter study on the orthotropic plate model has been carried out. In this parameter study, the focus will be on the parameters defining the transverse stiffness of the deck. These parameters are: the transverse bending stiffness (D_{11}), the transverse shear stiffness (D_{44}) and the torsional stiffness (D_{33}). For each of the stiffness quantities, the base value from the orthotropic plate model was taken, this value was multiplied with a factor 0.5 and 2.0. These factored stiffness parameters, as well as the base value (used for the Blankenburg case), can be seen in table 7.3. During the parameter study, only one stiffness parameter was increased or decreased at a time, the other input parameters were left unchanged. The effect of the change in the stiffness parameters was quantified by looking at the longitudinal bending moments at mid-span.

Table 7.3: Input values parameter study

	symbol	**base value**	**x 0.5**	**x 2.0**	
Transverse bending stiffness	D_{11}	7.0079	3.5040	14.0158	10^3 MN m
Torsional stiffness	D_{33}	2.6420	1.3210	5.2840	10^3 MN m
Transverse shear stiffness	D_{44}	2.6205	1.3103	5.2410	10^2 MN/m

Figure 7.17 and 7.18 show the effect of a lower and higher stiffnesses on the longitudinal bending moments for load-case 3 and load-case 7. On the x-axes, the names of the longitudinal strips are indicated. The y-axes shows the change in longitudinal bending moment with respect to the longitudinal bending moment of the orthotropic plate model. For load-case 3, the loading is applied at grid-line B. For load-case 7, the load is applied at grid-line E and G, which means that the load is applied centric.

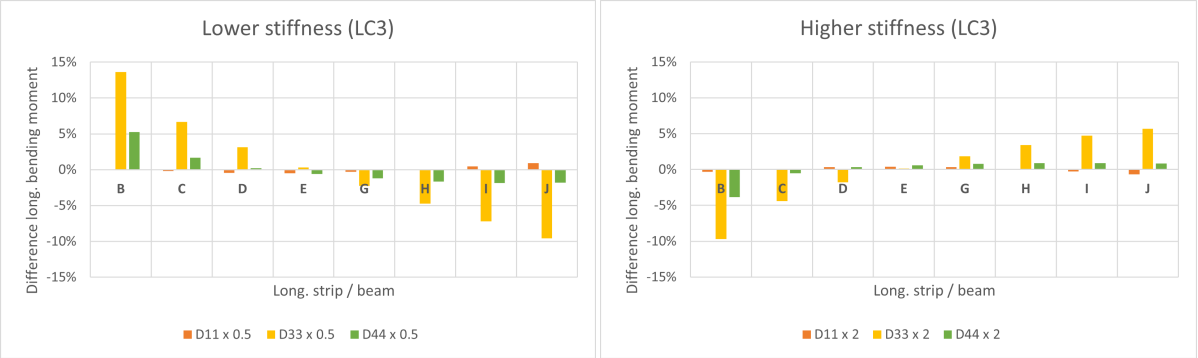

Figure 7.17: Difference longitudinal bending moment for lower/higher stiffnesses, LC3

From figure 7.17, it becomes clear that lower transverse stiffness parameters result into a higher longitudinal bending moment at the location where the load is applied. This means that there is less transverse load-spread when the transverse stiffness is lower. For higher stiffnesses, the bending moment under the point load decreases and increases on the opposite side of the deck. This indicates that a higher transverse stiffness means more transverse load-spread.

For load-case 3, the torsional stiffness (D_{33}) has the biggest influence on the transverse load-spread. For a lower stiffness, the longitudinal bending moment increases up to 14% and decreases up to almost 10%. When the torsional stiffness is a factor 2 higher compared to the orthotropic plate model, the effect is lower: the longitudinal bending moment decreases about 10% and increases up to 6%.

For load-case 3, the load is applied on the edge of the deck, this means that there is a quite amount of torsion. This declares why the torsional stiffness has a big influence on the transverse load-spread for this load-case. Another interesting load-case is load-case 7. This load-case involves 2 point loads in the middle of the deck. This means that the deck is loaded symmetrically.

Figure 7.18 shows how the longitudinal bending moments of the deck loaded with LC7 are influenced by the stiffness parameters that were taken into account in the parameter study. Again, the most important observation is that a lower stiffness results into less transverse load-spread and a higher stiffness leads to more transverse spread of the load.

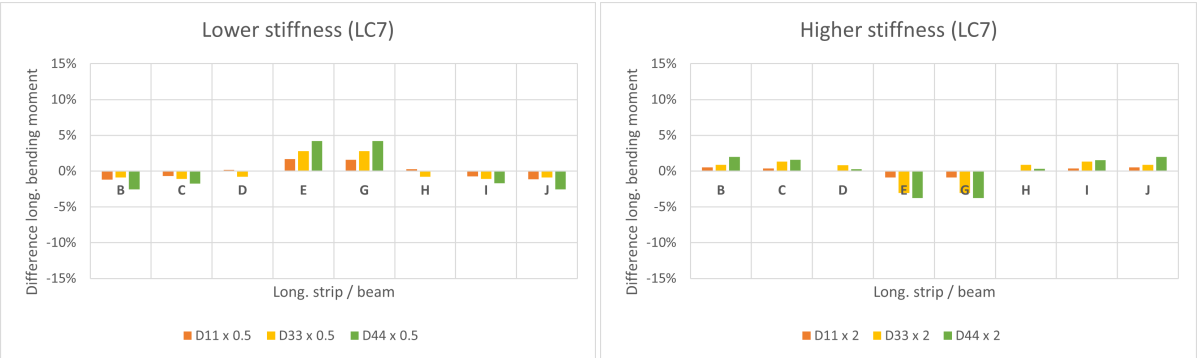

Figure 7.18: Difference in longitudinal bending moment for lower/higher stiffnesses, LC7

For LC7, the transverse shear stiffness has the biggest influence on the transverse load-spread. The change in maximum longitudinal bending moment is about 5%. For LC7, the effect on the transverse load-spread is much smaller compared to LC3.

7.4. Shear forces

For both the grillage model as well as the ortotropic plate model, the shear force in the plane of the transverse cross section of the deck can be extracted from the models. For the grillage model, this can be done by looking at the shear force V_z in the longitudinal beams. Due to the fact that the interaction between the longitudinal and transverse direction is concentrated in the nodes of the grillage model, the shear force diagram of each longitudinal beam shows big jumps in the nodes.

According to E.C. Hambly [3], the discontinuous results from the grillage model can be made continuous by averaging the results in the nodes. The values in the nodes can be interpolated by connecting the values in the nodes with straight lines. Figure 7.19 shows the grillage output of beam B for which the deck is subjected to LC3. The horizontal axis of this diagram shows the longitudinal position along the longitudinal beam, the total length of these beams is equal to 40 m. According to beam theory, the shear force diagram should be equal to the slope of the moment diagram. The grey line of figure 7.19 shows the slope of the moment diagram. It can be observed that the shear force output of the grillage model is almost equal to the slope of the bending moment diagram.

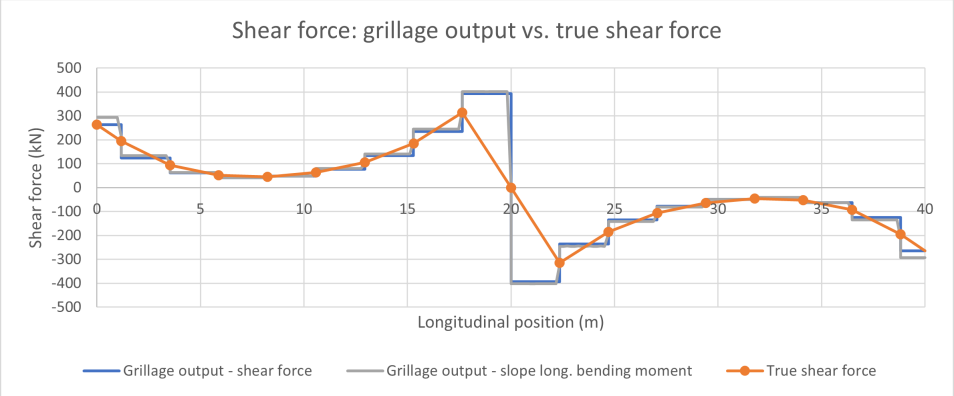

Figure 7.19: Shear force diagram: grillage output vs. true shear force. LC3, beam B

According to the procedure described above, the true shear force diagram of the grillage model is constructed by taking the average value in the nodes (where the longitudinal beam is connected to a transverse beam) and connect all the nodes. By doing this, the true shear force diagram can be obtained, see the orange line in the graph of figure 7.19.

The shear force diagrams of the orthotropic plate model can be obtained by creating integration strips in the longitudinal direction of the deck. The width of the integration strips is equal to the width of the longitudinal beams of the grillage model. This means that the orthotropic plate is divided into 8 integration strips, this integration strips have the same position as the 8 longitudinal beams of the grillage model. The shear force V_y of the integration strips can be compared to the shear fore diagram from the grillage model. Figure 7.20 shows the shear force diagrams of beam / integration strip B, C G and J for the deck subjected to LC3 (point load above the left stiffener). A complete overview of the shear force diagrams can be found in appendix E, page 154.

From figure 7.20, it becomes clear that the shear force diagrams deviate the most for the outer beams. It is expected that this difference is the result of the concentrated shear force. This concentrated force depends on the torsional moment. In the orthotropic plate model, the torsional moment is larger compared to the grillage model. For all other beams/strips the shear force diagrams of both models do not deviate much. Over each transverse cross-section, the sum of the shear force is equal to 500 kN, which is half the applied load.

The shear force at grid-line B shows a sharp jump in the area of the applied force. This jump is sharper for the orthotropic plate model compared to the grillage model. For the grillage model, the last node of the true shear force diagram is at 2.353 m before and after the point at which the load is applied. In between these 2 nodes, the shear force diagram runs trough 0, just like for the orthotropic plate model. As a result of the spacing of the transverse beams (which determines the spacing between the nodes of the true shear force diagram), the grillage model is less capable to capture the sharp jump in the area of the applied force.

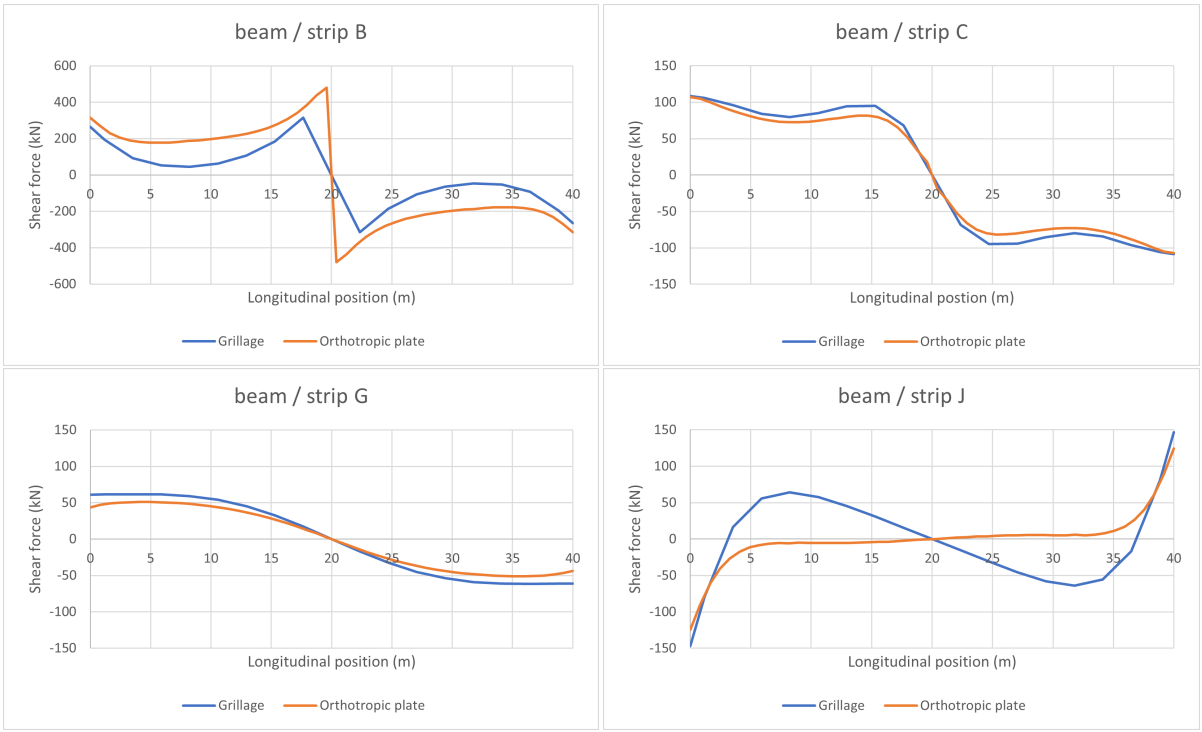

Figure 7.20: Shear forces LC3, longitudinal beam/strip B, C, G and J

In order to be able to make a better comparison between the grillage model and the orthotropic plate model, the shear force diagram for the loaded beam (beam B) of the grillage model is extrapolated towards the middle of the span. The extrapolation is done by fitting a 2nd order polynomial through the last 3 point before the middle of the span. The same is done for the 3 nodes behind mid-span.

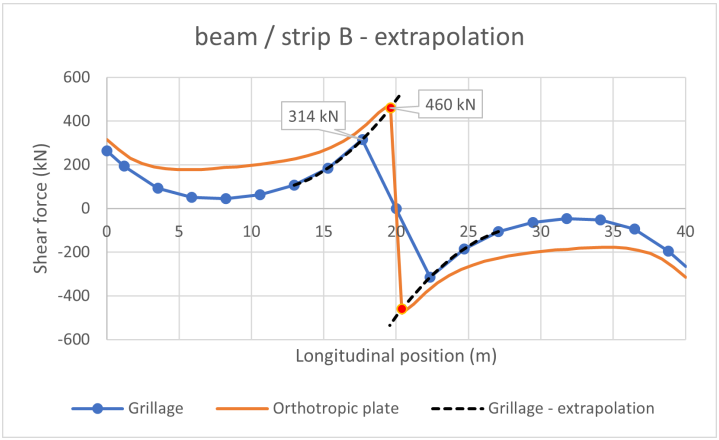

Figure 7.21: Shear force diagram grillage model extrapolated, LC3

Figure 7.21 shows the shear force diagram of the grillage model and the orthotropic plate model for beam / integration strip B. The extrapolation of the shear force of diagram of the grillage model is shown with the black striped line. The red dots mark the longitudinal position at which the shear force is maximum. At the red dots, the shear force of the grillage model is equal to $\pm$ 460 kN. For the orthotropic plate model, the maximum shear force is equal to $\pm$ 479 kN, which means that the difference between both models is about 4%. The direct output of the grillage model (with the jumps in it, see figure 7.19), gives a maximum shear force of $\pm$ 394 kN, this is 18% less compared to the maximum shear force of the orthotropic plate model.

The shear force diagrams can also be compared for a centric applied loading. Figure 7.22 shows

the shear forces for LC7. As the deck, loading and positioning of the longitudinal beams/strips is fully symmetrical, the results of the first 4 longitudinal beams/strips is identical to the other 4, but then mirrored over the middle of the deck. Again, for the grillage model, the true shear forces are plotted. The point loads of LC7 are applied on beam/strip E and G. At these beams/strips, the results of the grillage model are extrapolated near the point of application of the point loads.

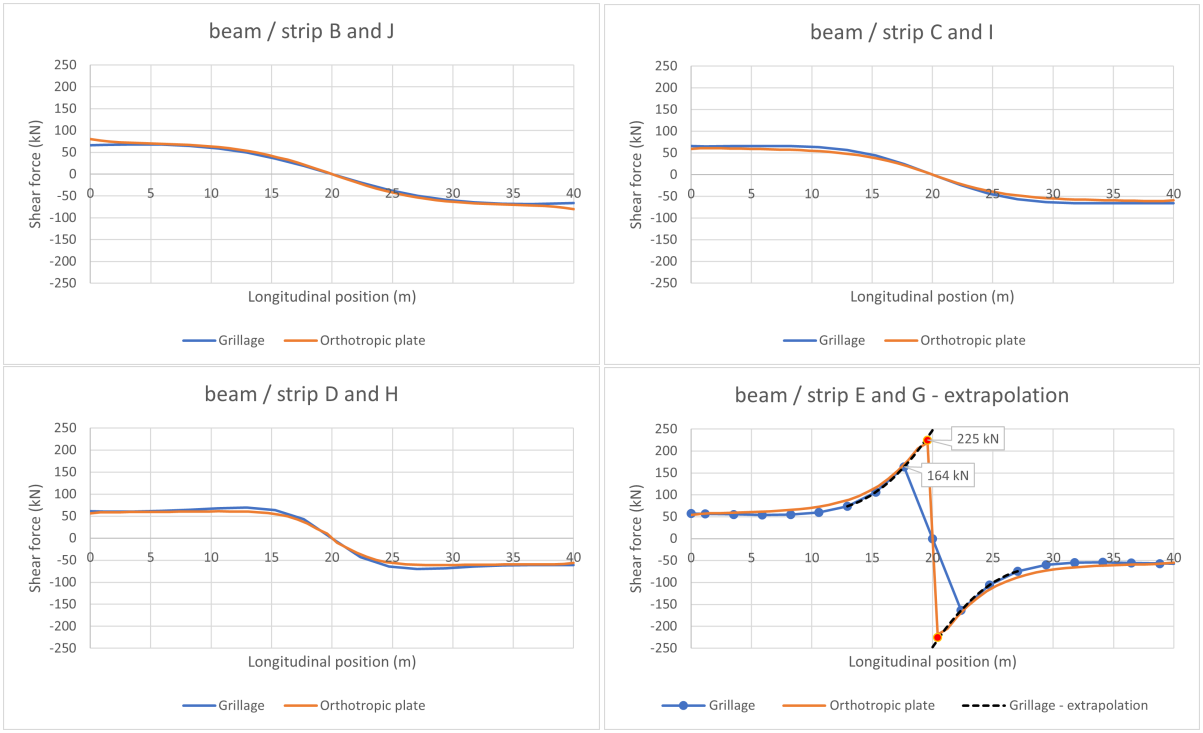

Figure 7.22: Shear forces LC7

From figure 7.22, it becomes clear that for LC7 the shear force diagrams are almost identical. The extrapolated maximum shear force of the grillage model is equal to $\pm$ 225 kN. For the orthotropic plate model, the maximum shear force is equal to $\pm$ 219 kN. This means that the maximum shear force of the grillage model is 2.3% larger compared to the orthotropic plate model.

The shear force diagrams of the 2 outer beams/strips do not deviate as much as they did for LC3. This means that the difference of the concentrated shear force between both models is relatively small compared to the shear force itself. Although the relative difference in torsional moment is big for LC7, the absolute difference is small (see table 7.2). Based upon this, it is assumed that the absolute difference in concentrated shear force between the grillage and orthotropic plate model is too small to be observed in the shear force diagram of beam/strip B and J.

Based upon the shear forces, it is hard to draw conclusions on the transverse load-spread. For the middle beams, the shear force diagrams of both models are almost identical. When the absolute difference between the torsional moment of the grillage and orthotropic plate model are large, the shear force diagram of the outer beams/strips deviate a lot. It is expected that this is the result of the concentrated shear force. This concentrated shear force depends on the torsional moment ($V = m_{xy}$).

7.5. Conclusions

Based upon the results of the straight bridge deck, the following conclusions can be drawn.

Reaction forces

- The reaction forces of the orthotropic plate and the 3D plate model much more agree compared to the reaction forces of the grillage model. Compared to the other to models, the reaction forces of the grillage model are more outliers.
- When the deck is loaded with a distributed load in the transverse direction of the deck (LC1), the reaction forces of the grillage model are almost equal for all supports. For the other two models, the outer supports take a larger part of the load, which can be contributed to the effect of the concentrated shear force.
- For LC2 through LC6, the grillage model shows the same peaks in support reaction for the outer supports as the other 2 models. This indicates that the grillage model can also show the effect of the concentrated shear force.

Mid-span deflections

- For all models and load-cases the mean mid-span deflection is almost the same. This means that the longitudinal stiffness of all bridge deck models is almost identical. This is in line with the conclusions of the strip models from chapter 6.
- The minimum and maximum deflections of the grillage model are significantly larger compared to the other 2 models. The mean deflection of the grillage model is almost equal to the mean deflection of the other 2 models. This means that the deck of the grillage model has an extra rotation compared to the orthotropic plate and 3D plate model.

Bending moments

- The longitudinal bending moment of the orthotropic plate and 3D plate model are almost identical. The biggest difference is found for LC2. This is a point load on the edge of the bridge deck. In the orthotropic plate model, this edge is a little bit too stiff. This most likely causes the difference in longitudinal bending moment distribution.
- The maximum longitudinal bending moment of the grillage model is larger compared to the orthotropic plate and the 3D plate model. This maximum can be found under the point load. Away from the point load, the longitudinal bending moment of the grillage model is smaller compared to the other 2 models.
- The difference in longitudinal bending moment distribution between the grillage model and the orthotropic plate and 3D plate model increases with increasing eccentricity.
- The transverse and torsional moment of the grillage model are smaller compared to the orthotropic plate model. The grillage model has no Poisson effect. This results into a lower transverse bending moment compared to the orthotropic plate model.

Parameter study

- Making the transverse bending, transverse shear and torsional stiffness of the orthotropic plate model 2 times larger, results into more transverse load-spread. Doing the opposite (2 times smaller stiffnesses) results into less transverse load-spread.
- The for the eccentric loaded bridge deck (LC3), the torsional stiffness (D_{33}) has the biggest influence on the transverse load-spread of the bridge deck. For a 2 times lower stiffness, the maximum longitudinal bending moment increases with 14%. When the torsional stiffness is 2 times larger, the maximum longitudinal bending moment decreases with 10%.
- For an eccentric loaded bridge deck (LC7), the transverse shear stiffness has the biggest influence on the transverse load-spread. Both for lower and higher transverse shear stiffness, the change in maximum longitudinal bending moment is about 5%.

Shear forces

- At the point at which the load is applied, there is a strong peak. The grillage model is not able to capture the peak value as the nearest transverse beam is already a several meters away from the peak value. This can be solved by extrapolating the graphs of the grillage model (figure 7.21)

- For both models, the sum of shear forces is equal to 500 kN (half the applied load) for each transverse cross-section.
- For both models, the shear force diagram is equal to the slope of the longitudinal bending moment diagram.
- For the inner beams/strips, the shear force diagrams of both models are quite identical. In case there is a big absolute difference between the torsional moment of the grillage and the orthotropic plate model, there is a big difference between the shear force diagrams for the outer beams/strips. It is assumed that this difference is caused by the difference in concentrated shear force. This concentrated shear force depends on the torsional moment.
- The shear force diagrams cannot be used to draw conclusions on the transverse load-spread.

8

Curved deck

This chapter shows the results of the curved bridge deck. First, the resultant of the reaction forces are compared for each of the 3 models. Using this, it can be checked whether all models are loaded with the same or equivalent load. Next the support reactions of all compared. This is done for the grillage, orthotropic plate and 3D plate model.

The bending moments (longitudinal, transverse and torsional) are compared for the grillage and orthotropic plate model only. Finally, the design bending moments for the reinforcement are compared. For this comparison, the effect of pre-stressing is included. The design bending moments are based upon Wood-Armer (1968). Based upon the design bending moments, it is determined which model results into more reinforcement.

The conclusions that can be drawn on the results of the curved bridge deck are shown in the last section of this chapter.

8.1. Reaction forces

Based upon the resultant of the reaction forces, it can be determined whether all different models are subjected to an equivalent loading. This can be done by looking at the resultant of the vertical reaction forces (R_z) and the bending moments M_x and M_y. Table 8.1 shows the resultant of the reaction forces per load case, and per model for the curved deck as well as for the curved and skewed deck.

Table 8.1: Resultants of the reaction forces

load	**model**	F_z (kN)	M_x (kNm)	M_y (kNm)
SW	grillage	12544	0.03	6589
	orthotropic plate	12543	0.05	6607
	3D plate	12544	0.03	6588
UDL	grillage	2905	0.34	6356
	orthotropic plate	2904	1.19	6346
	3D plate	2905	0.34	6356
TS	grillage	1200	0.22	5459
	orthotropic plate	1200	0.92	5460
	3D plate	1200	0.75	5420

Based upon table 8.1, it can be concluded that for all models the applied loading is equivalent, as for each of the load cases the difference between the resultant forces is very small. The maximum difference between the resultant for a specific load case is equal to 0.8%, excluding M_x of the curved bridge deck. As a result of symmetry, M_x is almost equal to zero for this deck. The non-zero bending moments M_x for the curved deck are most likely a result of rounding errors of the finite element analysis. The reaction forces for each of the load cases, as well as the sum of all load cases can be seen in figure 8.1. Along the horizontal axis of the graphs, the naming of the 8 supports is indicated. This naming

can be seen in figure 7.1. The curved deck is symmetrical with respect to the mid-span, which means that it suffices to show the reaction forces of one edge of the bridge deck only.

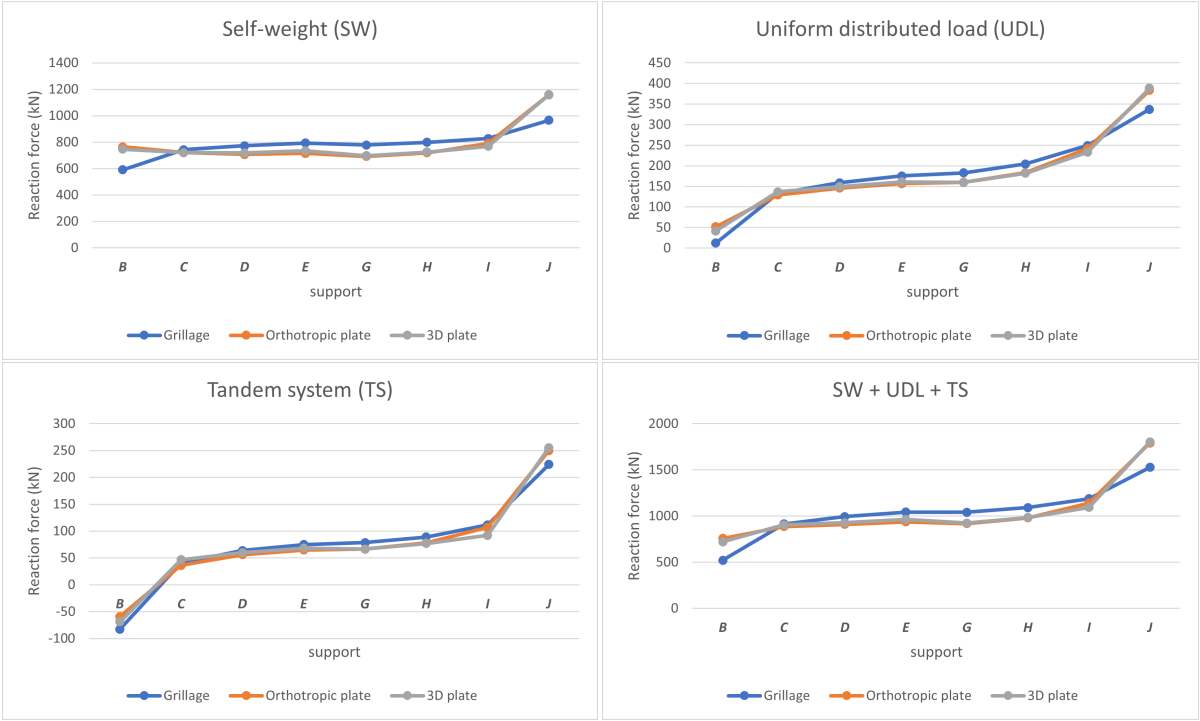

Figure 8.1: Reactions forces for each load case and the sum of all load cases

From figure 8.1, it becomes clear that the reaction forces of the orthotropic plate model and 3D plate model are almost identical for all load-cases. The reaction force diagram of the grillage model is an outlier compared to the other 2 models. For all load-cases, the grillage model shows lower support reactions on the outer supports. It is assumed that the concentrated shear force of the grillage model is smaller compared to the orthotropic plate and 3D plate model.

8.2. Bending moments

This section shows the results of the longitudinal, transverse and torsional moments of the curved bridge deck. The moment diagrams of the longitudinal and transverse bending moment are shown for the mid-span cross-section of the bridge deck.

8.2.1. Longitudinal bending moments

The longitudinal bending moments in the mid-span of the curved deck can be found in figure 8.2. This figure shows the longitudinal bending moments per 2.12 m deck with. For the grillage model, the longitudinal bending moments can be derived directly from the longitudinal beams. The longitudinal bending moments of the orthotropic plate model are determined in the same way as for the straight deck, for which 8 sections were created over the transverse mid-span of the deck.
Table 8.2 shows per model and per load case the maximum longitudinal bending moment, per 2.12 m. The last column of this table gives the relative difference between the grillage model and the orthotropic plate model. For the self-weight (SW), the difference between both the maximum longitudinal bending moments is 2.6%, while for the tandem load (TS), the difference is 10.5%.

The last 2 rows of table 8.2 give the maximum longitudinal bending moment for the 2 load-combinations. In the first load-combination, pre-stressing is not included. The second load-combinations includes pre-stressing. This is done by reducing the self-weight of the bridge with 65%.

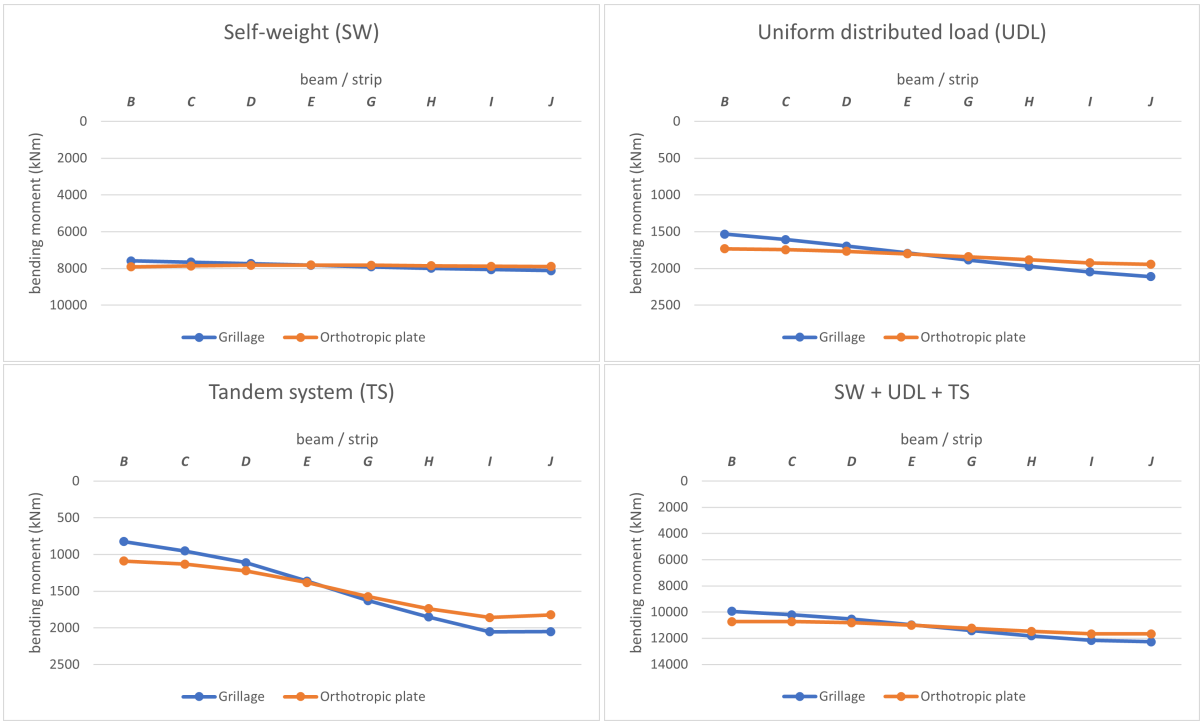

Figure 8.2: Longitudinal bending moment over mid-span cross-section

Table 8.2: Maximum longitudinal bending moments (kNm), per 2.12 m

load	**grillage**	**orthotropic plate**	**difference** (%)
SW	8113	7909	2.6
UDL	2112	1943	8.7
TS	2054	1859	10.5
SW + UDL + TS	**12275**	**11663**	**5.2**
0.35*SW + UDL + TS	**7002**	**6540**	**7.1**

Transverse load-spread of self-weight

From figure 8.2, it becomes clear that the difference in longitudinal bending moment is small for the self-weight. The bending moment diagram of the orthotropic plate model seems to be close to constant over the transverse cross-section. The grillage model shows a larger bending moment on the outer edge compared to the inner edge of the curved deck.

As a result of the curvature, the outer edge of the bridge deck is longer compared to the inner edge of the bridge. This means that the outer edge of the bridge deck contains more material. In case there will be no transverse load-spread of the self-weight, one expects larger longitudinal bending moments on the outer edge of the deck, which is observed in the results of the grillage model.

However, transverse load-spread of the self-weight of the curved deck may not be neglected. The outer edge of the curved deck has a longer span compared to the inner edge of the bridge deck. This means that the inner edge of the bridge deck is stiffer compared to the outer edge. Stiffer parts take more load compared to less stiff parts. So, it is expected that part of the self weight of the outer edge *travels* in the direction of the inner edge.

The transverse load-spread of the self-weight of the deck can be studied by looking at an equivalent distributed load for each longitudinal beam/strip. This equivalent distributed load can be calculated based upon the maximum longitudinal bending moment and the length of the span for each of the longitudinal beams/strips. The equation

$$M_{max} = \frac{1}{8} q l^2$$

can be re-written into:

$$q_{eq} = 8 \frac{M_{max}}{l^2}$$

Table 8.3 shows the equivalent distributed load for the grillage and orthotropic plate model loaded with the self-weight. The equivalent distributed load (q_{eq}) is calculated based upon the formula above. For both models, the mean of q_{eq} is about 39.3 kN/m. This is close to the applied self-weight per beam/strip of $q_{SW} = 39.20\,\text{kN/m}$.

Table 8.3: Equivalent distributed load, self-weight (kN/m)

beam/strip	grillage	orthotropic plate
B	39.89	41.61
C	39.67	40.74
D	39.51	40.00
E	39.41	39.39
G	39.30	38.88
H	39.16	38.45
I	38.94	38.07
J	38.64	37.61
mean	**39.32**	**39.34**

The values shown in table 8.3 can be divided by the applied self-weight of $q_{SW} = 39.20\,\text{kN/m}$. Figure 8.3 shows the ratio between q_{eq} and q_{SW} over the transverse direction of the bridge deck. From figure 8.3, it becomes clear that for both models the left edge of the bridge deck takes a larger part of the self-weight compared to the right part of the bridge. The stiffer inner edge is located on the left and the less stiff outer edge is located on the right.

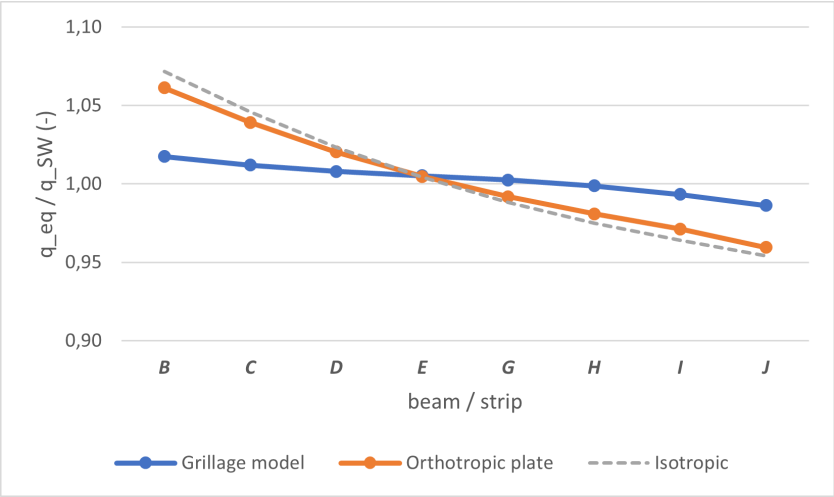

Figure 8.3: Transverse spread of self-weight

The effect of transverse load-spread of the self-weight is much stronger for the orthotropic plate model compared to the grillage model. For the grillage model, the ratio between q_{eq} and q_{SW} is much closer to 1.0 over the whole width of the bridge deck. This means that the equivalent distributed load is close to the distributed load of the applied self-weight. For the orthotropic plate model, there is a much stronger difference between the inner and the outer edge.

The gray dotted line of figure 8.3 shows the ratio between q_{eq} and q_{SW} for an isotropic plate. It can be seen that the load-spread of the self-weight of the orthotropic plate model is only a little bit smaller compared to an isotropic plate.

8.2.2. Transverse bending moments

The transverse bending moment diagrams of the curved bridge deck can be found in figure 8.4. The transverse bending moments are shown along the mid-span transverse cross-section of the bridge deck. Each graph shows the transverse bending moment per width of the mid-span transverse beam / strip, which has a width of 2.353 m.

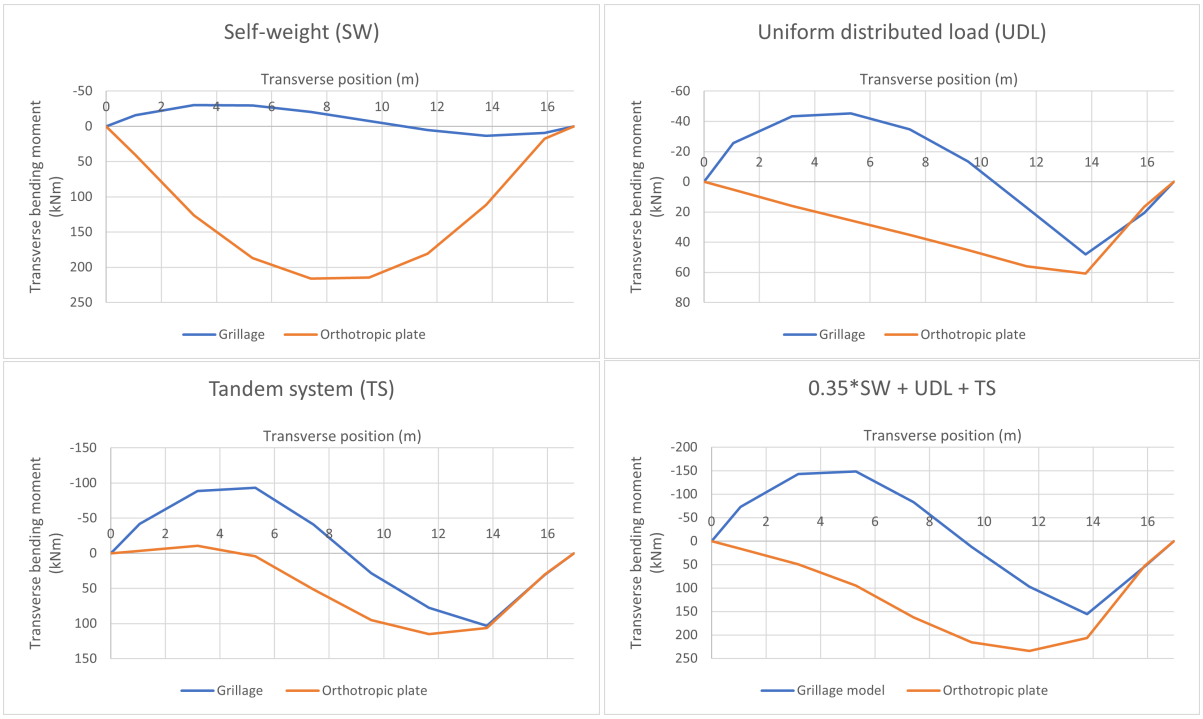

Figure 8.4: Transverse bending moment diagrams SW, UDL and TS and load-combination including pre-stressing

From figure 8.4 it becomes clear that the transverse bending moment of the grillage model is much lower compared to the orthotropic plate model. For the self-weight, the orthotropic plate model shows a parabolic line describing the transverse bending moment. For this load case, the transverse load-spread is relatively small (due to the curvature there is still some load-spread). The grillage model shows an S-like curve. Compared to the orthotropic plate model, the transverse bending moment of the grillage model is very small and close to 0. As the grillage model doesn't show any effect of lateral contraction, the transverse bending moment comes from transverse load-spread only. For the orthotropic plate model, the transverse bending moment is a combination of both lateral contraction (Poisson) as well as transverse load-spread.

8.2.3. Torsional moments

Figure 8.5 shows the contour plots of the torsional moment of the curved bridge deck modelled as a grillage model (left) and orthotropic plate model (right). The decks are loaded with the sum of all loads (including pre-stressing), which is load combination **0.35*SW+UDL+TS**.

From figure 8.5, it becomes clear that the torsional moments of the grillage model is smaller compared to the orthotropic plate model. The pattern of the torsional moment is also different. For the orthotropic plate model the biggest values are at the right part of the deck, while for the grillage model, the biggest values are at the left of the deck. In the middle of the span, the torsional moments are 0 for both models. In the orthotropic plate model, disturbances around the edges are observed. These disturbances are caused by the concentrated supports.

The maximum torsional moment of the grillage model is equal to $\pm$ 167 kNm/m. For the orthotropic

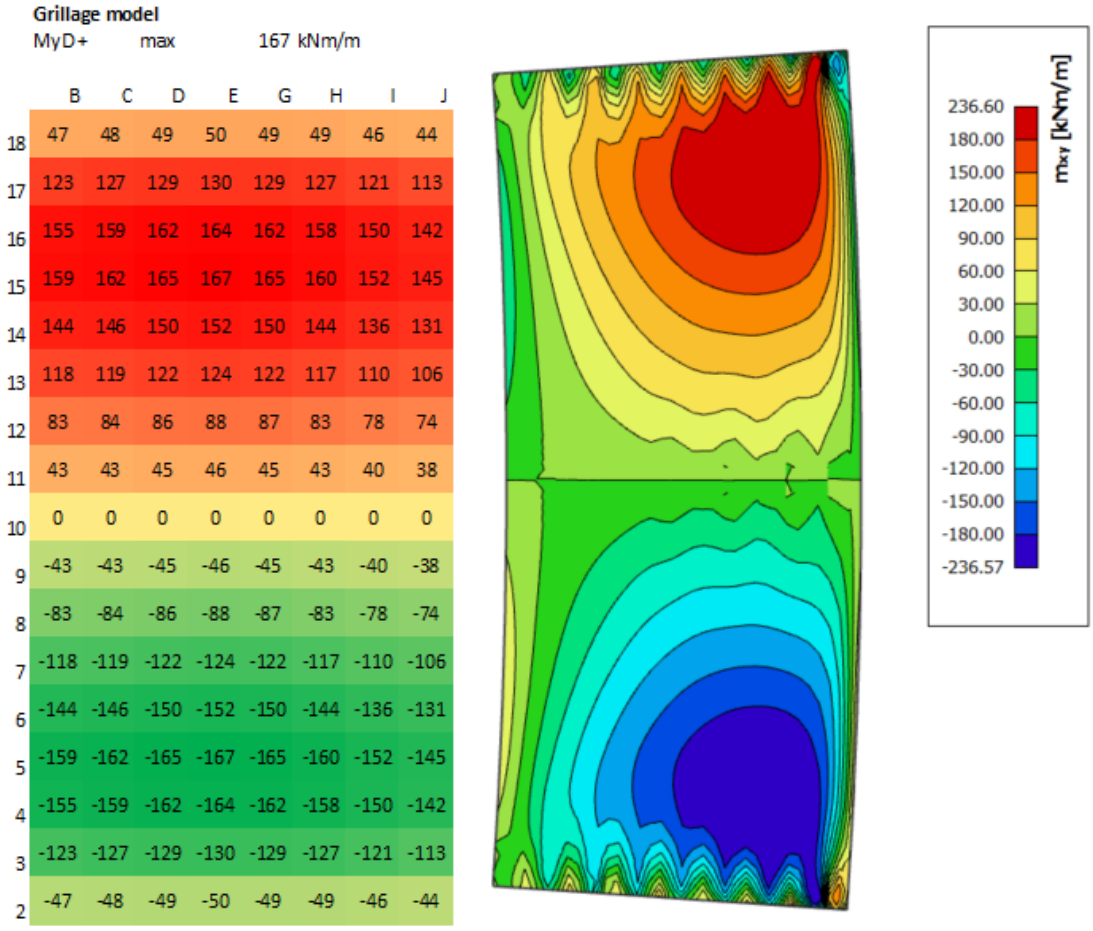

Figure 8.5: Torsional moment (kNm/m) grillage model (left) and orthotropic plate model (right)

plate model, the maximum torsional moment is equal to $\pm$ 237 kNm/m. However, this is a peak value. Taking the average torsional moment over a width that is equal to the width of the longitudinal beams of the grillage model results into an averaged torsional moment of $\pm$ 233 kNm/m. From this, it follows that the torsional moment of the grillage model is about 28% smaller compared to the orthotropic plate model.

8.3. Design bending moments

The reinforcement design of the bridge deck will eventually be based upon the Wood-Armer moments (1968). An overview of the calculation of the Wood-Armer moments can be found in appendix B (page 135). The Wood-Armer moments can aslo be called the *design bending moments*, as they are used to design the reinforcement.

It is assumed that orthogonal reinforcement is applied, in the x- (transverse) and y-direction (longitudinal) of the bridge deck. According to the Wood-Armer moments, the longitudinal reinforcement takes the longitudinal bending moment and the transverse reinforcement the transverse bending moment. The absolute value of the torsional moment needs to be added to both the longitudinal and the transverse reinforcement moments. The reinforcement on the top of the bridge deck takes the negative (hogging) bending moments and the bottom reinforcement takes the positive bending moments (sagging).

In case of the orthotropic plate model, the Wood-Armer moments can be extracted from *SCIA-engineer* directly. This can be done by choosing for *design values* and the values MxD+, MxD-, MyD+ and MyD-. These values are equal to the Wood-Armer moments, where $+/-$ stands for top/bottom reinforcement

and x and y for the direction of the reinforcement.

For the grillage model, it takes a little bit more effort to determine the design bending moments. For both the longitudinal as well as the transverse beams the bending moments M_y and torsional moments M_x were exported to excel for every node. Thereafter, the nodal results needed to be averages as each node can have to different bending moments per direction. One of these bending moments comes from the left and one from the right. The grillage model gives it's results over the whole width of the beam, so the bending moments needed to be divided by the width of the beams in order to have results per unit width.

The torsional moments of the longitudinal and transverse beams were averaged to end up with only one torsional moment per node instead of one torsional moment for each direction. Eventually, for each node of the grillage model, there are 3 benidng moments: longitudinal, transverse and torsional. Using the formulas of the Wood-Armer moments shown in appendix B (page 135), the design bending moments of the grillage model can be calculated.

Figure 8.6 shows the contour plots of the design bending moment for the bottom reinforcement in the longitudinal direction of the bridge deck (MyD-). These contour plots are based upon the load combination including the effect of pre-stressing The left plot shows the design bending moments of the grillage model, which is the result of the calculations in Excel. The right plot shows the result of the orthotropic plate model, which is extracted from SCIA-engineer directly. A complete overview of the design moments of the curved deck can be found in appendix F (page 157).

Table 8.4 shows the maximum values of the design bending moments per direction (x/y) and position of the reinforcement (top / bottom). The results of the grillage model are directly extracted from the calculations in Excel. For the orthotropic plate model, the peaks in the contour plot are averaged over the same width as the beams of the grillage model. This makes the comparison more fair as the results of the grillage model are indirectly also averaged over the width of the beams. The results of the orthotropic plate model were averaged using sections in longitudinal direction for the transverse bending moments and in transverse direction for the longitudinal bending moments.

For the transverse bending moments, the nodes of the grillage model start at about 1 m from the edge. This means that the first 1 m of the orthotropic plate model is not taken into account when determining the maximum design bending moments for the transverse direction.

Table 8.4: Design moments (kNm/m), including pre-stressing

design moment	**grillage**	**orthotropic plate**	**difference** (%)
MxD+	182	120	51.7
MxD-	185	207	-10.6
MyD+	0	0	0
MyD-	3303	3093	6.8
$\sum$	**3670**	**3437**	**7.3**

From table 8.4, it becomes clear that the reinforcement of the curved bridge deck mainly needs to be put at the bottom of the deck, in longitudinal direction. The relative difference between the grillage model and the orthotropic plate model is quite big for MxD+ (51.7%) and MxD- (-10.6%). However, the amount of reinforcement needed in these directions is very small compared to MyD-. For MyD-, the amount of reinforcement needed for the grillage model is 6.8% larger compared to the grillage model. This difference is slightly smaller than for my (7.1% table 8.2). This follows from the fact that for the grillage model, the torsional moment is smaller compared to the orthotropic plate model. This torsional moment is incorporated in the design bending moment.

The sum of the design bending moments is a measure for the total amount of reinforcement. For the grillage model, the sum of design bending moments is equal to 3670 kNm/m, for the orthotropic plate model this is equal to 3437 kNm/m. This means that the grillage model results in about 7.3% more reinforcement compared to the orthotropic plate model. From this, it becomes clear that theortically 7.3% reinforcement can be reduced when the curved deck is modelled using the orthotropic plate model instead of a grillage model.

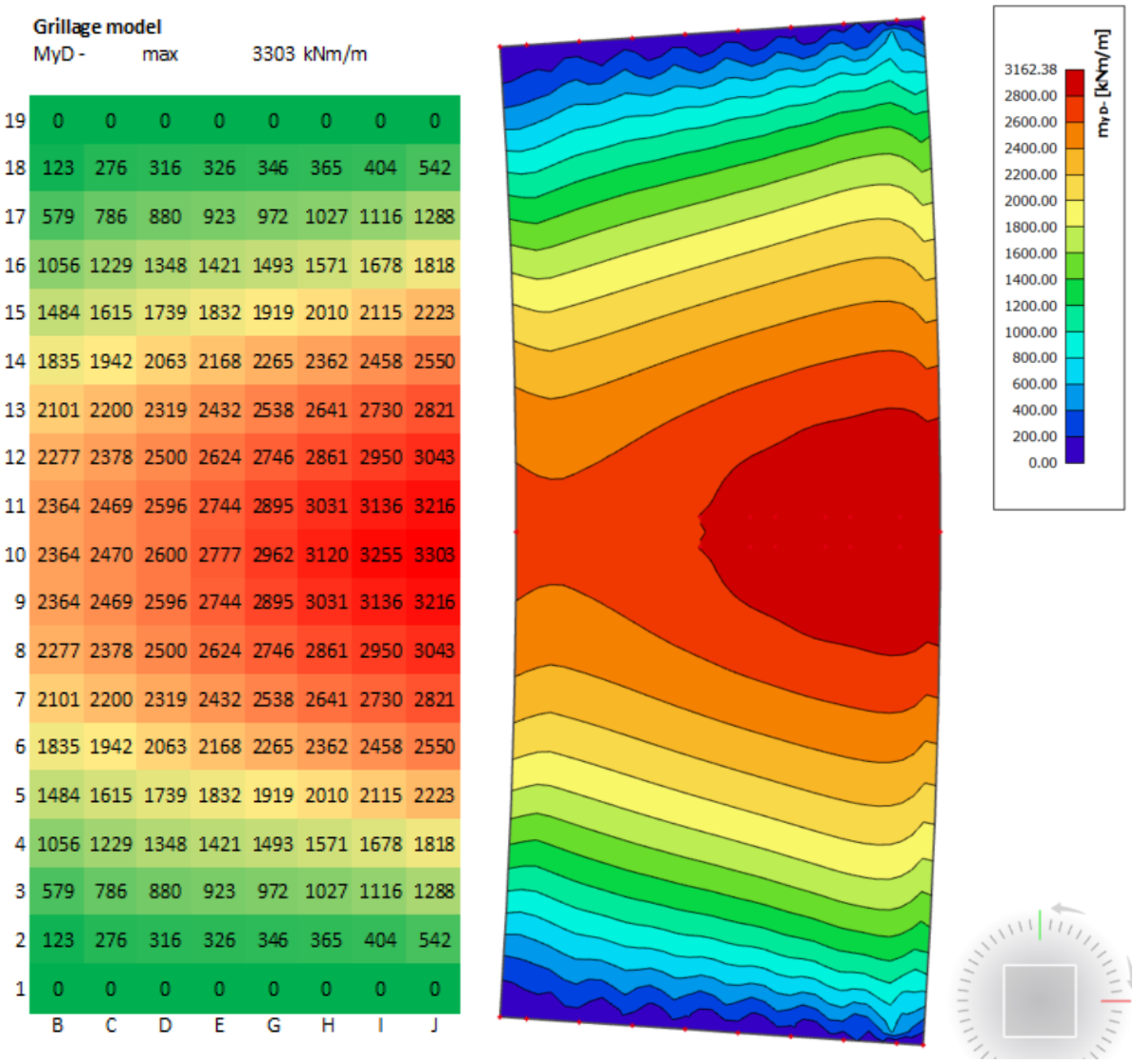

Figure 8.6: MyD-, grillage model (left) and orthotropic plate model (right) (kNm/m)

Reinforcement design in practice

In practice, the design of the reinforcement is limited by the space in which the reinforcement must be put, the allowed spacing between the reinforcement bars and the available and applicable reinforcement bar diameters. Appendix H shows an example of the longitudinal reinforcement design for the bottom plate of the deck (MyD-). In this appendix, the possible total amounts of reinforcement (mm^2/m) are shown. These amounts of reinforcement are based upon the available space in between the shear reinforcement, the possible spacing and the available bar diameters.

Eventually, all possible amounts of reinforcement (based upon possible spacing and bar diameters) are listed and sorted from small to big. See figure H.4, page 169. In the last column of this list, the step-size in the total amount of reinforcement is shown as a percentage. From this column, it becomes clear that for realistic spacing and bar diameters the step-size in the amount of reinforcement lies between 4% and 26%. The mean step-size is equal to 10%.

From the example shown in appendix H, it becomes clear that in practice it could be hard to reduce for example 5% of reinforcement as the possibilities in the reinforcement design are limited due to for example requirements on spacing and available bar diameters. Following the requirements on crack width, also not every available bar diameter can be used.

8.4. Conclusions

Based upon the results of the curved bridge deck, the following conclusions can be drawn.

Loading and reaction forces

- The resultant of the reaction forces is almost equal for all 3 models. This means that all the models are loaded with and identical or equivalent load.
- The reaction forces of the orthotropic plate and 3D plate model are almost identical for all load-cases. The reaction force diagram of the grillage model deviates from the other 2 models.

Bending moments

- The uniform distributed load and the tandem system show the biggest difference in load-spread. The difference in maximum moment is equal to 8.7% and 10.5 % respectively.
- The self-weight shows some difference in load-spread. The self-weight spreads out as a result of the curved layout of the bridge deck. The inner curve is stiffer and will take a relatively larger portion of the loads.
- When pre-stressing is taken into account, the difference between the maximum longitudinal bending moment of the grillage and orthotropic plate model increases as the self-weight becomes less dominant. The difference between the maximum longitudinal bending moment of both models increases from 5.2% to 7.1%.
- The transverse bending moment of the grillage model is smaller compared to the orthotropic plate model. Based upon the self-weight, it can be concluded that indeed the effect of lateral contraction is not taken into account in the grillage model.

Transverse load-spread of self-weight

- Due to the curvature of the bridge deck, the inner edge is stiffer compared to the outer edge of the deck. This means that also the self-weight of the bridge spreads in transverse direction. This transverse load-spread is less stronger for the grillage model compared to the orthotropic plate model.
- For evenly distributed loads (i.e.: self-weight) there can also be transverse load-spread, depending on the shape of the bridge deck. For a curved bridge deck, the inner edge is stiffer compared to the outer edge. This results into transverse load-spread and into differences in transverse load-spread between the grillage and orthotropic plate model.

Design bending moments

- For bottom reinforcement in the longitudinal direction of the bridge deck, the difference between both models is 6.8%. This is slightly less compared to the difference between the longitudinal bending moment (7.1%). For the grillage model, the torsional moment is lower, which decreases the difference between the results for MyD-.
- In transverse direction, the grillage model requires more top reinforcement compared to the orthotropic plate model (51.7%) and less bottom reinforcement (-10.6%). As the transverse design bending moments are small compared to the longitudinal design bending moment for bottom reinforcement, their impact on the total amount of reinforcement is very small.
- For the grillage model, the sum of design bending moments is 7.3% larger compared to the orthotropic plate model (table 8.4). As the sum of all design bending moments is a measure for the total amount of reinforcement needed, the grillage model requires about 7.3% more reinforcement compared to the orthotropic plate model.
- Compared to the practical possibilities to save reinforcement (appendix H), the theoretical difference (7.3%) between the amount of reinforcement of the grillage an orthotropic plate model is small.

9

Curved and skewed deck

This chapter shows the results of the curved and skewed bridge deck. Also for this deck, the resultants of the reaction forces are used to check whether all models were loaded equivalently. For curved and skewed bridge deck, the same comparisons were made as for the curved bridge deck (chapter 8).

The conclusions that can be drawn on the results of the curved and skewed bridge deck are shown in the last section of this chapter.

9.1. Reaction forces

First, the reaction forces of the curved and skewed bridge deck are used to check whether all models were loaded with equivalent loading. Table 9.1 shows the resultant of the reaction forces per load case and per model. These resultants consist of the sum of vertical reaction forces (F_z) and their resultant bending moment around both axis (M_x and M_y).

Table 9.1: Resultants of the reaction forces

load	model	F_z (kN)	M_x (kNm)	M_y (kNm)
SW	grillage	12543	1079	6647
	orthotropic plate	12543	1088	6659
	3D plate	12543	1079	6647
UDL	grillage	2906	5081	6370
	orthotropic plate	2906	5075	6365
	3D plate	2906	5081	6370
TS	grillage	1200	4666	5463
	orthotropic plate	1200	4665	5464
	3D plate	1200	4665	5464

From table 9.1 it becomes clear that for each type of loading (SW, UDL and TS), the resultant of the reaction forces is almost identical for all models. The biggest relative difference can be found for M_x of the self-weight. For this load the maximum relative difference is 0.8%. Such a small error can be attributed to rounding errors in the input and in the finite element calculation itself. So, it can be concluded that all models are loaded with an equivalent loading.

Figure 9.1 (bottom edge) and figure 9.2 (top edge) show the reaction forces for each of the 2 edges of the curved and skewed bridge deck. As a result of asymmetry, the reaction forces on each of the edges are different for this bridge deck layout.

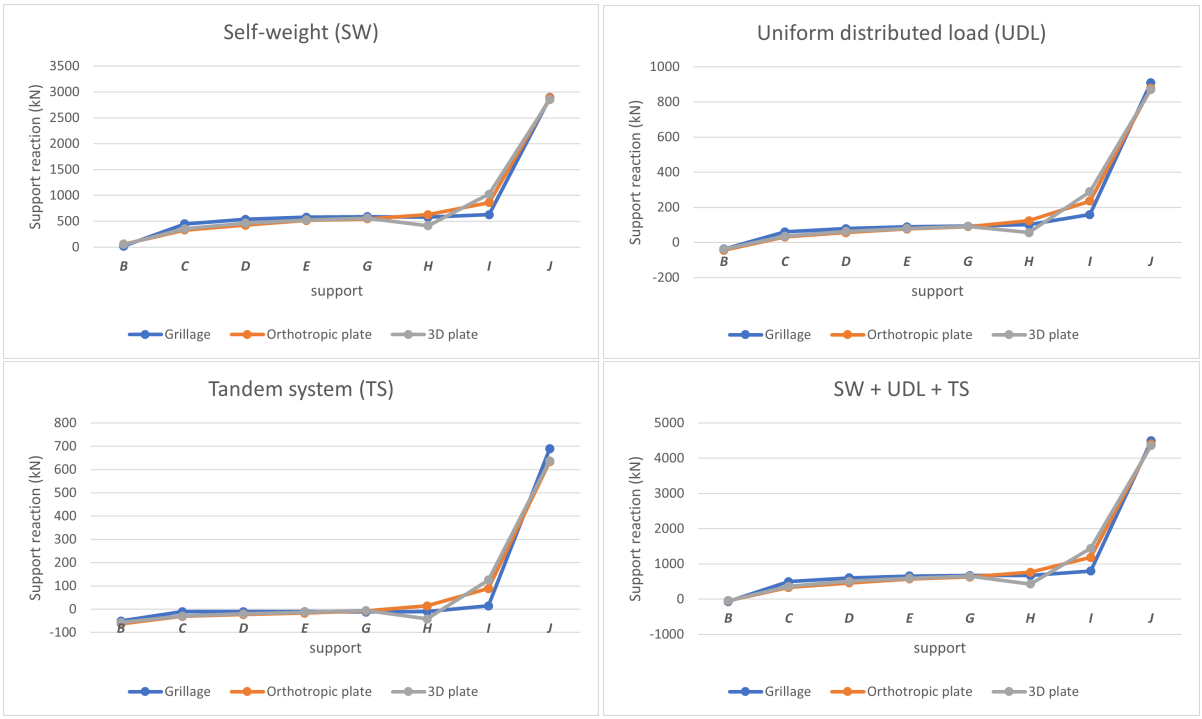

Figure 9.1: Reactions forces bottom edge

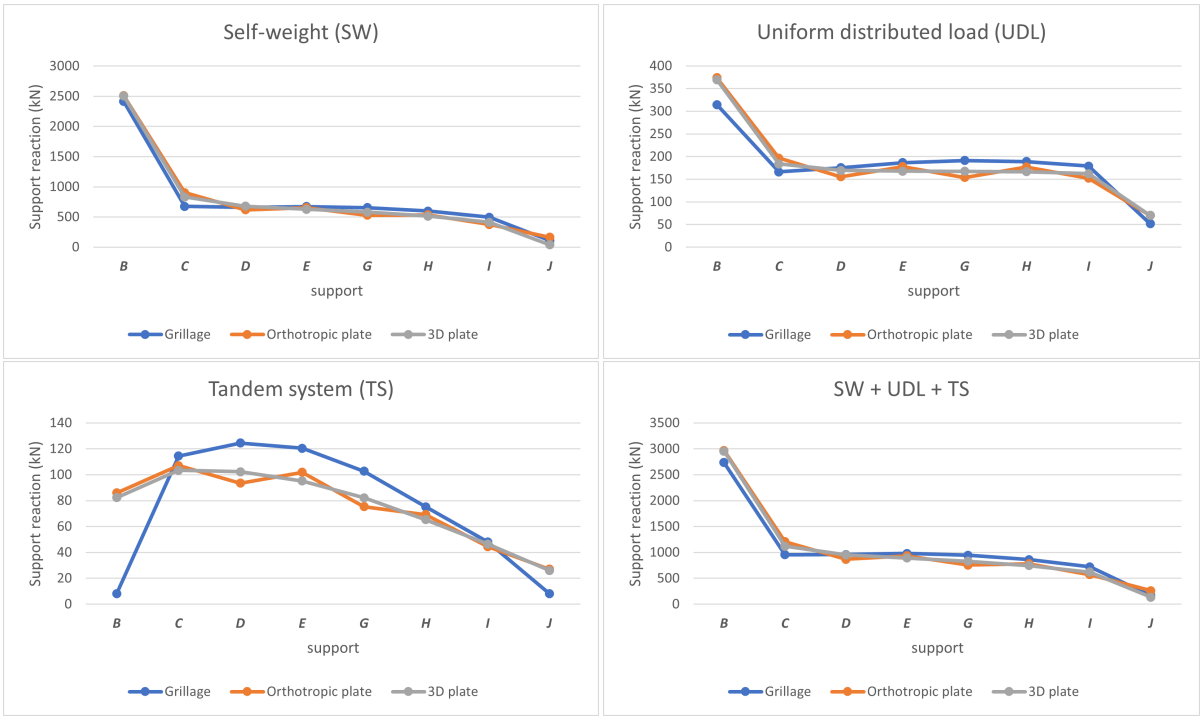

Figure 9.2: Reactions forces top edge

For all models, a clear pattern in the reaction forces can be observed. On the bottom edge, the right support is situated near the obtuse corner. For the edge on the opposite side of the bridge deck (top edge), the obtuse corner is near the left support. The support near the obtuse angle takes much more load compared to all the other supports. For a relative big part of the bridge deck, the support near the obtuse corner is the nearest support. This means that the biggest part of the load *travels* to these supports.

The most deviating support reaction is for the top edge of the grillage model loaded with the tandem system. For this load, the support reactions of the grillage model are much different compared to the orthotropic plate and 3D plate model. The difference between the grillage model and the other models is mainly the much lower support reaction at the support near the obtuse corner. Compared to the other models, the grillage model seems to have trouble to transfer the load towards support B.

For both edges, the support reactions for the sum of all loads does not deviate much. All 3 models follow the same pattern. In contrast to the straight and curved bridge decks, for the curved and skewed bridge deck the sum of support reactions of the grillage model are not an outlier compared to the orthotropic plate and 3D plate model.

9.2. Bending moments

This section shows the results of the longitudinal, transverse and torsional moments of the curved bridge deck. The moment diagram of the longitudinal bending moment shows the maximum bending moment per beam/strip. The transverse bending moment diagram is taken along transverse beam 13.

9.2.1. Longitudinal bending moments

Figure 9.3 shows the maximum longitudinal bending moments per longitudinal beam / strip. As a result of the skew, these maximum longitudinal bending moments are not aligned along one particular transverse cross-section. For the other 2 bridge deck layouts, the longitudinal bending moments were plotted along the mid-span transverse cross-section, as that is the location where the maximum longitudinal bending moment can be found. In case of the curved and skewed deck, also the maximum bending longitudinal bending moments are plotted, but the location differs per load case and per model, also the maximum bending moments do not lay on a perfectly straight line.

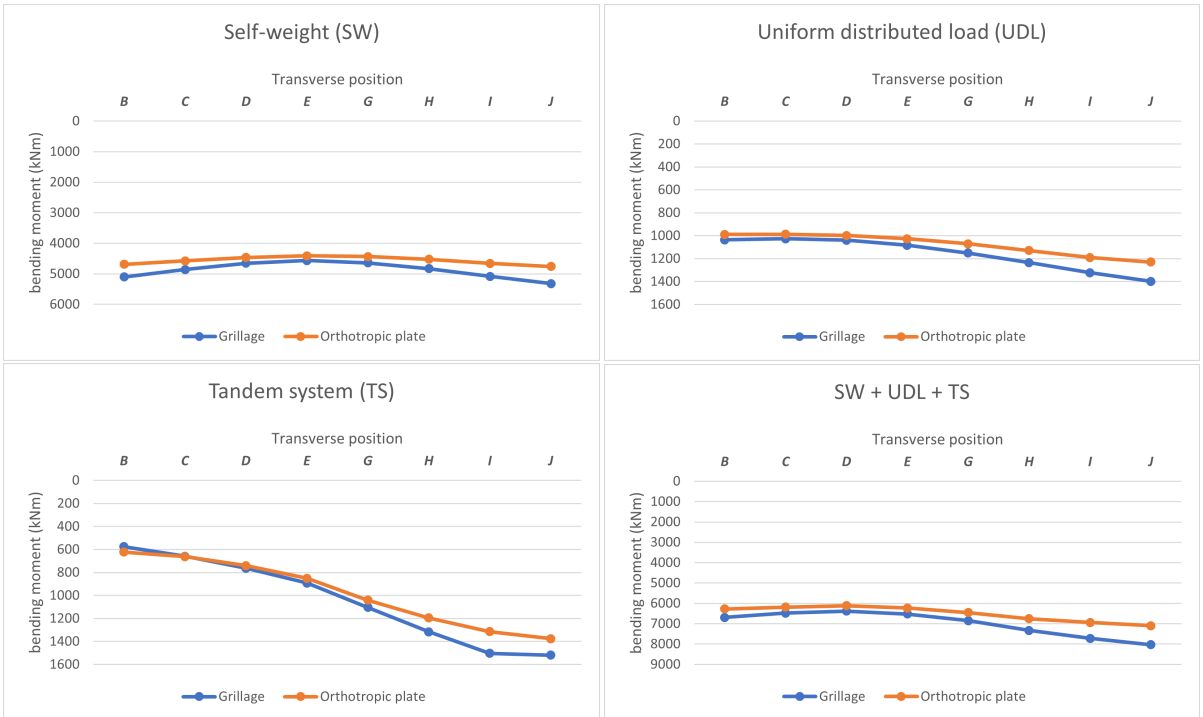

Figure 9.3: Maximum longitudinal bending moment

From figure 9.3 it becomes clear that the also for the curved ans skewed bridge deck the maximum longitudinal bending moment is larger for the grillage model. This can be observed for all types of loading. In contrast to the longitudinal bending moments of the straight and curved bridge deck, the sum of longitudinal bending moments is not the same for both models.

For the orthotropic plate model, the total longitudinal bending moment is smaller compared to the grillage model. As a result of the skew, part of the load is transferred in the transverse direction of the

deck, instead of the longitudinal direction. The load is transferred towards the nearest support. This means that not all the loading is transferred in longitudinal direction. As the orthotropic plate model has more transverse load-spread, it is easier for the orthotropic plate model to transfer part of the load in transverse direction which means that the bending moment in longitudinal direction becomes lower.

The maximum longitudinal bending moments are shown in table 9.2. This table shows the longitudinal bending moments per 2.12 m width if the bridge deck. The last column of the table shows the relative difference between the grillage and orthotropic plate model. The last rows show the maximum longitudinal bending moment for all loads combined (SW + UDL + TS) and all loads including pre-stressing (0.35*SW + UDL + TS).

Table 9.2: Maximum longitudinal bending moments (kNm), per 2.12 m

load	**grillage**	**orthotropic plate**	**difference** (%)
SW	5322	4759	11.8
UDL	1399	1230	13.7
TS	1518	1376	10.4
SW + UDL + TS	**8029**	**7099**	**13.1**
0.35*SW + UDL + TS	**4668**	**4145**	**12.6**

Table 9.2 shows that the maximum difference in load-spread can be found for the uniform distributed load (13.7%) and the self-weight of the bridge deck (11.8%). For both loads, the maximum longitudinal bending moment of the grillage model is larger compared to the orthotropic plate model. The difference for the total load is equal to 13.1%. Taking into account pre-stressing lower the difference a bit as the relatively big difference for the self-weight becomes less dominant. When pre-stressing is taken into account, the maximum longitudinal bending moment of the grillage model is 12.6% larger compared to the orthotropic plate model.

9.2.2. Transverse bending moments

The transverse bending moment diagrams of the curved bridge deck can be found in figure 9.4. The transverse bending moments are shown along transverse beam 13 of the grillage model of the skewed deck. In the grillage model of the straight and curved decks, this transverse beam is located at mid-span. Each graph shows the transverse bending moment over a width of 2.353 m.

From figure 9.4 it becomes clear that also for the deck with the skew angle, the transverse bending moment of the grillage model is smaller compared to the orthotropic plate model. For all load cases, the transverse bending moment of the grillage model follows the same shape as the transverse bending moment of the orthotropic plate model. However, for the grillage model the transverse bending moment is smaller. This is in line with which was expected. Both the absence of lateral contraction as well as the difference in load-spread will result into less transverse bending moment for the grillage model, see the hypothesis (page 6).

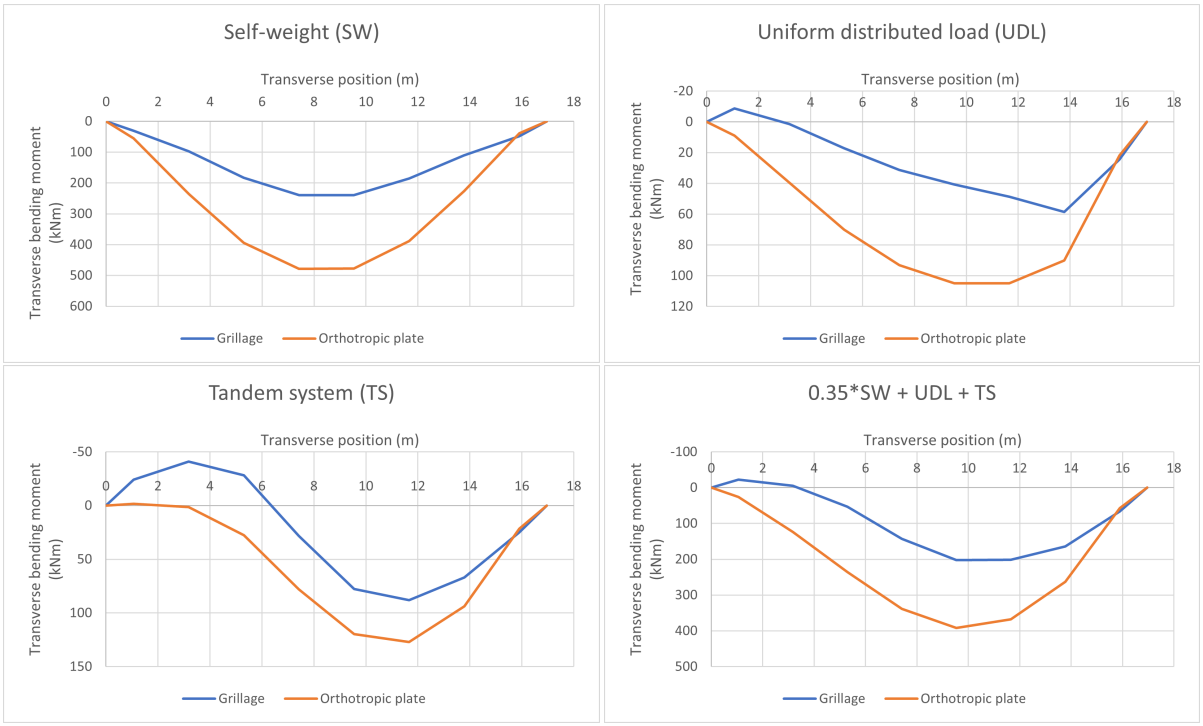

Figure 9.4: Transverse bending moment diagrams SW, UDL and TS and load-combination including pre-stressing

9.2.3. Torsional moments

Figure 9.5 shows the contour plots of the torsional moment of the skewed deck modelled as a grillage model (left) and orthotropic plate model (right). The decks are loaded with the sum of all loads (including pre-stressing), which is load combination **0.35*SW+UDL+TS**.

From figure 9.5, it becomes clear that the torsional moments of the grillage model is much smaller compared to the orthotropic plate model. The pattern of the torsional moment is similar for both models. The maximum torsional moment can be found in the lower right corner of the bridge deck. In the orthotropic plate model, disturbances around the edges are observed. These disturbances are caused by the concentrated supports.

The maximum torsional moment of the grillage model is equal to -615 kNm/m. For the orthotropic plate model, the maximum torsional moment is equal to -1089 kNm/m. However, this is a peak value. Taking the average torsional moment over a width that is equal to the width of the longitudinal beams of the grillage model results into an averaged torsional moment of -942 kNm/m. From this, it follows that the torsional moment of the grillage model is about 35% smaller compared to the orthotropic plate model.

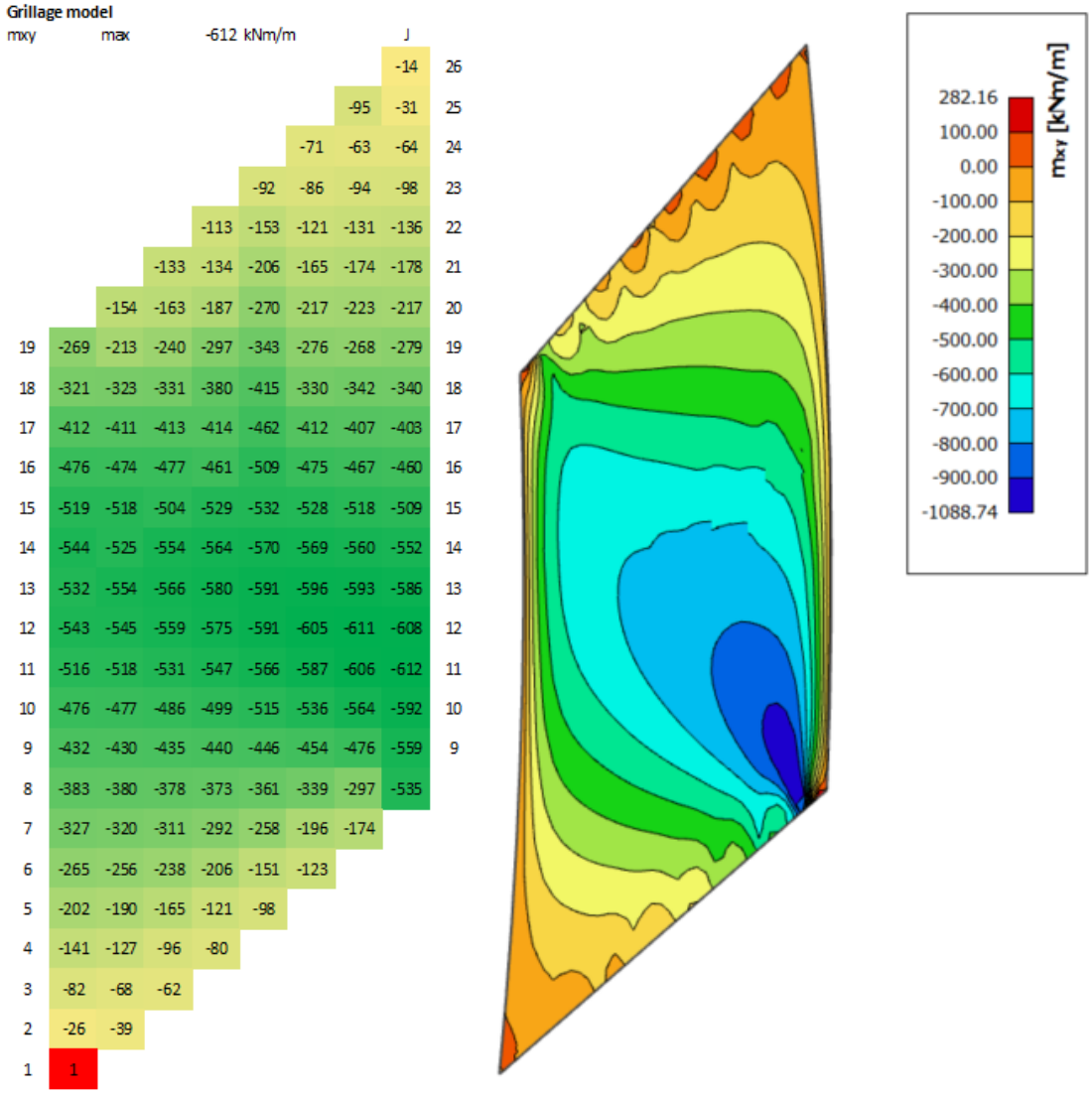

Figure 9.5: Torsional moment (kNm/m) grillage model (left) and orthotropic plate model (right)

9.3. Design bending moments

Also for the curved and skewed bridge deck, the bending moments for reinforcement design are extracted from the models. In the design bending moments, the effect of pre-stressing is included. For the grillage model the Wood-Armer moments are determined using excel, while for the orthotropic plate model, the Wood-Armer moments are extracted directly from SCIA-engineer.

Figure 9.6 shows the contour plots of the design bending moment for the bottom reinforcement in the longitudinal direction of the bridge deck (MyD-). The left plot is from the grillage model and the right plot is from the orthotropic plate model. The plots for the remaining reinforcement design bending moments can be found in appendix G (page 161)

The maximum design bending moments are shown in table 9.3. For the longitudinal bending moment, the difference between both models was equal to 12.6%. When the torsional moment is taken into account, the bending moment to design the longitudinal bottom reinforcement (MyD-) has become only 4.7%. This follows from the fact that the torsional moments of the grillage model are smaller compared to the orthotropic plate model.

For all other design bending moments, the results of the orthotropic plate model is smaller compared to the grillage model. In the skewed bridge deck, there are much larger torsional moments compared to the straight and curved bridge deck. So, the torsional moment has a relatively big contribution to

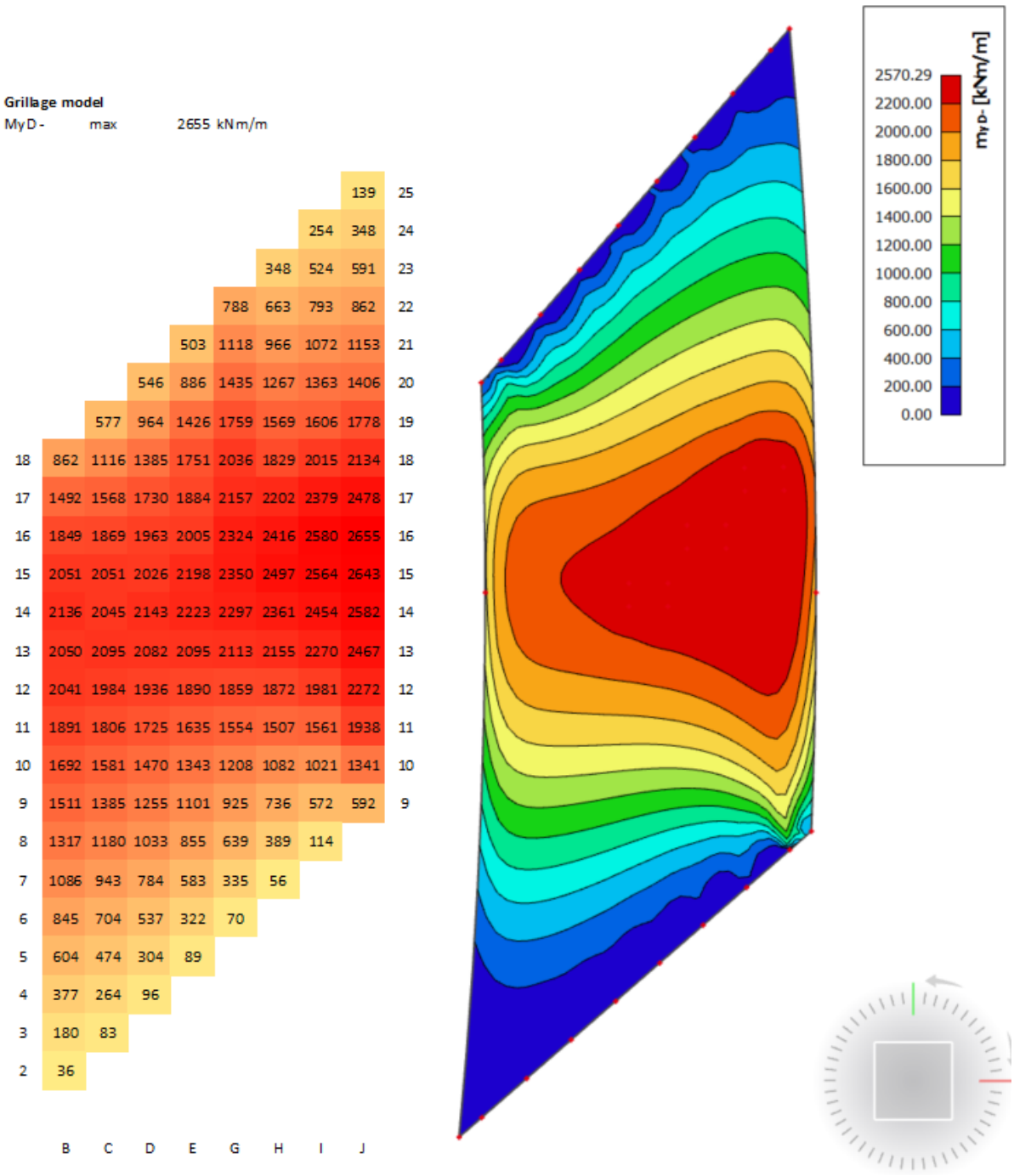

Figure 9.6: MyD-, grillage model (left) and orthotropic plate model (right) (kNm/m)

the Wood-Armer design bending moments. For the grillage model, the torsional moments are smaller compared to the orthotropic plate model, which results into lower design bending moments for MxD+, MxD- and MyD+.

The sum of design bending moments shows that the grillage model results into 11.7% less reinforcement compared to the orthotropic plate model. However, the design bending moments of the orthotropic plate exceed the maximum design bending moments of the grillage model in a very small part of the deck. This can be checked by looking at the results of the orthotropic plate model per node. In only 4% of the deck, MxD+ of the orthotropic plate is larger than the design bending moment of the grillage model (627 kNm/m). For MxD- this is 21% and for MyD+ also 4%. This means that the area

Table 9.3: Design moments (kNm/m), including pre-stressing

design moment	**grillage**	**orthotropic plate**	**difference** (%)
MxD+	627	982	-36.2
MxD-	793	1025	-22.6
MyD+	526	671	-21.6
MyD-	2655	2535	4.7
$\sum$	**4601**	**5213**	**-11.7**

in which the orthotropic plate model needs more reinforcement compared to the grillage model is very small.

9.4. Conclusions

From the results of the curved and skewed bridge deck layout, the conclusions listed below can be drawn.

Loading and reaction forces

- The resultant of the reaction forces is almost equal for all 3 models. This means that all the models are loaded with and identical or equivalent load.
- The support near the obtuse corner takes most of the load. This support is the nearest support for a relative big area of the bridge deck.
- The support reactions for the sum of all loads are almost identical for all 3 models. In contrast to the straight and curved deck, the sum of support reactions of the grillage model are not an outlier compared to the other 2 models.

Bending moments

- Also for the self-weight there is a significant difference in maximum longitudinal bending moment between the grillage and orthotropic plate model (11.8%). For the skewed deck, also the self-weight causes torsional bending moments. The biggest difference in maximum bending moment can be found for the uniform distributed load (13.7%).
- For the sum of all loads, the maximum longitudinal bending moment of the grillage model is 13.1% larger compared to the orthotropic plate model. Taking into account pre-stresssing, lowers the difference between both models to 12.6%.
- In the orthotropic plate model, the total longitudinal bending moment is smaller compared to the grillage model. Due to the skew, part of the load is transferred in transverse direction as this is the shortest path to the support. In the grillage model, a smaller part of the load seems to be transferred in the transverse direction, resulting into a larger total longitudinal bending moment.
- Both the transverse as well as the torsional bending moment of the grillage model are lower compared to the orthotropic plate model.

Design bending moments

- The design bending moment for longitudinal bottom reinforcement is 4.7% higher for the grillage model.
- For the other design bending moments, the orthotropic plate model gives higher maximum values. However, by looking at the design bending moments on node level, it can be concluded that the design bending moments of the orthotropic plat models exceeds the design bending moments of the grillage model in a small area of the bridge deck only (4%-21%). This means that the orthotropic plate model needs extra reinforcement in a relatively small area only.
- As the extra reinforcement of the orthotropic plate model is needed in a small area only, it is neglected. This results into an upper-bound of the extra amount of reinforcement needed for the grillage model. This upper-bound is equal to 4.7%.
- Compared to the practical possibilities to save reinforcement (see chapter 7, page 110) or appendix H, page 167), the theoretical difference (up to 4.7%) between the amount of reinforcement of the grillage an orthotropic plate model is small.

III

Conclusion

10

Discussion, conclusions and recommendations

In this chapter, the discussion, conclusions and recommendations for further research can be found. The conclusions are split-up into the conclusions to the sub-questions presented in chapter 1 (page 5) and the answer to the main research question of this thesis. The main research question shown in chapter 1, is repeated below. The conclusion to this study can be expanded and supported by follow-up research. Suggestions for a follow-up research can be found in the recommendations.

10.1. Discussion

This section shows the discussion to the study presented in this thesis. The discussion is categorized per topic.

Case simplification

- The stiffer edges of the bridge deck are left out of the the cross-section of the bridge as these stiffer parts could not easily be incorporated in the orthotropic plate model. Leaving out the edge beams made the comparison between the models more fair. However, the real bridge decks are stiffer on the edges compared to the created models. The stiffer edge of the bridge deck can have effects on the load distribution, which is not included in this study.
- Leaving out the stiffer edges of the bridge deck was not needed for the grillage model. The benefit of the grillage model compared to the orthotropic plate model is that in the grillage model every longitudinal beam can have a different cross-section. This means that the edge beams of the real cross-section of the bridge deck (figure 2.1, page 9) can be modeled in the grillage model Using the grillage model, the real cross-section of the bridge can be modeled more accurately compared to the orthotropic plate model.
- Above the supports the bridge decks have a solid cross-section. This solid cross-section was not included in the case study. In the real bridge deck, this solid cross-section provides a relative big torsional stiffness compared to the voided bridge deck in the span. These effects are not included.
- The bridge decks of the Blankenburgverbinding consists of multiple statically indeterminate spans, while this study considered a single simple supported span. In further research, the same study presented in this thesis could be applied to a multiple statically indeterminate bridge decks.

Software

- In this study, it was decided to create all models using SCIA-engineer. By doing this, it was ensured that for all models the material properties were identical. Eventually, these material properties comes down to the Young's modulus E of the concrete only, as only linear material behaviour was considered in this study. In retrospect, it can be concluded that (for the material properties) it may not have been necessary to create all models with SCIA-engineer.

- For this study, the grid of the grillage model was created by hand using SCIA-engineer. Instead of using SCIA-engineer, it would have been easier to create the grillage model using Midas civil, as this software provides a spacial wizard to create the grillage model. The downside of such a wizard is that it could be a kind of *black-box*. If a wizard is not described very well, it can be hard to determine whether certain effects are included in the model or not and what other assumptions are made. By using SCIA-engineer, this potential *black-box* was avoided as the grillage model was completely created by hand.

Torsional stiffness

- Using the strips taken out of the deck, the longitudinal and transverse stiffness of the 3 models were compared to each other and the analytical solution of the Timoshenko beam. The longitudinal and transverse strip showed that all models have almost identical longitudinal and transverse stiffness. From the strips, it cannot be concluded whether the torsional stiffness is the same for all models.

Bending moment 3D plate model

- The longitudinal bending moments of the 3D plate model were determined indirectly. This was done by looking at the ratio in slopes of normal force diagrams and divide the total longitudinal bending moment over the whole cross-section accordingly. For the other 2 models, the bending moments were extracted from the results directly.

Design bending moments

- In the comparison of the design bending moments, it is assumed that the reinforcement design is identical over the whole length or width of the bridge. In reality, the bridge deck will be divided into zones. For each of these zones (i.e. near the edge and the rest of the field) the reinforcement design can be different. For the design bending moments of the orthotropic plate model of the curved and skewed deck, the area over which the design bending moments of the orthotropic plate model exceed the design bending moments of the grillage model is taken into account. This area was equal to 4% - 21% of the bridge deck.
- For the straight bridge deck, the design bending moments were not studied. It is expected that result of the straight bridge deck is similar to the result of the curved deck. For the straight deck, there is no transverse distribution of self-weight. Based upon this, it is expected that the difference between the longitudinal bending moment of the grillage and orthotropic plate model becomes slightly smaller, which is beneficial for the design moments of the grillage model. Due to the shape of the deck, it is also expected that the torsional moment of the straight deck is slightly smaller compared to the curved deck, which is not beneficial for the design moments of the grillage model. The net effect of these 2 contributions (longitudinal and torsional moment) is expected to be small.

10.2. Conclusions

This section gives an overview of the answers to the sub-questions and the main research question stated in section 1.2 on page 5 of the report.

Sub-questions
Validation of the models

- All models have the same longitudinal and transverse stiffness, this follows from the strip models of chapter 6 (page 79).
- The deflections of the orthotropic plate model and the 3D plate model are almost identical. For all models, the reaction forces are quite close to each other. The ortotropic plate and 3D plate model show more agreement compared to the reaction forces of the grillage model (page 81).
- The orthotropic plate model describes the behaviour of the bridge deck correctly. The results of the orthotropic deck were validated using a 3D plate model. This validation showed agreement on at least the stiffness, reaction forces and transverse load-spread (chapter 7).

Differences in load-spread

- For the grillage model, the maximum longitudinal bending moment is larger compared to the orthotropic plate model. Away from the point of application of the force, the longitudinal bending moments is lower compared to the orthotropic plate model. The transverse bending moment as well as the torsional moment of the grillage model are lower compared to the orthotropic plate model. From these observations, it can be concluded that the grillage model has less transverse load-spread compared to the orthotropic plate model.
- The difference in load-spread increases with increasing eccentricity of the applied load (page 89).
- The transverse load-spread is mainly influenced by stiffness parameters D_{33} (torsional stiffness) and D_{44} (transverse shear stiffness). For lower stiffnesses, the load-spread decreases and for higher stiffnesses, the transverse load-spread decreases (page 95).
- For the curved bridge deck, the tandem system (TS) of the traffic load results into the biggest difference in load-spread. The smallest difference in load spread is observed for the self-weight . When pre-stressing is taken into account, the difference in transverse load-spread between both models becomes larger as the self-weight becomes smaller (page 105).
- In case of the curved and skewed bridge deck, also the self-weight results into a relative big difference in transverse load-spread. As a result of the skew, the self-weight causes torsion of the bridge deck (page 117). Taking into account pre-stressing has a minor effect on the difference in load-spread of the curved and skewed deck (page 116).

Design bending moments

- When looking at the design bending moments of the curved deck, the difference in load-spread between the grillage and orthotropic plate model becomes slightly smaller, as the torsional moments of the grillage model are smaller compared to the orthotropic plate model (page 107 and page 117). In case of the curved and skewed deck, the difference between the load-spread becomes a lot smaller when looking at the design bending moments compared to the longitudinal bending moments. This follows from the fact that the skewed deck has a lot more torsion compared to the curved deck.
- The difference in design bending moment depends on the layout of the bridge deck. The skewed deck has much more torsional moment, which is in favour of the grillage model. This means that for the grillage model, the result of the skewed bridge deck is less conservative compared to the curved bridge deck layout.
- The grillage model of the curved deck results in about 7.3% more reinforcement compared to the orthotropic plate model (page 109), for the curved and skewed deck, this is equal to 4.7%, which is an upper-bound (page 120).

Reinforcement design in practice

- The possibilities in the reinforcement design are limited by detailing requirements (i.e.: spacing, applicable bar diameters) and available bar diameters. The example of appendix H (page 167) showed that the step-size in the amount of reinforcement can be up to 26%. For this example, the mean step-size between the different amounts of reinforcement is equal to 10%.

Final conclusion
to which extend does the transverse load-spread of a voided orthotropic bridge deck modeled as a grillage model differ from an orthotropic plate model. And what does this mean for the practical usability of the grillage model in engineering practice?

It can be concluded that the grillage model results in less transverse load-spread. The follows from the fact that the maximum longitudinal bending moments of the grillage model are larger compared to the orthotropic plate model and the transverse bending moments of grillage model are smaller compared to the orthotropic plate model. The difference in transverse load-spread increases for increasing eccentricity. This means that there is no need to reject the hypothesis presented in chapter 1.

The differences in design bending moment between the grillage and orthotropic plate model are up to 4.7% for the curved and skewed deck and about 7.3% for the curved deck. The difference between both models is relatively small. In engineering practice it can be hard to save for example 5% of reinforcement. This has mainly to do with the fact that the solutions space of the reinforcement design is limited. Examples of limitations are: the available space, possible spacing, requirements from detailing (crack-width control) and the available bar diameters. The spacing of the reinforcement bars may not be to big, otherwise it is not possible to walk on it during the construction. On the other hand, the spacing may not be too small, otherwise the concrete segregates during casting.

The theoretical difference between the reinforcement design of the grillage and orthotropic plate model could become very small or even completely vanish as a result of the effects discussed above and due to rounding differences. This means that the theoretical difference in the amount of reinforcement doesn't have to mean that the design of the reinforcement is also different in practice. For some cases, the theoretical difference also translates into a practical difference in the amount of reinforcement and for some cases the possibilities to reduce reinforcement are limited which could result into (almost) the same amount of reinforcement for both models. Based upon this, it can be concluded that the grillage model doesn't necessarily results into a less economical reinforcement design, as a result of the discrete nature of the design possibilities the engineer has.

Eventually, it depends on the situation (i.e.: type of project and phase of the design) whether it is beneficial to use a grillage model or not. When a lot of the same bridges or spans need to be designed, the model of the bridge has to be created only once. In that case, a possibly (small) reduction on the amount of reinforcement for only one bridge deck, can have a significant impact on the total amount of reinforcement for the whole project. For such a project, the extra effort that is needed to create the orthotropic plate model is probably smaller, than the benefit from saving reinforcement when the orthotropic plate model is used instead of a grillage model.

For the bridge decks of the Blankenburgverbinding, every single span is different. This means that it is beneficial to model the bridge decks of the Blankenburgverbinding using a grillage model, as all spans need to be modeled. The cross-section of the Blankenburgverbinding also has stiffer edge beams. These edge beams can perfectly be modeled in the grillage model, while for the orthotropic plate model, the edge beams cannot be modeled. The benefits of the grillage model (i.e.: shorter calculation time and easier to apply pre-stressing) outweigh the probability that for some spans, the design of the reinforcement is less economical compared to the orthotropic plate model.

Also the phase of the design can play a role in the decision making. During a tender phase, the most important question is *"is the design technically feasible and what are the approximate costs to build it?"*. As there are still a lot of uncertainty's, the grillage model is accurate enough for this phase of the design.

In order to be able to make a better decision which model to use, it is advised to investigate - and where possible quantify - the benefits (such as modelling time, calculation time, applying pre-stressing, etc.) of the grillage model, compared to the orthotropic plate model. This can be done in a follow-up research. Together with the results following from this study, the results of this follow-up research will give a more complete overview from which the structural engineer can decide to use a grillage model or not.

10.3. Recommendations

The assumptions and choices made in this study make it hard to draw conclusions on the practical benefits of the grillage model compared to the orthotropic plate model. It is recommended to do a follow-up research in which the following aspects of the grillage and orthotropic plate model will be compared:

- Which software to use
- Effort to set-up the models
- Applying pre-stressing
- Calculation time
- Optimization of cross-section
- Extraction of results

In this study, it was chosen to make all models in SCIA-engineer. This was done to be sure that all material parameters, load-application and the presentation of the results were as uniform as possible. However, the software Midas civil provides a special wizard to create a grillage model automatically. When the effort to set-up the grillage model is compared to the orthotropic plate model, it would be more fair to make use of such a wizard. It is expected that with the help of this wizard in Midas, the grillage model can be set-up more easily. Based upon the cross-section of the deck, Midas calculates the stiffness properties of the longitudinal and transverse beams and creates the grid of the model automatically.

In SCIA-engineer, all beams need to be drawn by hand. In a follow-up research, it is advised to use the most suitable software for each model. By doing this, the comparison on the effort to set-up the models is fair. However, when a wizard is used, it is also important to investigate the background of the such a wizard. For example, which types of deformations are taken into account in the stiffness properties and what other assumptions does the wizard make?

The tandem system of the traffic load was applied for one location only. In practice, the traffic load will be applied to the bridge deck for a lot more locations, in order to find out the most unfavourable position of the tandem system. This results into a lot more load-cases and a lot more load-combinations. When the number of load-cases increases, the difference in calculation time between both models will become more clear. For the number of load-cases used in this study, there is no significant difference between the calculation time of the grillage model and the orthotropic plate model.

In further research, it is needed to apply the tandem system of the traffic load at all possible positions in the longitudinal direction of the bridge deck. For each load-case, the tandem system has moved for example 10 cm. It is expected that for a lot of load-cases and a lot of load-combinations, the calculation time of the grillage model is much shorter compared to the orthotropic plate model. The orthotropic plate model has much more nodes compared to the grillage model. This means that the matrix that has to be solved for every load-case is much smaller for the grillage model. A smaller matrix means a shorter calculation time.

A shorter calculation time also means that it is easier to adjust the cross-section a bit and to see the effects of this adjustment quicker. Expecting a shorter calculation time for the grillage model, also means that it is expected that it is easier to do optimizations of the cross-section.

For this current study, the pre-stressing was applied indirectly. This was done by lowering the self-weight of the bridge deck. In practice, the pre-stressing would be applied as an external load. For the grillage model, the external load of the pre-stressing force can be applied to the longitudinal beams directly. In case of the orthotropic plate model, first some auxiliary bars needs to be created, before the pre-stressing can be applied. As a result of this, it is expected that is easier to apply pre-stressing to the grillage model, compared to the orthotropic plate model. For a follow-up research it is advised to apply the pre-stressing force as an external load, in order to find out for which model it is easier to apply the pre-stressing.

In a follow-up research, the grillage and orthotropic plate model can be compared based upon the criteria discussed above. Where possible, the differences between both models can be quantified (time to set-up the model, calculation time, number of nodes, etc.). The results of the follow-up research can be taken into account next to the observed difference in transverse load-spread, to make a better consideration whether to use a grillage model or not.

IV

Appendices

A

Definition torsional stiffness SCIA-engineer

In order to be sure that *SCIA-engineer* uses the same definition for the torsional stiffness as used in this thesis, two identical plates were loaded in pure torsion. The plates have a dimension of 10 x 10 m and a uniform thickness of 200 mm. Both plates are made out of concrete, with strength class C45/55. This means that: $E = 36\,300$ MPa and $G = 15\,125$ MPa. The plates are supported in two diagonal corners, and is loaded with 2 point loads of $F = 1000$ kN in the other two diagonal corners, see figure A.1. In literature, this load-case is also known as the *Nadai's plate*.

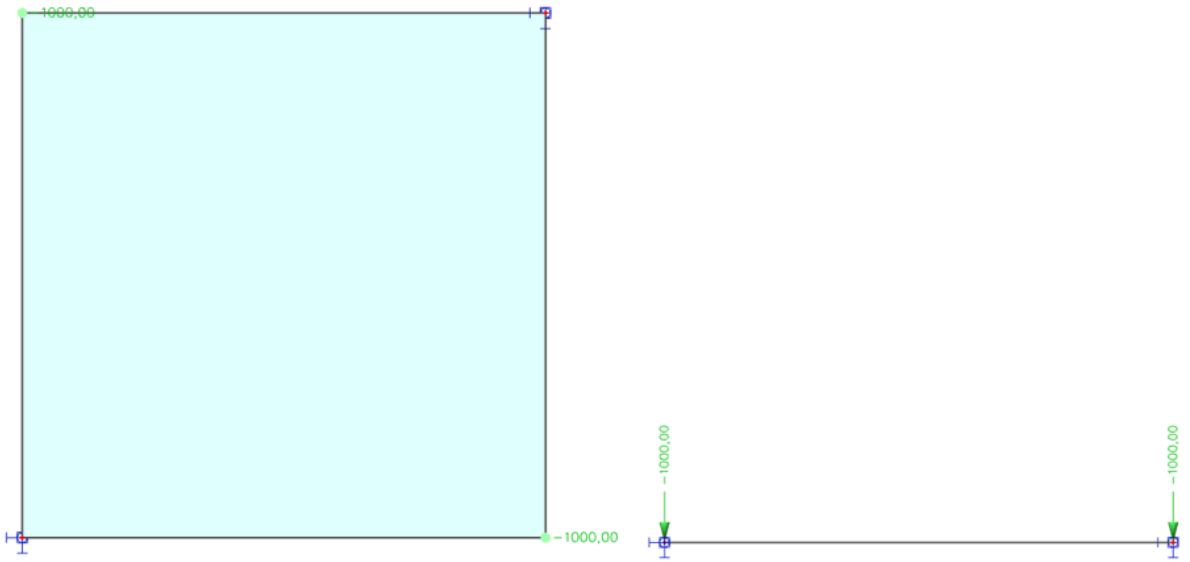

Figure A.1: Nadai's plate. *left: top view, right: side view*

Both the isotropic and the orthotropic plate were modelled in *SCIA-engineer*. One of the plates was modelled using an ordinary isotropic plate, the other plate was modelled using an orthotrpic plate. The stiffness parameters of the orthotrpic plate were calculated as if it was an isotropic plate with a uniform thickness of 200 mm and uniform material parameters. In case the torsional stiffness has been calculated according to the same definition as *SCIA-engineer* uses, both plates will show identical torsional deformation.

Torsional stiffness calculation

In this thesis, the torsional stiffness is calculated using the following equations [2]:

$$\begin{aligned} i_{xy} &= \frac{I_t}{2b} \\ i_{yx} &= \frac{I_t}{2b} \\ i_{av} &= \frac{1}{2}\left(i_{xy} + i_{yx}\right) \\ D_{33} &= G\frac{i_{av}}{2} \end{aligned} \tag{A.1}$$

The cross-section of the plate is a rectangle, for both directions of the plate the torsional stiffness is equal to:

$$I_t = \frac{1}{3}bt^3 \tag{A.2}$$

This results in to the following equation to calculate the torsional stiffness D_{33}:

$$\begin{aligned} i_{xy} = i_{yx} &= \frac{1}{6}t^3 \\ i_{av} &= \frac{1}{6}t^3 \\ D_{33} &= \frac{1}{12}Gt^3 \end{aligned} \tag{A.3}$$

Filling in $t = 200\,\text{mm}$ and $G = 15\,125\,\text{MPa}$, it follows that the torsional stiffness is equal to:

$$D_{33} = \frac{1}{12} \cdot 15\,125 \cdot 0.2^3 = 1.0083 \times 10^1\,\text{MN/m}$$

The other stiffness parameters of the orthotropic plate were calculated automatically by *SCIA-engineer*. An overview of those parameters can be found in figure A.2. The *d*-components refer to the in-plane stiffnesses and the *D*-components to the out-of-plane stiffness properties.

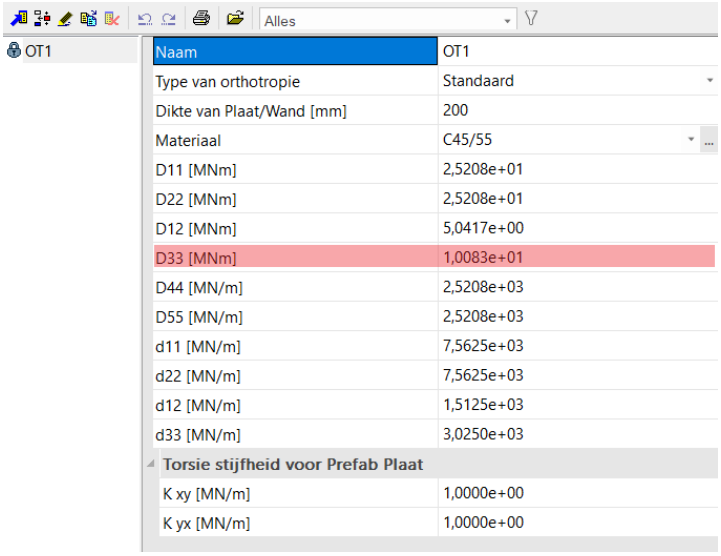

Figure A.2: Stiffness parameters ortotropic Nadai's plate

Results and conclusion

Figure A.3 shows the deformed shape of both the isotropic as well as the orthotropic Nadai's plate. The maximum deflection of the isotropic plate is 1254.9 mm, for the orthotropic plate the maximum deflection is equal to 1254.7 mm. This means that both plates result into an identical deformation due to torsion, under the exact same loading and support conditions. From this, it can be concluded that the manually calculated torsional stiffness of the orthotropic plate is identical to the torsional stiffness of the isotropic plate calculated by *SCIA-engineer*. This means that the definition of the torsional stiffness used in this thesis is equal to the definition that *SCIA-engineer* uses.

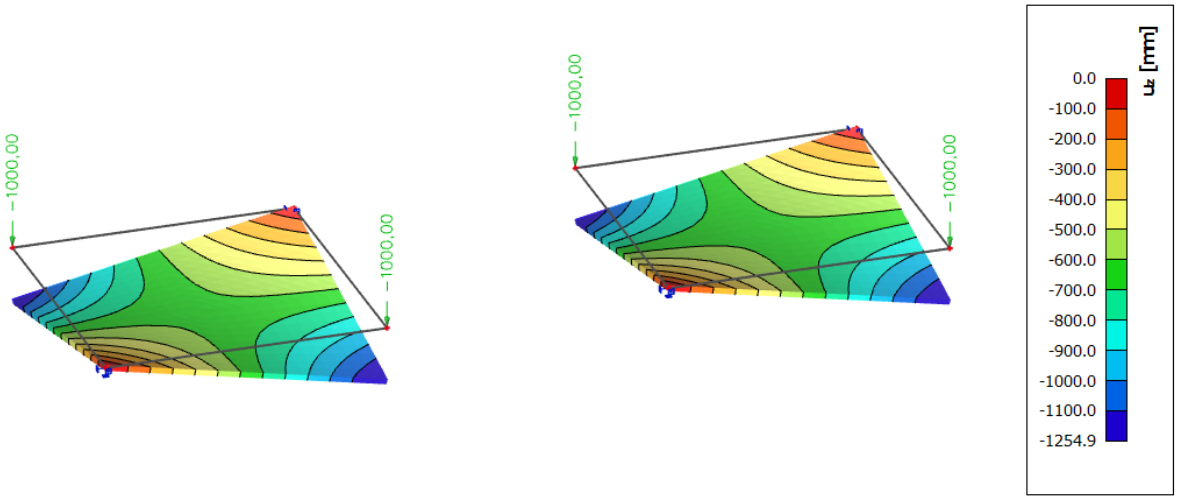

Figure A.3: Torsional deformation Nadai's plates. isotropic plate (left), orthotropic plate (right)

B

Wood-Armer moments

This appendix shows the formulas to calculate the Wood-Armer moments (Wood-Armer, 1968). These moments can be used to design the reinforcement of a plate in 2 orthogonal directions. The Wood-Armer moments are a combination of the bending moments in the direction of the reinforcement itself plus the absolute value of the torsional moment. For the reinforcement, there are 4 different design bending moments, in 2 directions at the bottom and in 2 direction at the top of the plate.

The definition of these 4 design bending moments can be found in figure B.1. This figure shows 2 cuts in 2 directions. For each direction, the top and bottom reinforcement is shown. The positive direction of the Wood-Armer moments is such that there is always tension in the reinforcement bars. This corresponds to the main purpose of the reinforcement: taking tensile forces. This also means that the Wood-Armer moments must always be ≥ 0.

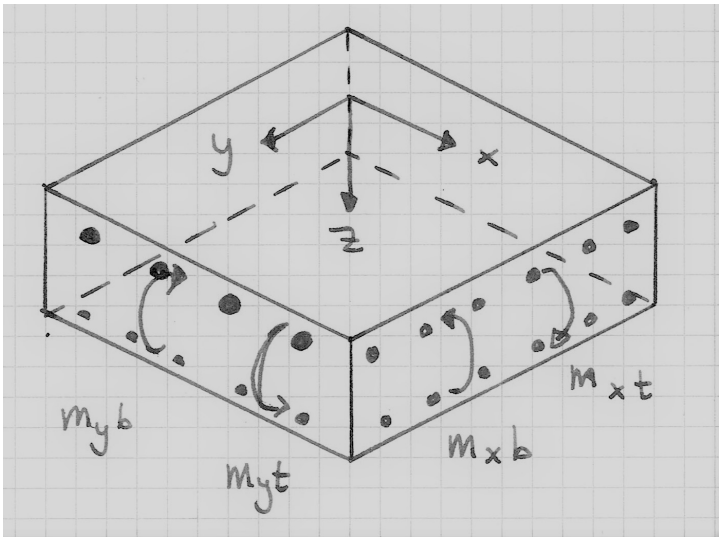

Figure B.1: Definition Wood-Armer moments

If the z-axis of the plate points downwards, the bending moments m_{xx} and m_{yy} of the plate are positive for sagging and negative for hogging bending moments. For the bottom reinforcement, the positive definition of the Wood-Armer moments corresponds to the positive definition of m_{xx} and m_{yy}. For the top reinforcement, the positive definition of the Wood-Armer moments is opposite. For the bottom reinforcement, the negative values of m_{xx} and m_{yy} are taken. The formulas of the Wood-Armer moments are shown on the next page.

Bottom reinforcement

$$\begin{aligned} m_{xb} &= m_{xx} + |m_{xy}| \\ m_{yb} &= m_{yy} + |m_{xy}| \end{aligned} \tag{B.1}$$

When m_{xb} would be ≤ 0

$$\begin{aligned} m_{xb} &= 0 \\ m_{yb} &= m_{yy} - \frac{m_{xy}^2}{m_{xx}} \end{aligned} \tag{B.2}$$

When m_{yb} would be ≤ 0

$$\begin{aligned} m_{xb} &= m_{xx} - \frac{m_{xy}^2}{m_{yy}} \\ m_{yb} &= 0 \end{aligned} \tag{B.3}$$

When m_{xb} and m_{yb} would be ≤ 0

$$\begin{aligned} m_{xb} &= 0 \\ m_{yb} &= 0 \end{aligned} \tag{B.4}$$

Top reinforcement

$$\begin{aligned} m_{xt} &= -m_{xx} + |m_{xy}| \\ m_{yt} &= -m_{yy} + |m_{xy}| \end{aligned} \tag{B.5}$$

When m_{xt} would be ≤ 0

$$\begin{aligned} m_{xt} &= 0 \\ m_{yt} &= -m_{yy} + \frac{m_{xy}^2}{m_{xx}} \end{aligned} \tag{B.6}$$

When m_{yt} would be ≤ 0

$$\begin{aligned} m_{xt} &= -m_{xx} + \frac{m_{xy}^2}{m_{yy}} \\ m_{yt} &= 0 \end{aligned} \tag{B.7}$$

When m_{xt} and m_{yt} would be ≤ 0

$$\begin{aligned} m_{xt} &= 0 \\ m_{yt} &= 0 \end{aligned} \tag{B.8}$$

C

Transverse shear stiffness

In the transverse direction, the bridge deck of the Blankenburg case is Vierendeeel-like cross-section. This means that next to bending deformation, there can be a lot of shear deformation as well.

The shear stiffness in transverse direction can be determined by modelling a shear frame in a framework program, such as *MatrixFrame*. A frame in a framework program is able to deform due to bending and axial deformation. In order to determine the shear deformation of the frame only, the axial deformation of the rods in the framework must be eliminated. In *MatrixFrame* the user is able to assign the following cross-sectional properties: Young's Modulus (E), cross-sectional area (A) and second moment of inertia (I). The axial deformation of the rods can be eliminated by setting the cross-sectional area A to infinity, as this also means that the axial stiffness EA becomes infinite. For E and I, the real values can be assigned.

The shear frame consists of rigidly connected vertical and horizontal rods. The shear frame represents one box of the bridge deck in the transverse direction, see figure C.1. This 2120 mm wide box is loaded with a shear force of $V = 10$ MN per meter in the longitudinal direction of the bridge deck.

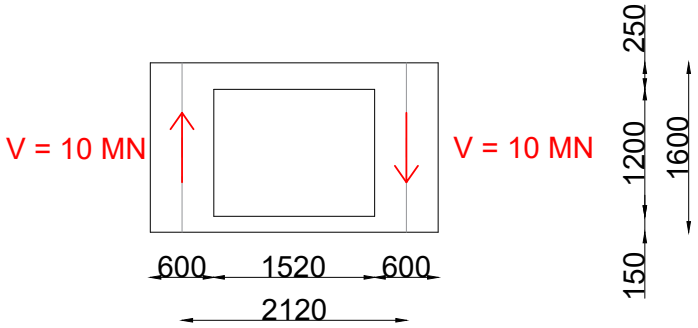

Figure C.1: Shear element

Upper- and lower-bound shear frame models

Initially, two shear frames are created, one frame being a lower-bound and one being an upper-bound. The dimensions, loading and boundary conditions of these shear frames are shown in figure C.2. For the lower-bound shear frame, the system lines of all rods follow the centre lines of the considered box (see figure C.1). The upper-bound shear frame follows the inner edges of the web-parts and the centre lines of the top and bottom plate. In reality, the horizontal top and bottom plate are rigidly connected to the web. This means that in case of the lower-bound shear frame shown in figure C.2, the bending stiffness of the top and bottom plate is underestimated in the zone of the web. This is because the top and bottom plate are not only rigidly connected to the webs, they also experience bending stiffness over the thickness of the web.

A shear frame that follows the centre lines of the elements is expected to deliver a lower-bound of the shear stiffness, as the top and bottom plate are able to rotate around the centre line of the web. An

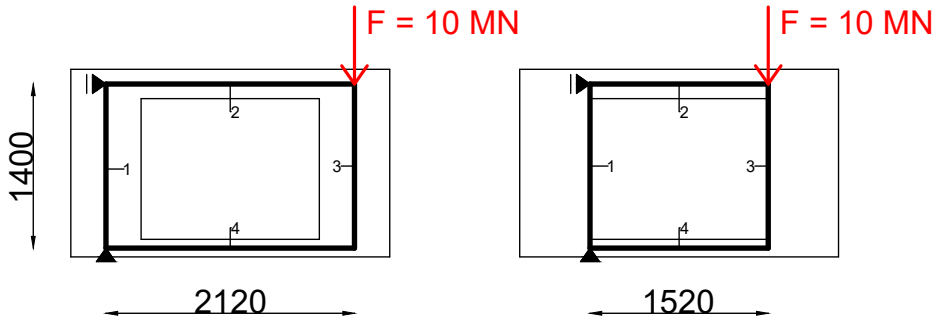

Figure C.2: Shear frames, lower-bound (left), upper-bound (right)

upper-bound of the shear stiffness can be found when the system lines of the shear frame are located at the edges of the web. This shear frame is expected to be too stiff as the top and bottom plate can rotate around the inner corners of the web. Rotations of the top and bottom plate relatively to the web are completely neglected in this model. The cross-sectional properties of the elements of the shear frame models can be found in table C.1. All rods have a unit width of 1 m (in the longitudinal direction of the deck), a Young's modulus of $E = 36\,300$ MPa. The cross-sectional area is set to $A = 1 \times 10^{10}$ m^2, in order to set the axial stiffness EA to infinity.

Table C.1: Cross-sectional properties shear frame models

#	height h (mm)	I_y (10^{-2} m^4)
1	600	18.00
2	250	1.302
3	600	18.00
4	250	0.281

Both shear frames are loaded with a shear force of $V = 10$ MN. One of these shear forces is the reaction force and one is an external applied force $F = 10$ MN. It must be kept in mind that both models are not fully comparable, as the external applied loads do not deliver the same bending moment for both models. Figure C.3 shows the deflection of the upper- and lower-bound shear frame models.

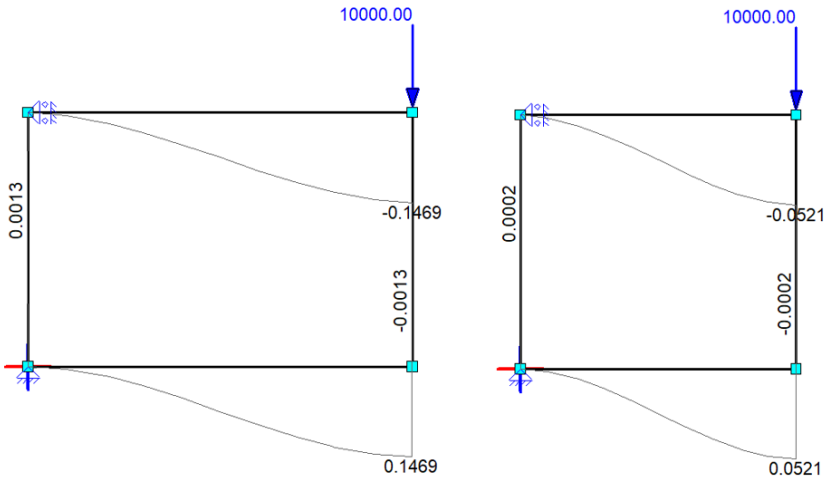

Figure C.3: Deflected shear frames (m). *left: lower-bound, right: upper-bound*

The lower-bound shear frame shows a deflection of $\delta_{lower} = 146.9$ mm, the upper-bound shear frame shows a deflection of $\delta_{upper} = 52.1$ mm. The width of the lower-bound shear frame model is

equal to the considered width of 2120 mm. The width of the upper-bound model is smaller than the width of the considered shear element of figure C.1. This means that the deflection of the upper-bound model could be extrapolated from the inner edges of the web towards the centre line of the web. However, in figure C.3 it can be seen that the end rotations of the top and bottom plate are very small. This means that, extrapolating the deflection line of the top and bottom plate according to the analogy of the "tail-wagging-effect" gives a limited extra deflection. For that reason, it is assumed that the deflection of the upper-bound shear frame model belongs to an element with a width of 2120 mm.

The shear deformation of the upper-bound model is almost 3 times bigger than the lower-bound model. As the gap between both models is significantly large, there is a need for a more elaborate shear frame model. This more elaborate shear frame is introduced in the following section.

More elaborate shear frame model

A more advanced model of the shear frame can be obtained by adding extra stiffness to the top and bottom plate in the zone of the web. The dimensions (width and height) of the more elaborate shear frame model are equal to the dimensions of the lower-bound shear frame. However, in the more elaborate shear frame model, the top and bottom plate have a higher thickness over the width of the web. The height over which the web is activated is determined in section 5.2.1, page 59, this extra height is added to the thickness of the top and bottom plate. The more elaborate shear frame model is shown in figure C.4. The blue elements (2,4,6 and 8) are the thicker top and bottom plates in the web-zone.

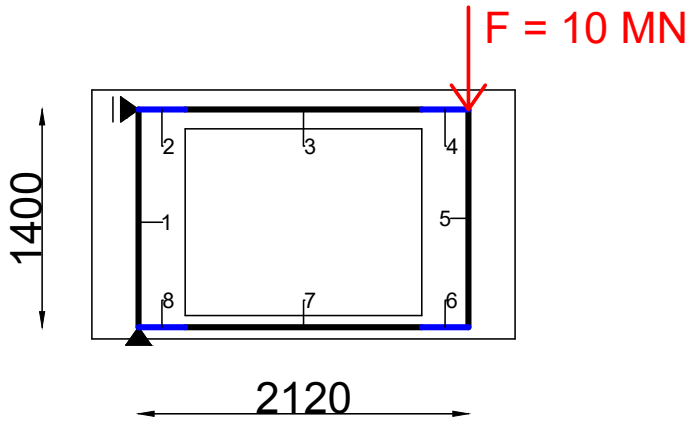

Figure C.4: More elaborate shear frame model

The shear frame presented in figure C.4 consists of 8 rods, an overview of their cross-sectional properties is shown in table C.2. The shear frame is analysed in *MatrixFrame*, this results into the deformed shape shown in figure C.5. All rods have a unit width of 1 m (in the longitudinal direction of the bridge deck), a Young's modulus of $E = 36\,300$ MPa. The cross-sectional area is set to $A = 1 \times 10^{10}$ m^2 in order to set the axial stiffness EA to infinity.

Table C.2: Cross-sectional properties elaborate shear frame model

#	length l (mm)	height h (mm)	e (mm)	I_y (10^{-2} m^4)
1	1400	600	-	18.00
2	300	357	53.5	4.821
3	1520	250	-	1.302
4	300	357	53.5	4.821
5	1400	600	-	18.00
6	300	240	45.0	1.634
7	1520	150	-	0.281
8	300	240	45.0	1.634

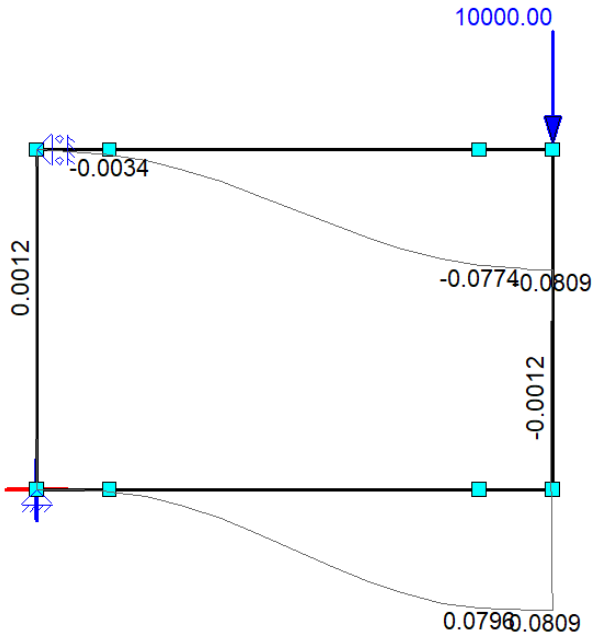

Figure C.5: Deflected more elaborate shear frame (m)

From figure C.5 it becomes clear that the more elaborate shear frame model has a deflection of $\delta = 78.0\,\text{mm}$. This deflection is in between the earlier found lower- and upper-bound ($\delta = 52.1 - 146.9\,\text{mm}$) The reliability of the elaborate shear frame model can be checked by comparing it to the analytical solution of a semi-rigid supported beam with support settlement. This model is introduced in the following section.

Analytical model

The shear frame model analysed in *MatrixFrame* can be validated by comparing it to the analytical solution of a semi-rigid supported beam with support settlement, which is shown in figure C.6.

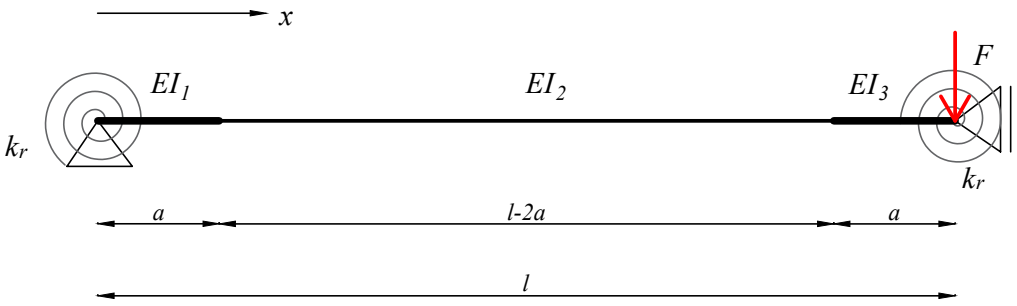

Figure C.6: Semi-rigid supported beam with support settlement

In this model, the top and bottom plate act together as a parallel system. This means that the bending stiffness of the beam is equal to sum of the bending stiffnesses of the top and bottom plate of the bridge deck. Over the width of the web (a), the bending stiffness of the beam depends on the higher plate thickness. On both ends, the beam is supported with rotational springs with stiffness k. The analytical solution of this case can be determined based upon the ordinary differential equation for a Euler-Bernoulli beam [4] (equation C.1). Using the relations of equation C.2 and the boundary and interface conditions (table C.3), the analytical solution for the case shown in figure C.6 can be solved.

$$EI\frac{\mathrm{d}^4 w}{\mathrm{d}x^4} = q \tag{C.1}$$

$$\begin{aligned} q &= 0 \\ \phi &= -\frac{\mathrm{d}w}{\mathrm{d}x} \\ M &= -EI\frac{\mathrm{d}^2w}{\mathrm{d}x^2} \\ V &= -EI\frac{\mathrm{d}^3w}{\mathrm{d}x^3} \end{aligned} \tag{C.2}$$

As the bending stiffness varies over the length of the beam, the beam must be divided into 3 parts. These 3 beams are rigidly connected using interface conditions. The beams are numbered from left to right. The boundary and interface conditions of the case shown in figure C.6 are shown in table C.3 below.

Table C.3: Overview of boundary and interface conditions

boundary conditions		**interface conditions**	
$x = 0$	$x = L$	$x = a$	$x = L - a$
$w_1 = 0$	$V_3 = F$	$w_1 = w_2$	$w_2 = w_3$
$\phi_1 = \frac{M_1}{k}$	$\phi_3 = -\frac{M_3}{k}$	$\phi_1 = \phi_2$	$\phi_2 = \phi_3$
		$V_1 = V_2$	$V_2 = V_3$
		$M_1 = M_2$	$M_2 = M_3$

Using the boundary and interface conditions shown above, the support settlement (which is equal to the deflection at the right end of the beam) can be determined. The bending stiffness has been calculated based upon the bending stiffness of the top and bottom plate. On both ends, the bending stiffness is higher due to the interaction with the web. The higher stiffness is present over a length $a = 300$ mm, which is half the thickness of the web. For these parts, the equivalent effective height of the web-zone is taken into account, which was introduced in section 5.2.1, page 59. The bending stiffness of the 3 different zones of the beam can be calculated as follows:

$$EI_1 = EI_3 = 36.3 \cdot 1000 \cdot \left(\frac{1}{12} \cdot 357^3 + 357 \cdot 53.5^2 + \frac{1}{12} \cdot 240^3 + 240 \cdot 45.0^2\right) = 2.34 \times 10^{11}\ \text{kN mm}^2$$

$$EI_2 = 36.3 \cdot \frac{1}{12} \cdot 1000 \cdot \left(250^3 + 150^3\right) = 5.75 \times 10^{11}\ \text{kN mm}^2$$

The magnitude of the force (F) is equal to 10 MN. The length is equal to $L = 2120$ mm. The only unknown is the stiffness of the rotational spring (k) on both ends of the beam, this k is determined and validated in the section below.

Rotational stiffness k

The rotational stiffness k is determined based upon the relation between the bending moments and rotations of the more elaborate shear frame analysed in *MatrixFrame*. The outcome of this calculation will be validated with an analytical solution. This analytical solution is based upon the approximation that the web-parts contribute to the rotational stiffness only. It is expected that the web-parts provide the biggest part of the rotational stiffness, as these parts have much more bending stiffness (they are thicker and shorter). The definition of the rotational stiffness k is shown in equation C.3.

$$k = \frac{M}{\phi} \tag{C.3}$$

For the elaborate shear frame model, the moments and rotations of the ends of the top and bottom plate are shown in table C.4. Based upon the bending moments and the rotations of the elaborate shear frame modelled in *MatrixFrame*, the rotational stiffness k = 3.567 × 10^9 kN mm.

Table C.4: Rotational stiffness k based upon M_y and ϕ from elaborate shear frame model

corner	M_y (10^3 kN mm)	ϕ (10^{-3} rad)	$k = M_y/\phi$ (10^9 kN mm)
top	8218.12	5.019	1.637
bottom	2380.61	1.234	1.929
$\sum$	-	-	**3.567**

Analytical solution rotational stiffness k

The reliability of the rotational stiffness based upon the shear frame model can be checked with an analytical solution. To do this, it is assumed that the web-parts contribute to the rotational stiffness only. This assumption can be made, because the web-parts are much stiffer compared to the plate parts: they have a bigger moment of inertia and they are shorter compared to the top and bottom plate. Equation C.4 gives the relationship between the end-rotation of a simply supported beam with length l, bending stiffness EI, subjected to a moment M. This end-rotation is on the same end of the beam at which the moment is applied.

$$\phi = \frac{1}{3}\frac{Ml}{EI} \tag{C.4}$$

According to equation C.3, this means that one end of the web delivers a rotational stiffness of:

$$k = \frac{M}{\phi} = \frac{3EI}{l} \tag{C.5}$$

The other end of the web contributes with the same magnitude to the rotational stiffness. This means that the web provides a total rotational stiffness of:

$$k = 2 \times \frac{3EI}{l} = \frac{6EI}{l} \tag{C.6}$$

The web has a thickness of $t = 600$ mm, this means that $EI_{web} = 6.534 \times 10^{11}$ kN mm^2. The web has a length of $l = 1400$ mm. Filling in these values into equation C.6, it follows that $k_{web} = 3.267 \times 10^9$ kNmm.

Based upon the web only, the rotational stiffness is 91.6% of the rotational stiffness based upon the shear frame result. It is assumed that the other 8.4% of the rotational stiffness comes from the top and bottom plate of the bridge deck. As expected, it turned out that the web has the biggest contribution to the rotational stiffness. The rotational stiffness based upon the elaborate shear frame model ($k = 3.567 \times 10^9$ kNmm, table C.4) is used to determine the deflection of the semi-rigid supported beam with support settlement.

Result

The solution to the semi-rigid supported beam with support settlement was found using a script in *Maple*. Figure C.7 shows the deflection of the semi-rigid supported beam with support settlement. From this solution it becomes clear that $\delta = 78.6$ mm. This deflection is slightly less (3%) compared to the deflection of the elaborate shear frame model, for which $\delta = 80.9$ mm.

It is chosen that the shear stiffness can be based upon the result of the elaborate shear frame model. According to this model, the shear deformation is equal to $\delta = 80.9$ mm, when the applied shear load is equal to F= 10 MN.

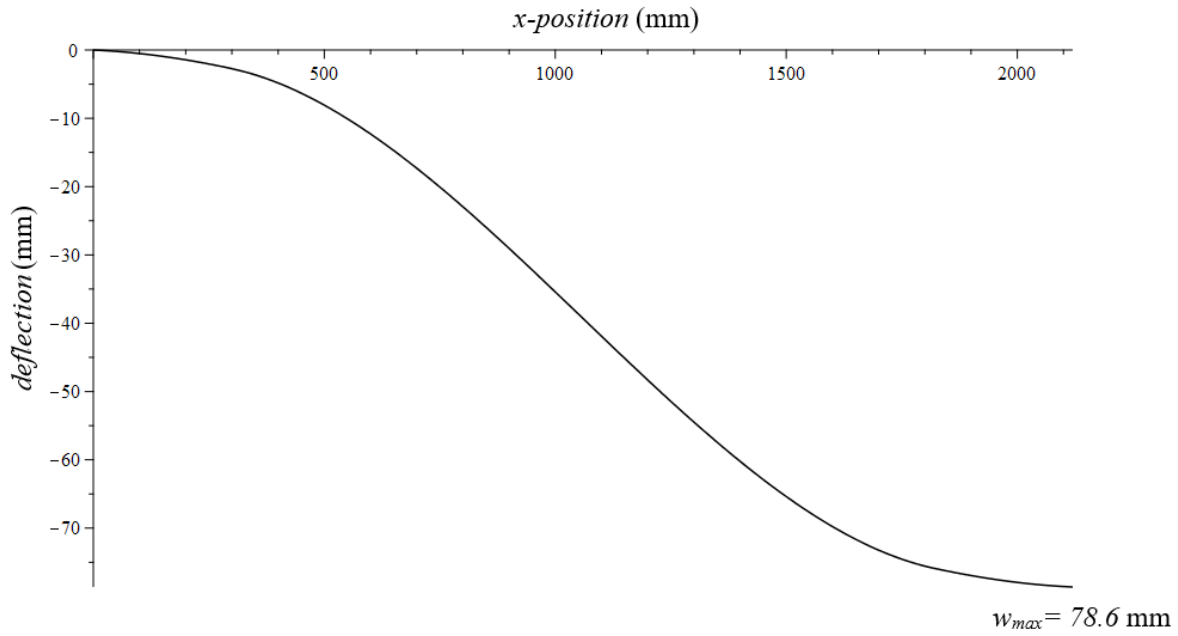

Figure C.7: Deflection $w(x)$ semi-rigid supported beam with support settlement

D

Guyon-Massonnet-Bareš method

In this thesis, the Guyon-Massonnet-Bareš method is used to verify and compared the mid-span deflection of the 3 different models. This is done for the straight deck loaded with load case LC3 (point load at grid-line B) and LC7 (point load at grid-line E and G). The theory presented below is extracted from *Analysis of beam grids and orthotropic plates, by the Guyon-Massonnet-Bareš method* [1]

Theory

In the Guyon-Massonnet-Bareš method, the reaction forces and bending moments of a bridge deck can be calculated using the coefficient of lateral distribution (k). For 9 different positions along an transverse section, the coefficients of lateral distribution (k) can be found in tables. The coefficients k can are defined as the local deflection along a transverse section ($w(y)$) divided by the mean deflection over the same transverse section (w_0):

$$k = \frac{w(y)}{w_0} \tag{D.1}$$

The width of the bridge is defined as $2b$ and the bridge deck runs from $-b$ till b. The nodes in for which the coefficients of lateral distribution can be found in tables are: $-b$, $-\frac{3}{4}b$, $-\frac{1}{2}b$, $-\frac{1}{4}b$, 0, $\frac{1}{4}b$, $\frac{1}{2}b$, $\frac{3}{4}b$ and b, see figure D.1. These nodes are also called *reference stations*.

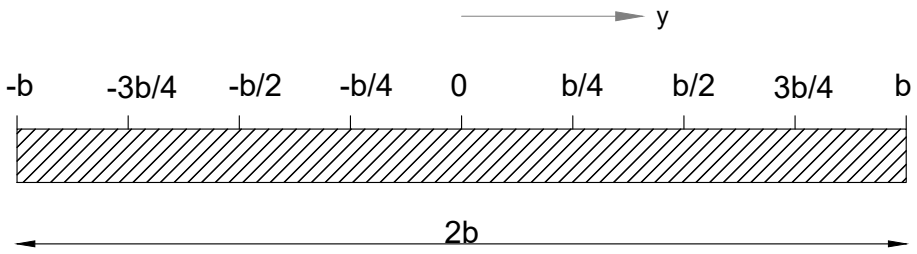

Figure D.1: Reference stations Guyon-Massonnet-Bareš

The coefficients of lateral distribution are based upon the parameters θ and α. Parameter θ is a measure for the ratio between the transverse and torsional bending stiffness and α is a measure for the rotational stiffness.

θ can be calculated using:

$$\theta = \frac{b}{l}\sqrt[4]{\frac{\rho_x}{\rho_y}} \tag{D.2}$$

In equation D.2, b is half the width of the bridge deck and l is the length of the bridge deck. ρ_x is the longitudinal bending stiffness per unit width and ρ_y is the transverse bending stiffness per unit width.

The torsional stiffness parameter α can be calculated using:

$$\alpha = \frac{C_x + C_y}{2 \cdot \sqrt{\rho_x \rho_y}} \tag{D.3}$$

Here, C_x and C_y are the torsional stiffness per unit width in the transverse and longitudinal direction of the bridge deck.

The k-values for the specific values of θ and α can be found by using interpolation. First, the tables for k_0 (torsion weak) and k_1 (torsion stiff) must be calculated for the correct value of θ. This can be done by linear interpolation. So, the k-values for $\theta = 0.43$, can be found by interpolation of $\theta = 0.40$ and $\theta = 0.50$. Next, the α-factor can be used to interpolate between the torsion weak (k_0) and torsion stiff (k_1) values. To do this, for this interpolation, equation D.4 must be used.

$$k_\alpha = k_0 + (k_1 - k_0) \cdot \sqrt{\alpha} \tag{D.4}$$

Blankenburg case

In case of the bridge decks of the Blankenburgverbinding, the width of the bridge deck ($2b$) and the length (l) are:

$$2b = 16.96\,\text{m}$$
$$l = 40\,\text{m}$$

The bending stiffness per unit width is equal to (see table 3.1, page 26):

$$\rho_x = 8.759 \times 10^6\,\text{kNm}$$
$$\rho_y = 7.008 \times 10^6\,\text{kNm}$$

This means that according to equation D.2, θ is equal to:

$$\theta = \frac{8.48}{40} \sqrt[4]{\frac{8.759 \times 10^6}{7.008 \times 10^6}} = 0.22$$

The transverse cross-section of the bridge deck of the Blankenburg case study has a torsional stiffness of (see page 31):

$$I_t = 11.85\,\text{m}^4$$

Using $G = 15\,125\,\text{MPa}$, this means that the torsional stiffness of a transverse section is equal to:

$$C_x = \frac{11.85}{16.96} \cdot 15\,125 = 1.057 \times 10^7\,\text{kNm}$$

In longitudinal direction, the cross-section consists of a 150 mm and a 250 mm thick plate. In longitudinal direction, the torsional stiffness per unit width is equal to:

$$C_y = \frac{1}{6} \cdot (150^3 + 250^3) \cdot 15\,125 = 4.790 \times 10^4\,\text{kNm}$$

According to equation D.3 the torsional stiffness parameter α is equal to:

$$\alpha = \frac{1.057 \times 10^7 + 4.790 \times 10^4}{2 \cdot \sqrt{8.759 \times 10^6 \cdot 7.008 \times 10^6}} = 0.68$$

Tables with k-values

Table D.1, D.2, D.3 and D.4 are taken from [1]. In these tables, y is the position of the node and e the position of the load. This means that each row of the tables is the influence line for one different load position. As the positioning of the nodes is symmetrical, only the values for loads located on the positive side of the bridge deck are shown. The influence lines for loads applied on the left part of the bridge deck can be obtained by mirroring.

The values k_0 and k_1 for $\theta = 0.22$ can be found by interpolation the tables for $\theta = 0.20$ and $\theta = 0.25$. The interpolated tables are table D.5 (k_0) an table D.6 (k_1).

Table D.1: k_0, $\theta = 0.20$

	y								
e	-b	-3b/4	-b/2	-b/4	0	b/4	b/2	3b/4	b
0	+0.9884	+0.9948	+1.0009	+1.0057	+1.0078	+1.0057	+1.0009	+0.9948	+0.9884
b/4	+0.2421	+0.4336	+0.6251	+0.8160	+1.0057	+1.1929	+1.3767	+1.5583	+1.7394
b/2	-0.5008	-0.1257	+0.2495	+0.6251	+1.0009	+1.3767	+1.7514	+2.1242	+2.4961
3b/4	-1.2418	-0.6839	-0.1257	+0.4336	+0.9948	+1.5583	+2.1242	+2.6913	+3.2581
b	-1.9823	-1.2418	-0.5008	+0.2421	+0.9884	+1.7394	+2.4961	+3.2581	+4.0236

Table D.2: k_0, $\theta = 0.25$

	y								
e	-b	-3b/4	-b/2	-b/4	0	b/4	b/2	3b/4	b
0	+0.9718	+0.9874	+1.0021	+1.0138	+1.0188	+1.0138	+1.0021	+0.9874	+0.9718
b/4	+0.2309	+0.4281	+0.6251	+0.8210	+1.0138	+1.2007	+1.3791	+1.5524	+1.7244
b/2	-0.5019	-0.1267	+0.2489	+0.6251	+1.0021	+1.3791	+1.7535	+2.1230	+2.4905
3b/4	-1.2302	-0.6789	-0.1267	+0.4281	+0.9874	+1.5524	+2.1230	+2.6966	+3.2696
b	-1.9571	-1.2302	-0.5019	+0.2309	+0.9718	+1.7244	+2.4905	+3.2696	+4.0574

Table D.3: k_1, $\theta = 0.20$

	y								
e	-b	-3b/4	-b/2	-b/4	0	b/4	b/2	3b/4	b
0	+0.9912	+0.9960	+1.0006	+1.0044	+1.0061	+1.0044	+1.0006	+0.9960	+0.9912
b/4	+0.9468	+0.9610	+0.9755	+0.9902	+1.0044	+1.0167	+1.0257	+1.0328	+1.0392
b/2	+0.9058	+0.9281	+0.9513	+0.9755	+1.0006	+1.0257	+1.0496	+1.0708	+1.0906
3b/4	+0.8674	+0.8972	+0.9281	+0.9610	+0.9960	+1.0328	+1.0708	+1.1086	+1.1449
b	+0.8305	+0.8674	+0.9058	+0.9468	+0.9912	+1.0392	+1.0906	+1.1449	+1.2009

Table D.4: k_1, $\theta = 0.25$

	y								
e	-b	-3b/4	-b/2	-b/4	0	b/4	b/2	3b/4	b
0	+0.9812	+0.9912	+1.0011	+1.0095	+1.0133	+1.0095	+1.0011	+0.9912	+0.9812
b/4	+0.9156	+0.9382	+0.9619	+0.9862	+1.0095	+1.0287	+1.0407	+1.0484	+1.0546
b/2	+0.8569	+0.8899	+0.9246	+0.9619	+1.0011	+1.0407	+1.0773	+1.1079	+1.1354
3b/4	+0.8038	+0.8456	+0.8899	+0.9382	+0.9912	+1.0484	+1.1079	+1.1669	+1.2225
b	+0.7539	+0.8038	+0.8569	+0.9156	+0.9812	+1.0546	+1.1354	+1.2225	+1.3133

Table D.5: k_0, $\theta = 0.22$ (interpolation of table D.1 and table D.2)

	y								
e	-b	-3b/4	-b/2	-b/4	0	b/4	b/2	3b/4	b
0	+0.9804	+0.9912	+1.0015	+1.0096	+1.0131	+1.0096	+1.0015	+0.9912	+0.9804
b/4	+0.2367	+0.4310	+0.6251	+0.8184	+1.0096	+1.1967	+1.3779	+1.5555	+1.7322
b/2	-0,5013	-0.1262	+0.2493	+0.6251	+1.0015	+1.3779	+1.7524	+2.1236	+2.4934
3b/4	-1.2362	-0.6815	-0.1262	+0.4309	+0.9912	+1.5554	+2.1236	+2.6938	+3.2637
b	-1.9701	+1.2362	+0.5013	+0.2367	+0.9804	+1.7322	+2.4934	+3.2637	+4.0399

Table D.6: k_1, $\theta = 0.22$ (interpolation of table D.3 and table D.4)

	y								
e	-b	-3b/4	-b/2	-b/4	0	b/4	b/2	3b/4	b
0	+0.9864	+0.9937	+1.0009	+1.0069	+1.0096	+1.0069	+1.0009	+0.9937	+0.9864
b/4	+0.9317	+0.9500	+0.9689	+0.9883	+1.0069	+1.0225	+1.0329	+1.0403	+1.0466
b/2	+0.8822	+0.9096	+0.9384	+0.9689	+1.0009	+1.0329	+1.0630	+1.0887	+1.1122
3b/4	+0.8367	+0.8723	+0.9096	+0.9500	+0.9937	+1.0399	+1.0887	+1.1368	+1.1824
b	+0.7935	+0.8367	+0.8822	+0.9317	+0.9864	+1.0466	+1.1122	+1.1824	+1.2552

Using the interpolation formula of equation D.4, the values of table D.5 and table D.6 can be interpolated to get the values for k_α, with $\alpha = 0.68$. The values of $k_{0.68}$ can be found in table D.7.

Table D.7: $k_{0.68}$, $\theta = 0.22$

	y								
e	-b	-3b/4	-b/2	-b/4	0	b/4	b/2	3b/4	b
0	+0.9853	+0.9932	+1.0010	+1.0074	+1.0102	+1.0074	+1.0010	+0.9932	+0.9853
b/4	+0.8088	+0.8582	+0.9081	+0.9582	+1.0074	+1.0533	+1.0940	+1.1315	+1.1679
b/2	+0.6374	+0.7264	+0.8165	+0.9081	+1.0010	+1.0940	+1.1849	+1.2718	+1.3566
3b/4	+0.4700	+0.5974	+0.7264	+0.8582	+0.9932	+1.1311	+1.2718	+1.4122	+1.5506
b	+0.3046	+0.4700	+0.6374	+0.8088	+0.9853	+1.1679	+1.3566	+1.5506	+1.7478

The k-values shown in table D.7 can be plotted in a graph, see figure D.2. The different lines shown in this graph are for different positions (e) of the load. As the position of the nodes is symmetrical, the influence lines for loads applied to the positive right part of the bridge deck can be mirrored for loads positioned on the left part of the deck.

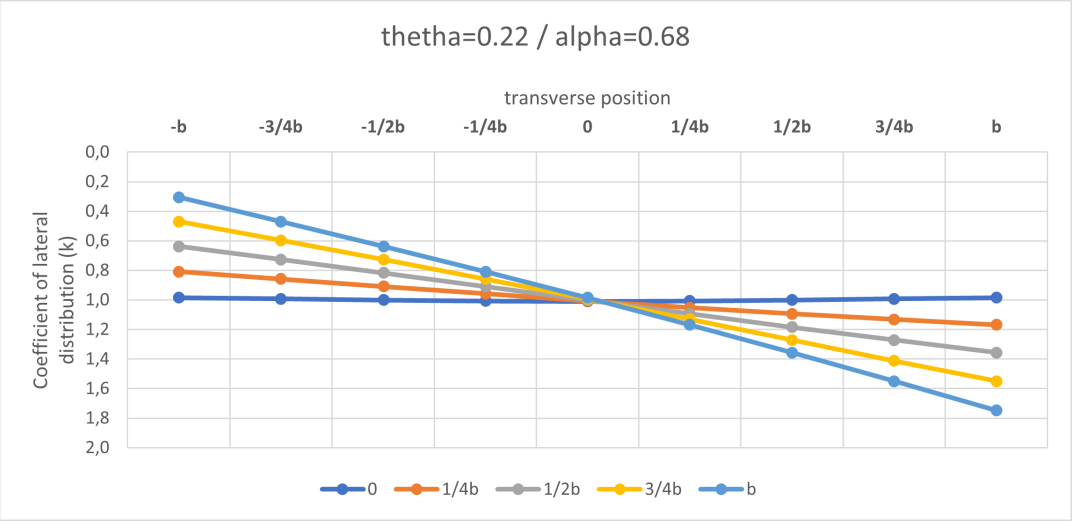

Figure D.2: Coefficients of lateral distribution (k), for $\theta = 0.22$ and $\alpha = 0.68$

E

Results straight deck

This appendix gives an overview of the results of the straight bridge deck. The reaction forces, longitudinal bending moments are shown for each of the 7 load-cases of the dummy loads. Also the shear forces diagrams for load-case 3 and load-case 7 are shown.

Figure E.1 gives an overview of the load-cases (LC1 till LC7) of the dummy applied to the straight bridge deck.

Load-cases dummy loads

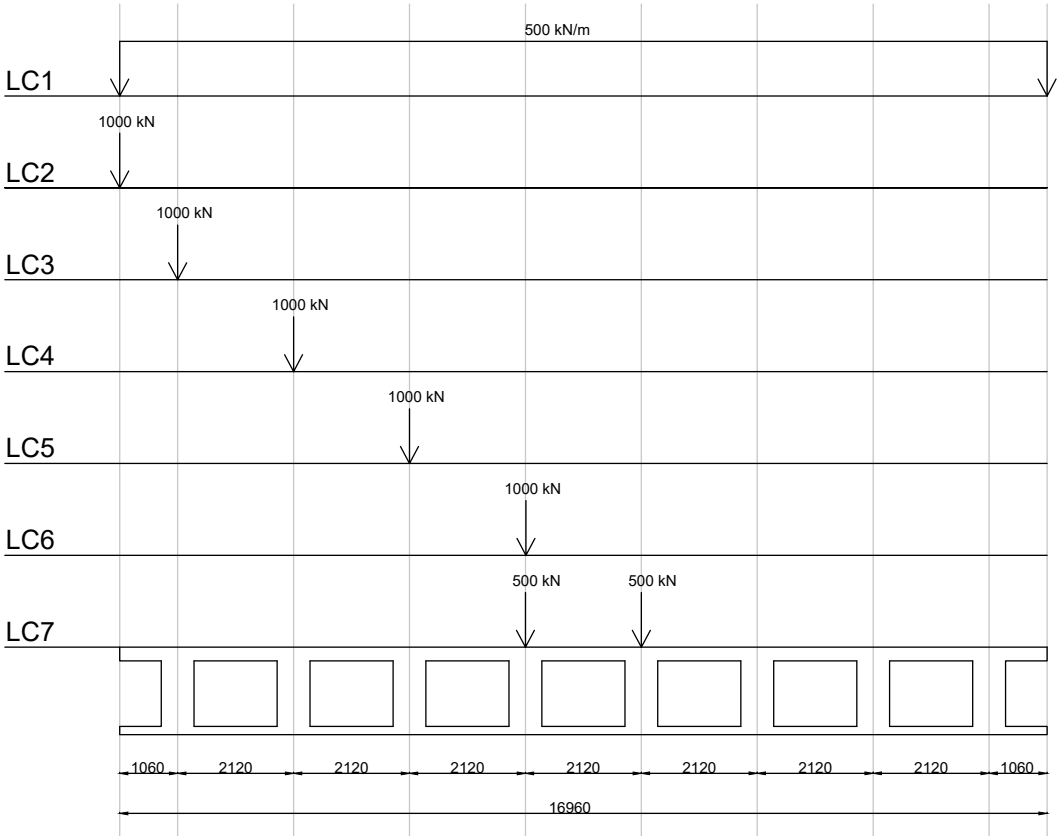

Figure E.1: Load cases of the dummy loads, positioned along the transverse cross-section, in the middle of the span [mm]

Reaction forces

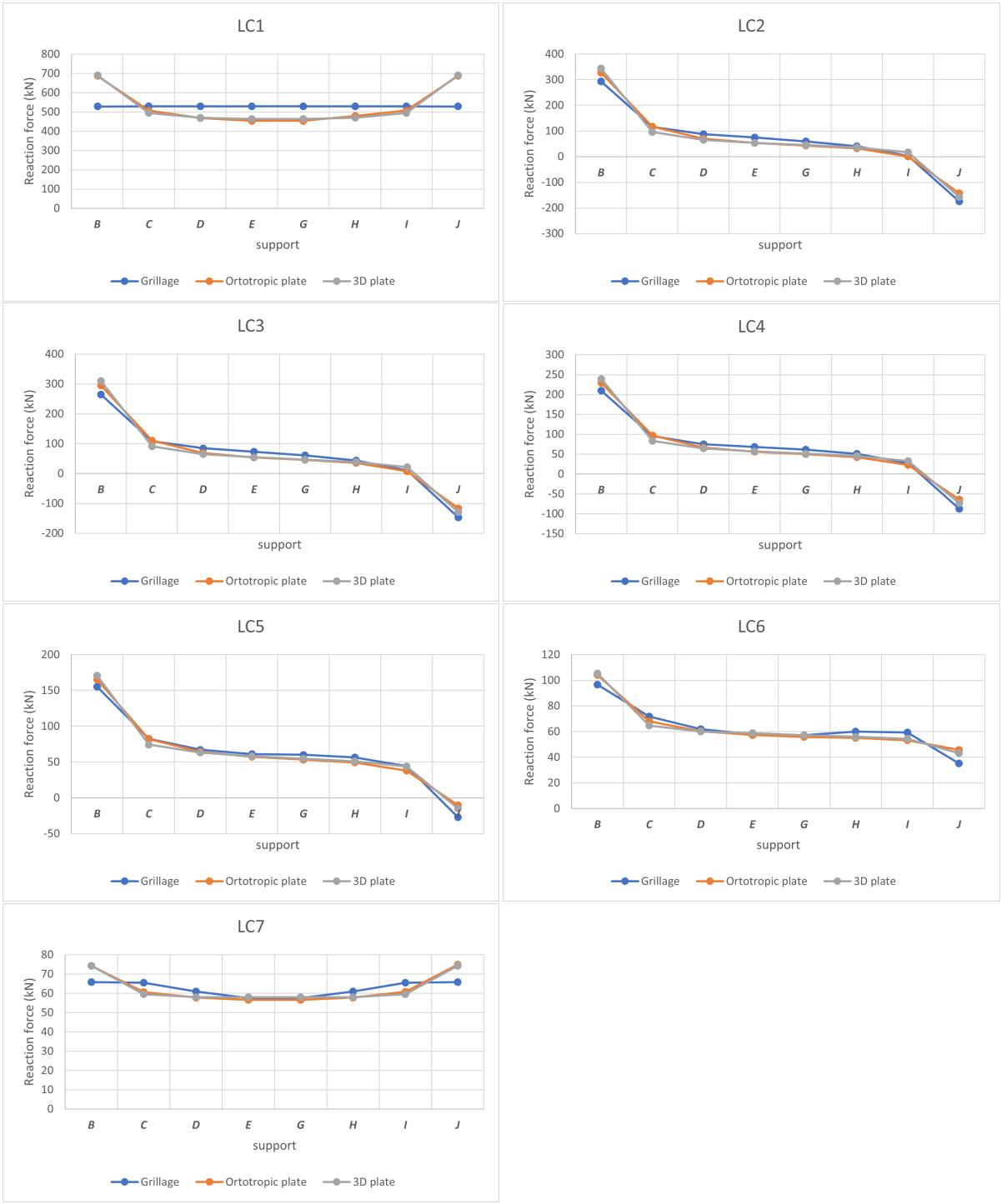

Figure E.2: Reaction forces straight deck

Longitudinal bending moments

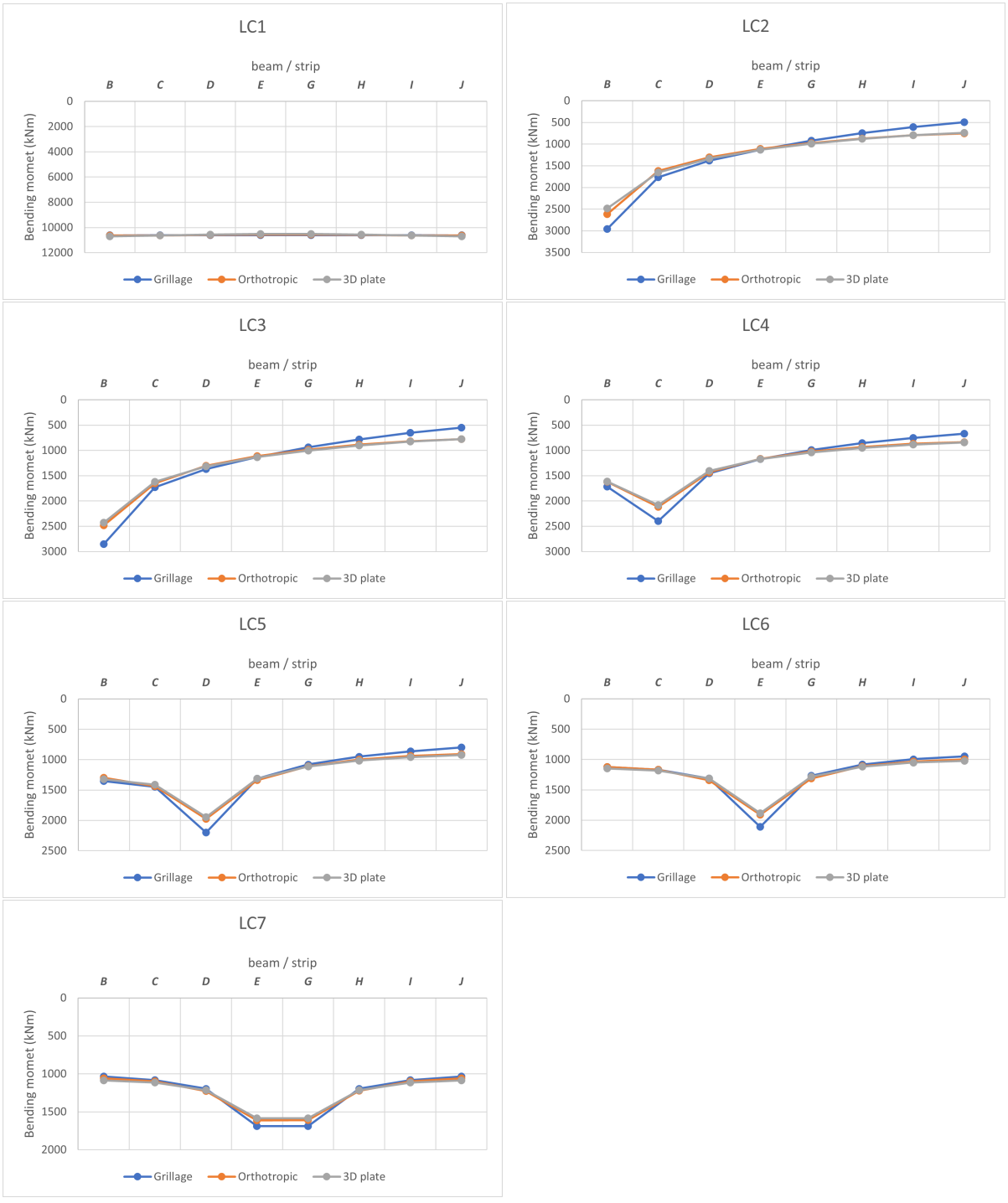

Figure E.3: Longitudinal bending moments LC1 till LC7

Shear forces LC3

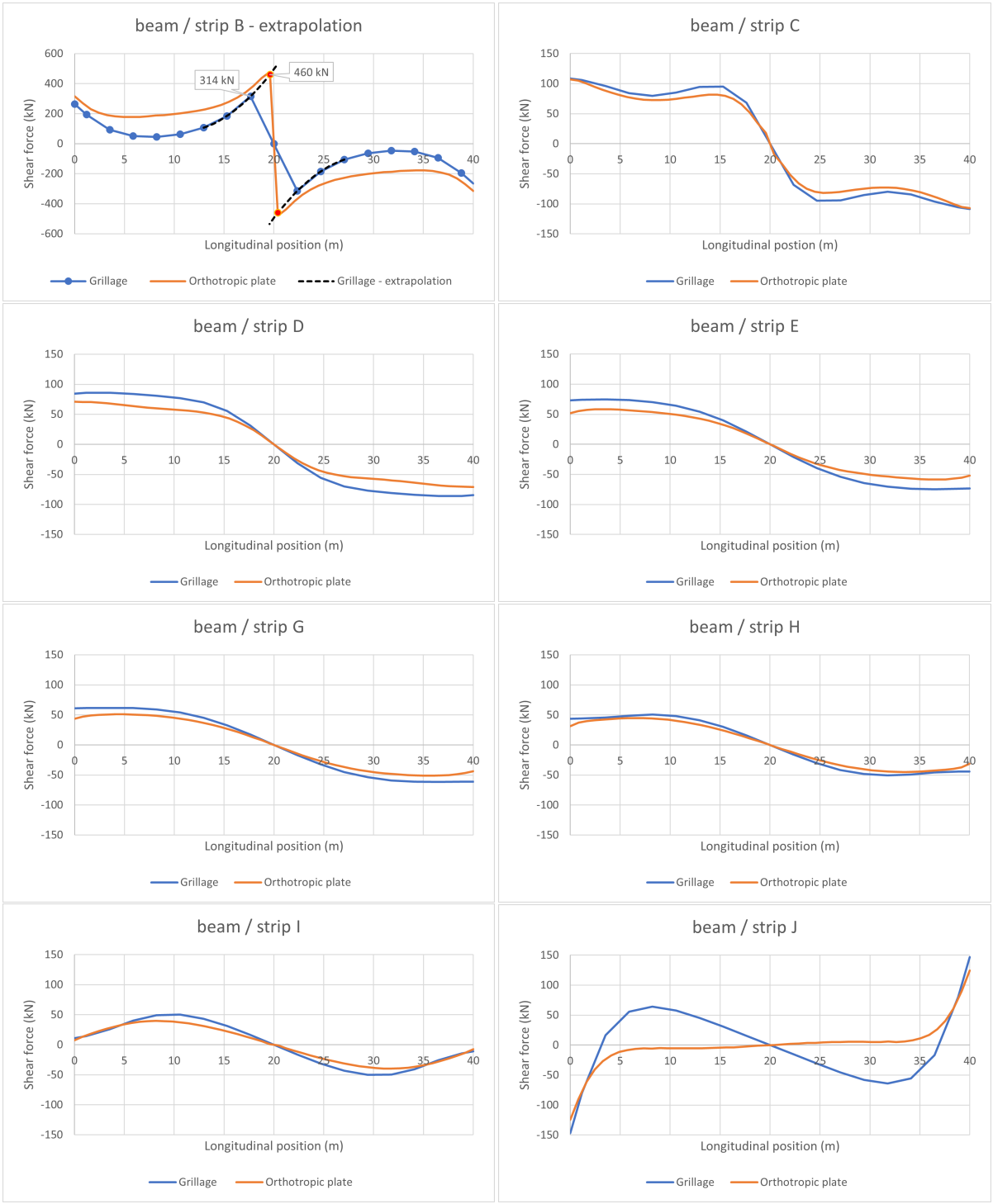

Figure E.4: Shear forces LC3, longitudinal beam / strip B, C, D, E, G, H, I and J

Shear forces LC7

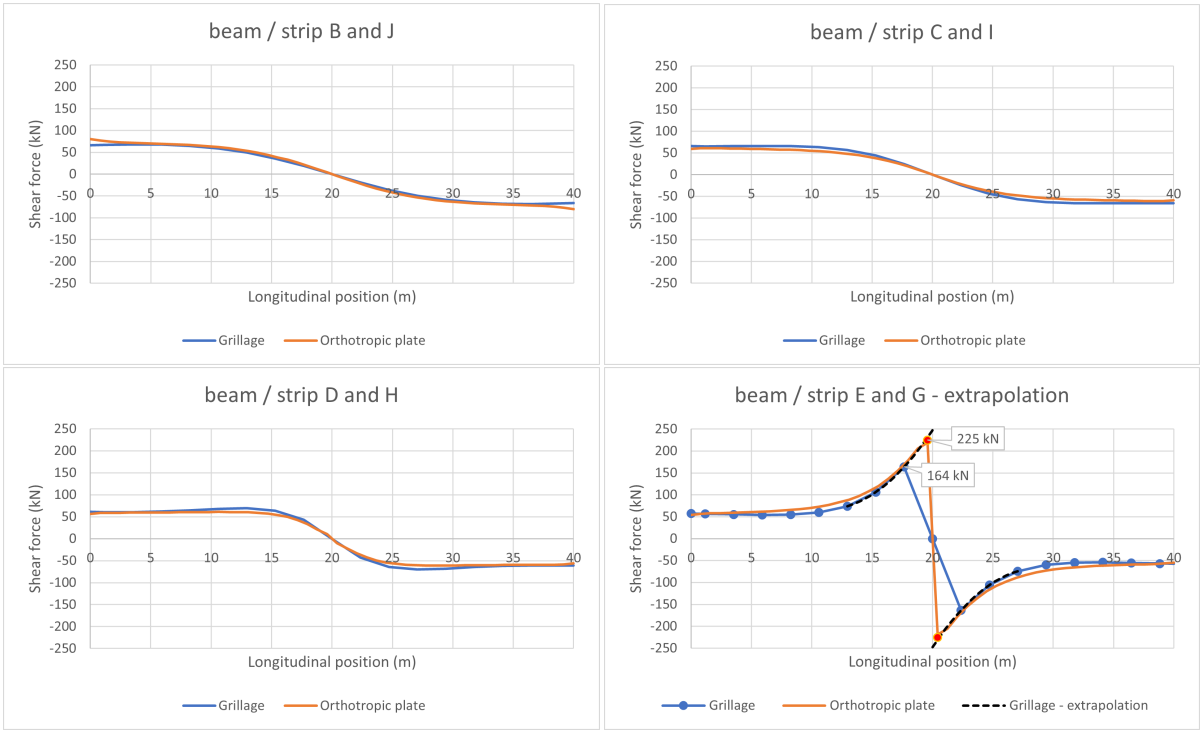

Figure E.5: Shear forces LC7, longitudinal beam / strip B, C, D, E, G, H, I and J

F

Results curved deck

This appendix shows the contour plots of the design bending moments (MxD+, MxD-, MyD+ and MyD-) of the curved bridge deck. The left plots are from the grillage model. These plots are created using excel. The right plots are from the orthotropic plate model. These plots are extracted from *SCIA-engineer* directly.

Grillage model

MxD+ max 182 kNm/m

	B	C	D	E	G	H	I	J
18	0	0	14	38	54	75	99	129
17	77	78	102	124	141	156	163	158
16	139	133	148	164	177	182	173	160
15	162	159	168	176	179	173	155	146
14	158	164	168	168	159	142	120	121
13	139	154	157	147	127	101	77	90
12	110	132	134	117	87	54	30	54
11	73	101	104	79	42	5	0	15
10	31	61	63	35	0	0	0	0
9	73	101	104	79	42	5	0	15
8	110	132	134	117	87	54	30	54
7	139	154	157	147	127	101	77	90
6	158	164	168	168	159	142	120	121
5	162	159	168	176	179	173	155	146
4	139	133	148	164	177	182	173	160
3	77	78	102	124	141	156	163	158
2	0	0	14	38	54	75	99	129

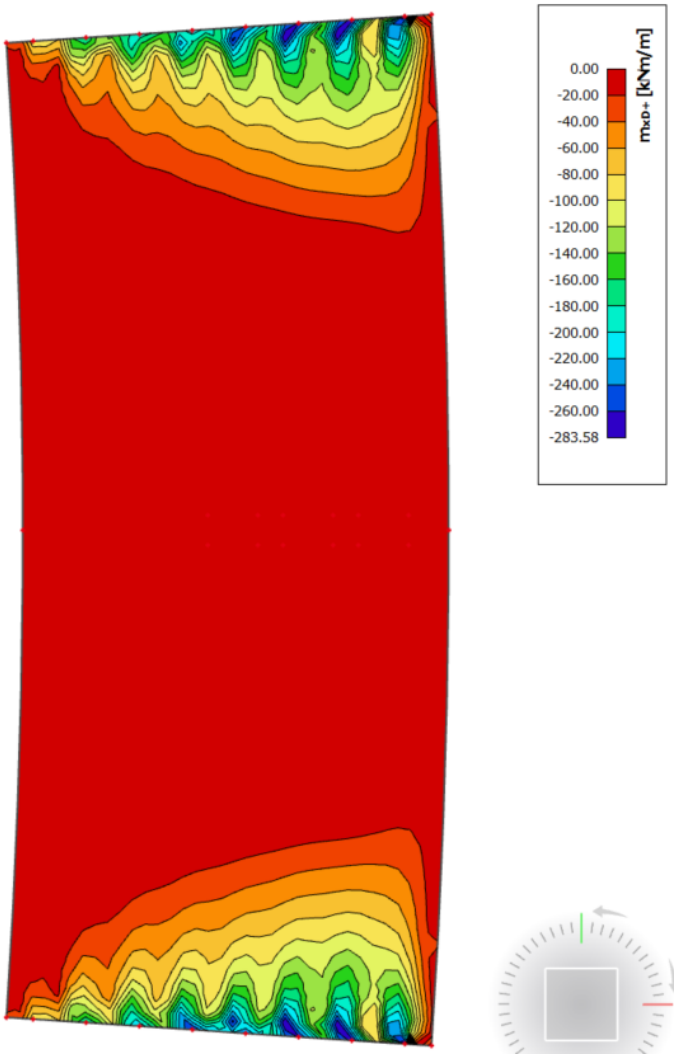

Figure F.1: MxD+, grillage model (left) and orthotropic plate model (right) (kNm/m)

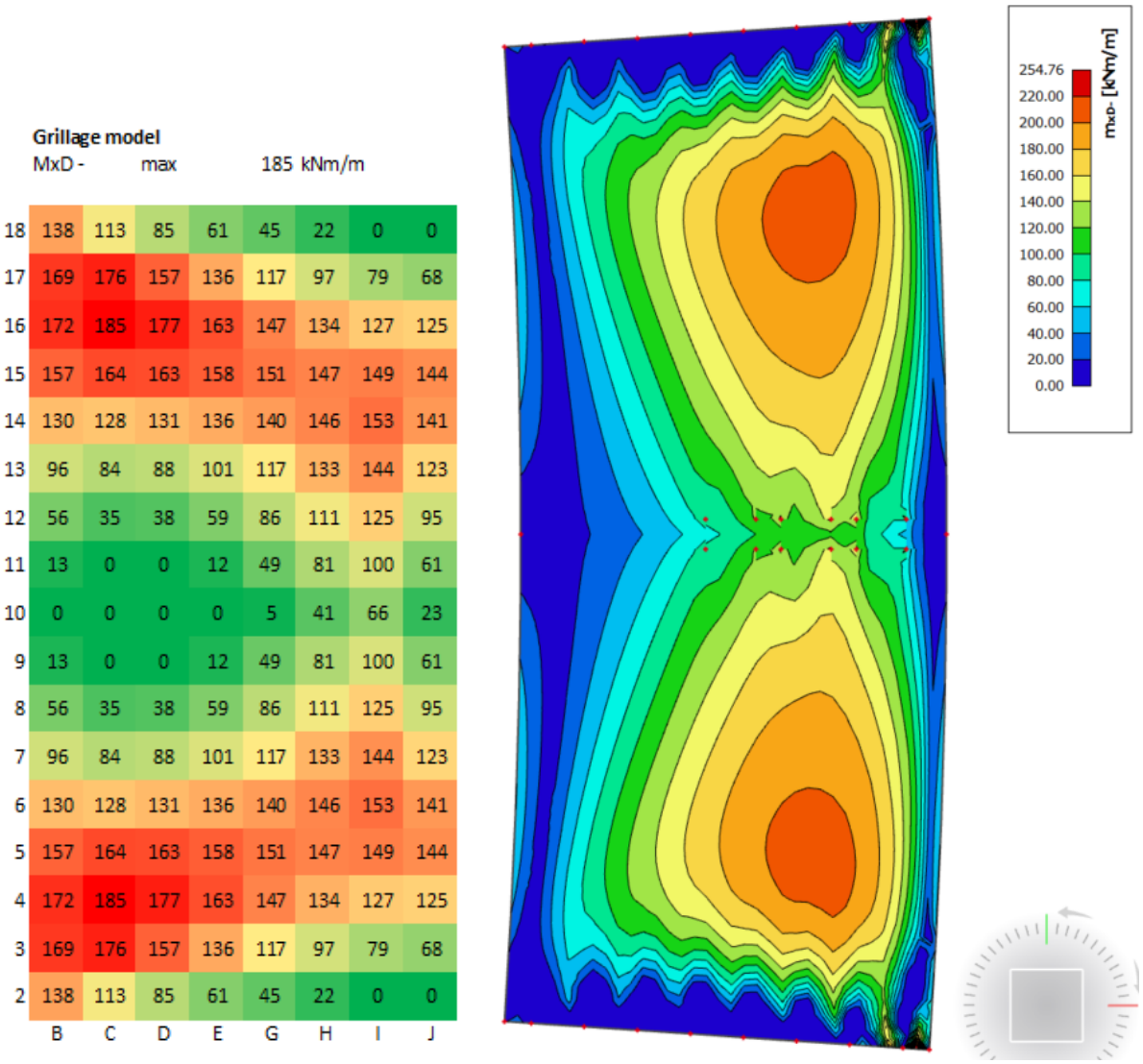

Figure F.2: MxD-, grillage model (left) and orthotropic plate model (right) (kNm/m)

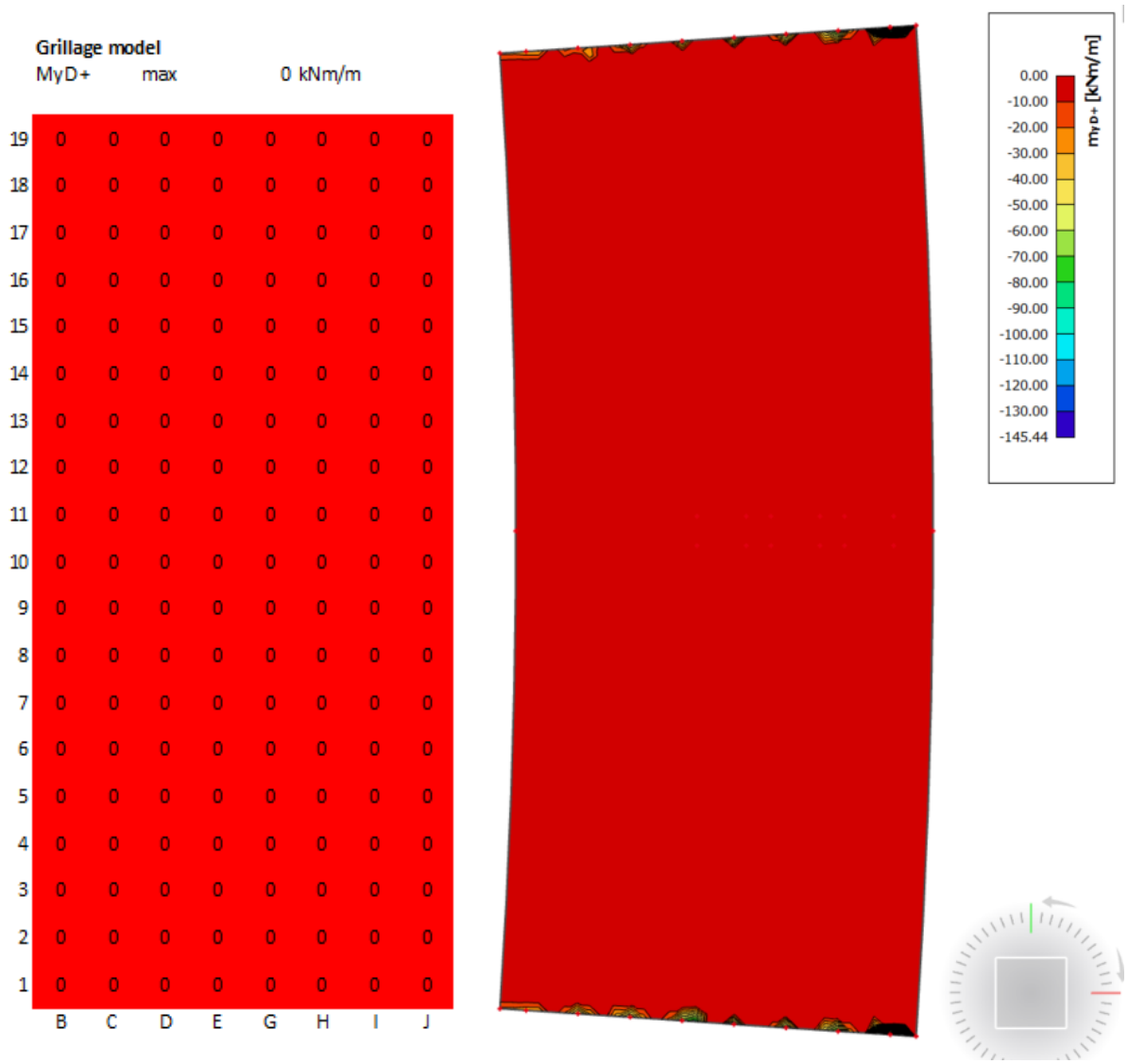

Figure F.3: MyD+, grillage model (left) and orthotropic plate model (right) (kNm/m)

Grillage model

MyD - max 3303 kNm/m

	B	C	D	E	G	H	I	J
19	0	0	0	0	0	0	0	0
18	123	276	316	326	346	365	404	542
17	579	786	880	923	972	1027	1116	1288
16	1056	1229	1348	1421	1493	1571	1678	1818
15	1484	1615	1739	1832	1919	2010	2115	2223
14	1835	1942	2063	2168	2265	2362	2458	2550
13	2101	2200	2319	2432	2538	2641	2730	2821
12	2277	2378	2500	2624	2746	2861	2950	3043
11	2364	2469	2596	2744	2895	3031	3136	3216
10	2364	2470	2600	2777	2962	3120	3255	3303
9	2364	2469	2596	2744	2895	3031	3136	3216
8	2277	2378	2500	2624	2746	2861	2950	3043
7	2101	2200	2319	2432	2538	2641	2730	2821
6	1835	1942	2063	2168	2265	2362	2458	2550
5	1484	1615	1739	1832	1919	2010	2115	2223
4	1056	1229	1348	1421	1493	1571	1678	1818
3	579	786	880	923	972	1027	1116	1288
2	123	276	316	326	346	365	404	542
1	0	0	0	0	0	0	0	0

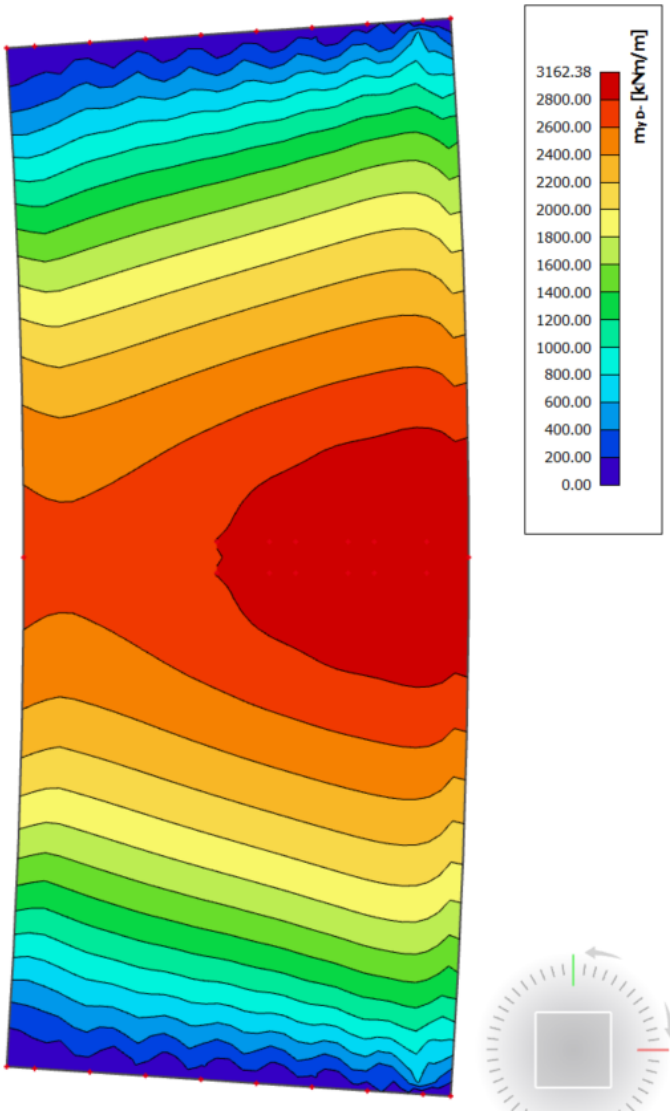

Figure F.4: MyD-, grillage model (left) and orthotropic plate model (right) (kNm/m)

G

Results curved and skewed deck

This appendix shows the contour plots of the design bending moments (MxD+, MxD-, MyD+ and MyD-) of the curved and skewed bridge deck. The left plots are from the grillage model. These plots are created using excel. The right plots are from the orthotropic plate model. These plots are extracted from *SCIA-engineer* directly.

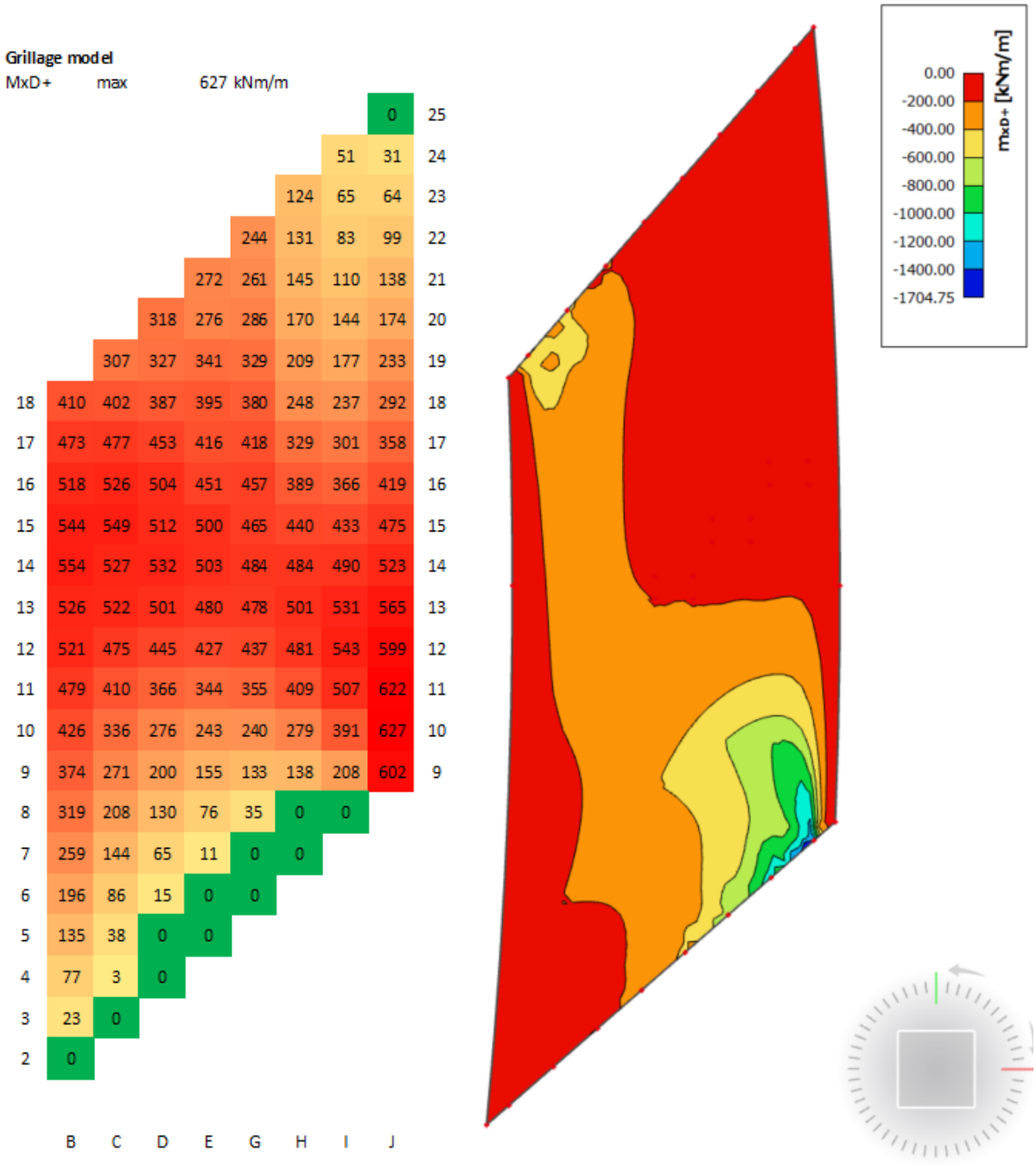

Figure G.1: MxD+, grillage model (left) and orthotropic plate model (right) (kNm/m)

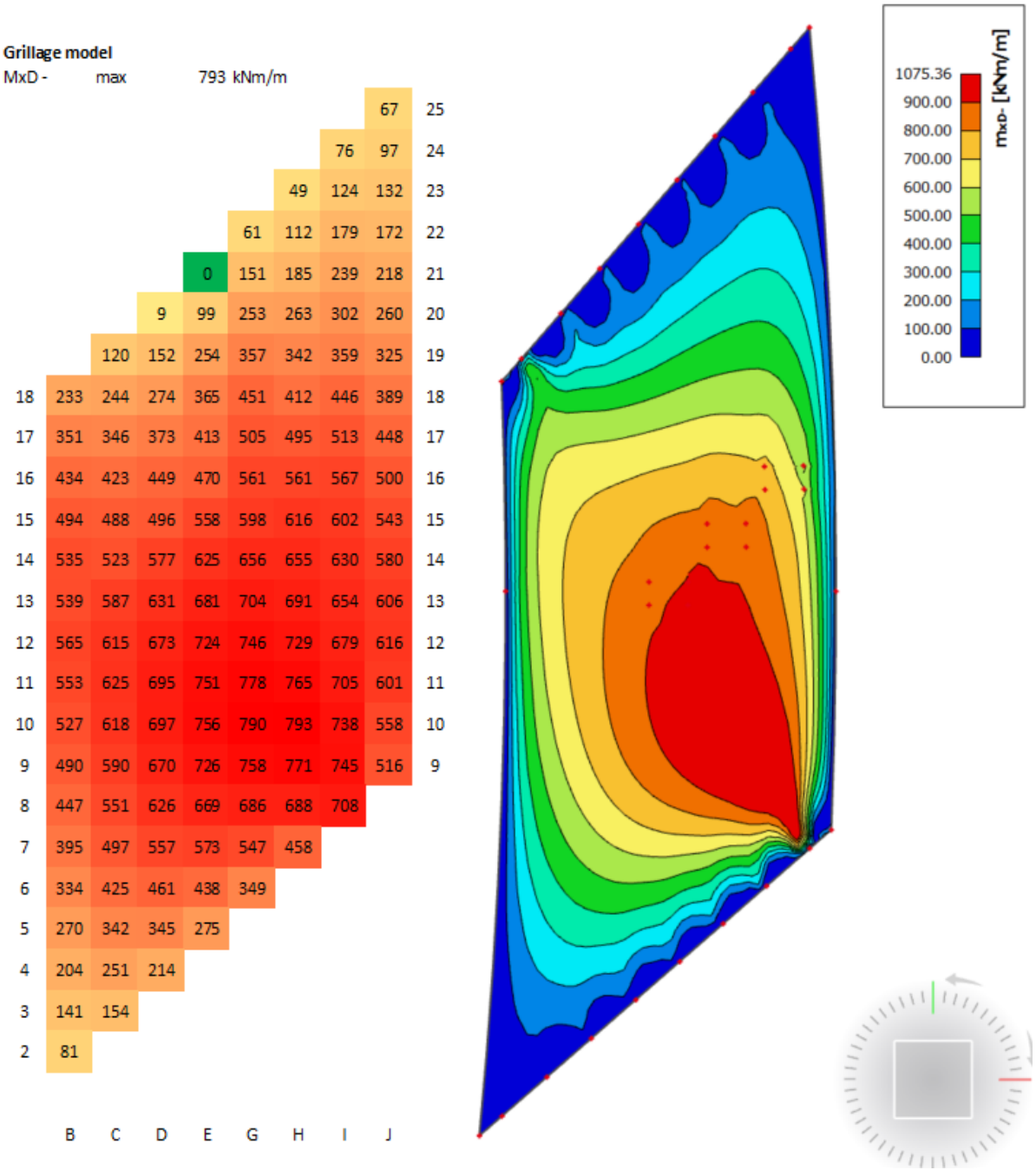

Figure G.2: MxD-, grillage model (left) and orthotropic plate model (right) (kNm/m)

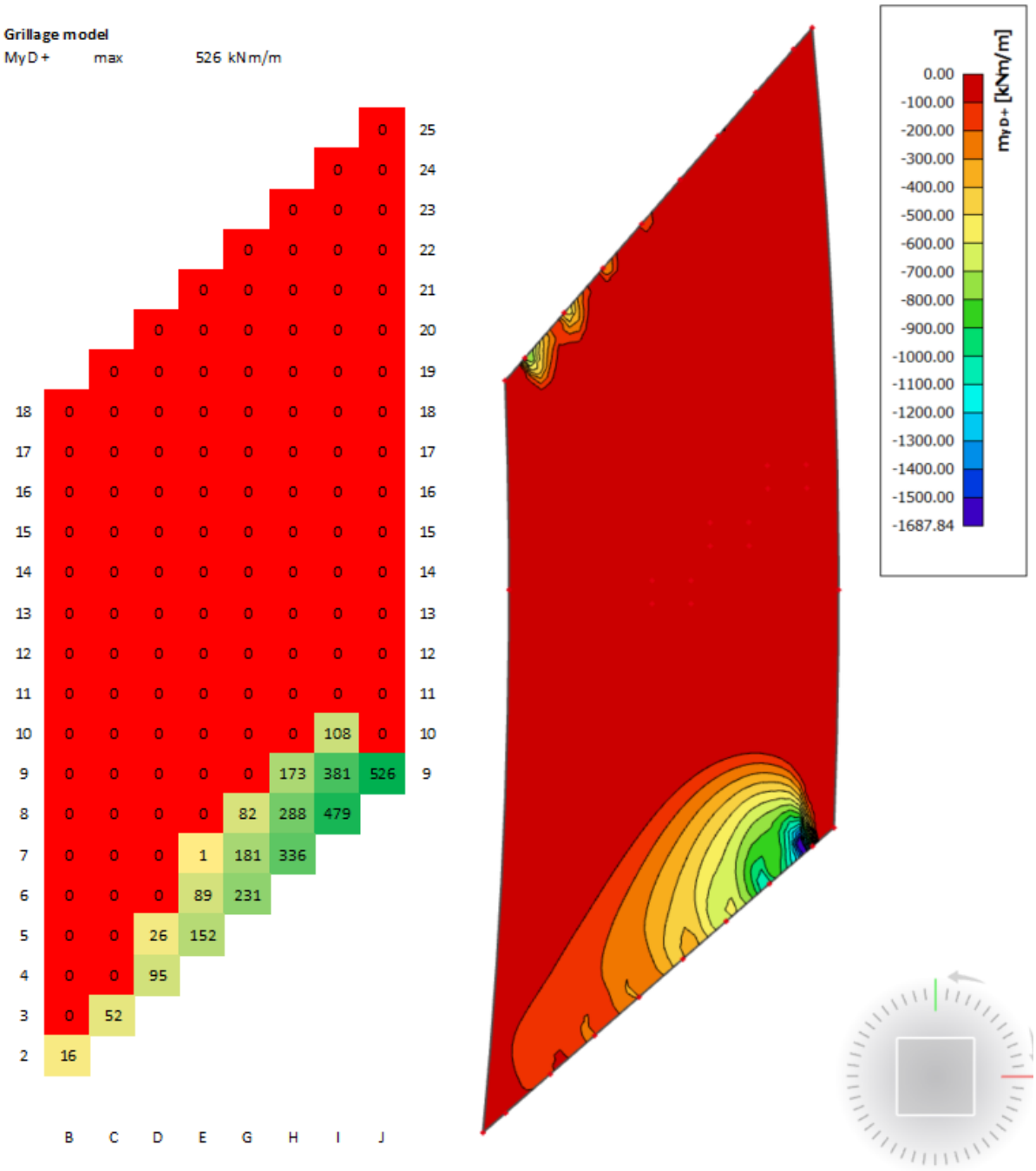

Figure G.3: MyD+, grillage model (left) and orthotropic plate model (right) (kNm/m)

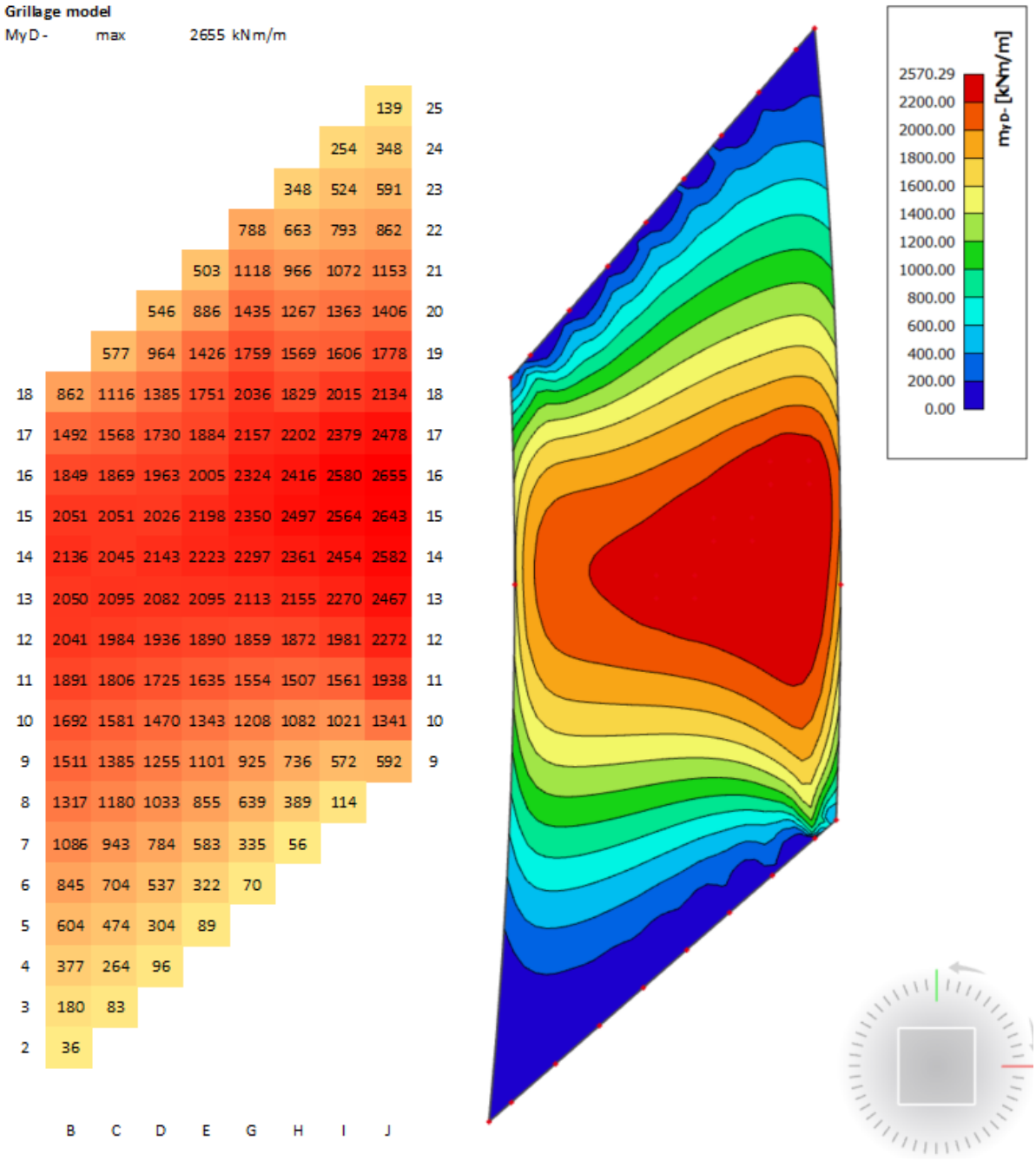

Figure G.4: MyD-, grillage model (left) and orthotropic plate model (right) (kNm/m)

H

Reinforcement design possibilities (practical example)

This appendix shows an example of the design possibilities for the reinforcement design of the longitudinal reinforcement at the bottom of the bridge deck (MyD-) of the Blankenburg case. This example shows which total amounts of reinforcement can be used for different realistic spacing and bar diameters.

For the bridge decks of the Blankenburgverbinding, the longitudinal reinforcement of the bottom plate is placed in between the shear reinforcement. The distance between the shear reinforcement is about 1.5 m, see figure H.1 and figure H.2 for a picture of the situation in practice. This means that for this example it is assumed that there must be an integer number of longitudinal reinforcement bars per 1.5 m.

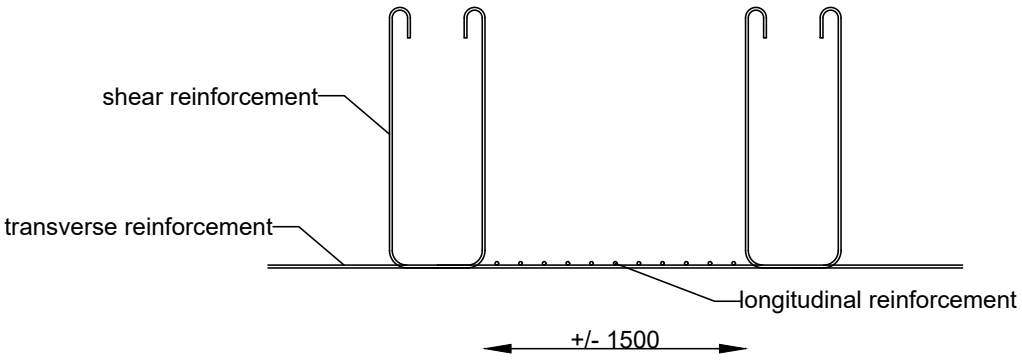

Figure H.1: Longitudinal and transverse reinforcement bottom plate, Blankenburg case (mm)

Bar diameters
For infra projects, the common minimum bar diameter is a reinforcement bar with a diameter of 12 mm (R12). However, this diameter is mainly used as so-called *practical* reinforcement. The practical reinforcement is for example used to help the main reinforcement holding its shape. For the main reinforcement, the most command bar diameters for infra project are R16, R20 and R25. These diameters are the most regular and easiest available ones.

Figure H.2: Picture longitudinal, transverse and shear reinforcement Blankenburg case

Spacing

For the spacing of the reinforcement bars, there are 2 important requirements. The spacing between the bars may not be too small, otherwise the concrete mixture segregates during casting. If the space between the bars is too small, the bigger aggregates are retained by the reinforcement bars. This results into an undesired in-homogeneous concrete. Depending on the bar diameter, the spacing can be translated into a minimum required center to center distance of the reinforcement. For R16, the minimum center to center distance is 100 mm. For bigger bar diameters, the minimum spacing as assumed to be 110 or 115 mm.

The other requirement follows from the safety of the workers on building site. The spacing of the reinforcement bars may not be too big, otherwise it would be unsafe to walk on the reinforcement. Workers have to walk on the reinforcement just before casting (the reinforcement has to be checked by a structural engineer) and during the casting of the concrete. In order to be able to walk on the reinforcement safely, it is advised to use a maximum center to center distance of 150 mm.

Example: step-sizes longitudinal reinforcement

As shown in figure H.1, the spacing between the shear reinforcement is about 1.5 m. Within this 1.5 m, there must be an integer number of reinforcement bars. Based upon the allowed center to center distance of 100 till 150 mm, there can be 10, 11, 12, 13, 14 or 15 longitudinal reinforcement bars in between the shear reinforcement. It is assumed that these bars can have a diameter of R16, R20, R25 or R32 mm.

Figure H.3 shows a table in which the total amount of reinforcement (mm^2/m) is shown for different spacing and bar diameters. As said, for R20 or bigger, the minimum spacing is 110 / 115 mm. The spacing for 14 and 15 reinforcement bars over a width of 1.5 m is equal to 107 and 100 mm. For these 2 spacing's, only bars with a diameter of 16 mm is considered.

All possible amounts of reinforcement per meter width shown in figure H.3 are put on a list. This list is sorted from small to large amount of reinforcement. The sorted list can be seen in figure H.4. For each step in the list shown in figure H.4, the step-size in the amount of reinforcement is shown in the last column. For example, the first step size in the total amount of reinforcement per meter width is equal to

$$\frac{1474 - 1340}{1340} = 10\%$$

Number of bars per 1.5 m		10	11	12	13	14	15
Center to center distance (mm)		150	136	125	115	107	100
Bar diameter (mm)	Cross-sectional area (mm^2)	Amount of reinforcement (mm^2/m)					
16	201	1340	1474	1608	1743	1877	2011
20	314	2094	2304	2513	2723	x	x
25	491	3272	3600	3927	4254	x	x
32	804	5362	5898	6434	6970	x	x

Figure H.3: Amount of reinforcement for different spacing and bar diameter

For realistic bar diameters (R16-R32) and realistic spacing (100-150 mm), the step-size in the amount of reinforcement varies from 4% till 26%. The mean step-size in the amount of reinforcement is 10%. Requirements on crack width could require that (some of) the biggest bar diameters could not be used. This could for example be a bar with a diameter of 32 mm. Excluding R32 results into a mean step-size of 9%.

Adjustments on the reinforcement design can be made by using different spacing and different bar diameters. If needed, also multiple layers of longitudinal reinforcement bars can be used. This option was not considered in the example presented in this appendix.

Amount of reinforcement (mm^2/m)	Diameter (mm)	Center to center distance (mm)	Step-size
1340	16	150	x
1474	16	136	10%
1608	16	125	9%
1743	16	115	8%
1877	16	107	8%
2011	16	100	7%
2094	20	150	4%
2304	20	136	10%
2513	20	125	9%
2723	20	115	8%
3272	25	150	20%
3600	25	136	10%
3927	25	125	9%
4254	25	115	8%
5362	32	150	26%
5898	32	136	10%
6434	32	125	9%
6970	32	115	8%
Mean step-size			10%

Figure H.4: Steps in the amount of reinforcement

Bibliography

[1] Richard Bares and Charles Massonnet. *Analysis of Beam Grids and Orthotropic Plates by the Guyon-Massonnet-Bares Method*. Crosby Lockwood Son LTD, 1968.

[2] Johan Blaauwendraad. *Plates and FEM: Surprises and Pitfalls*. Springfield, 2010.

[3] E. C. Hambly. *Bridge Deck Behaviour*. E FN Spon, 2nd edition, 1991.

[4] Coenraad Hartsuijker and Hans Welleman. *Mechanica: Statisch onbepaalde constructies en bezwijkanalyse*. Boom uitgevers Amsterdam, 2016.

[5] P. C. J. Hoogenboom. *Aantekeningen over wringing*. 5th edition, 2019.

[6] NEN. *NEN EN 1991-2: Traffic loads on bridges*. Delft, 2003.

[7] R Shreedhar and Rashmi Kharde. Comparative study of grillage method and finite element method of rcc bridge deck. *International Journal of Scientific & Engineering Research*, 4(2):1–10, 2013.

[8] Angelo Simone. *An Introduction to the Analysis of Slender Structures*. 2011.

TU Delft

Ballast Nedam